

Cover Page



Universiteit Leiden



The handle <http://hdl.handle.net/1887/35942> holds various files of this Leiden University dissertation

Author: Ent, Wietske van der

Title: *In vivo* modelling of Ewing sarcoma in zebrafish

Issue Date: 2015-10-22

***In vivo* modelling of
Ewing sarcoma in zebrafish**

Wietske van der Ent

ISBN 978-94-6203-932-2
Printed by CPI Koninklijke Wöhrmann
Research funded by Stichting Kinderen Kankervrij

***In vivo* modelling of Ewing sarcoma in zebrafish**

Proefschrift

Ter verkrijging van
de graad van Doctor aan de Universiteit Leiden,
op gezag van Rector Magnificus prof.mr. C.J.J.M. Stolker,
volgens besluit van het College voor Promoties
te verdedigen op donderdag 22 oktober 2015
klokke 16.15 uur

door

Wietske van der Ent

geboren te Albrandswaard

op 19 mei 1986

Promotoren: Prof. Dr. P.C.W. Hogendoorn
Prof. Dr. H.P. Spaink
Co-promotor: Dr. B. E. Snaar-Jagalska
Promotiecommissie: Prof. Dr. C.L. Mummery
Prof. Dr. P. ten Dijke
Prof. Dr. J. den Hertog
Dr. K. Szuhai

Table of contents

Chapter 1	Outline of the thesis	11
Chapter 2	Introduction on Ewing sarcoma	15
Chapter 3	Automation and manipulations for cancer discovery	33
Chapter 4	Ewing sarcoma inhibition by disruption of EWSR1-FLI1 transcriptional activity and reactivation of p53	57
Chapter 5	Suppression of deacetylase SIRT1 mediates tumor-suppressive NOTCH response and offers a novel treatment option in metastatic Ewing Sarcoma	85
Chapter 6	Development of a high-throughput zebrafish xenograft model for Ewing sarcoma drug discovery	109
Chapter 7	A versatile transgenic zebrafish model recapitulates genetic and histological features of Ewing sarcoma	129
Chapter 8	Quantitative analysis of protein expression in zebrafish embryos neuronally expressing human EWSR1-ERG oncogene	151
Chapter 9	Summary and concluding remarks	167
Chapter 10	Nederlandse samenvatting	173
Chapter 11	Curriculum Vitae	181
Chapter 12	List of publications	185
Chapter 13	List of abbreviations	189

The cure for anything is salt water: sweat, tears or the sea.

- Isak Dinesen, The Deluge at Norderney, 1934

Chapter 1

Outline of the thesis

Ewing sarcoma is the second most common pediatric sarcoma affecting bone, after osteosarcoma. This aggressive small blue round cell tumour also occurs in soft tissue, predominantly at older age, however in general the majority of patients are under the age of 20. Ewing sarcoma has an annual incidence rate of 2.93 cases per million, and responds well to chemotherapy combined with surgery and/or radiation. However, a quarter of all patients present with metastases at the time of diagnosis, and their outlook is unfavourable with event-free survival rates of 20-30%. In order to devise and improve treatment options for these patients, Ewing sarcoma is studied in a variety of assays ranging from cell culture to murine models. As the precise origin of Ewing sarcoma has not been determined as of yet, generating transgenic models to accurately recapitulate the disease has proven to be problematic. Various attempt at generating a murine transgenic line resulted in embryonic lethality.

In the last 15 years, the zebrafish (*Danio rerio*) has steadily been gaining ground as a model organism for cancer research. Transgenic lines have been made for various types of cancer, and xeno- and allotransplantation of cancer cells has been performed in both adult and embryonic zebrafish. Engraftment of cancer cells in an embryonic zebrafish is especially attractive for several reasons: large numbers of transparent embryos can be obtained from one pair of adults, they are transparent and thus highly suitable for non-invasive live imaging of various cancer-related processes. This imaging is aided by the wide availability of transgenic fluorescent reporter lines. Furthermore, development of the innate and adaptive immune systems are segregated in time, preventing graft rejection. In this thesis we have employed the zebrafish as a model organism for Ewing sarcoma research.

The two following chapters are written to provide background knowledge for the research performed in the other chapters. Chapter 2 provides a general introduction on Ewing sarcoma, with an overview on what is currently known about the genetics and molecular processes affected in this disease. It summarizes current disease management, and alternative treatment regimens considered based on novel insights. Chapter 3 reviews zebrafish as a model for cancer. The main focus of the chapter lies on automation, and how state-of-the-art technologies aid in increasing the throughput of the various zebrafish cancer models.

In chapter 4, we introduce a zebrafish Ewing sarcoma xenograft model. The behaviour of Ewing sarcoma cells is described, as well as their interaction with the host innate immune system. Furthermore, a combinatory treatment targeting both p53 regulation and transcriptional activity of the EWSR1-FLI1 oncogenic driver gene is presented.

Chapter 5 covers the mechanism of NOTCH-induced tumour suppression,

via Sirtuin 1 (SIRT1) inhibition. SIRT1 is a protein that suppresses p53 activation via deacetylation, and is associated with metastatic Ewing sarcoma. Restoration of NOTCH signaling, which is abrogated in Ewing sarcoma, leads to suppression of SIRT1 via HEY1. The subsequent activation of p53 by lack of SIRT1 suppression leads to cell death in vitro and inhibition of proliferation and metastatic spread in vivo.

In chapter 6, the previously established Ewing sarcoma xenograft model is altered to investigate its potential for high-throughput drug screening. We investigate how behavior of Ewing sarcoma cells robotically implanted in zebrafish embryos at blastula stage differs from that of Ewing sarcoma engraftments in the 2-day-old xenograft model, and compare the applicability both models for different drug efficacy testing .

Chapter 7 describes a transgenic zebrafish model for Ewing sarcoma. By placing the EWSR1-ERG driver gene under an UAS promoter, it is solely in cells where GAL4 is also expressed. With this binary system, the effects of EWSR1-ERG expression could be examined in various tissues. RNAseq analysis is performed on embryos expressing EWSR1-ERG in neurons. In chapter 8 investigations using this model are continued, by relating the alterations in protein expression as a consequence of EWSR1-ERG expression in the neurons.

Finally, in chapter 9, an overview is given of the different zebrafish models developed for Ewing sarcoma research. The chapter highlights the benefits and limitations of each model, and for which type of study they are most suited. Novel findings using the models as described in this thesis are summarized and their significance to the field of Ewing sarcoma research is discussed.

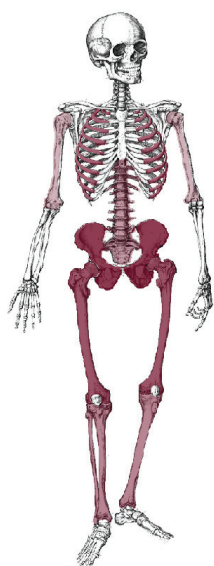
Chapter 2

Introduction on Ewing sarcoma

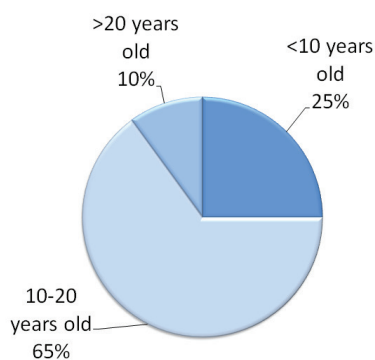
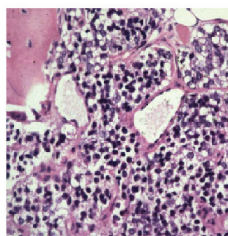
Ewing sarcoma (EWS) is the second most common bone- and soft tissue sarcoma affecting children and young adults, and is most prevalent in Caucasian males under the age of 20 (Figure 1).^{1,2} First described by James Ewing in 1921 as “diffuse endothelioma of bone”³, this tumour is composed of small round cells expressing CD99 on the membrane, and is characterised by an *EWSR1-ETS* translocation, most commonly *EWSR1-FLI1*.¹

Tumour localisation and site of origin

Common sites of skeletal involvement (~85%)



Long bones ~35%
Pelvis and ribs ~30%



Common sites of soft tissue involvement (~15%)

Lower extremities
Paravertebral region

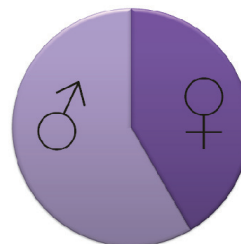


Figure 1. Characteristic of Ewing sarcoma. Histological presentation of EWS is characterised as small, blue round cells expressing CD99 on the membrane, usually with glycogen deposition. Peak incidence is between 10 and 20 years old, with a slight majority of male patients (1.4:1 ratio). Most common sites of skeletal involvement (~85% of all cases) are the long bones, pelvis and ribs (Darker red indicates higher incidence of involvement).¹ Most common sites of extraskelatal involvement (~15% of all cases) are the lower extremities and paravertebral region.^{1,4}

EWS occurs primarily in the long bones and pelvis.² Circa 25% of patients present with metastasis at the time of diagnosis⁵⁻⁷, most commonly in the lung, but also in bone and bone marrow.² It is currently unknown from which cell type EWS arises. Based on ultrastructural features and biomarkers, it has been ascribed to endothelial, reticuloendothelial, hematopoietical, neural crest and mesenchymal cells.⁸⁻¹⁰ Evidence points to the latter two as the most likely candidates, and in the following paragraphs arguments supporting these theories are expanded on.

A neural-crest derived cell has long been hypothesised to be the EWS cell of origin. Upon stimulation with cyclic adenosine monophosphate, EWS cells may undergo neural differentiation and express neural-associated enzymes like enolase 2 and choline esterase.¹¹ Gene expression profiling confirms a high expression of neuroectodermal associated genes.^{12,13} Occasionally, tumours have rosette ultrastructures comparable to Homer-Wright rosettes found in neuroblastoma.¹⁴ However, expression of *EWSR1-FLI1* or *EWSR1-ETV1* can drive neural differentiation in cells of various origins, not only derived from the neural crest.^{15,16} This suggests that not the cell of origin but the oncogene is responsible for these features.

Various studies showed that introduction of *EWSR1-ETS* was only tolerated by immortalised cells, or cells lacking p19^{ARF}, p16^{INK4A}, or TP53.¹⁷⁻¹⁹ Such deletions are not found in the majority of EWS tumours²⁰, pointing to the existence of a non-mutated primary cell type that can tolerate expression of *EWSR1-ETS* without adverse effects.²¹ Murine bone-marrow derived mesenchymal progenitor cells (MPCs) were first shown to be able to sustain proliferation upon expression of the fusion gene, without the presence of other genetic adaptations. MCPs expressing *EWSR1-FLI1* adopted histological and genetic hallmarks of EWS.²¹ Later, human mesenchymal stem cells (MSCs) with ectopic *EWSR1-ETS* expression also displayed similar gene expression profiles to EWS tumours.^{22,23} Inversely, when *EWSR1-ETS* knockdown was performed in EWS, cells took on features of MSCs^{24,25}. The discovery that MSCs can derive from the neural crest²⁶⁻²⁸ is an interesting point in the debate on the origin of EWS, and may reconcile the two lines of thought.

Genetic alterations

In 85% of all EWS cases, there is a reciprocal t(11;22)(q24;q12) translocation, merging *EWSR1* (ES Breakpoint region 1) to *FLI1* (Friend leukemia virus integration site 1)(Figure 2).¹ The fusion of *EWSR1* with *ERG*, t(21;22)(q11;q12), makes up for another 10% of EWS cases.^{29,30} Both *FLI1* and *ERG* are members of the erythroblast transformation-specific (ETS) transcription factor family and share a conserved DNA binding domain structure. Fusion of the N-terminal region of *EWSR1*, which contains a transcriptional activation domain^{31,32}, and these DNA

binding domains causes aberrant transcription of a multitude of genes. In addition to the more common *EWSR1-FLI1* and *EWSR1-ERG* translocation events, other fusions between members of the TET family of proteins (including *EWSR1* and *FUS*) and members of the ETS transcription factor family have been identified. In some cases, tumours with histological, radiological and clinical features are identified without rearrangement between TET members and ETS members. These 'Ewing-like' tumour do bear other chromosomal translocations, such as the *CIC-DUX4* or *BCOR-CCNB3*.^{34,35} An overview of these more rare type of translocations found in EWS is given in Table 1.

Besides the characteristic *EWSR1-ETS* translocation, other genetic events are observed in EWS. Chromosomal copy number alterations such as a gain of chromosomes 8, 12, 2, 5 or 9 have been described with various implications for clinical outcome.⁴⁸⁻⁵³ An unbalanced *der(16)t(1;16)* translocation leading to partial tri- or tetrasomy of 1q and partial monosomy of 16 is found in 10 to 30% of cases.^{48,54-56} Gain of 1q was repeatedly correlated to an adverse clinical prognosis^{51,52,57} and overexpression of *CDT2*, encoding a protein involved in the ubiquitin ligase activity, is suggested to underlie this aggressive phenotype.⁵⁷ Mutation or downregulation of *CDNK2A* is reported in 10 to 30% of EWS cases.^{20,58-61} Encoding P16^{INK4A}, loss of *CDNK2A* has been shown to correlate with a poor prognosis.^{20,59,62} Other mutations, such as in *TP53* have also been shown to lead to a poor prognosis, although these mutations are infrequent (less than 15% of cases).⁶³ Inactivating mutations in *STAG2* are reported in 9 to 21% of EWS cases^{64,65}, appear to be mutually exclusive with *CDKN2A*, while co-associating with *TP53* mutations.⁶⁶ This latter combination of mutations leads to a poor outlook with the current treatment regimes, and alternative therapies should be considered for these patients.

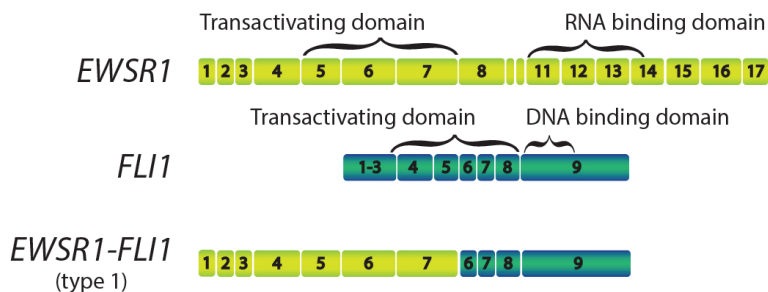


Figure 2. Scheme of the *t(11;22)(q24;q12)* translocation resulting in the *EWSR1-FLI1* fusion gene. Adapted from Burchill, 2008.³³

Table 1. Rare chromosomal rearrangements found in Ewing sarcoma.

Table 1. Rare chromosomal rearrangements found in Ewing sarcoma	Fusion gene	Chromosomal rearrangement	Reference
<i>Rearrangement between TET and ETS family of genes</i>	EWSR1-ETV1	t(7;22)(p22;q12)	Jeon <i>et al.</i> ³⁶
	EWSR1-ETV4	t(17;22)(q21;q12)	Urano <i>et al.</i> ³⁷
	EWSR1-FEV	t(2;22)(q35;q12)	Peter <i>et al.</i> ³⁸
	FUS-ERG	t(16;21)(p11;q22)	Shing <i>et al.</i> ³⁹
	FUS-FEV	t(2;16)(q35;p11)	Ng <i>et al.</i> ⁴⁰
<i>Rearrangement between TET and non-ETS family of genes</i>	EWSR1-NFATC2	t(20;22)(q13;q12)	Szuhai <i>et al.</i> ⁴¹
	EWSR1-POU5F1	t(20;22)(p21;q12)	Yamaguchi <i>et al.</i> ⁴²
	EWSR1-SMARCA5	t(4;22)(q31;q12)	Sumegi <i>et al.</i> ⁴³
	EWSR1-PATZ	t(1;22)(p36.1;q12)(with inv(22))	Mastrangelo <i>et al.</i> ⁴⁴
	EWSR1-SP3	t(2;22)(q31;q12)	Wang <i>et al.</i> ⁴⁵
<i>Rearrangement between non-TET and non-ETS family of genes</i>	CIC-DUX4	t(4;19)(q35;q13)	Kawamura-Saito <i>et al.</i> ³⁴
	CIC-FOXO4	t(X;19)(q13;q13.3)	Brohl <i>et al.</i> ⁴⁶ Sugita <i>et al.</i> ⁴⁷
	BCOR-CCNB3	inv(X)(p11.4p11.22)	Pierron <i>et al.</i> ³⁵

Current treatment regime and clinical outcome

Overall survival rates of EWS patients with localised disease have starkly improved since the introduction of systemic therapy to the treatment regime.² Patients with localised disease currently have an overall event free survival of 60% to 70%.⁶⁷ In a quarter of patients, metastatic disease is observed at the time of diagnosis. These patients have an unfavourable prognosis, with event-free survival rates of 20% to 30%.^{5-7,68,69} Patients who solely have lung-metastases seem to fare somewhat better than patients with metastases in bone or bone-marrow.^{7,70}

Standard protocol for treatment of Ewing sarcoma upon diagnosis is chemotherapy followed by surgical resection and/or radiotherapy.^{71,72}

In Europe, the chemotherapeutic regime consists of multiple cycles of vincristine, ifosfamide, doxorubicine and etoposide (VIDE, see table 2.).^{72,73}

When patients have recurrent disease, the 5 year post-recurrence event free survival rates have been reported between 5% and 35%.⁷⁴⁻⁷⁶ For these patients, no standardised therapeutic protocol is in place. Further treatment depends on the site of recurrence and prior methods of treatment. Strategies include surgery, radiation and further (high-dose) chemotherapy followed by autologous stem cell rescue.⁷⁷ High-dose therapy was found to improve the prognosis of patients with both bone(marrow) and lung metastases, or patients with an early relapse event (<2 years after initial treatment).⁷⁸⁻⁸⁰ However, incidence of relapse

remains high and more targeted therapeutic strategies are desirable to improve the prognostic outlook for these patients.

2

Molecular processes affected in Ewing sarcoma

Immunoprecipitation and yeast two-hybrid studies show that EWSR1-FLI1 protein interacts with a multitude of other proteins involved in transcription and mRNA splicing. Such interactions can increase the transactivating potency of EWSR1-FLI1, leading to an increase of deviant transcriptional activity.^{81,82} Moreover, some resultant alternative transcriptional products regulate transcription themselves, like ID2, GLI1 and EGR1.^{81,83-85} This leads to a higher amount of aberrant transcription, which complicates determining which expressional changes are critical for oncogenesis, versus those whose differential expression plays no significant part. Nonetheless, in recent years several signalling pathways have been implicated to play a key role in the pathogenesis of EWS and were proposed as candidates for targeted therapy.

One of these candidate targets for treatment is the IGF-pathway: both the IGF ligand and the IGF1 receptor (IGF1R) are upregulated in a vast majority of EWS cases, resulting in an autocrine loop.⁸⁶ The activation of the IGF-pathway leads to MAPK and PI3K-AKT-mTOR signalling, resulting in cellular proliferation and survival.⁸⁷ Inhibitors interfering with IGF1R signalling were shown to be effective both *in vitro* and *in vivo*⁸⁸⁻⁹⁰, although primary results from clinical trials were disappointing. In the clinic, only ~10% of patients showed partial response to treatment with antibodies against IGF1R⁹¹, indicating that alternative signalling routes are involved. Potratz *et al.* show that sensitivity to IGF1R kinase inhibitor could be induced in highly drug-resistant cell lines by targeting MST1R

Table 2. Class and action of therapeutics used in Ewing sarcoma treatment.

Name	Class	Mode of action
Vincristine	Vinca alkaloid	Inhibition of microtubule formation
Ifosfamide	Nitrogen mustard alkylating agent	DNA alkylation
Doxorubicine	Anthracycline antibiotic	DNA intercalation, free radical production
Etoposide	Podophyllotoxin	Topoisomerase II inhibitor

(Macrophage Stimulating 1 Receptor, a cMET related tyrosine kinase, also known as RON) with siRNA.⁹² OSI-906, a dual inhibitor targeting IR in addition to IGF1R is also being tested, and may provide a better therapeutic benefit, though as of yet there are not enough clinical data to support this.⁸⁷ Besides IGF1R, other tyrosine kinases receptors such as PDGFR⁹³⁻⁹⁵, KIT^{93,95-97} and FGFR1^{98,99}, are also found to be upregulated in cases of EWS. These kinase receptors may provide an alternative route to migrational and proliferational activation. Additionally, the serine/threonine kinase receptor TGF β -RII, which has a tumour-suppressive function, is down-regulated by EWSR1-ETS proteins.^{100,101}

Not only kinase receptors are targeted by EWSR1-FLI1. In cell cycle regulation, EWSR1-FLI1 downregulates p21^{WAF1} expression, possibly by impairing the histone deacetylation activity of transcriptional coactivator p300.¹⁰² Loss of p21^{WAF1} expression is observed in ~55% of the Ewing family of tumours.⁶⁰ Low expression of another cell cycle inhibitor, p57^{KIP} is also found in EWS cell lines.¹⁰³ Induced expression or depletion of EWSR1-FLI1 caused respectively a decrease or increase of p57^{KIP} expression.^{103,104} The protein kinase PKC- β (PRKCB) was upregulated by EWSR1-FLI1 presence, and plays a role in modulation of various signalling pathways crucial for EWS survival, as well as affecting transcriptional regulation by chromatin remodelling.

Mechanisms of intrinsic chemotherapy resistance are also worth considering, as circa 23% of the patients show little to no response to initial chemotherapy.¹⁰⁵ EWS tumours have been described to express *ABCB1* (P-glycoprotein) and/or *ABCC1* (previously *MRP1*).¹⁰⁵ Both genes belong to the ATP-Binding Cassete transporter family, and their products function as transmembrane drug-efflux proteins. One study shows that at mRNA level, *ABCC1* is expressed in 80% of samples, independent of prior chemochemical treatment, while *ABCB1* is expressed in only 30% of samples.¹⁰⁶ Another study, investigating *ABCB1* expression via immunohistochemistry, observed P-glycoprotein expression in 51 to 62% samples.¹⁰⁷ They also observed that half the tumours negative for P-glycoprotein before treatment did have expression after treatment. Besides ABC transporters, glutathione-S-transferase enzyme 4 (*GSTM4*, involved in detoxification of xenobiotics) expression is regulated by EWSR1-FLI1. Inhibition of this enzyme has been shown to confer an increased sensitivity to some chemotherapeutics.^{108,109}

Most studies on potential novel treatment regimens are initially conducted *in vitro*, then tested in murine models, before being considered for clinical trials. While testing of compounds in mammalian models is an essential step before moving on the patient trials, the high cost and long duration of these experiments limits the rate at which compounds can be screened. We propose the zebrafish as an additional model organism in the process of getting novel treatment from bench to bedside. Zebrafish can provide a model in which to screen promising compounds *in vivo* in rapid and cost-effective fashion. In this thesis, various different zebrafish models for Ewing sarcoma research are described, from

xenotransplantation models to transgenic models.

2

References

- 1 de Alava, E., Lessnick, S. L. & Sorensen, P. H. in *WHO classification of tumours of soft tissue and bone* (eds C.D.M Fletcher, J. A. Bridge, P.C.W. Hogendoorn, & F. Mertens) p. 305-309 (IARC Press, 2013).
- 2 Hawkins, D. S. *et al.* in *Principles and practice of pediatric oncology* (eds Philip A. Pizzo & David G. Poplack) Ch. 33, 987-1014, 1531 p. (Wolters Kluwer Health/Lippincott Williams & Wilkins, 2011).
- 3 Ewing, J. Diffuse endothelioma of bone. *Proceedings of the New York Pathological Society* **21**, 17-24 (1921).
- 4 Geens, L., Robays, J. V., Geert, V. & der Speeten, K. V. An Unusual Location of Extraosseous Ewing's Sarcoma. *Case reports in oncology* **6**, 293-302, doi:10.1159/000351836 (2013).
- 5 Bernstein, M. *et al.* Ewing's sarcoma family of tumors: current management. *Oncologist* **11**, 503-519, doi:10.1634/theoncologist.11-5-503 (2006).
- 6 Cotterill, S. J. *et al.* Prognostic factors in Ewing's tumor of bone: analysis of 975 patients from the European Intergroup Cooperative Ewing's Sarcoma Study Group. *Journal of clinical oncology : official journal of the American Society of Clinical Oncology* **18**, 3108-3114 (2000).
- 7 Paulussen, M. *et al.* Primary metastatic (stage IV) Ewing tumor: survival analysis of 171 patients from the EICESS studies. European Intergroup Cooperative Ewing Sarcoma Studies. *Annals of oncology : official journal of the European Society for Medical Oncology / ESMO* **9**, 275-281 (1998).
- 8 Lizard-Nacol, S., Lizard, G., Justrabo, E. & Turc-Carel, C. Immunologic characterization of Ewing's sarcoma using mesenchymal and neural markers. *Am J Pathol* **135**, 847-855 (1989).
- 9 Maurer, H. M. Current concepts in cancer. Solid tumors in children. *N Engl J Med* **299**, 1345-1348, doi:10.1056/NEJM197812142992406 (1978).
- 10 Toomey, E. C., Schiffman, J. D. & Lessnick, S. L. Recent advances in the molecular pathogenesis of Ewing's sarcoma. *Oncogene* **29**, 4504-4516, doi:10.1038/onc.2010.205 (2010).
- 11 Cavazzana, A. O., Miser, J. S., Jefferson, J. & Triche, T. J. Experimental evidence for a neural origin of Ewing's sarcoma of bone. *Am J Pathol* **127**, 507-518 (1987).
- 12 Khan, J. *et al.* Classification and diagnostic prediction of cancers using gene expression profiling and artificial neural networks. *Nat Med* **7**, 673-679, doi:10.1038/89044 (2001).

- 13 Staeger, M. S. *et al.* DNA microarrays reveal relationship of Ewing family tumors to both endothelial and fetal neural crest-derived cells and define novel targets. *Cancer Res* **64**, 8213-8221, doi:10.1158/0008-5472.CAN-03-4059 (2004).
- 14 Suh, C. H., Ordonez, N. G., Hicks, J. & Mackay, B. Ultrastructure of the Ewing's sarcoma family of tumors. *Ultrastructural pathology* **26**, 67-76, doi:10.1080/01913120252959236 (2002).
- 15 Hu-Lieskovan, S. *et al.* EWS-FLI1 fusion protein up-regulates critical genes in neural crest development and is responsible for the observed phenotype of Ewing's family of tumors. *Cancer Res* **65**, 4633-4644, doi:10.1158/0008-5472.CAN-04-2857 (2005).
- 16 Teitell, M. A. *et al.* EWS/ETS fusion genes induce epithelial and neuroectodermal differentiation in NIH 3T3 fibroblasts. *Laboratory investigation; a journal of technical methods and pathology* **79**, 1535-1543 (1999).
- 17 Deneen, B. & Denny, C. T. Loss of p16 pathways stabilizes EWS/FLI1 expression and complements EWS/FLI1 mediated transformation. *Oncogene* **20**, 6731-6741, doi:10.1038/sj.onc.1204875 (2001).
- 18 Lessnick, S. L., Dacwag, C. S. & Golub, T. R. The Ewing's sarcoma oncoprotein EWS/FLI induces a p53-dependent growth arrest in primary human fibroblasts. *Cancer Cell* **1**, 393-401 (2002).
- 19 Thompson, A. D., Teitell, M. A., Arvand, A. & Denny, C. T. Divergent Ewing's sarcoma EWS/ETS fusions confer a common tumorigenic phenotype on NIH3T3 cells. *Oncogene* **18**, 5506-5513, doi:10.1038/sj.onc.1202928 (1999).
- 20 Wei, G. *et al.* Prognostic impact of INK4A deletion in Ewing sarcoma. *Cancer* **89**, 793-799 (2000).
- 21 Riggi, N. *et al.* Development of Ewing's sarcoma from primary bone marrow-derived mesenchymal progenitor cells. *Cancer Res* **65**, 11459-11468, doi:10.1158/0008-5472.CAN-05-1696 (2005).
- 22 Riggi, N. *et al.* EWS-FLI-1 expression triggers a Ewing's sarcoma initiation program in primary human mesenchymal stem cells. *Cancer Res* **68**, 2176-2185, doi:10.1158/0008-5472.CAN-07-1761 (2008).
- 23 Miyagawa, Y. *et al.* Inducible expression of chimeric EWS/ETS proteins confers Ewing's family tumor-like phenotypes to human mesenchymal progenitor cells. *Mol Cell Biol* **28**, 2125-2137, doi:10.1128/MCB.00740-07 (2008).
- 24 Tirode, F. *et al.* Mesenchymal stem cell features of Ewing tumors. *Cancer Cell* **11**, 421-429, doi:10.1016/j.ccr.2007.02.027 (2007).
- 25 Potikyan, G. *et al.* Genetically defined EWS/FLI1 model system suggests mesenchymal origin of Ewing's family tumors. *Laboratory investigation; a journal of technical methods and pathology* **88**, 1291-1302, doi:10.1038/labinvest.2008.99 (2008).
- 26 Takashima, Y. *et al.* Neuroepithelial cells supply an initial transient wave of MSC

differentiation. *Cell* **129**, 1377-1388, doi:10.1016/j.cell.2007.04.028 (2007).

- 27 Morikawa, S. *et al.* Development of mesenchymal stem cells partially originate from the neural crest. *Biochem Biophys Res Commun* **379**, 1114-1119, doi:10.1016/j.bbrc.2009.01.031 (2009).
- 28 Nagoshi, N. *et al.* Neural crest-derived stem cells display a wide variety of characteristics. *J Cell Biochem* **107**, 1046-1052, doi:10.1002/jcb.22213 (2009).
- 29 Sorensen, P. H. *et al.* A second Ewing's sarcoma translocation, t(21;22), fuses the EWS gene to another ETS-family transcription factor, ERG. *Nat Genet* **6**, 146-151, doi:10.1038/ng0294-146 (1994).
- 30 Zucman, J. *et al.* Combinatorial generation of variable fusion proteins in the Ewing family of tumours. *EMBO J* **12**, 4481-4487 (1993).
- 31 Arvand, A. & Denny, C. T. Biology of EWS/ETS fusions in Ewing's family tumors. *Oncogene* **20**, 5747-5754, doi:10.1038/sj.onc.1204598 (2001).
- 32 Ohno, T., Rao, V. N. & Reddy, E. S. EWS/Fli-1 chimeric protein is a transcriptional activator. *Cancer Res* **53**, 5859-5863 (1993).
- 33 Burchill, S. A. Molecular abnormalities in Ewing's sarcoma. *Expert Rev Anticancer Ther* **8**, 1675-1687, doi:10.1586/14737140.8.10.1675 (2008).
- 34 Kawamura-Saito, M. *et al.* Fusion between CIC and DUX4 up-regulates PEA3 family genes in Ewing-like sarcomas with t(4;19)(q35;q13) translocation. *Hum Mol Genet* **15**, 2125-2137, doi:10.1093/hmg/ddl136 (2006).
- 35 Pierron, G. *et al.* A new subtype of bone sarcoma defined by BCOR-CCNB3 gene fusion. *Nat Genet* **44**, 461-466, doi:10.1038/ng.1107 (2012).
- 36 Jeon, I. S. *et al.* A variant Ewing's sarcoma translocation (7;22) fuses the EWS gene to the ETS gene ETV1. *Oncogene* **10**, 1229-1234 (1995).
- 37 Urano, F. *et al.* Molecular analysis of Ewing's sarcoma: another fusion gene, EWS-E1AF, available for diagnosis. *Japanese journal of cancer research : Gann* **89**, 703-711 (1998).
- 38 Peter, M. *et al.* A new member of the ETS family fused to EWS in Ewing tumors. *Oncogene* **14**, 1159-1164, doi:10.1038/sj.onc.1200933 (1997).
- 39 Shing, D. C. *et al.* FUS/ERG gene fusions in Ewing's tumors. *Cancer Res* **63**, 4568-4576 (2003).
- 40 Ng, T. L. *et al.* Ewing sarcoma with novel translocation t(2;16) producing an in-frame fusion of FUS and FEV. *The Journal of molecular diagnostics : JMD* **9**, 459-463, doi:10.2353/jmoldx.2007.070009 (2007).
- 41 Szuhai, K. *et al.* The NFATc2 gene is involved in a novel cloned translocation in a Ewing sarcoma variant that couples its function in immunology to oncology. *Clin Cancer Res* **15**, 2259-2268, doi:10.1158/1078-0432.CCR-08-2184 (2009).

- 42 Yamaguchi, S. *et al.* EWSR1 is fused to POU5F1 in a bone tumor with translocation t(6;22)(p21;q12). *Genes Chromosomes Cancer* **43**, 217-222, doi:10.1002/gcc.20171 (2005).
- 43 Sumegi, J. *et al.* A novel t(4;22)(q31;q12) produces an EWSR1-SMARCA5 fusion in extraskeletal Ewing sarcoma/primitive neuroectodermal tumor. *Mod Pathol* **24**, 333-342, doi:10.1038/modpathol.2010.201 (2011).
- 44 Mastrangelo, T. *et al.* A novel zinc finger gene is fused to EWS in small round cell tumor. *Oncogene* **19**, 3799-3804, doi:10.1038/sj.onc.1203762 (2000).
- 45 Wang, L. *et al.* Undifferentiated small round cell sarcomas with rare EWS gene fusions: identification of a novel EWS-SP3 fusion and of additional cases with the EWS-ETV1 and EWS-FEV fusions. *The Journal of molecular diagnostics : JMD* **9**, 498-509, doi:10.2353/jmoldx.2007.070053 (2007).
- 46 Brohl, A. S. *et al.* The genomic landscape of the Ewing Sarcoma family of tumors reveals recurrent STAG2 mutation. *PLoS Genet* **10**, e1004475, doi:10.1371/journal.pgen.1004475 (2014).
- 47 Sugita, S. *et al.* A novel CIC-FOXO4 gene fusion in undifferentiated small round cell sarcoma: a genetically distinct variant of Ewing-like sarcoma. *Am J Surg Pathol* **38**, 1571-1576, doi:10.1097/PAS.0000000000000286 (2014).
- 48 Mugneret, F., Lizard, S., Aurias, A. & Turc-Carel, C. Chromosomes in Ewing's sarcoma. II. Nonrandom additional changes, trisomy 8 and der(16)t(1;16). *Cancer Genet Cytogenet* **32**, 239-245 (1988).
- 49 Kullendorff, C. M. *et al.* Cytogenetic aberrations in Ewing sarcoma: are secondary changes associated with clinical outcome? *Med Pediatr Oncol* **32**, 79-83 (1999).
- 50 Armengol, G. *et al.* Recurrent gains of 1q, 8 and 12 in the Ewing family of tumours by comparative genomic hybridization. *Br J Cancer* **75**, 1403-1409 (1997).
- 51 Brisset, S. *et al.* CGH analysis of secondary genetic changes in Ewing tumors: correlation with metastatic disease in a series of 43 cases. *Cancer Genet Cytogenet* **130**, 57-61 (2001).
- 52 Hattinger, C. M. *et al.* Prognostic impact of chromosomal aberrations in Ewing tumours. *Br J Cancer* **86**, 1763-1769, doi:10.1038/sj.bjc.6600332 (2002).
- 53 Tarkkanen, M. *et al.* Clinical correlations of genetic changes by comparative genomic hybridization in Ewing sarcoma and related tumors. *Cancer Genet Cytogenet* **114**, 35-41 (1999).
- 54 Douglass, E. C. *et al.* A second nonrandom translocation, der(16)t(1;16)(q21;q13), in Ewing sarcoma and peripheral neuroectodermal tumor. *Cytogenetics and cell genetics* **53**, 87-90 (1990).
- 55 Sandberg, A. A. & Bridge, J. A. Updates on cytogenetics and molecular genetics of bone and soft tissue tumors: Ewing sarcoma and peripheral primitive

neuroectodermal tumors. *Cancer Genet Cytogenet* **123**, 1-26 (2000).

- 56 Hattinger, C. M. *et al.* Demonstration of the translocation der(16)t(1;16)(q12;q11.2) in interphase nuclei of Ewing tumors. *Genes Chromosomes Cancer* **17**, 141-150, doi:10.1002/(SICI)1098-2264(199611)17:3<141::AID-GCC1>3.0.CO;2-4 (1996).
- 57 Mackintosh, C. *et al.* 1q gain and CDT2 overexpression underlie an aggressive and highly proliferative form of Ewing sarcoma. *Oncogene* **31**, 1287-1298, doi:10.1038/onc.2011.317 (2012).
- 58 Kovar, H. *et al.* Among genes involved in the RB dependent cell cycle regulatory cascade, the p16 tumor suppressor gene is frequently lost in the Ewing family of tumors. *Oncogene* **15**, 2225-2232, doi:10.1038/sj.onc.1201397 (1997).
- 59 Tsuchiya, T. *et al.* Analysis of the p16INK4, p14ARF, p15, TP53, and MDM2 genes and their prognostic implications in osteosarcoma and Ewing sarcoma. *Cancer Genet Cytogenet* **120**, 91-98 (2000).
- 60 Maitra, A., Roberts, H., Weinberg, A. G. & Geradts, J. Aberrant expression of tumor suppressor proteins in the Ewing family of tumors. *Archives of pathology & laboratory medicine* **125**, 1207-1212, doi:10.1043/0003-9985(2001)125<1207:AEOTSP>2.0.CO;2 (2001).
- 61 Brownhill, S. C., Taylor, C. & Burchill, S. A. Chromosome 9p21 gene copy number and prognostic significance of p16 in ESFT. *Br J Cancer* **96**, 1914-1923, doi:10.1038/sj.bjc.6603819 (2007).
- 62 Honoki, K. *et al.* Prognostic significance of p16 INK4a alteration for Ewing sarcoma: a meta-analysis. *Cancer* **110**, 1351-1360, doi:10.1002/cncr.22908 (2007).
- 63 Huang, H. Y. *et al.* Ewing sarcomas with p53 mutation or p16/p14ARF homozygous deletion: a highly lethal subset associated with poor chemoresponse. *Journal of clinical oncology* **23**, 548-558, doi:10.1200/JCO.2005.02.081 (2005).
- 64 Solomon, D. A. *et al.* Mutational inactivation of STAG2 causes aneuploidy in human cancer. *Science* **333**, 1039-1043, doi:10.1126/science.1203619 (2011).
- 65 Solomon, D. A. *et al.* Frequent truncating mutations of STAG2 in bladder cancer. *Nat Genet* **45**, 1428-1430, doi:10.1038/ng.2800 (2013).
- 66 Tirode, F. *et al.* Genomic landscape of Ewing sarcoma defines an aggressive subtype with co-association of STAG2 and TP53 mutations. *Cancer discovery* **4**, 1342-1353, doi:10.1158/2159-8290.CD-14-0622 (2014).
- 67 Bacci, G. *et al.* Prognostic factors in non-metastatic Ewing's sarcoma tumor of bone: an analysis of 579 patients treated at a single institution with adjuvant or neoadjuvant chemotherapy between 1972 and 1998. *Acta Oncol* **45**, 469-475, doi:10.1080/02841860500519760 (2006).
- 68 Meyers, P. A. *et al.* High-dose melphalan, etoposide, total-body irradiation, and autologous stem-cell reconstitution as consolidation therapy for high-risk

- Ewing's sarcoma does not improve prognosis. *Journal of clinical oncology : official journal of the American Society of Clinical Oncology* **19**, 2812-2820 (2001).
- 69 Balamuth, N. J. & Womer, R. B. Ewing's sarcoma. *Lancet Oncol* **11**, 184-192, doi:10.1016/S1470-2045(09)70286-4 (2010).
- 70 Miser, J. S. *et al.* Treatment of metastatic Ewing's sarcoma or primitive neuroectodermal tumor of bone: evaluation of combination ifosfamide and etoposide--a Children's Cancer Group and Pediatric Oncology Group study. *J Clin Oncol* **22**, 2873-2876, doi:10.1200/JCO.2004.01.041 (2004).
- 71 Drabko, K. *et al.* Consolidation of first-line therapy with busulphan and melphalan, and autologous stem cell rescue in children with Ewing's sarcoma. *Bone Marrow Transplant* **47**, 1530-1534, doi:10.1038/bmt.2012.78 (2012).
- 72 Ladenstein, R. *et al.* Primary disseminated multifocal Ewing sarcoma: results of the Euro-EWING 99 trial. *Journal of clinical oncology : official journal of the American Society of Clinical Oncology* **28**, 3284-3291, doi:10.1200/JCO.2009.22.9864 (2010).
- 73 Juergens, C. *et al.* Safety assessment of intensive induction with vincristine, ifosfamide, doxorubicin, and etoposide (VIDE) in the treatment of Ewing tumors in the EURO-E.W.I.N.G. 99 clinical trial. *Pediatr Blood Cancer* **47**, 22-29, doi:10.1002/pbc.20820 (2006).
- 74 Barker, L. M., Pendergrass, T. W., Sanders, J. E. & Hawkins, D. S. Survival after recurrence of Ewing's sarcoma family of tumors. *J Clin Oncol* **23**, 4354-4362, doi:10.1200/JCO.2005.05.105 (2005).
- 75 Rodriguez-Galindo, C. *et al.* Survival after recurrence of Ewing tumors: the St Jude Children's Research Hospital experience, 1979-1999. *Cancer* **94**, 561-569, doi:10.1002/cncr.10192 (2002).
- 76 Stahl, M. *et al.* Risk of recurrence and survival after relapse in patients with Ewing sarcoma. *Pediatr Blood Cancer* **57**, 549-553, doi:10.1002/pbc.23040 (2011).
- 77 Rasper, M. *et al.* The value of high-dose chemotherapy in patients with first relapsed Ewing sarcoma. *Pediatr Blood Cancer* **61**, 1382-1386, doi:10.1002/pbc.25042 (2014).
- 78 Ladenstein, R. *et al.* Impact of megatherapy in children with high-risk Ewing's tumours in complete remission: a report from the EBMT Solid Tumour Registry. *Bone Marrow Transplant* **15**, 697-705 (1995).
- 79 Frohlich, B. *et al.* [High-dosage chemotherapy in primary metastasized and relapsed Ewing's sarcoma. (Ei)CESS]. *Klin Padiatr* **211**, 284-290, doi:10.1055/s-2008-1043801 (1999).
- 80 Oberlin, O. *et al.* Impact of high-dose busulfan plus melphalan as consolidation in metastatic Ewing tumors: a study by the Societe Francaise des Cancers de l'Enfant. *J Clin Oncol* **24**, 3997-4002, doi:10.1200/JCO.2006.05.7059 (2006).

- 81 Erkizan, H. V., Uversky, V. N. & Toretsky, J. A. Oncogenic partnerships: EWS-FLI1 protein interactions initiate key pathways of Ewing's sarcoma. *Clin Cancer Res* **16**, 4077-4083, doi:10.1158/1078-0432.CCR-09-2261 (2010).
- 82 Petermann, R. *et al.* Oncogenic EWS-Fli1 interacts with hsRPB7, a subunit of human RNA polymerase II. *Oncogene* **17**, 603-610, doi:10.1038/sj.onc.1201964 (1998).
- 83 Nishimori, H. *et al.* The Id2 gene is a novel target of transcriptional activation by EWS-ETS fusion proteins in Ewing family tumors. *Oncogene* **21**, 8302-8309, doi:10.1038/sj.onc.1206025 (2002).
- 84 Watson, D. K. *et al.* FLI1 and EWS-FLI1 function as ternary complex factors and ELK1 and SAP1a function as ternary and quaternary complex factors on the Egr1 promoter serum response elements. *Oncogene* **14**, 213-221, doi:10.1038/sj.onc.1200839 (1997).
- 85 Zwerner, J. P. *et al.* The EWS/FLI1 oncogenic transcription factor deregulates GLI1. *Oncogene* **27**, 3282-3291, doi:10.1038/sj.onc.1210991 (2008).
- 86 Scotlandi, K. *et al.* Insulin-like growth factor I receptor-mediated circuit in Ewing's sarcoma/peripheral neuroectodermal tumor: a possible therapeutic target. *Cancer Res* **56**, 4570-4574 (1996).
- 87 Olmos, D. *et al.* Targeting the Insulin-Like Growth Factor 1 Receptor in Ewing's Sarcoma: Reality and Expectations. *Sarcoma* **2011**, 402508, doi:10.1155/2011/402508 (2011).
- 88 Scotlandi, K. *et al.* Blockage of insulin-like growth factor-I receptor inhibits the growth of Ewing's sarcoma in athymic mice. *Cancer Res* **58**, 4127-4131 (1998).
- 89 Sabbatini, P. *et al.* GSK1838705A inhibits the insulin-like growth factor-1 receptor and anaplastic lymphoma kinase and shows antitumor activity in experimental models of human cancers. *Mol Cancer Ther* **8**, 2811-2820, doi:10.1158/1535-7163.MCT-09-0423 (2009).
- 90 Manara, M. C. *et al.* Preclinical in vivo study of new insulin-like growth factor-I receptor--specific inhibitor in Ewing's sarcoma. *Clin Cancer Res* **13**, 1322-1330, doi:10.1158/1078-0432.CCR-06-1518 (2007).
- 91 Fleuren, E. D., Versleijen-Jonkers, Y. M., Boerman, O. C. & van der Graaf, W. T. Targeting receptor tyrosine kinases in osteosarcoma and Ewing sarcoma: current hurdles and future perspectives. *Biochim Biophys Acta* **1845**, 266-276, doi:10.1016/j.bbcan.2014.02.005 (2014).
- 92 Potratz, J. C. *et al.* Synthetic lethality screens reveal RPS6 and MST1R as modifiers of insulin-like growth factor-1 receptor inhibitor activity in childhood sarcomas. *Cancer Res* **70**, 8770-8781, doi:10.1158/0008-5472.CAN-10-1093 (2010).
- 93 Merchant, M. S., Woo, C. W., Mackall, C. L. & Thiele, C. J. Potential use of imatinib in Ewing's Sarcoma: evidence for in vitro and in vivo activity. *J Natl Cancer Inst* **94**, 1673-1679 (2002).

- 94 Uren, A. *et al.* Beta-platelet-derived growth factor receptor mediates motility and growth of Ewing's sarcoma cells. *Oncogene* **22**, 2334-2342, doi:10.1038/sj.onc.1206330 (2003).
- 95 Bozzi, F. *et al.* Evidence for activation of KIT, PDGFRalpha, and PDGFRbeta receptors in the Ewing sarcoma family of tumors. *Cancer* **109**, 1638-1645, doi:10.1002/cncr.22587 (2007).
- 96 Gonzalez, I. *et al.* Imatinib inhibits proliferation of Ewing tumor cells mediated by the stem cell factor/KIT receptor pathway, and sensitizes cells to vincristine and doxorubicin-induced apoptosis. *Clin Cancer Res* **10**, 751-761 (2004).
- 97 Smithey, B. E., Pappo, A. S. & Hill, D. A. C-kit expression in pediatric solid tumors: a comparative immunohistochemical study. *Am J Surg Pathol* **26**, 486-492 (2002).
- 98 Girnita, L. *et al.* A link between basic fibroblast growth factor (bFGF) and EWS/FLI-1 in Ewing's sarcoma cells. *Oncogene* **19**, 4298-4301, doi:10.1038/sj.onc.1203755 (2000).
- 99 Kamura, S. *et al.* Basic fibroblast growth factor in the bone microenvironment enhances cell motility and invasion of Ewing's sarcoma family of tumours by activating the FGFR1-PI3K-Rac1 pathway. *Br J Cancer* **103**, 370-381, doi:10.1038/sj.bjc.6605775 (2010).
- 100 Hahm, K. B. *et al.* Repression of the gene encoding the TGF-beta type II receptor is a major target of the EWS-FLI1 oncoprotein. *Nat Genet* **23**, 222-227, doi:10.1038/13854 (1999).
- 101 Im, Y. H. *et al.* EWS-FLI1, EWS-ERG, and EWS-ETV1 oncoproteins of Ewing tumor family all suppress transcription of transforming growth factor beta type II receptor gene. *Cancer Res* **60**, 1536-1540 (2000).
- 102 Nakatani, F. *et al.* Identification of p21WAF1/CIP1 as a direct target of EWS-Fli1 oncogenic fusion protein. *J Biol Chem* **278**, 15105-15115, doi:10.1074/jbc.M211470200 (2003).
- 103 Dauphinot, L. *et al.* Analysis of the expression of cell cycle regulators in Ewing cell lines: EWS-FLI-1 modulates p57KIP2 and c-Myc expression. *Oncogene* **20**, 3258-3265, doi:10.1038/sj.onc.1204437 (2001).
- 104 Hu, H. M. *et al.* EWS/FLI1 suppresses retinoblastoma protein function and senescence in Ewing's sarcoma cells. *Journal of orthopaedic research : official publication of the Orthopaedic Research Society* **26**, 886-893, doi:10.1002/jor.20597 (2008).
- 105 Roundhill, E. & Burchill, S. Membrane expression of MRP-1, but not MRP-1 splicing or Pgp expression, predicts survival in patients with ESFT. *Br J Cancer* **109**, 195-206, doi:10.1038/bjc.2013.168 (2013).
- 106 Oda, Y., Dockhorn-Dworniczak, B., Jurgens, H. & Roessner, A. Expression of multidrug resistance-associated protein gene in Ewing's sarcoma and malignant peripheral neuroectodermal tumor of bone. *Journal of cancer research and*

clinical oncology **123**, 237-239 (1997).

- 107 Hijazi, Y. M. *et al.* Immunohistochemical detection of P-glycoprotein in Ewing's sarcoma and peripheral primitive neuroectodermal tumors before and after chemotherapy. *Am J Clin Pathol* **102**, 61-67 (1994).
- 108 Luo, W. *et al.* GSTM4 is a microsatellite-containing EWS/FLI target involved in Ewing's sarcoma oncogenesis and therapeutic resistance. *Oncogene* **28**, 4126-4132, doi:10.1038/onc.2009.262 (2009).
- 109 Pasello, M. *et al.* Targeting glutathione-S transferase enzymes in musculoskeletal sarcomas: a promising therapeutic strategy. *Analytical cellular pathology* **34**, 131-145, doi:10.3233/ACP-2011-012 (2011).

Chapter 3

Automation and manipulations for cancer discovery

van der Ent W, Veneman WJ, Groenewoud A, Chen L, Tulotta C, Hogendoorn
PCW, Spaik HP, Snaar-Jagalska BE.

Accepted in Springer publication 'Cancer and Zebrafish: Mechanisms,
Techniques, and Models'

Abstract

3 Zebrafish embryos can be obtained for research purposes in large numbers at low costs, embryos develop externally and in limited space, making them highly suitable for high-throughput cancer studies and drug screens. Non-invasive live imaging of various processes and their manipulations within the larvae is possible due to their transparency during development, and a multitude of available fluorescent transgenic reporter lines.

In high-throughput studies, handling large amounts of embryos and larvae is involved. With such high numbers, even the most minute tasks may become time-consuming and arduous. In this chapter, an overview is given of the developments in the automation of various steps of large scale zebrafish cancer research for discovering important cancer pathways and drugs for the treatment of human disease. The focus will lie on various tools designed for cancer cell implantation, embryo handling and sorting, microfluidic systems for imaging and drug treatment, and image acquisition and analysis. Examples will be given of employment of these devices within the fields of toxicology and cancer research.

Introduction

The use of zebrafish in cancer research has become increasingly widespread, and different models have been generated for a variety of cancer types. In initial models, tumour development was induced by the exposure of embryos, fry or adult fish to carcinogens, and gave rise to hepatic, mesenchymal, neural and epithelial neoplasms.¹⁻³ Then, with improvement of techniques to generate transgenic animals, Langenau *et al.* designed the first transgenic cancer model in zebrafish, in which expression of murine *mMyc* in lymphoid cells drove the onset of leukemia.⁴ Other transgenic cancer models followed⁵⁻¹⁵, such as activated human *BRAF*^{V600E} leading to invasive melanoma formation in p53-deficient fish⁷, or an embryonic model for rhabdomyosarcoma induced by activated human *RAS*.⁹ In addition to transgenic models, xenotransplantation models were developed, and tumours cells from a range of cancer types and species were shown to be able to proliferate, migrate and induce neovascularization in zebrafish.¹⁶⁻²⁴ In these models, cells can be implanted at different stages, from blastula and embryonic stages to (immunosuppressed) adults, as well as in different sites, like the yolk, Duct of Cuvier²⁵, perivitelline space¹⁷ or brain cavity.²⁶ In addition to xenotransplantation with cancer cells of human or murine origin, allotransplantation with cells from transgenic zebrafish cancer models or zebrafish transformed cells have been performed.^{27,28}

Many papers highlight the opportunity provided by these animals to perform large-scale chemical screens in aid of finding novel anti-

cancer drugs. Before gaining ground as a model for cancer, zebrafish embryos were used in a screen identifying small molecules affecting development²⁹, and immersion of embryos in compounds is now an established technique for treatment.^{30,31} With the development of various cancer models in zebrafish, performing screens with large libraries of compounds to find improved treatment strategies for patients is a logical next step. However, performing large scale screens can be a labour-intensive, monotonous task, and automation of different steps of the process would both increase speed, precision and reproducibility of results.

Automated systems for injection, compound treatment, imaging and data analysis are being developed. Many of these new systems are designed with zebrafish embryos in mind, not adults, so the main application will be for engraftment models, or transgenic models where there is a distinct phenotype in larval stages. Here, we will provide an overview of the advances in automation regarding each stage of cancer research in zebrafish embryos and larvae.

Automated microinjection systems

Microinjection is an indispensable technique in zebrafish research, with many applications. Microinjection is used for generation of transgenic lines, mutant lines (using the TALEN or CRISPR/Cas9 system), transient gene knock-down (using morpholinos, siRNA or antibodies), transient gene overexpression (by mRNA injection), infection studies (by injection of microbes) and cancer cell engraftment. Most of these injections are performed in embryos up to 16 cell stage, and currently available automated injection systems are designed with this stage in mind. At these early stages, the yolk cell is the largest cell in the embryo, and compounds injected there will be taken up by neighboring cells. However, with the rapid development that embryos are undergoing, injections have to be performed at high rate, to ensure proper uptake by all the cells of the embryo.

Two automated injection systems for zebrafish were reported in 2007. In the first system, published by Wang *et al.*, embryos were positioned using a 5x5 vacuum-based holding grid.³² Using image recognition software, different structures in the embryos could be recognized, and the site of injection was determined based on this information. In this first injection system, twenty-five embryos were injected per 2-minute run, with an accuracy of 99%. The second injection system, published by Hogg *et al.*, was primarily designed for injection of south-African clawed frog *Xenopus laevis* oocytes, but utility for zebrafish microinjections was also shown.³³ Here, embryos were placed in commercially available 96-well microplates with conical wells, and the site of injection was based on the spacing between wells. This negated the need for image capturing and recognition software. The setup had

a plunger-driven injection system, which allowed automated cleaning and refilling of the injection needle, making it possible to inject up to 7 different solutions. Up to 600 injections could be performed per hour.

In 2011 Carvalho *et al.* published an automated injection system that, in addition to being suitable for gene disruption injection in early-stage embryos, could also be applied to inject pathogens such as *Mycobacterium marinum* into the yolk of embryos of up to 1024-cell stage.³⁴ In this injection system, embryos were positioned in an agarose grid with a honeycomb pattern of hemispherical wells, and the site of injection was based on the consistent spacing between the wells (Figure 1A). The freshly cast agarose grid could be designed according to the experiment in mind, with a variety in number of wells for small or large scale experiments, or multiple small grids of wells to distinguish groups of embryos injected with different compounds or parameters (Figure 1B). With a built-in camera, the volume of the injected droplet could be calibrated on-screen, and easily adapted during the run of the experiment, if desired. With this robotic injection method, the authors showed that embryos could be infected with *M. marinum* bacteria at a rate of 2000 embryos per hour. High rate of infection makes it an attractive tool for high-throughput screens. Furthermore, successful morpholino injection at 1-2 cell stage has been described in this system, as well as the possibility to perform gene knockdown by injection of antibodies or siRNAs, and generating transgenic lines by DNA injection.³⁵ For additional details, refer to publications by Veneman *et al.* for an overview of the setup³⁶, and its application in *Staphylococcus epidermidis* infection.³⁷

The possibilities to do cancer research in zebrafish by manual xenotransplantation has been shown in a large number of papers. Therefore the applicability of this automated injection system for cancer cell xenografts was also investigated. A follow-up paper from the group of Prof. H. Spaink reports that cells of a number of different cancer types could be successfully injected into the yolk of embryos between 2 and 4 hours post-fertilisation (hpf) (Figure 1C).³⁵ Osteosarcoma cells (from the SJSA-1 cell line), cutaneous melanoma (Mel57), and prostate cancer cells (PC3 and LNCap) were all found to disseminate and proliferate at 6 days post-injection (dpi) and onwards. The injection system operated largely in the same manner as described by Carvalho *et al.*, with only a few adaptations to injection parameters. Due to the larger size of tumour cells when compared to bacteria, needles with a larger opening were used for these injections. Additionally, the larger tumour cells tended to sediment in the needle more rapidly, and clump together, which could cause needle clogging. A higher concentration of 14% polyvinylpyrrolidone-40 (PVP-40) carrier solution PVP was used to prevent this from happening. With these two changes, successful implantation rates were 80 to 90%, and showcases the suitability of the system for high-throughput applications. Some optimization of injection parameters may have to be performed for each cancer cell line to be injected. In addition, it is recommended to exclude the possible effects

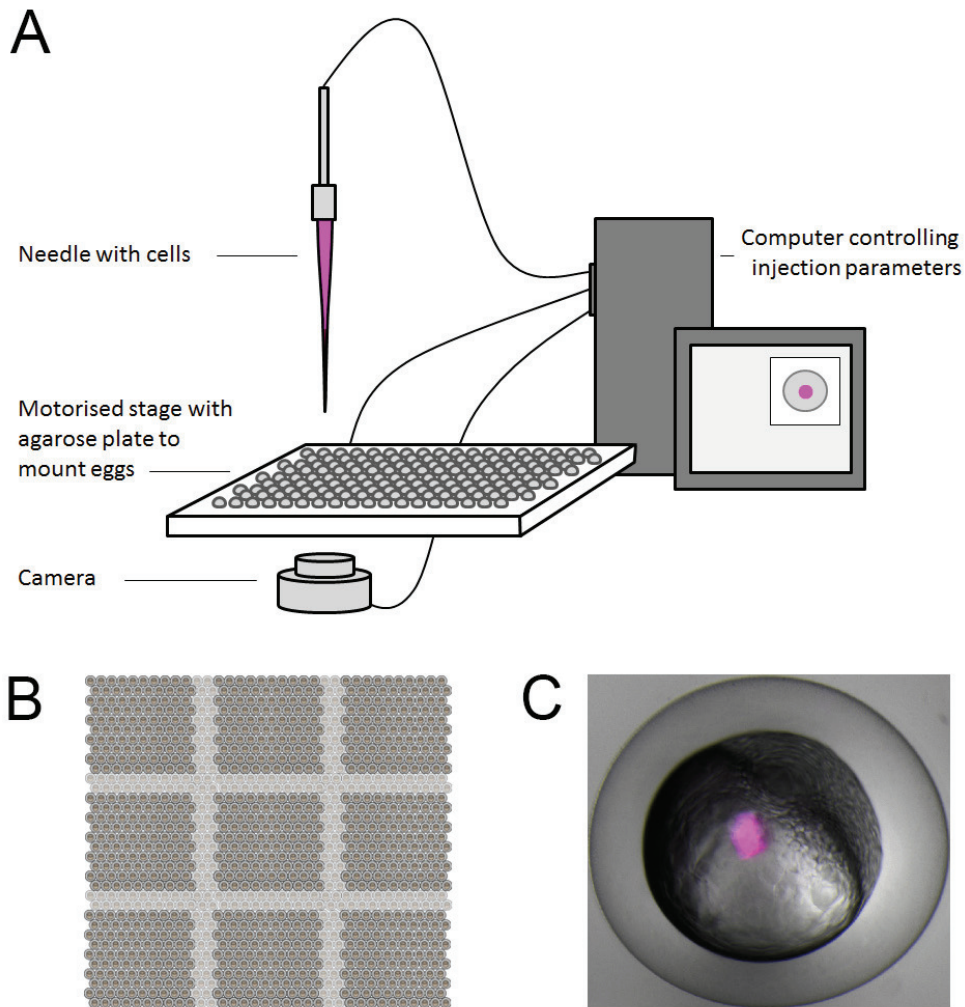


Figure 1. High-throughput injection platform for zebrafish embryos. A) Schematic representation of the injection platform described by Carvalho *et al.*³⁴ Embryos are positioned into an agarose-cast grid of hemispherical wells. The agarose grid is cast on a glass slide, the size of a well plate. A needle filled with cancer cells, mounted above the agarose plate, is computer-controlled to deliver one or multiple injections per embryo. A camera mounted beneath the agarose plate is used in calibrating the parameters of injection at the beginning of the experiment. The motorised stage moves between injections, positioning each embryo beneath the stationary needle. **B)** Example of agarose cast grid in different forms: the dark grey areas show a grid-pattern when multiple injection parameters are used, or different compounds are injected. Each dark grey square holds 100 embryos. The light and dark grey areas combined can hold up to 1024 embryos. Grid-molds for holding up to 2580 embryos are available. **C)** Embryo injected with cancer cells (magenta), 30 minutes after implantation.

of the embryonic developmental program on the cancer cells injected at this stage.³⁸

3 Thus far, the described automated injection systems are primarily used to achieve injections into the yolk cell of early stage embryos. However, when looking at cancer cell engraftment models established in zebrafish, often engraftment takes place in the yolk of older embryos from two days post fertilisation. At this point, the embryos are less fragile, and thus more likely to survive higher numbers of engrafted cells. As well as tolerating larger volumes, another key difference of older stages is that it is also possible to engraft in compartments other than the yolk sac. Engraftment into the bloodstream is achieved via injection into the Duct of Cuvier²⁵ or the heart cavity, and enables following extravasation processes and micrometastases formation. For studying angiogenesis, an engraftment model of cancer cells into the perivitelline space (PVS) close to the subintestinal vessel complex has been described.¹⁷ The PVS was also used as an implantation site in a recent publication by the group of Prof. Y. Cao, which studies the effect of tumour associated macrophages in the tumour microenvironment on intravasation and metastasis formation.³⁹ The effect of the zebrafish microenvironment on Glioblastoma multiforme cells was investigated by performing injections to the midbrain/hindbrain boundary.²⁶ In infection studies, injection of bacteria in the hindbrain have been performed to study macrophage recruitment⁴⁰⁻⁴², and injection of bacteria into the otic vesicle induce macrophage and neutrophil recruitment.⁴³ Similar injections could be of use in investigation of leukocyte recruitment in cancer research. However, a limiting factor for achieving successful automation of these types of injections is the inter-individual variations in body shape of the embryos. As the injections mentioned in this paragraph are largely high-precision maneuvers concerning minute structures, the slightest deviation in injection site or depth will result in a failed engraftment. Furthermore, with the loss of radial symmetry during embryonic development, positioning of the embryos is also a more time-consuming process.

A system for performing these kinds of injections was recently published by the group of Prof. M.F. Yanik.⁴⁴ This system positions zebrafish larvae in an array of hydrogel droplets, using a microfluidic dispensing system. Each droplet contains one larva, which can be orientated in either a dorsal orientation by several pulses of mechanical vibration (eliciting the 'startle' response), or in the lateral orientation by addition of an anesthetic to the hydrogel. After orientation of the embryos, the hydrogel will solidify after a brief period of cooling. Using a high-speed camera and image-recognition software, the position of each embryo within a droplet is identified and can be zoomed in on. The eyes and posterior-anterior axis serve as reference coordinates to determine the site of implantation with a front-loaded micropipette. This system achieved a success rate between 84% and 93% of implanting 4 dpf larvae in different orientations in a variety of organs such as forebrain,

midbrain, ventricles, eyes, heart and liver.

Another aspect to consider when aiming to perform high-throughput screens, is the amount of embryos needed. Variation of response, loss of individual embryos during the experiment, and the intention to use multiple concentrations per compound means that tens of thousands of reproducibly injected embryos are needed to screen a typical compound library. While the robotic injection systems described above will allow these reproducible injections, acquiring such numbers of uniformly staged embryos is the first necessary step. Commonly, to acquire embryos at the same developmental stage, single couples of zebrafish are placed in small tanks in which a spacer is placed between the female and male. This spacer prevents the fish from spawning, and is only removed once spawning is desired. Setting up these types of crosses when very large amounts of eggs are required, is laborious and takes up large amounts of time and space. A solution for these was presented in a paper by Addato *et al.*, which describes development of a large breeding vessel, in which 180 zebrafish can be placed at a time.⁴⁵ In the breeding vessel, females and males are separated until the desired spawning time, when the researcher removes the barrier separating the fish. Subsequently, eggs can be harvested at multiple time intervals from the bottom of the vessel. In this way, in a relatively short time, around 8000 eggs were collected on average.

Embryo-to-plate dispensing systems

Commonly, drug testing in zebrafish is performed in 96- or 384- well plates. In these plates, individual embryos can be treated with small volumes of compound to be taken up from the water in which they are immersed. Benefits of this setup are that the required volumes are relatively small, and liquid handling robots for these standardized plates are commercially available, having been previously developed for cell culture systems. Furthermore, embryos may be imaged directly in the plates in which they receive compound treatment. Confocal microscopy is possible in plates with an optical bottom, or sideview plates in which prisms allow viewing embryos from two different angles.⁴⁶

Manually filling these plates with embryos is a laborious undertaking in large drug screens. Various systems have been developed to automate the dispensing of embryos to well plates, and are described in the following paragraphs.

Pfriem *et al.* developed a fish sorting system intended for dispensing embryos from a Petri dish to a well plate that works by taking a photograph of a plate with anaesthetized embryos (hatched or unhatched), and analyzing this image to determine coordinates of each embryo.⁴⁷ They are then subsequently taken up from the Petri dish via a pipette tip, whilst a built-in sensor detects if the embryos are indeed

aspirated. The same sensor is able to detect if the aspirated embryo is living or coagulated. Living embryos are transferred to the well plate, either of 96- or 384-well format. As no fluorescent screening step is incorporated, the simple design may be cheaper than other available embryo sorters. Notably, this fish sorting system is compatible with other robots performing a variety of different tasks, in a 'modular cube' system. This modular design allows the addition or removal of parts, dependent on the design and needs of the researcher.

A similar system is described by Mandrell *et al.*, where a 4-axis Selective Compliant Assembly Robot Arm (SCARA, Denso Inc.) picks up 5-6 hpf embryos from a Petridish based on coordinates obtained from a photograph.⁴⁸ Here, the distinction between living and dead embryos is made based on rapid analysis of the same photographic record. Living, semi-transparent embryos are taken up with the pipette mounted on the SCARA. Dead embryos will appear bright white and will not be aspirated.

In addition to such 'pick-and-place' devices, other flow-based sorting systems are available. One such system is the COPAS from Union Biometrica.⁴⁹ This 'Complex Object Parametric Analyzer and Sorter' takes up embryos from a reservoir in the system, and leads them through tubing past a sensor measuring the time-of-flight (to get an indication of length), the optical density (to get an indication of thickness), and the presence and intensity of fluorescent signal within the embryos. By gating the parameters, the system can deposit the embryos in well plates of various formats, or discard them if they do not comply with defined factors. Since it is possible to analyze the intensity and presence of fluorescent signal, this system can be employed to perform selection based on the presence and amount of fluorescent tumour cells. This can be particularly useful in combination with an automated injection system, to separate the embryos implanted with sufficient amounts of cancerous cells from those with little to no cells.

Another flow-based system, called the ZebraFactor, was described by Graf *et al.*⁵⁰ The ZebraFactor consists of two devices working in sync. The CellSorter unit uses a static and a sliding ring to create a circular fluidic channel in which suspended embryos are caught via drag and friction forces. Cameras placed to visualize a part of the channel can be used to observe and sort the embryos. Single embryos are pushed, by redirection of the buffer, into the WellPlateFeeder. This second unit will dispense the embryos in wells of a 96-well plate. This setup makes use of light barriers to control opening and closing of various valves, to ensure correct embryo placement.

Microfluidic systems

The ability to automate the dispense of embryos in microtiter plates is a great boon to zebrafish research. But the well plate format is not always the ideal experimental setup. When analysis of the embryos requires

a staining procedure, a multitude of washing steps are involved. Such steps are not easily carried out in the well plate format. An alternative are microfluidic systems, or Lab-On-Chip (LOC) devices. These devices have been designed to perform rapid fluid perfusion, and to allow in-device imaging. A number of devices are designed to generate a continuous flowthrough of fresh medium, which aids in the survival of embryos when they are kept in low volumes of medium.

An in-depth explanation of the rationale of design and mechanics of LOC devices for zebrafish handling can be read in the papers by Khoshmanesh *et al.*⁵¹ and Akagi *et al.*⁵², from the group of Dr D. Wlodkovic. In short, PDMS chips bonded to microscope slides are designed to have a small fluidic channel in which embryos are loaded. The channel goes past an array of interconnected embryo traps. When embryos (within their chorions) are introduced into this channel via the inlet of the LOC device, hydrodynamic forces cause the docking and immobilization of embryos at these traps, whilst allowing remaining embryos to pass. After loading the chip with embryos, drugs or dyes can be completely perfused through the system via the inlet and outlet in a matter of minutes, without disrupting the positioned embryos. The internal volume of the described LOC device in these papers was under 1 mL, highlighting the small amounts of fluids necessary. As the devices are made with microscopic glass slides, in-device microscopy can be performed for easy imaging and analyzing of the embryos.

As a proof of concept, Akagi *et al.* perform an on-chip angiogenesis assay.⁵² After loading transgenic *TG(fli1:EGFP)* embryos with fluorescent vasculature into the chip, they are perfused by eggwater with either vehicle control, or Tivozanib, a VEGFR inhibitor effectively inhibiting angiogenesis. The development of intersegmental blood vessels could be monitored in the array for a period of 48 hours. In follow-up papers, the group of Wlodkovic describe a further developed LOC device (Figure 2A).^{53,54} The new design includes a small suction channel connected to each well, to increase immobilization efficiency via combined gravitational sedimentation and low-pressure suction forces. Additionally, the chips are fitted out with an integrated electronic automation interface, and include an automated stage and fluorescent microscope. This integrated LOC device allows automated loading of embryos, liquid perfusion control, microenvironment maintenance, and fluorescent imaging of embryos over time.

Other presented LOC devices have their own unique features. The device described by Zheng *et al.*^{35,55} (Figure 2B) is a device where the embryos are loaded manually into the open wells of the chip. What makes this an interesting system is that actuator-regulated monolithic valves are present in the channels leading into and out of each individual well of the chip. This allows for rapid, automated aspiration and reperfusion of the wells. This LOC device was used to demonstrate the ability to monitor effects of drug treatment on the cancer-associated hedgehog pathway and vasculature development.⁵⁵ Both this study

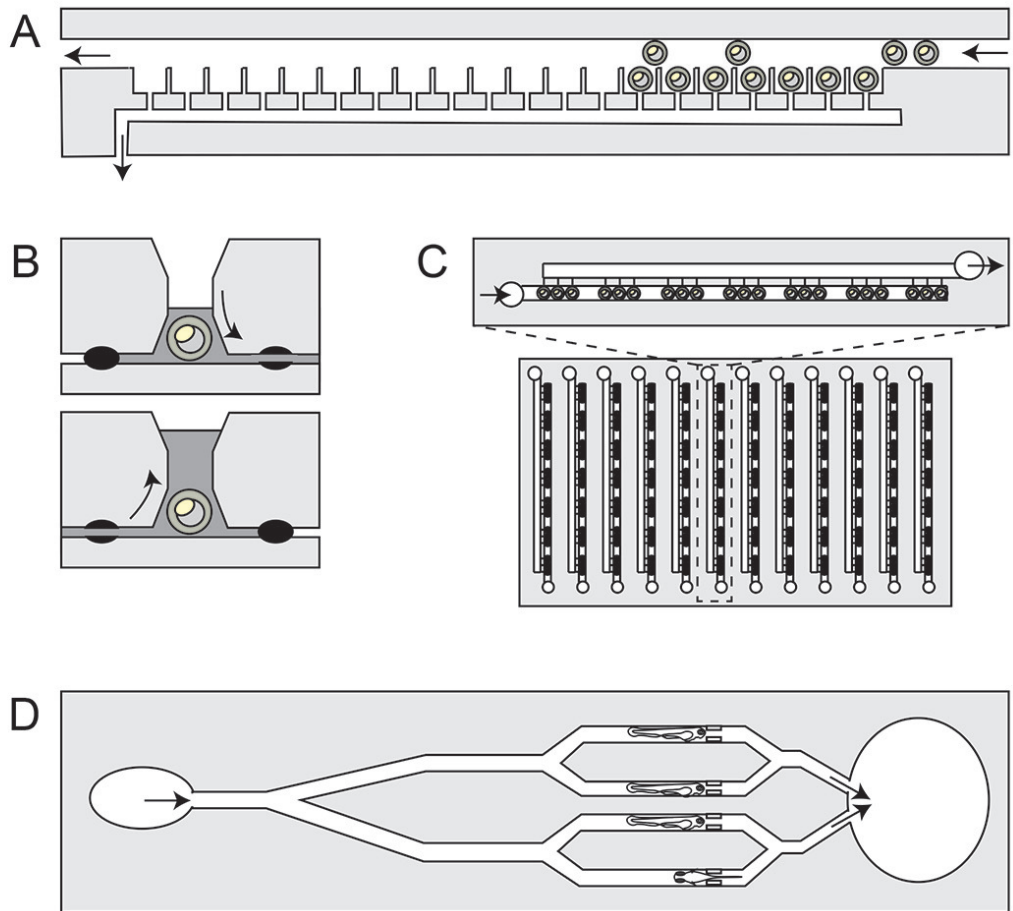


Figure 2. Microfluidic devices for imaging or compound treatment purposes. Arrows indicate the direction of flowthrough. **A)** Schematic representation of the cross-section a microfluidic device described by Wang *et al.*⁵⁴ Embryos are loaded at the inlet through the main channel, along which embryo traps are present. Each embryo trap is connected via a small channel to a suction channel underneath. Via combined gravitational sedimentation and low-pressure suction forces, embryos are immobilized in the embryo traps. In this LOC device, embryos can be imaged from above. The array was integrated in a platform with an electronic interface regulating automated embryo immobilization, culture, treatment and time-resolved image acquisition. **B)** Schematic representation of the cross-section of one well of a microfluidic device described by Zheng *et al.*⁵⁵ In this device, consisting of 24 wells of 40 μ l, each well is open and embryos are loaded from above. Channels feeding into the wells have actuator-controlled monolithic valves, which open and close independantly from eachother as old medium is removed (upper panel) and fresh medium is added (lower panel). **C)** Schematic representation of a microfluidic array, described by Zhu *et al.*⁵⁷ In this device, embryos are immobilized via combined gravitational sedimentation and low-pressure suction forces. As suction channels are positioned on the side of the embryo traps, imaging can be performed in both upright- and inverted imaging setups.

The whole array is the size of a 96-well plate, and can contain 252 embryos. **D)** Schematic representation of the ZEBRA device described by Bischel *et al.*⁵⁸ The device employs passive pumping to drive embryos through the device. Embryos are trapped in individual channels. Dependant on the manner of loading embryos (head-first or tail-first), embryos are trapped allowing side-view or in dorsal/ventral view.

and that of Akagi *et al.*⁵² show that it is possible to investigate cancer-related processes in these LOC devices, with only very small amounts of compound necessary.

In the device presented by Wielhouwer *et al.*⁵⁶, embryos are manually loaded into the wells of a chip, where a constant flow-through of medium is attained via the presence of multiple in- and outlet channels. Furthermore, this chip has integrated heating channels, making it possible to maintain stable temperature gradients on a small scale.

Another device, described by Zhu *et al.*⁵⁷ (Figure 2C) is an array of multiple identical microfluidic segments, the size of a 96-well plate. It employs combined gravitational and suction forces to trap the embryos, and can contain up to 252 individual embryos. The suction channels are positioned on the side of each embryo trap, enabling the possibility to image in both upright and inverted microscope settings. As the array is shaped as a conventional 96-well plate, it is compatible with automated imaging setups designed for well plates.

A limiting feature of the above described LOC devices, is that they are unsuitable for embryos older than 72 hpf, as at this time the larvae will break out of their chorions. A different microfluidic device, developed by Bischel *et al.* (Figure 2D), is designed for older embryos.⁵⁸ In the Zebrafish Entrapment By Restriction Array (ZEBRA), embryos are guided through small channels via surface-tension driven passive pumping. Depending on if embryos are loaded head-first or tail-first, they will be positioned laying on their side, or dorsal/ventral side facing upward, respectively. The design includes small access ports above the location where the larvae will be trapped, for an easy and rapid method to add dyes or compounds. This device was shown to be suitable for imaging 3-5 dpf larvae without the need for agarose embedding, which is time consuming and can impair embryonic development due to constriction.

Image acquisition

Much of the read-out of zebrafish experiments is based on microscopic imaging and analysis. Often, embedding in agarose with a low melting-temperature is used to fix embryos and larvae (anaesthetized with tricaine) in position for high-end microscopy. In this method, each embryo has to be positioned individually, before the agarose solidifies.

This technique is not suited for large-scale experiments. In the previous section on microfluidic devices, the possibility of doing image acquisition in the LOC devices has already been discussed. In microtiter plate format, optical glass bottom plates allow confocal imaging.^{59,60} As embryos are still small relative to one well of a 96-well plate, the use of predefined imaging coordinates is hampered. Plates can be modified with an array of agarose molds, to restrict the space the embryo will occupy.⁶¹ Additionally, Physical Sciences, Inc. (Andover, MA, USA) has manufactured the Sideview Microplate. In this plate, the wells are designed as narrow rectangles, so that embryos are limited in their orientation. Prisms placed adjacent to the wells allow imaging the embryos from the side of the well as well as the bottom. In a microscope with an automated stage, complete 96-well plates of consistently oriented embryos can be imaged with minimal effort of the investigator. Alternatively, if embryo orientation within the well is not fixed, microscopes are developed with integrated detection software to locate and recognize the orientation of the embryo.⁶³

A flow-based device, called the Vertebrate Automated Screening Technology (VAST, Figure 3A)^{63,64}, similarly takes up anesthetized embryos from a suspension cup or plate and leads them through tubing past a sensor. When an embryo is detected, the water flow is adjusted and eventually stopped so that the embryo is positioned in a glass capillary mounted under a microscope. This capillary is immersed in water and has a similar refractive index to it, making microscopy with high numeric aperture water dipping objectives possible. Motors drive the rotation of the capillary, so that the embryo within can be imaged from any angle. In this system, optic manipulations and even laser microsurgery can be performed⁶³, before the embryo is deposited in a bulk receptacle. Figure 3B shows low-magnification imaging of an 8 dpf zebrafish larvae engrafted with MDA-MB-157 breast cancer cells, imaged from multiple angles. Figure 3C shows high-magnification imaging of an 8 dpf zebrafish larvae engrafted with PC3-Pro4 prostate cancer cells, imaged from multiple angles.

Non-image based data acquisition

In various experimental setups, the final read-out of the assay is based on the presence or change in amount of fluorescence. Often, this is quantified post-experiment from microscopic images. However, this is not a necessity. In the section dealing with embryo-to-plate dispensing devices, the COPAS system has already been mentioned. As each individual embryo passes the beams of various lasers, excitation levels can be measured and recorded. This information is used in the selection and sorting of embryos during dispensing, but can be of equal use to analyze the difference in presence of various fluorescent markers in post-treatment groups. In this setup, no actual images of the embryos are generated as they pass through the system. However, there is a

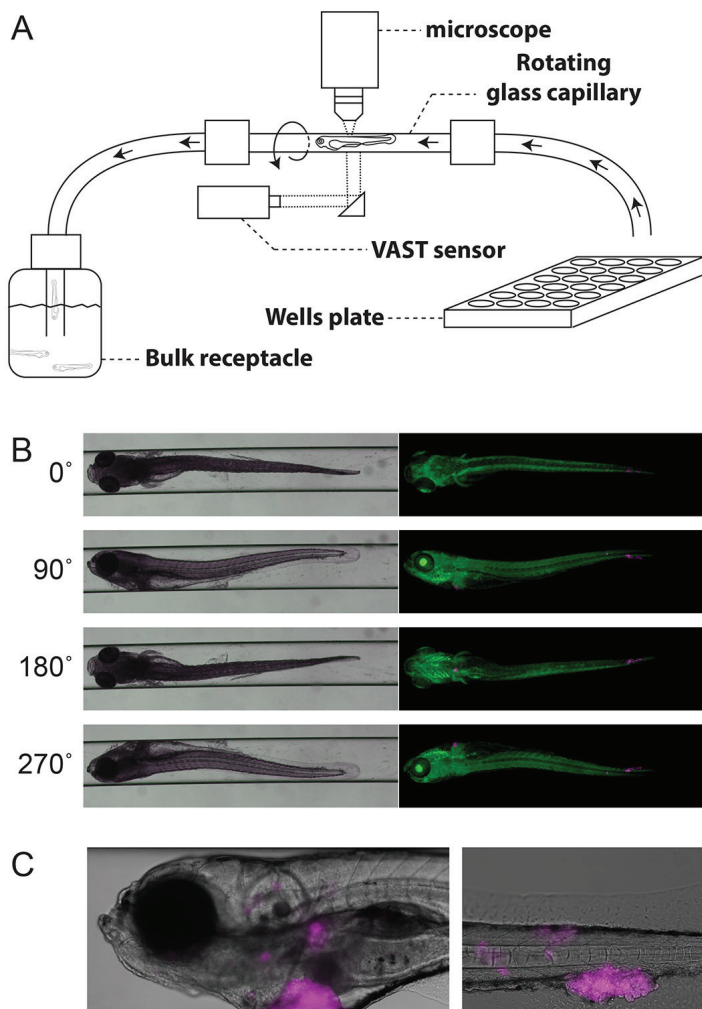


Figure 3. Automated imaging using Vertebrate Automated Screening Technology (VAST).

A) Schematic representation of the Vertebrate Automated Screening Technology (VAST) setup. Briefly, embryos are taken up from a well plate (or bulk receptacle) and guided through tubing past a sensor. As an embryo is detected by the sensor, fluid flowthrough stops or is reverted, until the embryo is positioned in a glass capillary mounted beneath a microscope. Two stepper motors on either end of the capillary can cause it to rotate, allowing the embryo to be imaged from multiple sides. After imaging, fluid flowthrough is reinitiated, and the embryo is guided to a bulk receptacle.

B) Example of images taken in the VAST setup, using a 2x objective. Bright-field and fluorescent overlays of fixed 6 dpi *TG(fli1:EGFP)* embryo (vasculature in green) implanted with breast-cancer cells (MDA-MB-157, magenta) are shown at multiple angles. **C)** Example of images taken in the VAST setup, using a 4x objective. Bright-field and fluorescent overlays of fixed 6 dpi embryo implanted with prostate-cancer cells (PC3-Pro4, magenta) are shown at multiple angles.

profile generated, showing the outline of the embryo in combination with the fluorescence signal. This could be used to detect where the fluorescent signal is located within the embryo body, and determine how much distance there is between the site of injection (yolk) and metastases (tail).

For high-throughput reporter-based assays in zebrafish, a tool called ARQiv (Automated Reporter Quantification in vivo) was presented by Walker *et al.*⁶⁵ ARQiv does not use image analysis, but quantifies the presence and intensity of fluorescent signal directly using a microplate reader. By eliminating microscopy from the process, higher throughput levels can be achieved than in other systems. The system was demonstrated to allow detection of inter-individual variation of expression of several reporters. ARQiv was shown to detect cell loss, although cell regeneration could not be as robustly measured. Furthermore, as the process is rapid and non-invasive, alterations of expression levels can be followed within individual embryos over time.

Image analysis

In development and toxicology research, alterations in phenotype of the embryo is an important readout. For this purpose, automated image analysis software packages designed for recognizing various structures within the embryo are now available.^{61, 66-69}

To assess fluorescent tumour cell burden in zebrafish, several different analysis programs are available, each with unique attributes. Pixel-counting programs are available and are a useful tool to quickly determine differences in fluorescent (tumour cell) burden. With this type of analysis, care needs to be taken that the detected fluorescent signal indeed comes from the tumour cells within the fish, and not from debris which may be visible in the background of an image. A way to reduce the interference of non-relevant signal, is to use recognition software to find the zebrafish body, and only count fluorescent signal within this area of the image.⁷⁰ Pixel-counting is a rapid analysis tool, but provides no information on the migration capabilities of cancer cells within the zebrafish.

An automated image analysis tool specifically designed for analyzing cancer cell engraftment models in zebrafish, was presented by Ghotra *et al.*⁶⁰ Here, a macro is able to detect the body of the larvae, no matter in which orientation the image was taken, and the fluorescent tumour cell burden within. Based on the body plan of the larva and its tumour cell burden, the site of implantation is determined. For each individual tumour cell cluster, the size and migration distance away from the site of implantation is determined (Figure 4).

In another program called zebIAT, developed by Annila *et al.*, a body plan is mapped to the image of engrafted embryos, and segregated

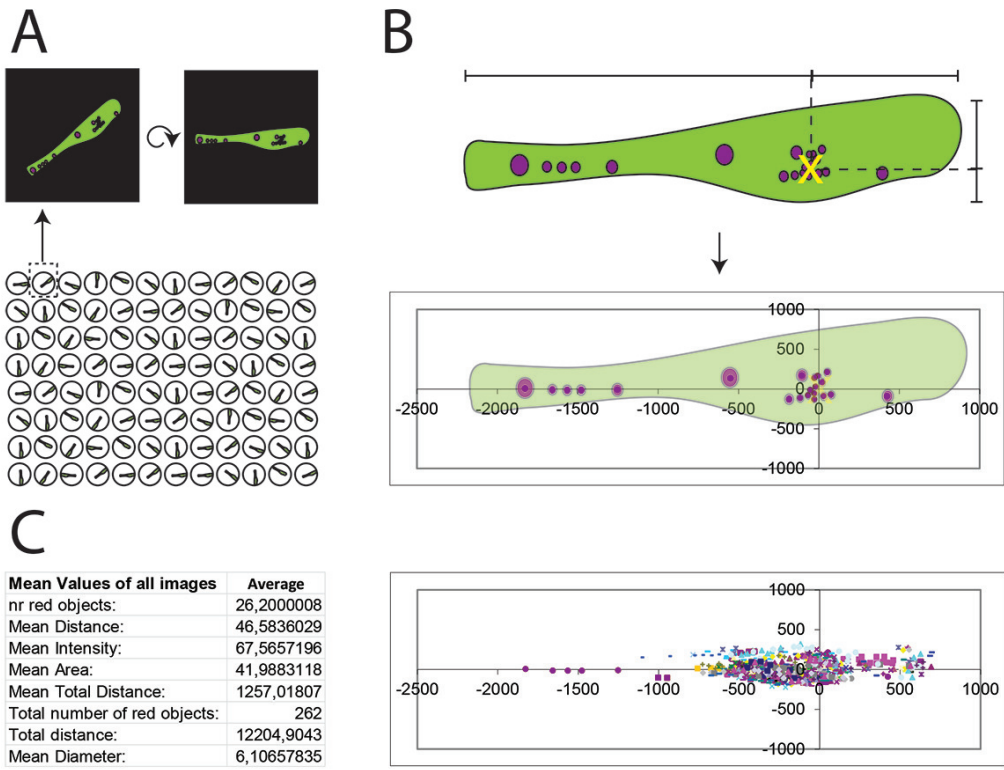


Figure 4. Automated image analysis tool. **A)** Schematic of embryos imaged in glass-bottom 96-well plate. Based on a macro written for Image-Pro Analyzer software (Media Cybernetics, USA) which determines the body axis of the larva based on signal of the green fluorescent channel, all images are rotated so that the body axes of all larvae align. **B)** In the correctly re-orientated images, the same macro uses the red fluorescent signal to identify all tumour cell foci (represented in magenta). Simultaneously, based on the larval body axes, the site of implantation (SOI) is determined (indicated by a yellow X, top panel). Of each larva, the number of tumour cell foci, the size and intensity, and the distance of migration away from the SOI is recorded. The coordinates of each tumour cell cluster is plotted in a dot plot, where the SOI corresponds to the origin (lower panel). **C)** A Microsoft Excell (Microsoft Corporation, USA) based macro is used to summarize data required from all embryos in one group (left panel), and generates a dot plot (right panel).

into 12 different tissues/structures.⁷¹ ZebiAT can then assess the presence of tumour cells per region. The program is not fully automated as of yet, as there is a requirement for manually identifications of part of the landmarks needed to map all structures. However, this software provides useful information on the seeding amount and preference of cells to home to certain organs or structures and warrants further development

to allow analysis of large data sets generated in engraftment screens.

One method to quantify the tumour burden, presented by Corkery *et al.*⁷² does not make use of images of whole embryos containing engrafted cells, but images fluorescent cancer cells *ex vivo*. For this purpose, engrafted embryos are dissociated, the cells pelleted and then resuspended in PBS. Images of fluorescent cells are analysed *in silico* using a semi-automated ImageJ (National Institutes of Health, USA) macro, and was shown to allow detecting of difference in proliferation between drug- treated and untreated groups. Although not providing information on migration or establishment of metastases, the sensitivity of this approach is advantageous for when there are only limited numbers of embryos per group, which is likely the case in large-scale drug screens.

Concluding remarks

The zebrafish is inherently a very suitable model organism for high-throughput applications. Adults can be housed relatively cheaply, embryos are produced in large numbers, and the external development makes them accessible for various kinds of manipulations. Furthermore, multiple well-characterized cancer models have been established in zebrafish on a smaller scale, ready to be adapted for large scale studies. In this chapter, we show the effort that has been made in recent years to conduct such studies. Development in automation has been achieved on all levels of zebrafish research, from embryo handling, to manipulation, drug screening, data acquisition and analysis. As these various tools are continuously being refined, we look forward to see how the described tools and methods will aid in taking the field of cancer research forward and prove the translational value of discoveries made in zebrafish for clinical application.

References

1. Beckwith LG, Moore JL, Tsao-Wu GS, Harshbarger JC, Cheng KC (2000) Ethylnitrosourea induces neoplasia in zebrafish (*Danio rerio*). *Lab Invest* 80 (3):379-385
2. Spitsbergen JM, Tsai HW, Reddy A, Miller T, Arbogast D, Hendricks JD, Bailey GS (2000) Neoplasia in zebrafish (*Danio rerio*) treated with N-methyl-N'-nitro-N-nitrosoguanidine by three exposure routes at different developmental stages. *Toxicologic pathology* 28 (5):716-725
3. Spitsbergen JM, Tsai HW, Reddy A, Miller T, Arbogast D, Hendricks JD, Bailey GS (2000) Neoplasia in zebrafish (*Danio rerio*) treated with 7,12-dimethylbenz[a]anthracene by two exposure routes at different developmental stages.

4. Langenau DM, Traver D, Ferrando AA, Kutok JL, Aster JC, Kanki JP, Lin S, Prochownik E, Trede NS, Zon LI, Look AT (2003) Myc-induced T cell leukemia in transgenic zebrafish. *Science* 299 (5608):887-890. doi:10.1126/science.1080280
5. Yang HW, Kutok JL, Lee NH, Piao HY, Fletcher CD, Kanki JP, Look AT (2004) Targeted expression of human MYCN selectively causes pancreatic neuroendocrine tumors in transgenic zebrafish. *Cancer Res* 64 (20):7256-7262. doi:10.1158/0008-5472.CAN-04-0931
6. Langenau DM, Jette C, Berghmans S, Palomero T, Kanki JP, Kutok JL, Look AT (2005) Suppression of apoptosis by bcl-2 overexpression in lymphoid cells of transgenic zebrafish. *Blood* 105 (8):3278-3285. doi:10.1182/blood-2004-08-3073
7. Patton EE, Widlund HR, Kutok JL, Kopani KR, Amatruda JF, Murphey RD, Berghmans S, Mayhall EA, Traver D, Fletcher CD, Aster JC, Granter SR, Look AT, Lee C, Fisher DE, Zon LI (2005) BRAF mutations are sufficient to promote nevi formation and cooperate with p53 in the genesis of melanoma. *Curr Biol* 15 (3):249-254. doi:10.1016/j.cub.2005.01.031
8. Feng H, Langenau DM, Madge JA, Quinkertz A, Gutierrez A, Neuberger DS, Kanki JP, Look AT (2007) Heat-shock induction of T-cell lymphoma/leukaemia in conditional Cre/lox-regulated transgenic zebrafish. *Br J Haematol* 138 (2):169-175. doi:10.1111/j.1365-2141.2007.06625.x
9. Langenau DM, Keefe MD, Storer NY, Guyon JR, Kutok JL, Le X, Goessling W, Neuberger DS, Kunkel LM, Zon LI (2007) Effects of RAS on the genesis of embryonal rhabdomyosarcoma. *Genes Dev* 21 (11):1382-1395. doi:10.1101/gad.1545007
10. Le X, Langenau DM, Keefe MD, Kutok JL, Neuberger DS, Zon LI (2007) Heat shock-inducible Cre/Lox approaches to induce diverse types of tumors and hyperplasia in transgenic zebrafish. *Proc Natl Acad Sci U S A* 104 (22):9410-9415. doi:10.1073/pnas.0611302104
11. Chen YH, Wang YH, Yu TH, Wu HJ, Pai CW (2009) Transgenic zebrafish line with over-expression of Hedgehog on the skin: a useful tool to screen Hedgehog-inhibiting compounds. *Transgenic Res* 18 (6):855-864. doi:10.1007/s11248-009-9275-y
12. Dovey M, White RM, Zon LI (2009) Oncogenic NRAS cooperates with p53 loss to generate melanoma in zebrafish. *Zebrafish* 6 (4):397-404. doi:10.1089/zeb.2009.0606
13. Ju B, Spitsbergen J, Eden CJ, Taylor MR, Chen W (2009) Co-activation of hedgehog and AKT pathways promote tumorigenesis in zebrafish. *Molecular cancer* 8:40. doi:10.1186/1476-4598-8-40
14. Santoriello C, Gennaro E, Anelli V, Distel M, Kelly A, Koster RW, Hurlstone A, Mione M (2010) Kita driven expression of oncogenic HRAS leads to early

onset and highly penetrant melanoma in zebrafish. *PLoS One* 5 (12):e15170. doi:10.1371/journal.pone.0015170

- 3
15. Leacock SW, Basse AN, Chandler GL, Kirk AM, Rakheja D, Amatruda JF (2012) A zebrafish transgenic model of Ewing's sarcoma reveals conserved mediators of EWS-FLI1 tumorigenesis. *Dis Model Mech* 5 (1):95-106. doi:10.1242/dmm.007401
 16. Lee LM, Seftor EA, Bonde G, Cornell RA, Hendrix MJ (2005) The fate of human malignant melanoma cells transplanted into zebrafish embryos: assessment of migration and cell division in the absence of tumor formation. *Dev Dyn* 233 (4):1560-1570. doi:10.1002/dvdy.20471
 17. Nicoli S, Ribatti D, Cotelli F, Presta M (2007) Mammalian tumor xenografts induce neovascularization in zebrafish embryos. *Cancer Res* 67 (7):2927-2931. doi:67/7/2927 [pii]
 18. Stoletov K, Montel V, Lester RD, Gonias SL, Klemke R (2007) High-resolution imaging of the dynamic tumor cell vascular interface in transparent zebrafish. *Proc Natl Acad Sci U S A* 104 (44):17406-17411. doi:10.1073/pnas.0703446104
 19. Marques IJ, Weiss FU, Vlecken DH, Nitsche C, Bakkers J, Lagendijk AK, Partecke LI, Heidecke CD, Lerch MM, Bagowski CP (2009) Metastatic behaviour of primary human tumours in a zebrafish xenotransplantation model. *BMC Cancer* 9:128. doi:10.1186/1471-2407-9-128
 20. Eguiara A, Holgado O, Beloqui I, Abalde L, Sanchez Y, Callol C, Martin AG (2011) Xenografts in zebrafish embryos as a rapid functional assay for breast cancer stem-like cell identification. *Cell Cycle* 10 (21):3751-3757. doi:10.4161/cc.10.21.17921
 21. Zhao C, Wang X, Zhao Y, Li Z, Lin S, Wei Y, Yang H (2011) A novel xenograft model in zebrafish for high-resolution investigating dynamics of neovascularization in tumors. *PLoS One* 6 (7):e21768. doi:10.1371/journal.pone.0021768
 22. Drabsch Y, He S, Zhang L, Snaar-Jagalska BE, ten Dijke P (2013) Transforming growth factor-beta signalling controls human breast cancer metastasis in a zebrafish xenograft model. *Breast cancer research : BCR* 15 (6):R106. doi:10.1186/bcr3573
 23. van der Ent W, Burrello C, Teunisse AF, Ksander BR, Van der Velden PA, Jager MJ, Jochemsen AG, Snaar-Jagalska BE (2014) Modelling of human uveal melanoma in Zebrafish xenograft embryos. *Invest Ophthalmol Vis Sci*. doi:10.1167/iovs.14-15202
 24. van der Ent W, Jochemsen AG, Teunisse AF, Krens SF, Szuhai K, Spaink HP, Hogendoorn PC, Snaar-Jagalska BE (2014) Ewing sarcoma inhibition by disruption of EWSR1-FLI1 transcriptional activity and reactivation of p53. *J Pathol* 233 (4):415-424. doi:10.1002/path.4378
 25. He S, Lamers GE, Beenakker JW, Cui C, Ghotra VP, Danen EH, Meijer AH, Spaink HP, Snaar-Jagalska BE (2012) Neutrophil-mediated experimental metastasis is enhanced by VEGFR inhibition in a zebrafish xenograft model. *J*

26. Rampazzo E, Persano L, Pistollato F, Moro E, Frasson C, Porazzi P, Della Puppa A, Bresolin S, Battilana G, Indraccolo S, Te Kronnie G, Argenton F, Tiso N, Basso G (2013) Wnt activation promotes neuronal differentiation of glioblastoma. *Cell death & disease* 4:e500. doi:10.1038/cddis.2013.32
27. Tang Q, Abdelfattah NS, Blackburn JS, Moore JC, Martinez SA, Moore FE, Lobbardi R, Tenente IM, Ignatius MS, Berman JN, Liwski RS, Houvras Y, Langenau DM (2014) Optimized cell transplantation using adult rag2 mutant zebrafish. *Nat Methods* 11 (8):821-824. doi:10.1038/nmeth.3031
28. He S, Krens SG, Zhan H, Gong Z, Hogendoorn PC, Spaink HP, Snaar-Jagalska BE (2011) A DeltaRaf1-ER-inducible oncogenic zebrafish liver cell model identifies hepatocellular carcinoma signatures. *J Pathol* 225 (1):19-28. doi:10.1002/path.2936
29. Peterson RT, Link BA, Dowling JE, Schreiber SL (2000) Small molecule developmental screens reveal the logic and timing of vertebrate development. *Proc Natl Acad Sci U S A* 97 (24):12965-12969. doi:10.1073/pnas.97.24.12965
30. Stern HM, Zon LI (2003) Cancer genetics and drug discovery in the zebrafish. *Nat Rev Cancer* 3 (7):533-539. doi:10.1038/nrc1126
31. Goessling W, North TE, Zon LI (2007) New waves of discovery: modeling cancer in zebrafish. *J Clin Oncol* 25 (17):2473-2479. doi:25/17/2473 [pii]
32. Wang W, Liu X, Gelinas D, Ciruna B, Sun Y (2007) A fully automated robotic system for microinjection of zebrafish embryos. *PLoS One* 2 (9):e862. doi:10.1371/journal.pone.0000862
33. Hogg RC, Bandelier F, Benoit A, Dosch R, Bertrand D (2008) An automated system for intracellular and intranuclear injection. *Journal of neuroscience methods* 169 (1):65-75. doi:10.1016/j.jneumeth.2007.11.028
34. Carvalho R, de Sonnevile J, Stockhammer OW, Savage ND, Veneman WJ, Ottenhoff TH, Dirks RP, Meijer AH, Spaink HP (2011) A high-throughput screen for tuberculosis progression. *PLoS One* 6 (2):e16779. doi:10.1371/journal.pone.0016779
35. Spaink HP, Cui C, Wiweger MI, Jansen HJ, Veneman WJ, Marin-Juez R, de Sonnevile J, Ordas A, Torraca V, van der Ent W, Leenders WP, Meijer AH, Snaar-Jagalska BE, Dirks RP (2013) Robotic injection of zebrafish embryos for high-throughput screening in disease models. *Methods* 62 (3):246-254. doi:10.1016/j.ymeth.2013.06.002
36. Veneman WJ, Marin-Juez R, de Sonnevile J, Ordas A, Jong-Raadsen S, Meijer AH, Spaink HP (2014) Establishment and optimization of a high throughput setup to study *Staphylococcus epidermidis* and *Mycobacterium marinum* infection as a model for drug discovery. *Journal of visualized experiments : JoVE* (88):e51649. doi:10.3791/51649
37. Veneman WJ, Stockhammer OW, de Boer L, Zaat SA, Meijer AH, Spaink HP

- (2013) A zebrafish high throughput screening system used for *Staphylococcus epidermidis* infection marker discovery. *BMC Genomics* 14:255. doi:10.1186/1471-2164-14-255
38. Hendrix MJ, Seftor EA, Seftor RE, Kasemeier-Kulesa J, Kulesa PM, Postovit LM (2007) Reprogramming metastatic tumour cells with embryonic microenvironments. *Nat Rev Cancer* 7 (4):246-255. doi:10.1038/nrc2108
39. Wang J, Cao Z, Zhang XM, Nakamura M, Sun M, Hartman J, Harris RA, Sun Y, Cao Y (2015) Novel mechanism of macrophage-mediated metastasis revealed in a zebrafish model of tumor development. *Cancer Res* 75 (2):306-315. doi:10.1158/0008-5472.CAN-14-2819
40. Herbomel P, Thisse B, Thisse C (1999) Ontogeny and behaviour of early macrophages in the zebrafish embryo. *Development* 126 (17):3735-3745
41. Davis JM, Clay H, Lewis JL, Ghori N, Herbomel P, Ramakrishnan L (2002) Real-time visualization of mycobacterium-macrophage interactions leading to initiation of granuloma formation in zebrafish embryos. *Immunity* 17 (6):693-702
42. Clay H, Davis JM, Beery D, Huttenlocher A, Lyons SE, Ramakrishnan L (2007) Dichotomous role of the macrophage in early *Mycobacterium marinum* infection of the zebrafish. *Cell Host Microbe* 2 (1):29-39. doi:10.1016/j.chom.2007.06.004
43. Le Guyader D, Redd MJ, Colucci-Guyon E, Murayama E, Kissa K, Briolat V, Mordelet E, Zapata A, Shinomiya H, Herbomel P (2008) Origins and unconventional behavior of neutrophils in developing zebrafish. *Blood* 111 (1):132-141. doi:10.1182/blood-2007-06-095398
44. Chang TY, Shi P, Steinmeyer JD, Chatnuntawech I, Tillberg P, Love KT, Eimon PM, Anderson DG, Yanik MF (2014) Organ-targeted high-throughput in vivo biologics screen identifies materials for RNA delivery. *Integrative biology : quantitative biosciences from nano to macro* 6 (10):926-934. doi:10.1039/c4ib00150h
45. Adatto I, Lawrence C, Thompson M, Zon LI (2011) A new system for the rapid collection of large numbers of developmentally staged zebrafish embryos. *PLoS One* 6 (6):e21715. doi:10.1371/journal.pone.0021715
46. Peterson RT, Fishman MC (2011) Designing zebrafish chemical screens. *Methods Cell Biol* 105:525-541. doi:10.1016/B978-0-12-381320-6.00023-0
47. Pfriem A, Pylatiuk C, Alshut R, Ziegner B, Schulz S, Bretthauer G (2012) A modular, low-cost robot for zebrafish handling. *Conf Proc IEEE Eng Med Biol Soc* 2012:980-983. doi:10.1109/EMBC.2012.6346097
48. Mandrell D, Truong L, Jephson C, Sarker MR, Moore A, Lang C, Simonich MT, Tanguay RL (2012) Automated zebrafish chorion removal and single embryo placement: optimizing throughput of zebrafish developmental toxicity screens. *Journal of laboratory automation* 17 (1):66-74. doi:10.1177/2211068211432197
49. Pulak R (2006) Techniques for analysis, sorting, and dispensing of *C. elegans* on

- the COPAS flow-sorting system. *Methods Mol Biol* 351:275-286. doi:10.1385/1-59745-151-7:275
50. Graf SF, Hotzel S, Liebel U, Stemmer A, Knapp HF (2011) Image-based fluidic sorting system for automated Zebrafish egg sorting into multiwell plates. *Journal of laboratory automation* 16 (2):105-111. doi:10.1016/j.jala.2010.11.002
 51. Khoshmanesh K, Akagi J, Hall CJ, Crosier KE, Crosier PS, Cooper JM, Wlodkowic D (2012) New rationale for large metazoan embryo manipulations on chip-based devices. *Biomicrofluidics* 6 (2):24102-2410214. doi:10.1063/1.3699971
 52. Akagi J, Khoshmanesh K, Evans B, Hall CJ, Crosier KE, Cooper JM, Crosier PS, Wlodkowic D (2012) Miniaturized embryo array for automated trapping, immobilization and microperfusion of zebrafish embryos. *PLoS One* 7 (5):e36630. doi:10.1371/journal.pone.0036630
 53. Akagi J, Zhu F, Hall CJ, Crosier KE, Crosier PS, Wlodkowic D (2014) Integrated chip-based physiometer for automated fish embryo toxicity biotests in pharmaceutical screening and ecotoxicology. *Cytometry Part A : the journal of the International Society for Analytical Cytology* 85 (6):537-547. doi:10.1002/cyto.a.22464
 54. Wang KI, Salcic Z, Yeh J, Akagi J, Zhu F, Hall CJ, Crosier KE, Crosier PS, Wlodkowic D (2013) Toward embedded laboratory automation for smart Lab-on-a-Chip embryo arrays. *Biosens Bioelectron* 48:188-196. doi:10.1016/j.bios.2013.04.033
 55. Zheng C, Zhou H, Liu X, Pang Y, Zhang B, Huang Y (2014) Fish in chips: an automated microfluidic device to study drug dynamics in vivo using zebrafish embryos. *Chem Commun (Camb)* 50 (8):981-984. doi:10.1039/c3cc47285j
 56. Wielhouwer EM, Ali S, Al-Afandi A, Blom MT, Riekerink MB, Poelma C, Westerweel J, Oonk J, Vrouwe EX, Buesink W, vanMil HG, Chicken J, van't Oever R, Richardson MK (2011) Zebrafish embryo development in a microfluidic flow-through system. *Lab on a chip* 11 (10):1815-1824. doi:10.1039/c0lc00443j
 57. Zhu F, Akagi J, Hall CJ, Crosier KE, Crosier PS, Delaage P, Wlodkowic D A high-throughput lab-on-a-chip interface for zebrafish embryo tests in drug discovery and ecotoxicology. In, 2013. pp 892345-892345-892349
 58. Bischel LL, Mader BR, Green JM, Huttenlocher A, Beebe DJ (2013) Zebrafish Entrapment By Restriction Array (ZEBRA) device: a low-cost, agarose-free zebrafish mounting technique for automated imaging. *Lab on a chip* 13 (9):1732-1736. doi:10.1039/c3lc50099c
 59. Takaki K, Cosma CL, Troll MA, Ramakrishnan L (2012) An in vivo platform for rapid high-throughput antitubercular drug discovery. *Cell reports* 2 (1):175-184. doi:10.1016/j.celrep.2012.06.008
 60. Ghotra VP, He S, de Bont H, van der Ent W, Spaik HP, van de Water B, Snaar-Jagalska BE, Danen EH (2012) Automated whole animal bio-imaging assay for human cancer dissemination. *PLoS One* 7 (2):e31281. doi:10.1371/journal.pone.0031281

61. Westhoff JH, Giselbrecht S, Schmidts M, Schindler S, Beales PL, Tonshoff B, Liebel U, Gehrig J (2013) Development of an automated imaging pipeline for the analysis of the zebrafish larval kidney. *PLoS One* 8 (12):e82137. doi:10.1371/journal.pone.0082137
62. Spomer W, Pfriem A, Alshut R, Just S, Pylatiuk C (2012) High-throughput screening of zebrafish embryos using automated heart detection and imaging. *Journal of laboratory automation* 17 (6):435-442. doi:10.1177/2211068212464223
63. Pardo-Martin C, Chang TY, Koo BK, Gilleland CL, Wasserman SC, Yanik MF (2010) High-throughput in vivo vertebrate screening. *Nat Methods* 7 (8):634-636. doi:10.1038/nmeth.1481
64. Chang TY, Pardo-Martin C, Allalou A, Wahlby C, Yanik MF (2012) Fully automated cellular-resolution vertebrate screening platform with parallel animal processing. *Lab on a chip* 12 (4):711-716. doi:10.1039/c1lc20849g
65. Walker SL, Ariga J, Mathias JR, Coothankandaswamy V, Xie X, Distel M, Koster RW, Parsons MJ, Bhalla KN, Saxena MT, Mumm JS (2012) Automated reporter quantification in vivo: high-throughput screening method for reporter-based assays in zebrafish. *PLoS One* 7 (1):e29916. doi:10.1371/journal.pone.0029916
66. Liu T, Li G, Nie J, Tarokh A, Zhou X, Guo L, Malicki J, Xia W, Wong ST (2008) An automated method for cell detection in zebrafish. *Neuroinformatics* 6 (1):5-21. doi:10.1007/s12021-007-9005-7
67. Kamali M, Day LJ, Brooks DH, Zhou X, O'Malley DM (2009) Automated identification of neurons in 3D confocal datasets from zebrafish brainstem. *Journal of microscopy* 233 (1):114-131. doi:10.1111/j.1365-2818.2008.03102.x
68. Peravali R, Gehrig J, Giselbrecht S, Lutjohann DS, Hadzhiev Y, Muller F, Liebel U (2011) Automated feature detection and imaging for high-resolution screening of zebrafish embryos. *Biotechniques* 50 (5):319-324. doi:10.2144/000113669
69. Eames BF, DeLaurier A, Ullmann B, Huycke TR, Nichols JT, Dowd J, McFadden M, Sasaki MM, Kimmel CB (2013) FishFace: interactive atlas of zebrafish craniofacial development at cellular resolution. *BMC developmental biology* 13:23. doi:10.1186/1471-213X-13-23
70. Nezhinsky A, Verbeek F (2010) Pattern Recognition for High Throughput Zebrafish Imaging Using Genetic Algorithm Optimization. In: Dijkstra TH, Tsivtsivadze E, Marchiori E, Heskes T (eds) *Pattern Recognition in Bioinformatics*, vol 6282. *Lecture Notes in Computer Science*. Springer Berlin Heidelberg, pp 301-312. doi:10.1007/978-3-642-16001-1_26
71. Annala T, Lihavainen E, Marques IJ, Williams DR, Yli-Harja O, Ribeiro A (2013) ZeBIAT, an image analysis tool for registering zebrafish embryos and quantifying cancer metastasis. *BMC Bioinformatics* 14 Suppl 10:S5. doi:10.1186/1471-2105-14-S10-S5
72. Corkery DP, Dellaire G, Berman JN (2011) Leukaemia xenotransplantation in zebrafish--chemotherapy response assay in vivo. *Br J Haematol* 153 (6):786-

789. doi:10.1111/j.1365-2141.2011.08661.x

3

Chapter 4

Ewing sarcoma inhibition by disruption of EWSR1-FLI1 transcriptional activity and reactivation of p53

van der Ent W, Jochemsen AG, Teunisse AF, Krens SF, Szuhai K, Spaink HP,
Hogendoorn PC, Snaar-Jagalska BE.

J Pathol. 2014 Aug;233(4):415-24

Abstract

Translocations involving ETS-transcription factors, most commonly leading to the EWSR1-FLI1 fusion protein, are the hallmark of Ewing sarcoma. Despite knowledge of this driving molecular event, an effective therapeutic strategy is lacking. To test potential treatment regimes, we established a novel Ewing sarcoma zebrafish engraftment model allowing time-effective, dynamic quantification of Ewing sarcoma progression and tumour burden *in vivo*, applicable for screening of single and combined compounds. In Ewing sarcoma the tumour-suppressor gene *TP53* is commonly found to be wild-type, thus providing an attractive target for treatment. Here, we study *TP53*-wild-type (EW7, CADO-ES1 and TC32) and *TP53*-deleted (SK-N-MC) Ewing sarcoma cell lines to investigate the potentiating effect of p53 reactivation by Nutlin-3 on treatment with YK-4-279 to block transcriptional activity of EWSR1-FLI1 protein. Blocking EWSR1-FLI1 transcriptional activity reduced Ewing sarcoma tumour cell burden irrespective of *TP53* status. We show that simultaneous YK-4-279 treatment with Nutlin-3 to stabilize p53 resulted in an additive inhibition of *TP53*-wild-type Ewing sarcoma cell burden, whilst not affecting *TP53*-deleted Ewing sarcoma cells. Improved inhibition of proliferation and migration by combinatorial treatment was confirmed *in vivo* with zebrafish engraftments. Mechanistically, both compounds together additively induced apoptosis of tumour cells *in vivo* by engaging distinct pathways. We propose reactivation of the p53 pathway in combination with complementary targeted therapy by EWSR1-FLI1 transcriptional activity disruption as a valuable strategy against p53-wild-type Ewing sarcoma.

Introduction

Ewing sarcoma (EWS) is the second most common sarcoma of bone in children and young adults.¹ Transformation is believed to be caused by a chromosomal translocation fusing the *EWSR1* gene to a member of the ETS transcription factor family of genes, resulting in a highly deregulated transcription factor.² The two most common gene fusions are *EWSR1-FLI1* (85% of the cases) and *EWSR1-ERG* (10% of the cases).^{3,4} Around 25% of patients have metastasis present at the time of diagnosis.⁵ Currently, these patients have a 2-year event-free survival of ~20%⁶ and a satisfactory treatment regime is lacking. Inactivation of the transcriptional activity of EWSR1-ETS oncogene in combination with reactivation of p53, which is wild-type in ~90% of these tumours, could provide a potential treatment strategy.⁷ To test this hypothesis, two potential drugs operating via a different mode of action were used in this study: Nutlin-3⁸, a p53 activator, and YK-4-279, a small-compound inhibiting the interaction between EWSR1-ETS protein and RNA helicase A and thereby inhibiting its gene-transactivating function.⁹

Individually, these compounds are known to modulate EWS tumour growth. Treatment with YK-4-279 elicited a marked reduction of EWS tumour growth in mice xenografts⁹, and reactivation of the p53 pathway by Nutlin-3 induced an apoptotic response of EWS cell lines *in vitro*.¹⁰ Here, we show how the combination of these compounds affects EWS tumour behaviour both in culture and in a newly-established zebrafish xenotransplantation model.

Zebrafish (*Danio rerio*) are increasingly used as a model organism to study cancer.¹¹ Benefits include large clutch size, *ex utero* development, temporal separation between innate and adaptive immunity, transparency and easy of manipulation of embryos.¹² There is high conservation of oncogenes and tumour-suppressor genes between zebrafish and human¹³, and various oncogenic transgenic zebrafish lines have been developed.¹⁴ The histology of zebrafish tumours has been shown to be highly similar to tumours found in human cancers.¹⁵ The adaptive immune system in zebrafish does not reach maturity until 4 weeks post-fertilisation¹⁶, allowing circumvention of cell graft-host rejection by using zebrafish in early stages.

Zebrafish embryos can absorb various small molecular weight compounds from water, which is advantageous when screening for anti-cancer compounds.¹⁷⁻²¹ Use of transgenic lines with fluorescent vasculature or neutrophil granulocytes^{22,23}, allows live imaging of cancer development and interaction with the microenvironment *in vivo* within 1 week.

We established a zebrafish model for EWS development, applicable for real-time *in vivo* monitoring of tumour progression at single cell level, by recording induction of angiogenesis, EWS proliferation and migration, as well as tumour cell interaction with the host immune system. The model was utilised to investigate combinatorial treatments with multiple drugs. Such multi-hit approaches have until now been limited in test animals due to lack of throughput.

In this chapter, we show both in culture and *in vivo* that p53 stabilisation by Nutlin-3 has an additive effect on the ability of YK-4-279 to reduce tumour burden via EWSR1-ETS transcriptional deactivation. Both compounds caused tumour cell apoptosis *in vivo* via distinct pathways. We propose p53 reactivation in combination with targeted EWSR1-ETS transcriptional deregulation as an attractive therapeutic strategy for patients with p53-wild-type Ewing sarcoma.

Materials and Methods

Cell culture

Ewing sarcoma cell lines (CADO-ES, EW3, EW7, L1062, TC32, TC71 and SK-N-MC) were present in the LUMC and authenticated by Promega Powerplex assay. Cells were cultured in IMDM (Life Technologies)

with 10% fetal bovine serum (Life Technologies) at 37°C and 5% CO₂. Stably fluorescent lines were produced by transduction with mCherry-expressing lentiviral vectors (kindly provided by Prof. Dr. Hoeber, LUMC). Non-fluorescent lines were labelled using Celltracker CM-Dil (Life Technologies), according to manufacturers instructions.

Zebrafish maintenance

ABTL, Albino, Casper, *TG(fli1:EGFP)*, *TG(mpo:GFP)i114* and *tp53^{M214K}* zebrafish lines were handled compliant to local animal welfare regulations and maintained according to standard protocols (www.ZFIN.org). Animal experiments were approved by the animal care committee of the Faculty of Medicine, Leiden University (UDEC10027).

4

Tumour cell implantation

Embryos or 35dpf juveniles were anaesthetized with 0.001% tricaine (Sigma-Aldrich). Single-cell suspension in 2% polyvinylpyrrolidone-40 (Sigma-Aldrich) was loaded into 1.0mm OD x 0.78mm ID borosilicate needles (Harvard Apparatus). 500-800 cells were injected into the yolk or eye, using a Pneumatic PicoPump (World Precision Instruments) (10-20 psi, 100-400 ms). Larvae were maintained at 34°C. For 35dpf juveniles, water temperature was raised from 28°C to 34°C over the course of a week prior to implantation. Juveniles were immunosuppressed by addition of 10 µg/mL dexamethazone (Sigma-Aldrich) to the water, refreshed every other day, starting 2 days before implantation.²⁴

In vivo toxicity test of chemical compounds and analysis

Racemic (±)Nutlin-3 (Cayman Chemical, USA) and racemic YK-4-279 (kindly provided by Dr. Toretsky) stock solutions were dissolved to a concentration of 1mM in DMSO. Six embryos were placed per well of a 24-well plate in a volume of 1mL Instant Ocean egg water supplemented with chemical compounds, with daily refreshing of the solutions. Embryos were fixed overnight (O/N) in 4% paraformaldehyde (PFA) at 4°C. Embryos were imaged in glass-bottom 96-wells plates using a NIKON3 confocal microscope (4x lens). Image processing was performed with ImageJ 1.43 (National Institutes of Health, USA). ImagePro Analyzer 7.0 (Media Cybernetics) analysis was performed as described previously.²⁵

Proliferation assay in cell culture

For measurement of relative EWS cell survival of each treatment, 3000 or 5000 cells/well were seeded in triplicate in full medium in a 96-wells microtiter plate. Next day, medium was replaced with medium containing indicated compound or vehicle concentrations. After indicated times, relative growth was measured using a WST-1-based colorimetric assay (Roche Diagnostics), according to the manufacturer's instructions. For

synergy studies, effects were calculated as 'affected fraction' of treated versus untreated cells, according to the method of Chou.²⁶ Dose–effect analyses were performed using CompuSyn software (Compusyn).

Western blotting

Western blots were performed as described previously.²⁷ Gels were loaded with 10-15 μ g total protein lysates. The following antibodies were used: Anti-p53 (DO-1 (1:500); Santa Cruz Biotechnology), Anti-HDM2 (SMP14 (1:500); Santa Cruz Biotechnology), Anti-HDMX (Rabbit polyclonal A300-287A (1:2000), Bethyl Laboratories or mouse monoclonal 8C6 (1:1000), Millipore), anti-p21 (CP74 (1:500), Upstate Biotechnology), anti-PARP (#9542 (1:1000), Cell Signaling Technology) and anti-Vinculin (hVIN1 (1:1000), Sigma-Aldrich).

4

Immunohistochemistry and TUNEL staining

Whole-mount zebrafish immunohistochemistry was performed as described previously.²⁸ The following antibodies were used: CD99-O13 (Covance), L-plastin (kindly provided by Dr. A. Huttenlocher), Alexa Fluor 488 (Life Technologies), Alexa Fluor 568 (Life Technologies). TUNEL staining was performed using ApopTag Peroxidase in situ apoptosis detection kit (Merck-Millipore) and TSA-Plus Fluorescein system (Perkin-Elmer). For tissue-section staining, embryos were fixed in 4% PFA, embedded in paraffin, cut into 4 micron sections and stained with H&E, CD99-O13 and Periodic acid-Schiff (PAS). Quantification of apoptosis was performed by counting TUNEL-positive versus TUNEL-negative cells, for >4 embryos per condition, and noted in the text as mean percentage apoptotic cells \pm SEM.

Statistical Analysis

A one-way ANOVA test with a Dunnet's post-test was utilized to determine the *in vivo* drug treatment effects. All statistical tests were two-sided. Values were expressed as means with 95% confidence intervals. P values less than 0.05 were considered statistically significant, and are indicated with one star (*). P values less than 0.01 were indicated with two stars (**). Statistical analyses were performed using GraphPad Prism V4.

Results

Characterization of the behaviour of EWS cells within the zebrafish xenotransplantation model

Previous reports have shown that zebrafish can be used as a host organism to study the progression of various types of cancer, either by

using transgenic or xenograft models.¹¹ To determine if zebrafish is a suitable model organism for Ewing Sarcoma progression, a panel of EWS cell lines was implanted in the yolk of two days post-fertilisation (dpf) embryos (Fig. 1A-C).

Cell lines derived from metastatic and primary tumours were selected for different translocation types, and status of the p53 pathway (Table 1). Induction of angiogenesis was scored 24 hours post-implantation (hpi) (Fig. 1D-F), as described by Nicoli and Presta.^{34,35} Implanted cell lines differed in potential to induce angiogenesis, ranging from angiogenesis observed in 25% of fish (EW3, n=52), to no observed angiogenesis (CADO-ES, n=31). To ensure specificity of the angiogenic response by implanted cells and exclude response to injection-induced wounding, zebrafish fibroblast cells and cancer cells that underwent several freeze-thaw cycles were implanted. Neither zebrafish cells nor cell fragments were able to elicit an angiogenic response (Supporting Information Fig 1, n≥35).

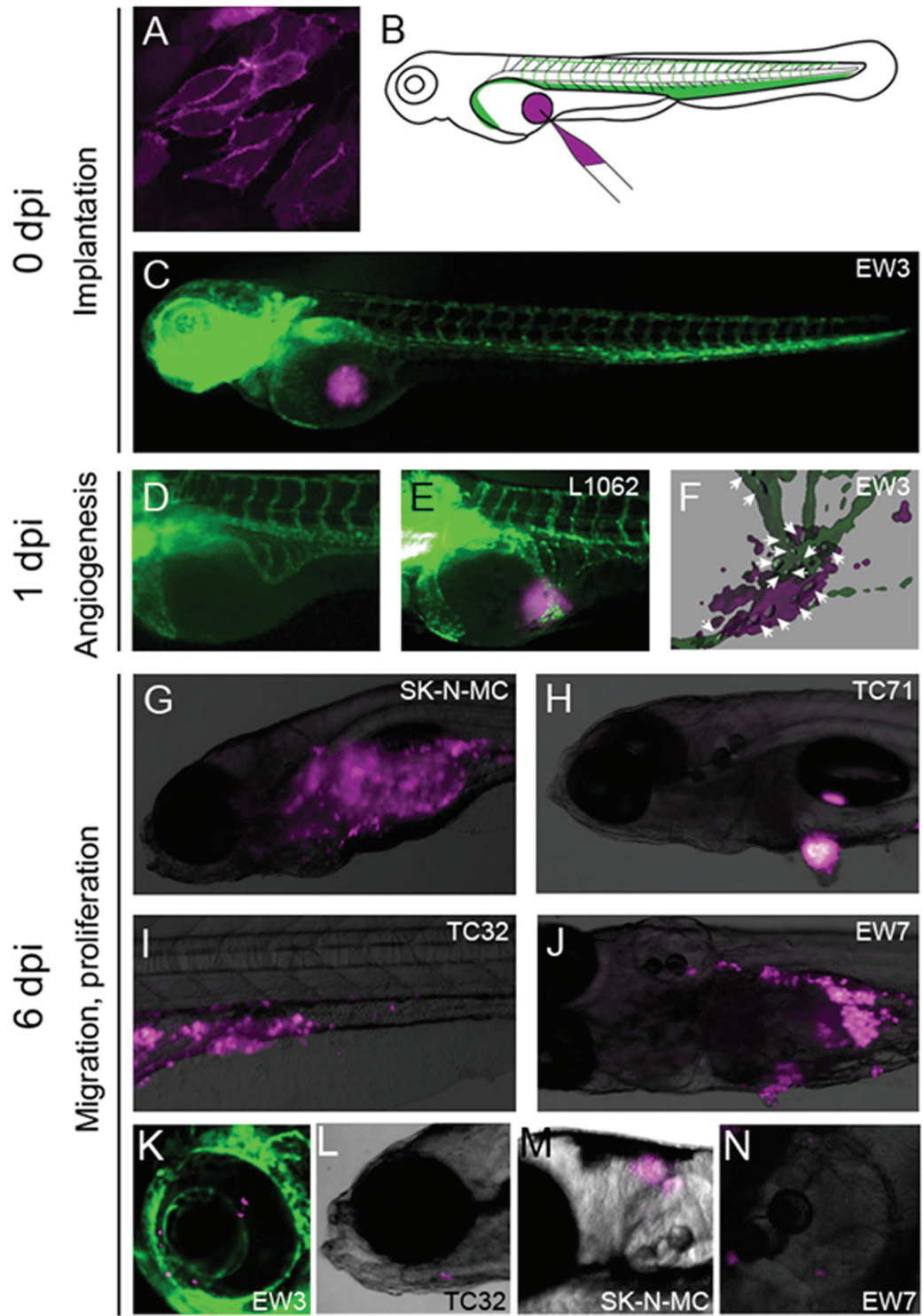
Haematogenous dissemination of all tested cell lines was observed to fins, head and body (Fig. 1G-N, Table 1) of the zebrafish larvae within 6 dpi. In addition, some cell lines (TC32, TC71, EW7) were capable of forming tumour-cell outgrowths, primarily in proximity of the abdomen (Fig. 1H). Proliferation of cells was scored by the amount of red fluorescent signal per larvae. At 6 dpi, a variation in the amount of cell burden could be observed for different cell lines.

All tested cell lines proliferate and migrate within the embryo and most EWS cells were showed the ability to induce angiogenic response (Table 1), independent of translocation type or p53 status, with EW7 having the most potent tumour progression properties.

Migration of EWS cell within the zebrafish host

EWS cells showed strong metastatic capacities in the zebrafish larvae.

Figure 1. Workflow of xenotransplantation experiment. **A)** Cells stably expressing mCherry or labelled with fluorescent membrane marker. **B)** Schematic view of injection in a 2 dpf embryo. Magenta: EWS cells; green: vasculature of tail and yolk. **C)** 2 dpf *TG(fli1:EGFP)* embryo with green vasculature²², injected with EWS cells (magenta), 3 hours after implantation. **D)** Regular development of the subintestinal vein complex of an uninjected 3 dpf *TG(fli1:EGFP)* embryo. **E)** Angiogenic sprouting of vessels from the subintestinal vein complex induced by the implanted EWS cells in *TG(fli1:EGFP)* embryo, 1 dpi. **F)** Interaction (white arrows) between implanted EWS cells and vasculature of *TG(fli1:EGFP)* embryo, 1dpi. **G, H, I, J)** Proliferation, outgrowth and migration to head of ABTL embryo implanted with EWS cells, 6 dpi. **K)** Migration to eye. **L)** Migration to jaw. **M)** Migration to brain. **N)** Migration to otic vesicle. Data are representative images of >10 independent, highly reproducible experiments.



Further analysis on engrafted larvae was performed to get an insight into the migration mechanism.

High-magnification imaging at sites of dissemination revealed that EWS cells resided both inside and out of the blood vessels (Fig. 2A, B), suggesting a role of the circulatory system in their migration. Immunohistochemistry demonstrated that migratory cells were positive for EWS markers (CD99, PAS) (Fig. 2C and Supporting Information Fig 2), thus retaining EWS properties *in vivo*.

Major organ systems are still in development in zebrafish larvae. To determine if EWS cells could home to specific organs, cells were implanted via vessels in the eye into the bloodstream of fully-developed 35 dpf Casper zebrafish juveniles lacking melanocytes and iridiophores³⁶, enabling non-invasive late-stage microscopy. Cells were observed in the abdomen of the zebrafish at 6 dpi with live stereo imaging. Immunohistochemical analysis at 6 dpi showed cells in the gut and kidney of the larvae (Supporting Information Fig 3, n=12), proving

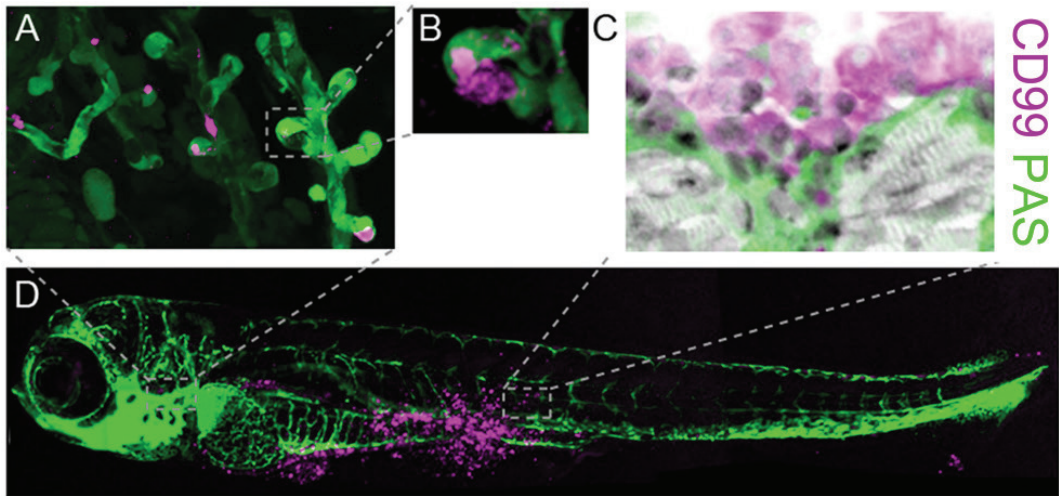
4

Table 1. Overview of EWS cell properties. Tumour burden is classified according to the following definitions: High – High tumour cell burden in >80% of larvae. Medium - High tumour cell burden in 50%-80% of larvae. Low – minimal amounts of tumour cells in >50% of larvae. Migration is represented as the percentage of embryos which showed cells migrating away from the site of implantation. All xenograft data was collected from 3 or more individual experiments with n>30 and no more than 80% lethality per group.

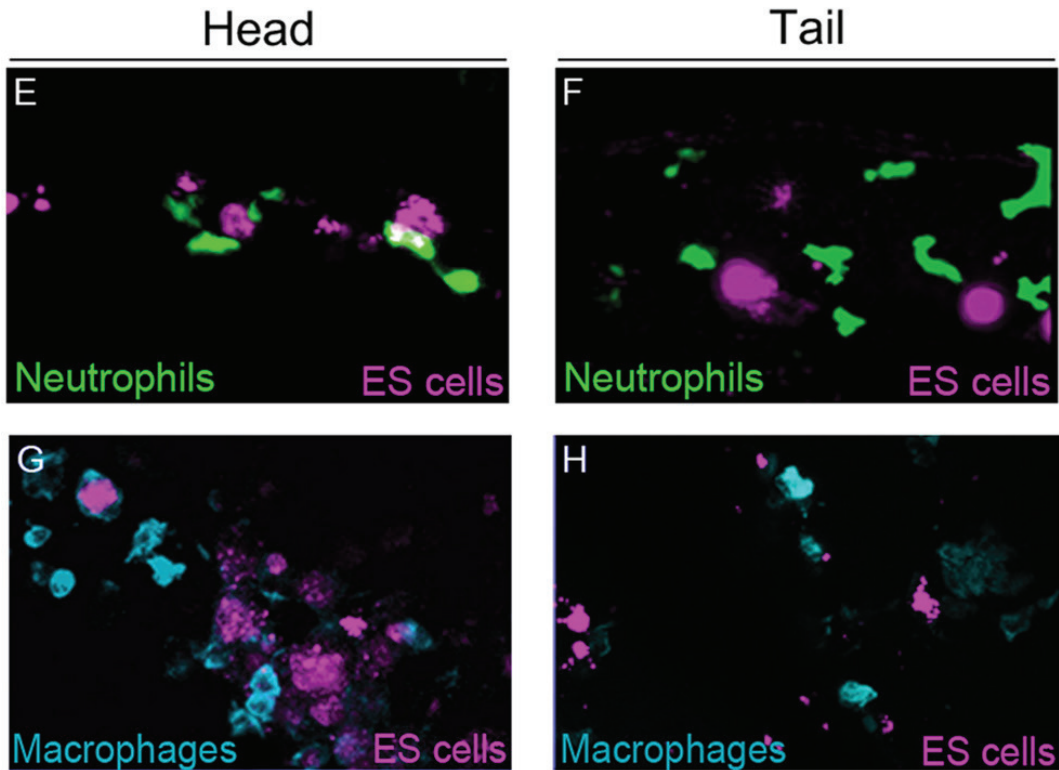
Behaviour in zebrafish embryonic xenograft

Cell line	Primary or metastasis	Translocation	TP53 status	Tumour burden	Migration (95% CI)	Angiogenesis
CADO-ES ²⁹	Metastasis	<i>EWSR1-ERG</i>	Wild-type	Medium	48.5%-86.1%	No
EW3 ²⁹	Primary	<i>EWSR1-ERG</i>	Wild-type	Low	57.2%-70.8%	Yes
EW7 ²⁹	Primary	<i>EWSR1-FLI1</i>	Wild-type	Medium	74.8%-78.6%	Yes
L1062 ³⁰	Primary	<i>EWSR1-FLI1</i>	Mutant	High	37.7%-62.3%	Yes
SK-N-MC ³¹	Metastasis	<i>EWSR1-FLI1</i>	Deletion	High	61.1%-92.3%	Yes
TC71 ³²	Recurrent	<i>EWSR1-FLI1</i>	Mutant	Medium	69.5%-73.3%	Not analysed
TC32 ³³	Metastasis	<i>EWSR1-FLI1</i>	Wild-type	Medium	56.7%-64.5%	Yes

Figure 2. Behaviour of EWS cells within embryo host. **A)** EWS cells (magenta) inside and next to blood vessels in the gills of *TG(fli1:EGFP)* embryo, 5 dpi. **B)** Detail of 2A, showing cells within the lumen of the blood vessel. **C)** Paraffin section of 5 dpi embryo with CD-99 positive EWS cells (magenta) in the muscle (Grey: H&E; magenta: CD99; green: PAS). **D)** Confocal overview image of *TG(fli1:EGFP)* embryo with EWS cells spreading to the head, muscles and fins, 5 dpi. **E)** *TG(mpx:GFP)i114* embryo showing EWS cells (magenta)



4



interacting with neutrophils (green), 5 dpi, head. **F**) *TG(mpx:GFP)ⁱ¹¹⁴* embryo showing EWS cells (magenta) interacting with neutrophils (green), 5 dpi, tail. **G**) ABTL embryo showing EWS cells (magenta) interacting with macrophages (blue), 5 dpi, head. **H**) ABTL embryo showing EWS cells (magenta) interacting with macrophages (blue), 5 dpi, tail. Data are representative images of >10 independent, reproducible experiments (each n>30).

that migration of EWS in embryos resembles metastatic behaviour in adult zebrafish stages.

To exclude false-positive results for migration due to cell debris taken up and transported by embryonic leukocytes (primarily neutrophils and macrophages at this stage of development), cells were implanted into embryos expressing GFP in the neutrophils.²³ Neutrophils and various EWS cells were shown to interact (Fig. 2E, F), but uptake of EWS cell material by neutrophils was not observed.

At the time of the experiment, transgenic embryos with fluorescent macrophages were not available yet. To examine if macrophages played a role in migration, leukocytes were detected by whole-mount immunohistochemistry against L-plastin (a zebrafish pan-leukocyte marker). Co-localization of L-plastin and red fluorescent cells showed that some, but not all EWS cells in the body of the larvae were taken up by leukocytes (Fig. 2G, H), suggesting that EWS cells disseminate mainly due to active migration. No neutrophil uptake was observed in previous experiments, indicating that macrophages are responsible for the observed partial phagocytosis of EWS cells.

Effect of Nutlin-3 and YK-4-279 on p53-wildtype and p53-deletion EWS cell lines

In ~90% of EWS tumours, p53 is found to be wild-type⁷, providing an interesting target for treatment strategies. Previous reports showed Nutlin-3 to have an adverse effect on the malignant potential of EWS cells³⁷, via the stabilization of the p53 protein and subsequent apoptotic pathway activation. Nevertheless, single-compound treatments may allow the escape of non-respondent cells, which can be reduced by adding drugs with a different target simultaneously. For this purpose, we used YK-4-279, a small molecule reported to disrupt EWS-FLI1 transcriptional activity by blocking the interaction between RNA helicase A and EWS-FLI1 protein⁹.

We tested the sensitivity of p53-wild-type EW7, CADO-ES1 and TC32 and p53-deletion SK-N-MC cell lines in culture for various concentrations of Nutlin-3 or YK-4-279, or a combination of both, by comparing the relative growth of the cells after 72h of treatment.

Nutlin-3 reduced the growth of EW7 in a dose-dependent manner (EC-50=0.97 μ M, Fig. 3A), as well as CADO-ES1 and TC32 (Supporting Information Fig. 4). SK-N-MC cells, which lack a full-length p53 protein, were essentially not affected by Nutlin-3 treatment (EC-50>100 μ M, Fig. 3B). YK-4-279 reduced growth of all four cell lines with SK-N-MC appearing slightly more sensitive than EW7 (respectively EC-50=0.46 μ M and EC-50=0.65 μ M, Fig. 3A, B, Supporting Information Fig. 4). The combination of Nutlin-3 and YK-4-279 was found to have a synergistic inhibitory effect on the growth of EW7, CADO-ES1 and TC32 but not on SK-N-MC (Fig. 3A, B, and Supporting Information Fig. 4).

Cell culture experiments confirmed that, as Nutlin-3 works largely in a p53-dependent and YK-4-279 mainly in a p53-independent manner,

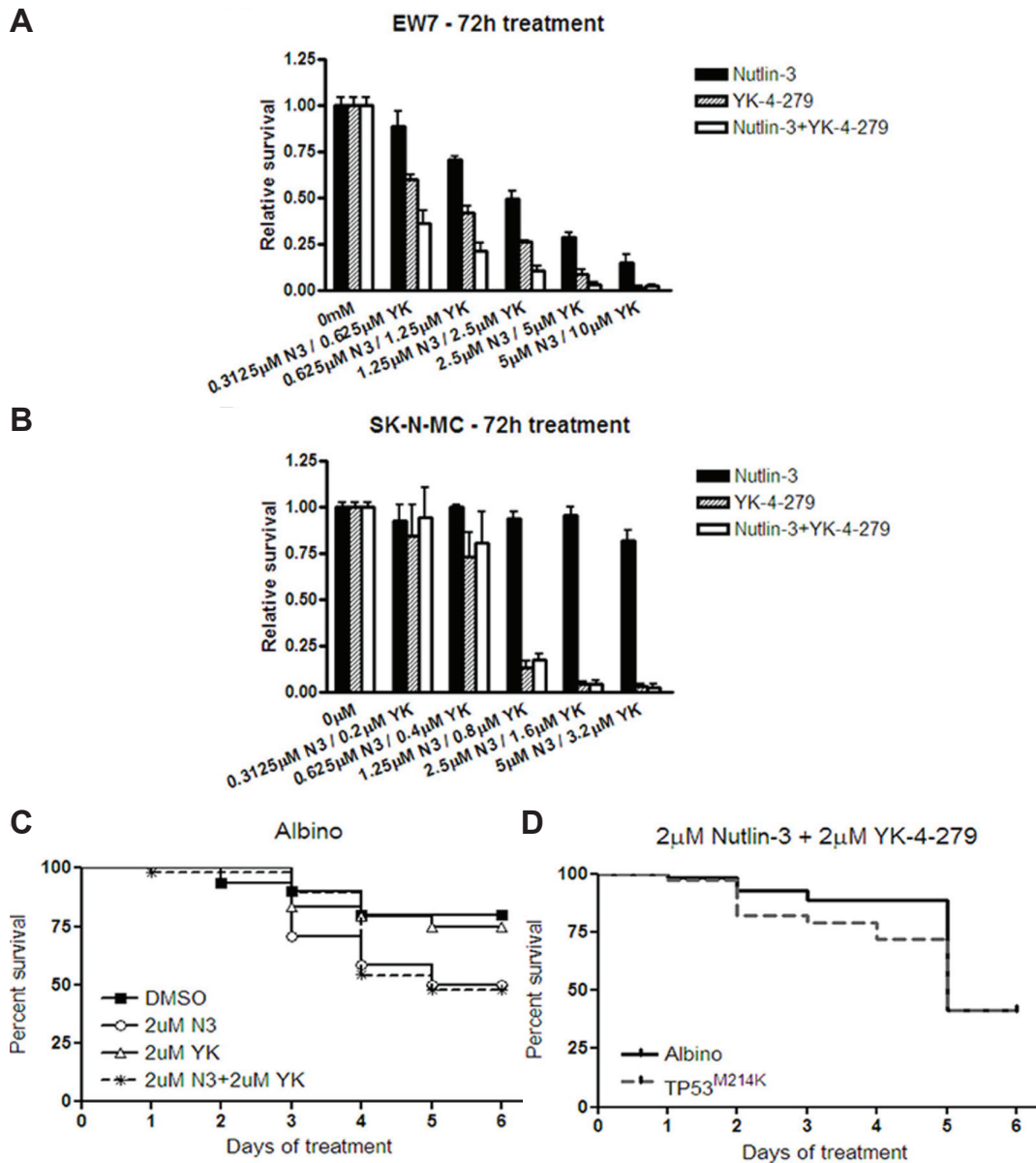


Figure 3. The effect of Nutlin-3 and YK-4-279 on EWS cells in culture and zebrafish embryos. **A)** WST-1 assay for measuring relative survival of EW7 cells treated for 72 hours with Nutlin-3 (EC-50: 0.97µM), YK-4-279 (EC-50: 0.65 µM) or a combination thereof. All measurements were performed in triplicates. Error bars represent 95% confidence interval. **B)** WST-1 assay for measuring relative survival of SK-N-MC cells treated for 72 hours with Nutlin-3 (EC-50 > 100 µM), YK-4-279 (EC-50: 0.46 µM) or a combination thereof. All measurements were performed in triplicates. Error bars represent 95% confidence interval. **C)** Toxicity test of compounds on albino embryos treated from 2 dpf onwards. N≥24 per condition. **D)** Effect of treatment on albino embryos compared to *tp53*^{M214K} embryos treated from 2 dpf onwards. N=72 per condition.

cell lines with a differential p53 expression have dissimilar responses to the applied compounds.

Effect of Nutlin-3 and YK-4-279 on p53-wild-type and p53-mutant zebrafish

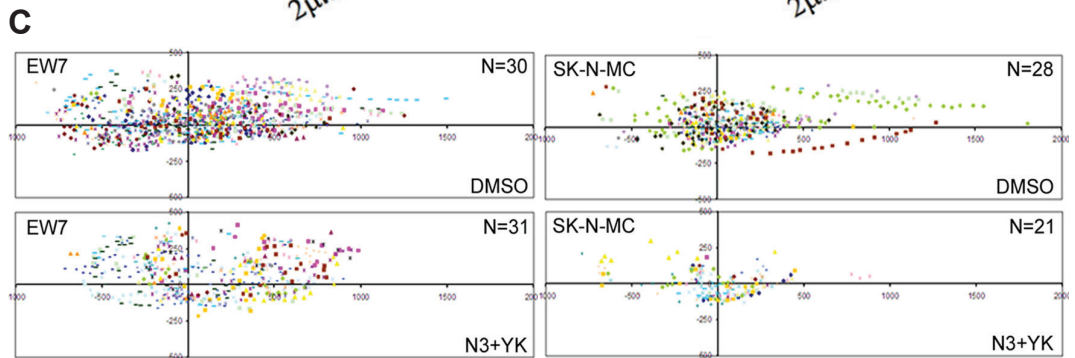
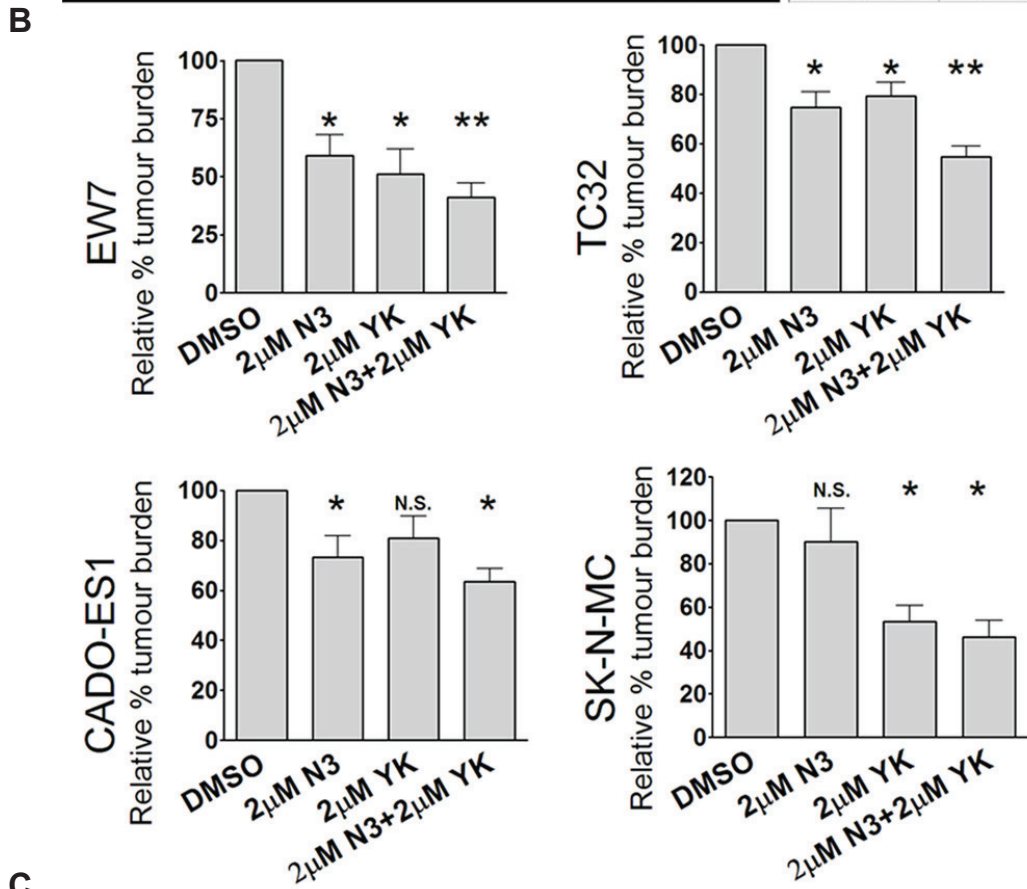
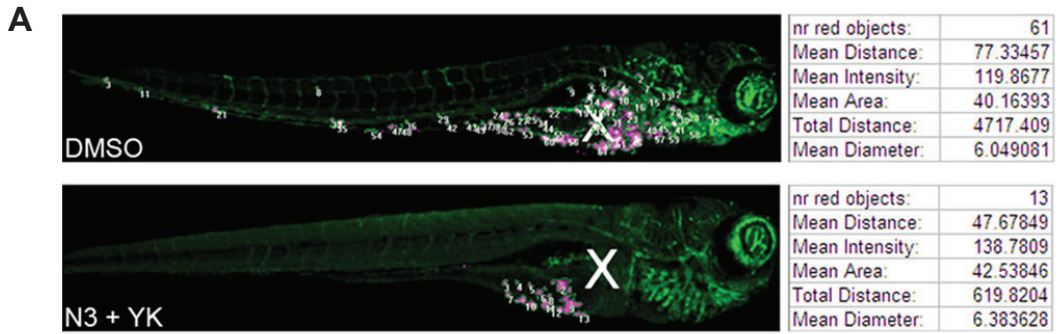
Immersion is a well-established method for drug treatment of zebrafish larvae.^{12,38} To determine if our xenotransplantation model was suitable for drug testing, Nutlin-3 and YK-4-279 were applied to embryos injected with EWS cells.

As pathways concerned with cancer can be involved in larval development, we initially performed toxicity tests on mock-injected larvae. For both compounds, a concentration of 2 μ M had a strong inhibitory effect in culture but allowed sufficient survival *in vivo* (Fig. 3C). No significant difference in lethality was observed when compounds were applied to *tp53*^{M214K} mutant zebrafish (Fig. 3D), excluding a lethal effect of Nutlin-3 by activation of wild-type zebrafish p53. In addition to stabilizing p53, Nutlin-3 may also upregulate TAp73 levels.^{39,40} This protein plays an important role in embryonic development of zebrafish, and may be responsible for the higher toxicity of Nutlin-3 in these experiments.⁴¹ At concentrations of 4 μ M, both Nutlin-3 and YK-4-279 caused >40% lethality (Supporting information Fig 5), so further experiments were performed with concentrations of 2 μ M, in p53-wild-type zebrafish, to simulate the typical microenvironment as close as possible.

Effect of Nutlin-3 and YK-4-279 on EWS cells in the xenotransplantation model

After implantation with EW7 and SK-N-MC cells in larvae, treatment with Nutlin-3, YK-4-279, or a combination thereof, was started 24 hpi. At 6 dpi, quantitative analysis was performed on confocal images, providing information on the amount, size and migration of tumour cell foci per embryo (Fig. 4A shows two examples of the readout). Mean reduction

Figure 4. The effect of Nutlin-3 and YK-4-279 on EWS cells *in vivo*. **A)** Quantitative analysis²⁵ of embryos implanted with SK-N-MC cells, treated with DMSO or Nutlin-3 and YK-4-279. Algorithms use the green channel to find the outline of the *TG(fli1:EGFP)* embryo and estimate the site of implantation (white X). Using the mCherry signal from EWS cells, all tumour cell foci (objects) are outlined and numbered. To determine tumour burden per embryo, number of objects was multiplied by the average size of objects. Migration away from the site of implantation was determined per object and represented in scatter dot plots. **B)** Tumour burden of EWS cells in embryos, 6 dpi, normalized against DMSO. Differences between means were obtained by one-way analysis of variance (ANOVA) with a Dunnett's post-test. One star indicates a P value < 0.05; two stars indicate a P value < 0.01; N.S. indicates no significant difference. Error bars represent 95% confidence interval. **C)** Scatter dot plot for migration. Each colour represents one embryo per group, each dot one cluster of tumour cells. Site of implantation: (X, Y = 0, 0).



of tumour burden (MR), as obtained by the cumulative area of tumour foci, and 95% confidence intervals (CI) was determined per group, compared to DMSO controls. Our quantification revealed that larvae treated with both Nutlin-3 and YK-4-279 showed a significantly reduced growth of EW7 (MR=41%, CI=1%-81%; $P<0.05$ and MR=48%, CI=8%-88%; $P<0.05$, respectively), as well as CADO-ES1 and TC32 (Fig. 4B). The combination of compounds had an additive effect on this decrease of wild-type EWS growth (EW7: MR=61.6%, CI=22.7%-100%; $P<0.01$). The growth of SK-N-MC was significantly reduced in the embryos treated with YK-4-279 (MR=46.6%, CI=7.3%-85.9%; $P<0.05$), but not by Nutlin-3, and minimal additive effects were observed for double treatment (MR=53.8%, CI=10.0%-97.6%; $P<0.05$).

Migration from the site of implantation was determined for all tumour foci per larvae ($N>20$ per panel) and represented per group in scatter dot plots (Fig. 4C, Supplementary Information Fig. 6). Quantification of these plots by mean cumulative migration distance of tumour cell foci (MCD, Supporting Information Fig. 7) indicate that treatment with both Nutlin-3 and YK-4-279 reduced the number of tumour cell foci migrating from the site of implantation.

Our *in vivo* results substantiate our findings regarding growth in cultured cells with equal treatment time (Supporting Information Fig. 7), as well as previously described research on single treatments with these compounds on EWS cells.^{9,37} Additionally, we managed to rapidly investigate the synergistic effects that these two compounds had on EWS, showing an additive effect of combined treatment on the reduction of tumour burden *in vivo*.

Induction of apoptosis by Nutlin-3 and YK-4-279 on EWS cells *in vivo* and in culture

To further assess the effect of Nutlin-3 and YK-4-279 on EW7 and SK-N-MC cells implanted in larvae, we performed whole-mount TUNEL staining to analyse the apoptotic response. DMSO-treated larvae revealed only a fraction of the grafted EWS cells undergoing apoptosis at 96 hpi (Fig. 5A). Upon administration of Nutlin-3 on grafted embryos, the apoptotic response was increased more effectively in EW7 cells than SK-N-MC cells (from 43.3%±15.7 to 71.0%±8.2 and 35.4%±8.3 to 40.8%±11.5 respectively), while both cell lines responded equally effectively to YK-4-279 treatment (to 86.4%±5.4 for EW7 and 86.6%±6.2 for SK-N-MC). Treatment with both compounds simultaneously showed that the majority of cells underwent apoptosis in both EW7 (92.0%±6.4) and SK-N-MC (90.6%±4.6).

Protein analysis of cells treated in culture (Fig. 5C, corresponding WST-1 proliferation assays for these conditions are found in Fig. 5B) revealed that in EW7, both compounds increased p53 protein levels, p21 and cleaved PARP. This increase resembles induction of cell-cycle arrest and apoptosis by both YK-4-279 and Nutlin-3. In SK-N-MC, full-length p53 and p21 are undetectable, but YK-4-279 could induce cleaved

PARP, an apoptotic marker.

The data obtained both *in vivo* and in culture show that YK-4-279 induces apoptosis in EWS cells in a p53-independent manner, whilst apoptosis induced by Nutlin-3 is p53-dependent. Combined treatment increased apoptosis of tumour cells by engaging these mechanistically distinct pathways simultaneously.

Discussion

In this study, we investigated the additive effect of p53 reactivation on disruption of EWSR1-FLI1 transcriptional activity as a therapeutic strategy against Ewing sarcoma. EWS is a highly aggressive, malignant bone and soft-tissue tumour for which currently, when presented with metastatic spread, no satisfactory treatment regime has been developed. *TP53* is wild-type in ~90% of EWS cases⁷, and up-regulation provides an attractive approach for intervention. EWS cells have been shown to lose viability upon forced wild-type p53 expression⁴². Alterations of *TP53* as well as *CDKN2A/CDKN2B* (p16), another important regulator of G1/S transition, are described to be correlated with an unfavourable prognosis.⁴³⁻⁴⁵

We applied a newly-developed zebrafish EWS-engraftment model to assess reactivation of p53 by Nutlin-3 as a treatment approach against these tumours. EWS cell lines implanted in zebrafish embryos could induce angiogenesis, migrate and proliferate within a week after implantation mimicking the human situation in a model system. As the embryos can take up a range of compounds from the water, the zebrafish model allows rapid medium-to-high-throughput screening of preclinical compounds in multiple subjects and can be a useful complement to established rodent models. Two practical matters need to be taken into account: the compounds need to be water-soluble and taken up by the embryo. Further, in the timeframe of the experiment embryonic cells are rapidly dividing and migrating, which might pose a problem, as these are features that many anti-cancer drugs are targeting. In treatment strategy design, we took into consideration that pathways that are important in cancer development can also be involved organ developmental processes. We observed less toxicity when compounds were applied at 3 dpf, when the larvae have already undergone some of the most crucial developmental processes. All compounds in the described experiments were tested for their toxicity; concentrations administered to engrafted embryos were chosen as high as possible to maximise the effect on EWS cells, whilst still ensuring sufficient survival to perform analyses. The use of *tp53*^{M214K} mutant larvae, which fail to undergo apoptosis in response to γ -radiation indicating aberrant p53 signalling⁴⁶, determined that Nutlin-3 worked specifically on EWS cells, and not via host cells.

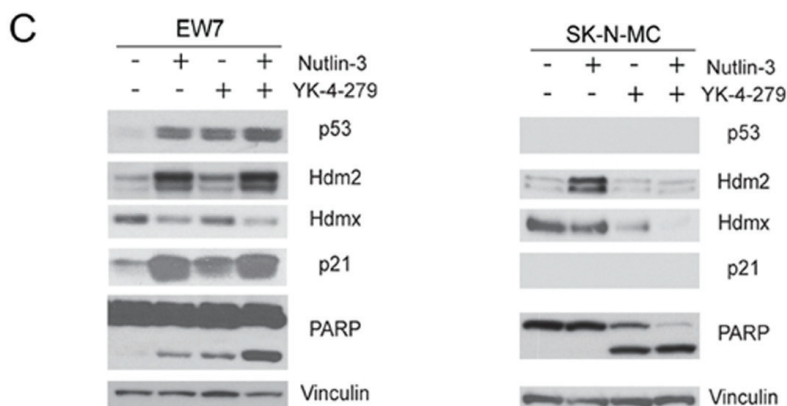
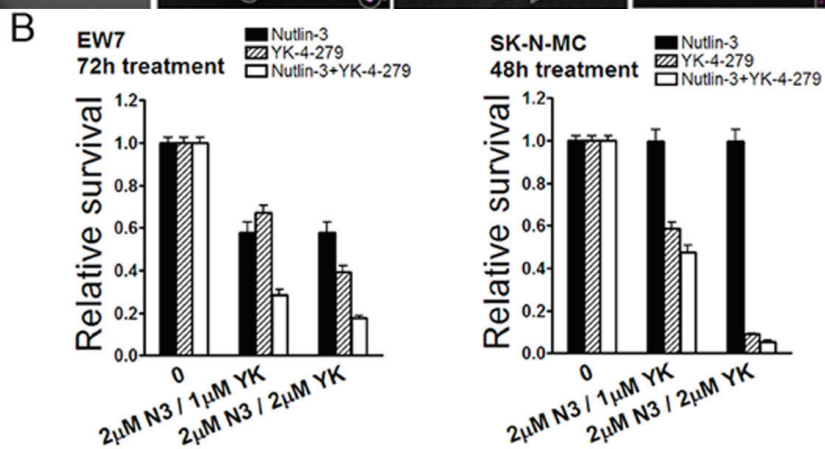
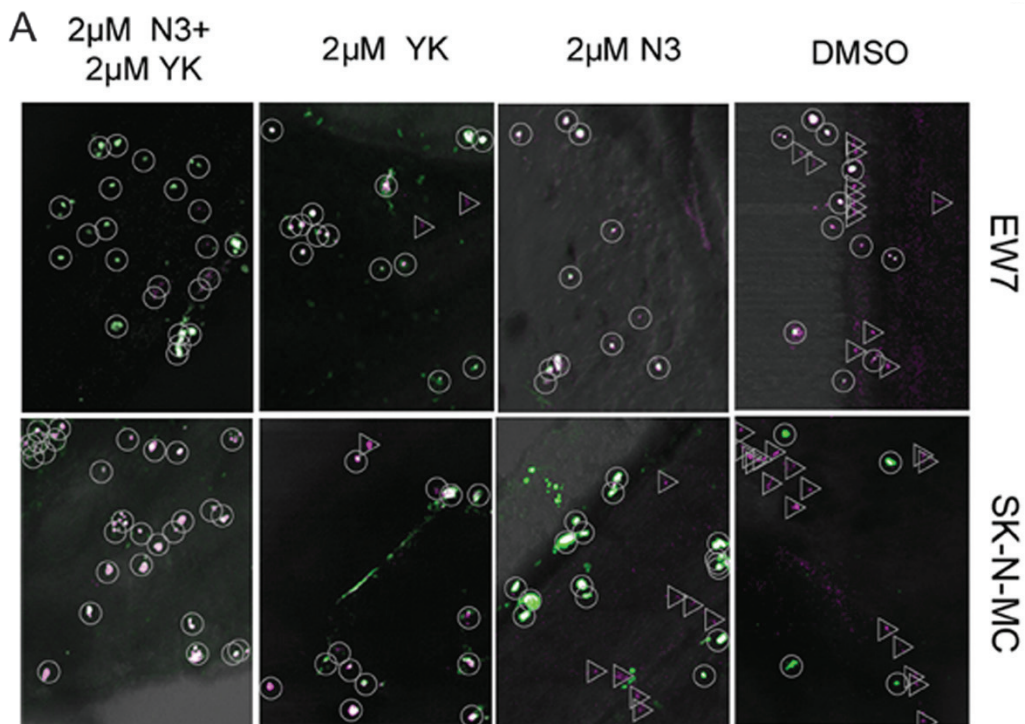
To inhibit EWS progression via inactivation of two essential tumourigenic mechanisms and investigate their therapeutic value *in vivo*,

we applied Nutlin-3 and YK-4-279 on EWS cell engraftments in zebrafish. Nutlin-3 was used to stabilise p53 by blocking its interaction with MDM2, whilst YK-4-279 blocks interaction between RNA helicase A and EWS-FLI1 protein, deregulating gene trans-activation and inducing apoptosis. EWS cells with a different p53 status were used, to show specificity of the reduction of tumour cell burden by these compounds *in vivo*. Tumour burden of both cell lines was significantly reduced by addition of YK-4-279, while Nutlin-3 reduced tumour growth only of the p53-wild-type cells. Interestingly, although the tumour burden of p53-deletion cells was not significantly affected by treatment with Nutlin-3, a slight induction of apoptosis *in vivo* was observed, suggesting a less straightforward response than found in culture data. Combinatory treatment had an additive effect on reduction of tumour burden of p53-wild-type cells by engaging distinct pathways of apoptosis, and confirmed that the model is applicable to study possible synergy between compounds.

In this model, treatments were applied relatively soon after implantation, to achieve the longest possible treatment time before additional immune-systems become activated and engraftments may be rejected. As Ewing sarcoma patients often present with metastases at time of diagnosis, any promising treatment found needs to be tested in a model where tumours are already established. Either immune-suppressed zebrafish or murine models should provide additional information before taking these compounds to clinical trials.

Several Phase I clinical trials with RO5045337, an analogue of Nutlin-3 suitable for oral administration, have been completed. Currently, a follow-up trial is active for various cancer types, amongst which patients presenting with soft tissue sarcoma (NCT01677780). Additionally, clinical trials with other HDM2 antagonists are also ongoing (NCT01877382, NCT01462175)⁴⁷, and could perform a similar synergistic function as Nutlin-3. A racemic mixture of YK-4-279 was used for all tests performed

Figure 5. Apoptosis of EWS cells in 4 dpi wild-type embryos. **A)** Whole-mount TUNEL staining of EWS cells in the muscle, fins or abdomen of ABTL embryo, 72h after treatment. Apoptotic EWS cells are indicated by circles, non-apoptotic EWS cells by triangles. A certain amount of background apoptosis (<5%) was observed in all groups, independent of treatment (unmarked green cells). Data are representative images of >3 independent experiments (each n>25). **B)** The relative survival of EW7 cells and SK-N-MC cells treated with various concentrations of Nutlin-3 and YK-4-279 or a combination thereof, for 72h (EW7) or for 48h (SK-N-MC) was determined by WST-1 assay as described in Materials and Methods. All measurements were performed in triplicates. Error bars represent 95% confidence interval. **C)** Western blot for EW7 and SK-N-MC cells treated for 72h or 48 h, respectively, with 2 μ M Nutlin-3, 2 μ M YK-4-279 or a combination thereof. The earlier time point was chosen for SK-N-MC because 2 μ M of YK-4-279 caused such a high lethality in SK-N-MC cells after 72h, making it impossible to harvest cells to make protein extracts.



in this study. Recent investigations show that the (S)-YK-4-279 enantiomer has enhanced therapeutic potency compared to a mixture of this compound.⁴⁸ This increased specificity could minimize off-target effects and brings this compound one step further to the initiation of clinical trials.

In conclusion, using the high throughput zebrafish model we found that simultaneous induction of the p53 pathway and disruption of EWS-FLI1 transcriptional activity to have an additive effect on the reduction of EWS malignancy *in vivo*. Combining different treatment strategies with reactivation of the p53 pathway in this tumour type may be a promising therapeutic strategy for the subset of EWS patients harbouring wild-type p53, and should be investigated in further detail in murine models, before initiating clinical trials.

Acknowledgements

The authors are grateful to Frans Prins for assistance with histology, Hans de Bont for assistance with confocal image analysis, and Rubén Marín-Juez for critical reading of the manuscript. This work was supported by Stichting Kinderen Kankervrij, Project 30677.

Author contributions

W.E. designed the experiments, performed the experiments, analyzed and interpreted the data, and wrote the paper. A.G.J. designed the experiments, performed the experiments, analyzed and interpreted the data and wrote the paper. A.F.A.S.T. performed the experiments, analyzed and interpreted the data. S.F.G.K. performed the experiments, interpreted the data and wrote the paper. K.S., H.P.S. and P.C.W.H. designed the experiments and interpreted the data and wrote the paper. B.E.S.-J. designed the experiments, interpreted the data, and wrote the paper.

References

1. Fletcher CDM, Bridge JA, Hogendoorn PCW, *et al.* WHO Classification of Tumours of Soft Tissue and Bone. 4 ed. IARC: Lyon 2013.
2. Burchill SA. Molecular abnormalities in Ewing's sarcoma. *Expert Rev Anticancer Ther* 2008; **8**: 1675-1687.
3. Delattre O, Zucman J, Plougastel B, *et al.* Gene fusion with an ETS DNA-binding domain caused by chromosome translocation in human tumours. *Nature* 1992; **359**: 162-165.

4. Sorensen PH, Lessnick SL, Lopez-Terrada D, *et al.* A second Ewing's sarcoma translocation, t(21;22), fuses the EWS gene to another ETS-family transcription factor, ERG. *Nat genet* 1994; **6**: 146-151.
5. Verhoeven DH, de Hooge AS, Mooiman EC, *et al.* NK cells recognize and lyse Ewing sarcoma cells through NKG2D and DNAM-1 receptor dependent pathways. *Mol Immunol* 2008; **45**: 3917-3925.
6. Balamuth NJ, Womer RB. Ewing's sarcoma. *Lancet Oncol* 2010; **11**: 184-192.
7. Neilsen PM, Pishas KI, Callen DF, *et al.* Targeting the p53 Pathway in Ewing Sarcoma. *Sarcoma* 2011; **2011**: 746939.
8. Vassilev LT, Vu BT, Graves B, *et al.* In vivo activation of the p53 pathway by small-molecule antagonists of MDM2. *Science* 2004; **303**: 844-848.
9. Erkizan HV, Kong Y, Merchant M, *et al.* A small molecule blocking oncogenic protein EWS-FLI1 interaction with RNA helicase A inhibits growth of Ewing's sarcoma. *Nat Med* 2009; **15**: 750-756.
10. Sonnemann J, Palani CD, Wittig S, *et al.* Anticancer effects of the p53 activator nutlin-3 in Ewing's sarcoma cells. *Eur J Cancer* 2011; **47**: 1432-1441.
11. Liu S, Leach SD. Zebrafish models for cancer. *Annu Rev Pathol* 2011; **6**: 71-93.
12. Goessling W, North TE, Zon LI. New waves of discovery: modeling cancer in zebrafish. *J Clin Oncol* 2007; **25**: 2473-2479.
13. Ung CY, Lam SH, Gong Z. Comparative transcriptome analyses revealed conserved biological and transcription factor target modules between the zebrafish and human tumors. *Zebrafish* 2009; **6**: 425-431.
14. Feitsma H, Cuppen E. Zebrafish as a cancer model. *Mol Cancer Res* 2008; **6**: 685-694.
15. Amatruda JF, Shepard JL, Stern HM, *et al.* Zebrafish as a cancer model system. *Cancer cell* 2002; **1**: 229-231.
16. Lam SH, Chua HL, Gong Z, *et al.* Development and maturation of the immune system in zebrafish, *Danio rerio*: a gene expression profiling, in situ hybridization and immunological study. *Dev Comp Immunol* 2004; **28**: 9-28.
17. Goessling W, North TE, Zon LI. New Waves of Discovery: Modeling Cancer in Zebrafish. *J Clin Oncol* 2007; **25**: 2473-2479.
18. Kari G, Rodeck U, Dicker AP. Zebrafish: an emerging model system for human disease and drug discovery. *Clin Pharmacol Ther* 2007; **82**: 70-80.
19. den Hertog J. Chemical genetics: Drug screens in Zebrafish. *Bioscience reports* 2005; **25**: 289-297.
20. Zon LI, Peterson RT. In vivo drug discovery in the zebrafish. *Nat Rev Drug*

Discovery 2005; **4**: 35-44.

21. Parng C, Seng WL, Semino C, *et al.* Zebrafish: a preclinical model for drug screening. *Assay Drug Dev Technol* 2002; **1**: 41-48.
22. Lawson ND, Weinstein BM. In vivo imaging of embryonic vascular development using transgenic zebrafish. *Dev Biol* 2002; **248**: 307-318.
23. Renshaw SA, Loynes CA, Trushell DM, *et al.* A transgenic zebrafish model of neutrophilic inflammation. *Blood* 2006; **108**: 3976-3978.
24. Langenau DM, Feng H, Berghmans S, *et al.* Cre/lox-regulated transgenic zebrafish model with conditional myc-induced T cell acute lymphoblastic leukemia. *Proc Natl Acad Sci U S A* 2005; **102**: 6068-6073.
25. Ghotra VP, He S, de Bont H, *et al.* Automated whole animal bio-imaging assay for human cancer dissemination. *PLoS one* 2012; **7**: e31281.
26. Chou TC. Theoretical basis, experimental design, and computerized simulation of synergism and antagonism in drug combination studies. *Pharmacological reviews* 2006; **58**: 621-681.
27. Lam S, Lodder K, Teunisse AF, *et al.* Role of Mdm4 in drug sensitivity of breast cancer cells. *Oncogene* 2010; **29**: 2415-2426.
28. Krens SF, He S, Lamers GE, *et al.* Distinct functions for ERK1 and ERK2 in cell migration processes during zebrafish gastrulation. *Dev Biol* 2008; **319**: 370-383.
29. Forbes SA, Tang G, Bindal N, *et al.* COSMIC (the Catalogue of Somatic Mutations in Cancer): a resource to investigate acquired mutations in human cancer. *Nucleic acids res* 2010; **38**: D652-657.
30. Szuhai K, Ijszenga M, Tanke HJ, *et al.* Molecular cytogenetic characterization of four previously established and two newly established Ewing sarcoma cell lines. *Cancer Genet Cytogenet* 2006; **166**: 173-179.
31. Moll UM, Ostermeyer AG, Haladay R, *et al.* Cytoplasmic sequestration of wild-type p53 protein impairs the G1 checkpoint after DNA damage. *Mol Cell Biol* 1996; **16**: 1126-1137.
32. Ottaviano L, Schaefer KL, Gajewski M, *et al.* Molecular characterization of commonly used cell lines for bone tumor research: a trans-European EuroBoNet effort. *Genes Chromosomes Cancer* 2010; **49**: 40-51.
33. Whang-Peng J, Triche TJ, Knutsen T, *et al.* Cytogenetic characterization of selected small round cell tumors of childhood. *Cancer Genet Cytogenet* 1986; **21**: 185-208.
34. Nicoli S, Presta M. The zebrafish/tumor xenograft angiogenesis assay. *Nat Protoc* 2007; **2**: 2918-2923.
35. Nicoli S, Ribatti D, Cotelli F, *et al.* Mammalian tumor xenografts induce

- neovascularization in zebrafish embryos. *Cancer Res* 2007; **67**: 2927-2931.
36. White RM, Sessa A, Burke C, *et al.* Transparent adult zebrafish as a tool for in vivo transplantation analysis. *Cell stem cell* 2008; **2**: 183-189.
 37. Pishas KI, Al-Ejeh F, Zinonos I, *et al.* Nutlin-3a is a potential therapeutic for ewing sarcoma. *Clin Cancer Res* 2011; **17**: 494-504.
 38. Stern HM, Zon LI. Cancer genetics and drug discovery in the zebrafish. *Nat Rev Cancer* 2003; **3**: 533-539.
 39. Peirce SK, Findley HW. The MDM2 antagonist nutlin-3 sensitizes p53-null neuroblastoma cells to doxorubicin via E2F1 and TAp73. *Int J Oncol* 2009; **34**: 1395-1402
 40. Ray RM, Bhattacharya S, Johnson LR. Mdm2 inhibition induces apoptosis in p53 deficient human colon cancer cells by activating p73- and E2F1-mediated expression of PUMA and Siva-1. *Apoptosis* 2011; **16**: 35-44.
 41. Rentzsch F, Kramer C, Hammerschmidt M. Specific and conserved roles of TAp73 during zebrafish development. *Gene* 2003; **323**: 19-30.
 42. Kovar H, Pospisilova S, Jug G, *et al.* Response of Ewing tumor cells to forced and activated p53 expression. *Oncogene* 2003; **22**: 3193-3204.
 43. Wei G, Antonescu CR, de Alava E, *et al.* Prognostic impact of INK4A deletion in Ewing sarcoma. *Cancer* 2000; **89**: 793-799.
 44. Lopez-Guerrero JA, Pellin A, Noguera R, *et al.* Molecular analysis of the 9p21 locus and p53 genes in Ewing family tumors. *Lab invest* 2001; **81**: 803-814.
 45. Huang HY, Illei PB, Zhao Z, *et al.* Ewing sarcomas with p53 mutation or p16/p14ARF homozygous deletion: a highly lethal subset associated with poor chemoresponse. *J Clin Oncol* 2005; **23**: 548-558.
 46. Berghmans S, Murphey RD, Wienholds E, *et al.* tp53 mutant zebrafish develop malignant peripheral nerve sheath tumors. *Proc Natl Acad Sci U S A* 2005; **102**: 407-412.
 47. Ji Z, Kumar R, Taylor M, *et al.* Vemurafenib synergizes with nutlin-3 to deplete survivin and suppresses melanoma viability and tumor growth. *Clin Cancer Res* 2013; **19**: 4383-4391.
 48. Barber-Rotenberg JS, Selvanathan SP, Kong Y, *et al.* Single enantiomer of YK-4-279 demonstrates specificity in targeting the oncogene EWS-FLI1. *Oncotarget* 2012; **3**: 172-182.

Supplementary information

4

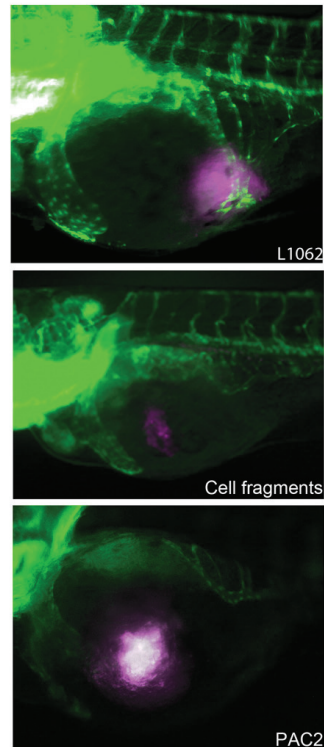
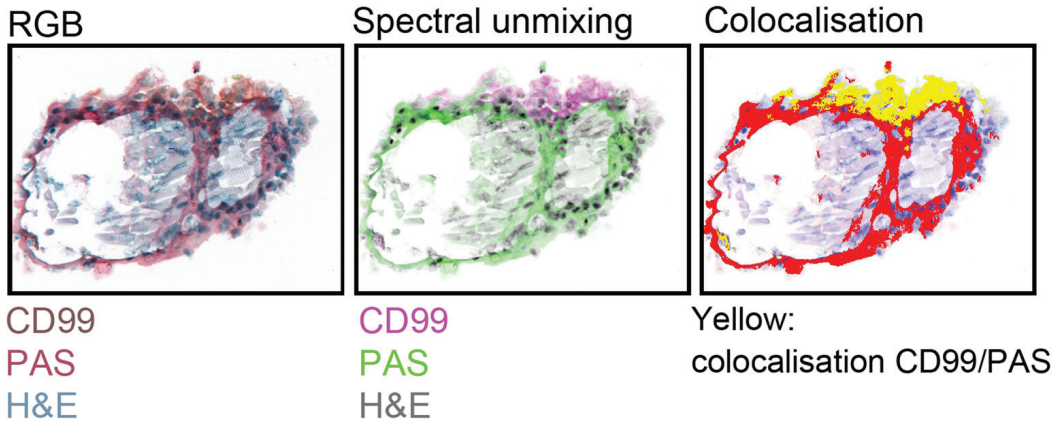


Figure S1. Angiogenesis controls. Upper panel) Angiogenic sprouting of vessels from the SIV complex induced by the implanted EWS cells L1062, 1dpi. **Middle panel)** Lack of angiogenic sprouting after cell fragment engraftment, 1 dpi. **Bottom panel)** Lack of angiogenic sprouting after engraftment of zebrafish fibroblasts PAC2, 1 dpi.



4

Figure S2. High-resolution histology images of 5 dpi embryo with CD-99 positive EWS cells. Left) RGB image of paraffin section. **Middle)** Spectral unmixing of paraffin section showing CD99 in magenta and PAS staining in green. **Right)** Colocalisation of CD99 and PAS, indicated in yellow.

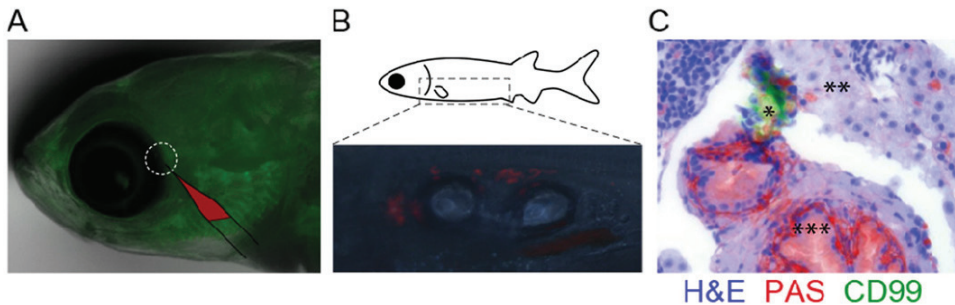


Figure S3. Implantation in bloodstream of 35 dpf zebrafish juveniles with EWS cells. A) Site of implantation into vessels behind the eye. **B)** Cells visible in abdomen of live fish, 6 dpi. **C)** Immunohistochemical analysis at 6 dpi showing cells in the gut of the larvae.

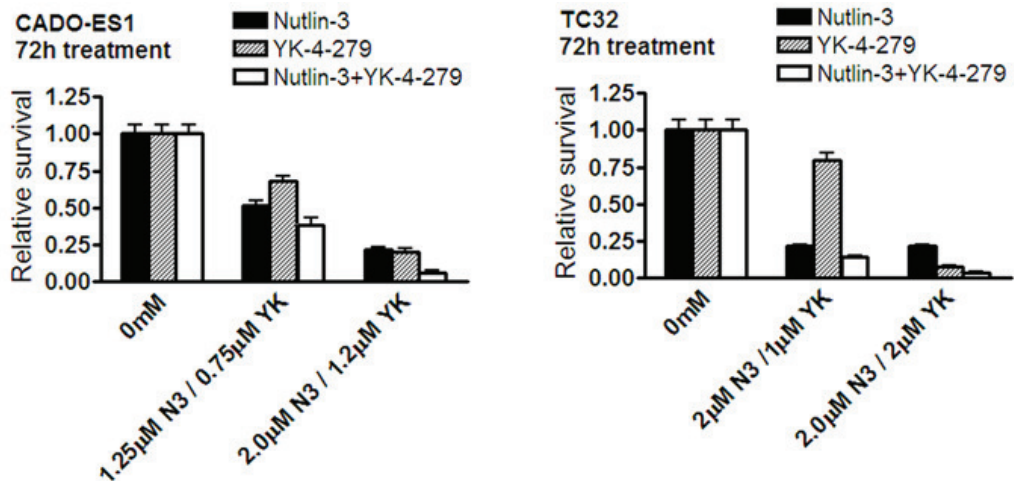


Figure S4. In culture effect of Nutlin-3 and YK-4-279 on TC32 and CADO-ES1. WST-1 assay for measuring relative survival of CADO-ES1 cells (Left) or TC32 cells (Right) treated for 72 hours with Nutlin-3, YK-4-279 or a combination thereof. All measurements were performed in triplicates. Error bars represent 95% confidence interval.

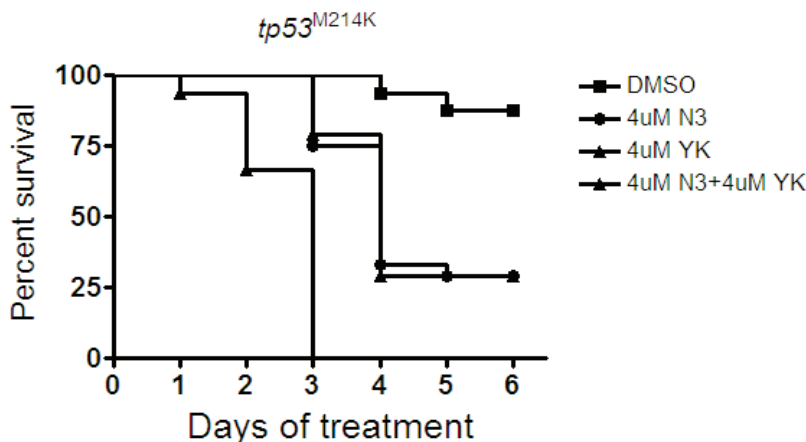


Figure S5. Zebrafish survival curves. Effect of treatment at 4μM compound concentrations on *tp53^{M214K}* embryos treated from 2 dpf onwards. N≥24per condition.

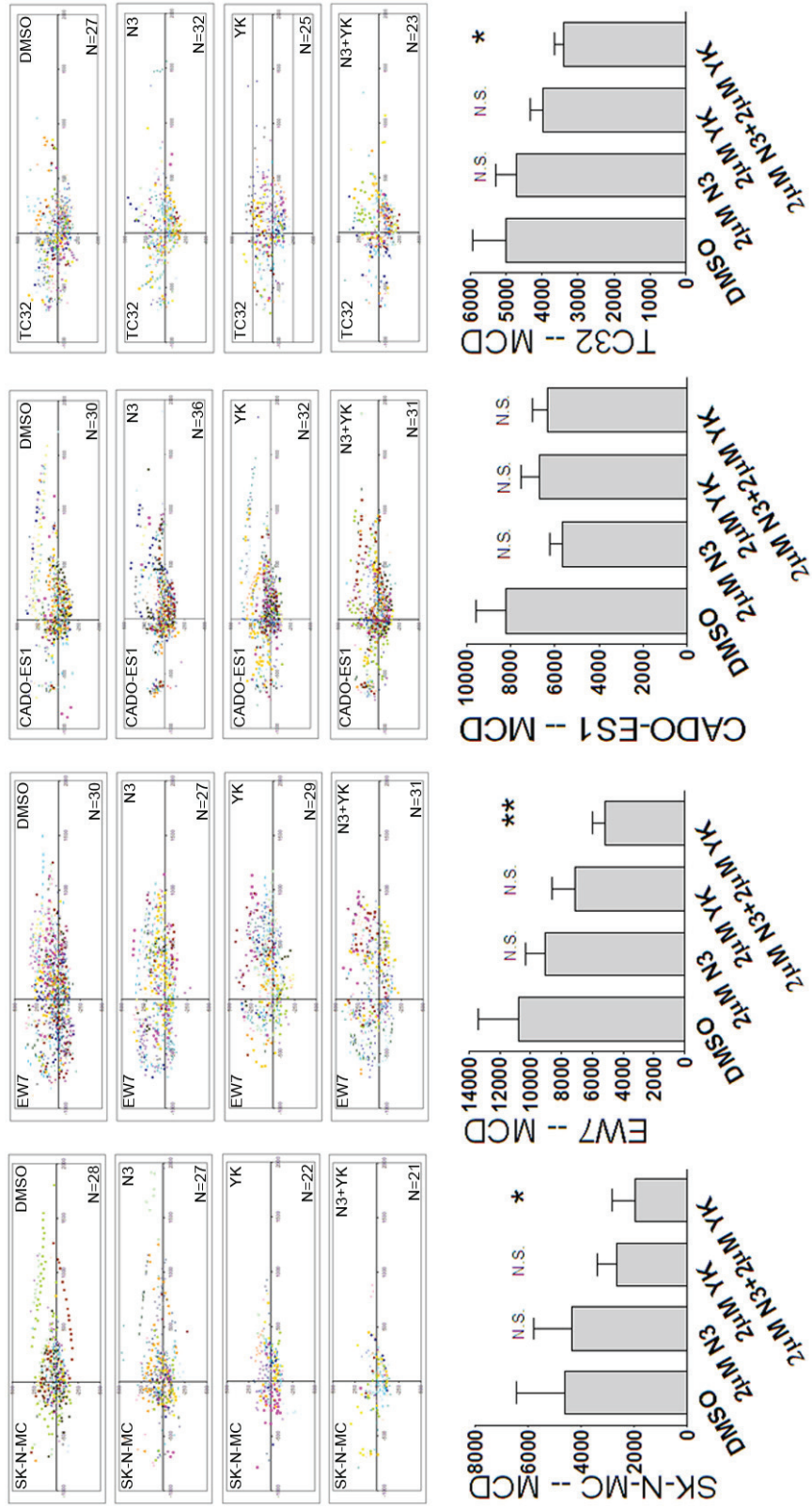


Figure S6. Quantification of migration of EWS cells in zebrafish. Migration from the site of implantation represented per group in scatter dot plots. Quantification of these plots by mean cumulative migration distance of tumour cell foci (MCD) are represented in the bar graphs below the scatterplots.

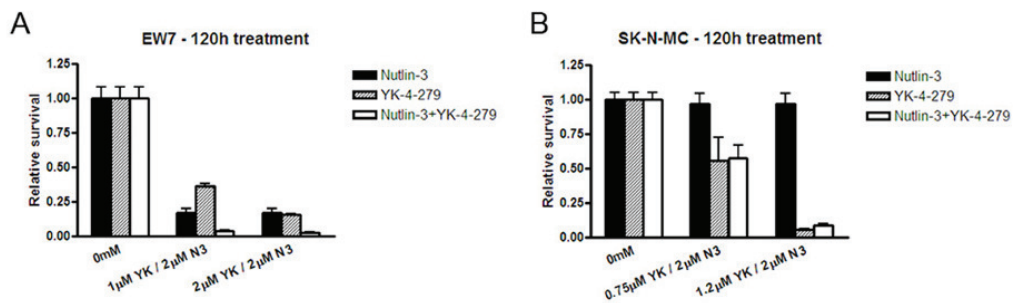


Figure S7. In culture effect of Nutlin-3 and YK-4-279 on EWS cells for prolonged exposure. WST-1 assay measuring relative survival of EW7 (Left) or SK-N-MC cells (Right) treated for 120 hours with Nutlin-3, YK-4-279 or a combination thereof. All measurements were performed in triplicates. Error bars represent 95% confidence interval.

Chapter 5

Suppression of deacetylase SIRT1 mediates tumor-suppressive NOTCH response and offers a novel treatment option in metastatic Ewing Sarcoma

Ban J, Aryee DN, Fourtouna A, **van der Ent W**, Kauer M, Niedan S, Machado I, Rodriguez-Galindo C, Tirado OM, Schwentner R, Picci P, Flanagan AM, Berg V, Strauss SJ, Scotlandi K, Lawlor ER, Snaar-Jagalska E, Lombart-Bosch A, Kovar H.

Cancer Res. 2014 Oct 3. pii: canres.1736.2014

Abstract

The developmental receptor NOTCH plays an important role in various human cancers as a consequence of oncogenic mutations. Here we describe a novel mechanism of NOTCH-induced tumor suppression involving modulation of the deacetylase SIRT1, providing a rationale for the use of SIRT1 inhibitors to treat cancers where this mechanism is inactivated because of SIRT1 overexpression. In Ewing sarcoma cells, NOTCH signaling is abrogated by the driver oncogene EWS-FLI1. Restoration of NOTCH signaling caused growth arrest due to activation of the NOTCH effector HEY1, directly suppressing SIRT1 and thereby activating p53. This mechanism of tumor suppression was validated in Ewing sarcoma cells, B-cell tumors, and human keratinocytes where NOTCH dysregulation has been implicated pathogenically. Notably, the SIRT1/2 inhibitor Tenovin-6 killed Ewing sarcoma cells *in vitro* and prohibited tumor growth and spread in an established xenograft model in zebrafish. Using immunohistochemistry to analyze primary tissue specimens, we found that high SIRT1 expression was associated with Ewing sarcoma metastasis and poor prognosis. Our findings suggest a mechanistic rationale for the use of SIRT1 inhibitors being developed to treat metastatic disease in patients with Ewing sarcoma.

5

Introduction

NOTCH signaling is an evolutionarily conserved pathway involved in tissue patterning and cell specification during normal development. It is initiated following interaction of a cell surface expressed ligand (JAG1, JAG2, DLL1, 3 and 4) with a transmembrane monomeric NOTCH receptor (NOTCH1–4). Binding of the ligand is followed by two successive proteolytic cleavage steps catalyzed by TNF α -converting enzyme and the presenilin- γ secretase complex that release the NOTCH intracellular domain (NICD) to the cytoplasm. Upon translocation to the nucleus, NICD activates the transcription factor CSL. The amplitude and duration of the NOTCH response are regulated by acetylation of NICD on specific lysine residues.¹ Only few CSL targets are known, most prominently the HES and HEY family of transcriptional repressors. In many mammalian cell types, the NOTCH pathway enhances stem cell potential and suppresses differentiation, whereas in others, it exerts an opposite role suppressing tumor development.² Oncogenic NOTCH pathway activation by mutation occurs in many cancers including T-cell leukemia and a variety of solid tumors including breast, colorectal, ovarian, and non-small cell lung cancers. Accordingly, a number of pharmacologic NOTCH inhibitors are currently in early clinical development. However, the consequences of activated NOTCH signaling are cell-type-specific and there is a growing list of tissues and neoplasms in which NOTCH activation has a tumor-suppressive effect, including keratinocytes, tumors of the prostate, liver, skin, lung, gastrointestinal stromal tumors, a

wide range of B-cell malignancies, and in Ewing sarcoma.³ Currently, the mechanisms of tumor-suppressive NOTCH signaling remain unknown.

Ewing sarcoma pathogenesis is driven by the chimeric ETS oncogene *EWS-FLI1*. *EWS-FLI1* acts as an aberrant oncogenic transcription factor with both activating and repressive gene regulatory properties.⁴ We have previously reported that *EWS-FLI1* represses *JAG1* expression keeping NOTCH signaling off.⁵ We found that silencing of *EWS-FLI1* results in activation of tumor cell autonomous NOTCH signaling, leading to a strong transcriptional induction of *HEY1*, which was paralleled by activation of the tumor suppressor *TP53* and consequently upregulation of the cell-cycle inhibitor *p21* and cell-cycle arrest.³ We showed that *HEY1* was sufficient to elicit a *TP53* response in Ewing sarcoma cell lines, but the mechanism of *TP53* activation remained unknown.

We here demonstrate that knockdown of *EWS-FLI1* and induction of *HEY1* result in *TP53* acetylation. Carboxy terminal acetylation by *p300* was demonstrated to be essential for *TP53* transcriptional activity.⁶ Consequently, factors that lead to deacetylation of *TP53* interfere with *TP53* stress response.⁷ We now report *SIRT1* as a *HEY1*-repressed deacetylase preventing *TP53* acetylation downstream of suppressed NOTCH signaling in Ewing sarcoma and other tissues in which NOTCH acts tumor suppressive.

Sirtuins are an evolutionarily highly conserved protein family homologous to yeast silent information regulator 2 (*sir2*) and link cellular metabolism to tissue homeostasis and differentiation. Sirtuins have recently attracted considerable interest due to their role in inflammation, protection from neurodegenerative diseases, organismal longevity, and their emerging importance for cancer.⁸ Of the seven members of this family in man, *SIRT1*, 3, 6, and 7 localize mainly to the nucleus, whereas *SIRT2* resides exclusively in the cytoplasm and *SIRT4* and 5 in mitochondria. *SIRT1*, 2, 3, and 5 catalyze NAD^+ -dependent deacetylation of targets, whereas *SIRT4* and 6 mediate ADP-ribosylation of protein substrates. *SIRT1* has originally been identified as a class III histone deacetylase removing histone H1K26, H3K9, H3K56, and H4K16 acetylation marks, thus facilitating heterochromatin formation. In addition, it plays a role in the repression of euchromatic gene regulation as part of a corepressor complex with the demethylase *LSD1* and associated proteins. Among others, this complex binds to *CSL* and represses genes regulated by the NOTCH signaling pathway including *HEY1*.⁹ In addition, *SIRT1* can modulate *NICD* activity by deacetylation as demonstrated in endothelial cells.¹ Gene regulation by *SIRT1* is also affected by deacetylation of other transcription factors including *AR*, *FOXO*, *E2F1*, *HIC1*, *BCL6*, *NF- κ B*, and notably *TP53* (for review, see ref. 10). *SIRT1* physically interacts with *TP53* and deacetylates Lys382, thus reducing the transcriptional activity of *TP53*.^{7,11} Knockdown of *SIRT1* allows for *TP53* acetylation, which is an indispensable prerequisite for the destabilization of the *TP53*–*MDM2* interaction, inducing transcriptional activity and enabling

TP53 stress response.¹²

We here report that modulation of SIRT1 by HEY1 provides a feedback mechanism that couples NOTCH signaling to TP53 activation in tissues in which NOTCH activity acts tumor suppressive. We demonstrate that in Ewing sarcoma, SIRT1 expression is specifically confined to metastases and that pharmacologic inhibition of SIRT1 activity efficiently kills SIRT1-positive Ewing sarcoma cells *in vitro* and prohibits growth and migration of tumor cells *in vivo*.

Materials and Methods

5

Cell lines, transfections, and drug treatments

Cell lines of this study are summarized in Supplementary Table S4A. All cell lines were verified by short tandem repeat (STR) analysis and are routinely subjected to mycoplasma and SMRV testing in regular intervals. Ewing sarcoma cell lines and keratinocytes were transfected with Lipofectamine Plus reagent (Invitrogen) and subjected to puromycin selection (1 $\mu\text{g}/\text{mL}$) the next day. Ninety-six hours posttransfection, puromycin-selected cells were harvested, washed, and subjected to RNA and protein extraction. “697” and Nalm-6 were transfected by electroporation (Gene Pulser XCell, Bio-Rad) using commercial electroporation buffers from Bio-Rad. Tenovin-6 (Tnv-6; DundeeCell) and MG132 (Alexis, Biochem) were used at concentrations and time periods indicated in the figures. Plasmids and siRNA targeting sequences used in the study have previously been published and are listed in Supplementary Table S4B and S4C.

Proliferation and viability assays

Cell viability was assessed using the colorimetric MTT metabolic activity assay. Briefly, Ewing sarcoma cells (2×10^4 cells per well) were cultured in 96-well plates at 37°C and exposed to varying concentrations of Tnv-6. Solvent (DMSO)-treated cells served as a negative control group. Seventy two hours after treatment, 20 μL of MTT solution (Sigma-Aldrich; 5 mg/mL in PBS) was then added and incubated for another 3 hours. Half-maximal inhibitory concentration (IC_{50}) values were calculated by using Spotfire (TIBCO; duplicate analysis).⁵⁰ All experiments were performed at least 3 times in quadruplicates.

Western blot analyses and immunoprecipitations

For immunoblot analysis, total proteins were resolved by 8.5% or 10% SDS-PAGE and processed according to standard protocols. Antibodies in the study are listed in Supplementary Table S4D. For monitoring antibody binding, blots were incubated for 1 hour with either horseradish

peroxidase–coupled secondary antibody for chemiluminescent detection with Super Signal West Pico chemiluminescent substrate (Pierce Biotechnology, THP) or with fluorescent dye–coupled secondary antibodies (DyLight 649 and DyLight 800, Pierce Biotechnology, THP) for detection by the Odyssey infrared imager (LI-COR Biosciences). TP53 was precipitated with either CM1 or DO1 antibodies and probed with either acetylation-specific or DO1 antibodies.

Reporter gene assays

For promoter activity analysis, TC252 Ewing sarcoma cells were plated at an initial concentration of 10^4 cells/mL into 24-well plates. Cells were transiently transfected with 50 ng of each SIRT1-firefly reporter construct plus 100 ng of pSport HEY1 and pSuper empty vector, using Lipofectamine (Invitrogen). Luciferase reporter assays were then performed using *Renilla* as internal control. All plasmids used are listed in Supplementary Table S4B.

Gene expression analysis

Changes in gene expression profiles upon knockdown of EWS-FLI1 were followed on Affymetrix HGU133A arrays (Affymetrix, Inc.) as previously reported.³

Quantitative real-time RT-PCR

Total RNA was extracted from cells using the RNeasy Mini Kit (QIAGEN) and quantitative analysis by TaqMan reverse transcriptase PCR (qRT-PCR) was performed as previously described [3]. The relative expression levels of the genes assessed were calculated by the $2^{(-\Delta\Delta C_t)}$ method.

Immunohistochemistry on tissue microarrays and formalin-fixed, paraffin-embedded tumor sections

Three different Ewing sarcoma tissue microarray (TMA) series were used in this study: one (TMA1) previously described¹³ containing 280 samples (277 Ewing sarcoma and three unclassified samples from Rizzoli Institute, Bologna, Italy); one (TMA2) containing 112 de-identified Ewing sarcoma samples from the University of Michigan (Ann Arbor, MI); and one previously described TMA from St. Jude Children's Hospital containing primary tumor samples with complete clinical follow-up from 43 patients (Supplementary Table S2; ref. 14). In addition, formalin-fixed, paraffin-embedded (FFPE) tissue blocks from 14 paired primary Ewing sarcoma tumor and corresponding metastasis tissues were obtained from the University College London (see also Supplementary Materials). Tissue processing, antibody staining (Supplementary Table S4C), and interpretation of staining results were performed as previously described.¹³ Two pathologists blind to the origin and identity of cases independently evaluated the percentage and intensity of stained cells (I. Machado, A. Llombart-Bosch). Statistical differences in staining patterns

were evaluated using the 2 × 2 Fisher exact (2-tailed) probability test.

Zebrafish embryo xenotransplantation and *in vivo* Tnv-6 treatment

TG(fli1:EGFP) zebrafish were handled compliant to local animal welfare regulations and maintained according to standard protocols (www.ZFIN.org). Two-day-old zebrafish embryos were anaesthetized with 0.001% tricaine (Sigma-Aldrich). TC252 and A673 stably expressing mCherry were loaded as a single-cell suspension in 2% polyvinylpyrrolidone-40 (Sigma-Aldrich) into 1.0 mm OD × 0.78 mm ID borosilicate needles (Harvard Apparatus). Circa 500 cells were injected into the yolk, using a Pneumatic PicoPump (World Precision Instruments, Inc.; 10–20 psi, 100–400 ms). Larvae were maintained at 34°C. One day after implantation, six embryos were placed per well of a 24-well plate, in a volume of 1 mL Instant Ocean eggwater supplemented with either DMSO or Tnv-6, with daily refreshing of the solutions. After 3 days of treatment, embryos were fixed overnight (O/N) in 4% paraformaldehyde at 4°C. Embryos were imaged in glass-bottom 96-well plates using a NIKON3 confocal microscope (4× lens). Image processing was performed with ImageJ 1.43 (NIH, Bethesda, MD). ImagePro Analyzer 7.0 (Media Cybernetics) analysis was performed as described previously.¹⁵

5

Results

Identification of candidate genes mediating HEY1 induced TP53 stabilization downstream of EWS-FLI1

We previously showed that the NOTCH effector HEY1 stabilizes and activates TP53 in Ewing sarcoma upon silencing of EWS-FLI1, but the mechanism behind remained unknown.³ Because TP53 stability is largely regulated by posttranslational modifications (PTM), we hypothesized that HEY1 represses a TP53 interacting protein involved in the destabilization of TP53. We considered either a repression of the MDM2/MDM4 ubiquitin ligase complex (Supplementary Results and Supplementary Fig. S1) or of an enzyme involved in destabilizing posttranslational TP53 modification.

HEY1 was ectopically expressed in TC252 cells and genome-wide gene expression changes were compared with the EWS-FLI1 signature previously obtained by knockdown in five different Ewing sarcoma cell lines (TC252, WE68, STA-ET-1, STA-ET-7.2, SK-N-MC; ref. 4). Of 45 genes with relevance to TP53 modification 16-18, five fulfilled the criterion of being significantly suppressed in response to both HEY1 expression in TC252 and EWS-FLI1 silencing in all five tested Ewing sarcoma cell lines (Supplementary Table S1): PRKDC, encoding DNA-dependent protein kinase; YEATS4, whose product GAS41 is involved in dephosphorylation of TP53 Ser36619; PPA1, stabilizing MDM4 and dephosphorylating TP53 at Ser1520,21; PPP2R5C, a

component of protein phosphatase 2A dephosphorylating TP53 at various residues including Thr55, Ser37, and Ser462-24, and SIRT1, a type III deacetylase known to target histone and non-histone proteins including TP53. While suppression of PRKDC is expected to perturb the DNA damage checkpoint²⁵, HEY1 mediated suppression of GAS41, or protein phosphatases 1 and 2, and specifically of the deacetylase SIRT1 has the potential to lead to TP53 stabilization and activation. We observed a marked upregulation of SIRT1 RNA expression in 59 primary Ewing sarcoma samples as compared with 89 normal tissues (Fig. 1A) and acetylation of TP53 in response to EWS-FLI1 knockdown and ectopic HEY1 expression in the Ewing sarcoma cell line TC252 (Fig. 1B). Because acetylation and deacetylation play a central role in the regulation of the TP53 pathway¹⁶, we therefore focused our further analysis on SIRT1.

SIRT1 mediates TP53 stabilization by HEY1 downstream of NOTCH and of EWS-FLI1 silencing

Ectopic HEY1 consistently reduced SIRT1 expression leading to TP53 stabilization and consequently to the induction of CDKN1A expression in wild-type *TP53* cell types, for which NOTCH activation has been reported to act tumor suppressive. This is demonstrated for three Ewing sarcoma cell lines (TC252, VH64, and WE68; Fig. 1C), the B-ALL cell line 697, the B-cell lymphoma cell line Nalm-6, and primary human keratinocytes lacking endogenous HEY1 expression (Supplementary Fig. S2). SIRT1 modulation is dependent on the concentration of ectopic HEY1 as demonstrated in HEK293 cells carrying doxycycline-inducible Flag-tagged HEY1, where it was completely reversible upon release from doxycycline-dependent HEY1 induction (Supplementary Fig. S3A). Conversely, knockdown of endogenous HEY1 in the osteosarcoma cell line U2OS by siRNA increased SIRT1 accompanied by TP53 modulation (Supplementary Fig. S3B). These results indicate that the mechanism of TP53 activation by HEY1-mediated SIRT1 suppression is not restricted to Ewing sarcoma but also operative in other tissues and tumors.

Consistent with HEY1 acting downstream of activated NOTCH signaling, ectopic NICD1 expression also induced SIRT1 downregulation and TP53 stabilization (Fig. 1D). To confirm dependence of EWS-FLI1-dependent SIRT1 regulation on HEY1 in Ewing sarcoma cells, we performed EWS-FLI1 knockdown in the absence and presence of siRNA to HEY1. Silencing of EWS-FLI1 by shRNA resulted in a marked induction of HEY1 and a strong downregulation of SIRT1, which was completely rescued upon concomitant inhibition of HEY1 expression (Fig. 1E).

HEY proteins are known to preferentially bind to class B E-box sequences.^{26,27} The SIRT1 promoter region contains a (GACGTG) motif at -373 base pairs from the transcriptional start site (Fig. 1F). In reporter gene assays with a 562 base pair SIRT1 promoter fragment driving luciferase expression in TC252 cells, HEY1 reduced the

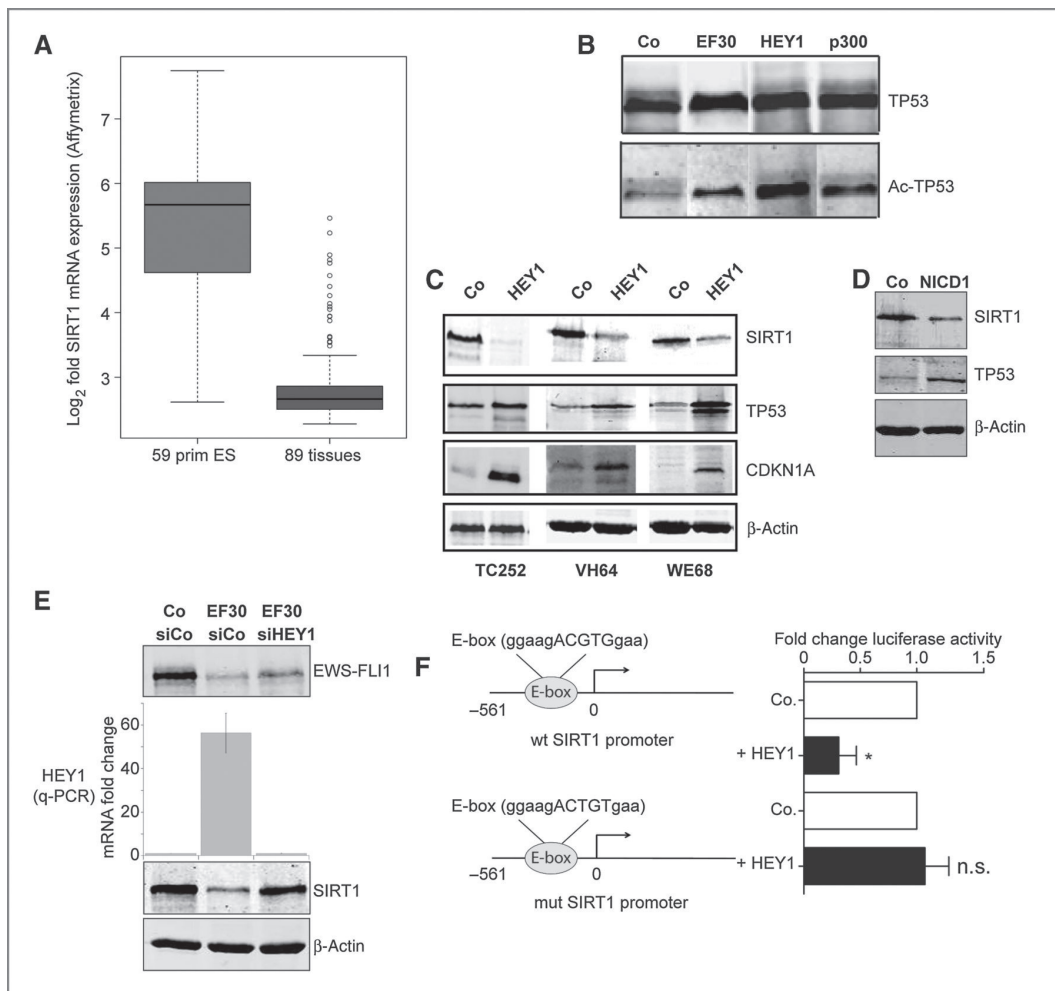
activity more than 3-fold. This transcriptional repressive effect was completely lost upon mutation of the E-box element (Fig. 1F). Together with published chromatin immunoprecipitation sequencing data from HEK293 embryonal kidney cells²⁶, K562 myeloid leukemia, and HepG2 hepatocellular carcinoma cells (ENCODE; ref. 28) that demonstrated HEY1 binding to the SIRT1 promoter at about 300 base pairs upstream of the transcription start site, these results confirm SIRT1 as a direct HEY1 target gene.

Inhibition of SIRT1 leads to Ewing sarcoma cell death *in vitro*

Modulation of SIRT1 in Ewing sarcoma cells was sufficient to induce acetylation of TP53 and activation of TP53 target genes such as *CDKN1A* (Fig. 2A), as also observed upon HEY1 expression (Fig. 1C). In fact, ectopic expression of increasing amounts of SIRT1 in the presence of HEY1 was able to abolish HEY1-induced TP53 acetylation already at the lowest levels (Fig. 2B). These results suggest that SIRT1 expression in Ewing sarcoma is involved in functional impairment of TP53 activity, which can be restored by activation of the NOTCH signaling pathway through HEY1 induction upon knockdown of EWS-FLI1.

We next tested for the impact of SIRT1 modulation on cell fate of Ewing sarcoma cells. Knockdown of SIRT1 but not of SIRT2 induced TP53 acetylation and cell death in TC252 cells (Fig. 3A). This result suggested that SIRT1 expression may serve as a promising pharmacologic target in Ewing sarcoma. We therefore tested the sensitivity of Ewing sarcoma cell lines to the small-molecule SIRT1/2 inhibitor Tnv-6.²⁹ As shown in Fig. 3B, Tnv-6 killed Ewing sarcoma cell lines with IC_{50} values between 0.8 and 8.0 $\mu\text{mol/L}$. The lowest IC_{50} values were found in cell lines with wild-type *TP53*, which also expressed the highest levels of SIRT1,

Figure 1. HEY1 induces TP53 acetylation via direct modulation of deacetylase SIRT1 upon silencing of EWS-FLI1. A, SIRT1 RNA expression in 59 primary Ewing sarcoma (ES) samples as compared with 89 human tissues from the Novartis gene expression atlas. The box and whiskers plot shows the \log_2 expression levels on Affymetrix arrays as described (4). The box contains data within the upper and lower quartile; the median of the data is shown as horizontal line within the box; the whiskers extend at maximum to $1.5 \times$ IQD (interquartile distance = distance between upper and lower quartile); more extreme data points (outliers) are depicted as circles. The difference between the groups is highly significant ($P = 2.2e-16$, Wilcoxon test). See also Supplementary Table S1. B, immunoblot of immunopurified TP53. TC252 cells were transfected with control empty vector, EWS-FLI1 directed shRNA (EF30), HEY1 expression plasmid, or, for positive control, a p300 expression construct. Cells were lysed and TP53 was immunoprecipitated using anti-TP53 antibody. Equal amounts of immunopurified TP53 were probed with pan-acetylation antibody and for control of equal TP53 loading, DO-1. C, modulation of SIRT1 and induction of TP53 and *CDKN1A* by ectopic HEY1



expression in three Ewing sarcoma cell lines (TC252, VH64, and WE68). Co, empty vector control transfection. D, NICD1 downregulates SIRT1 and induces TP53 protein expression in TC252 cells. E, knockdown of EWS-FLI1 modulates SIRT1 expression in a HEY1-dependent way. TC252 cells were transfected with either control scrambled shRNA (Co) or EWS-FLI1 targeting shRNA EF30 in the presence of either nontargeting siRNA control (siCo) or HEY1-specific siRNA. Because of the unavailability of sensitive HEY1-specific antibodies, HEY1 expression was monitored by real-time quantitative RT-PCR (mean values \pm SEM of three determinations), whereas EWS-FLI1, SIRT1, and β -actin were followed on the protein level. F, HEY1 suppresses the SIRT1 promoter by binding to an E-box element. Firefly luciferase reporter assays were conducted in TC252 cells upon cotransfection of the indicated reporter vectors carrying a SIRT1 promoter fragment with the E-box in either wild-type or mutant configuration³⁹ with either empty vector control or HEY1 expression plasmid. Mean \pm SEM of three independent experiments is shown. *, significant ($P = 0.011$) by 1-sample t test. n.s., not significant ($P > 0.05$).

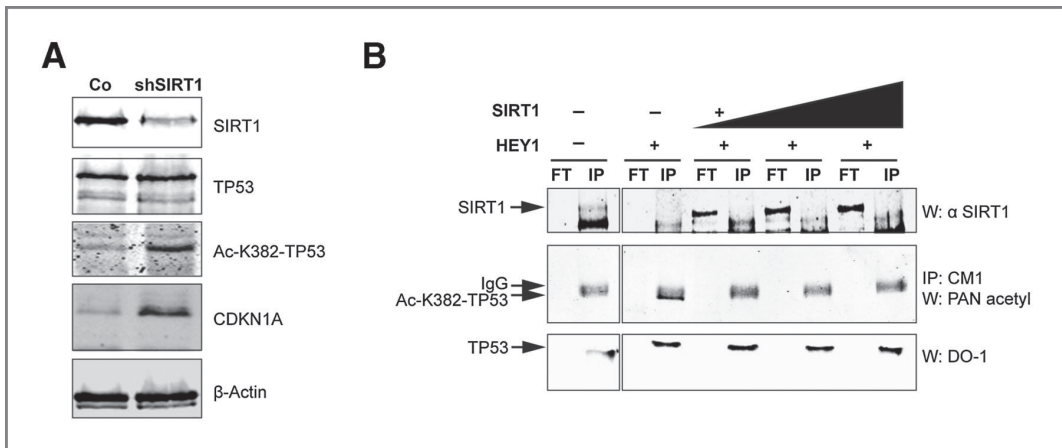


Figure 2. Modulation of SIRT1 results in TP53 acetylation. A, knockdown of SIRT1 in TC252 cells by shSIRT1 results in TP53 K382 acetylation and TP53 target gene activation (monitored representatively by CDKN1A induction). B, ectopic expression of SIRT1 counteracts HEY1-induced TP53 acetylation. TC252 cells were transfected with empty vector control or HEY1 expression vector plus increasing amounts of SIRT1 expression vector (left to right). TP53 was immunoprecipitated with rabbit polyclonal α TP53 antibody CM1, and Western blot analyses of flow-through and immunoprecipitates were probed with α SIRT1, pan-acetylation antibody, and pan-TP53 antibody DO1. Experiments indicate that in the absence of HEY1, TP53 remains deacetylated because of the activity of endogenous SIRT1. Upon HEY1 transfection, SIRT1 is suppressed and TP53 is acetylated. Titrating-in increasing amounts of SIRT1 rescues TP53 deacetylation in the presence of HEY1.

consistent with the induction of acetylated TP53 and of CDKN1A as a marker of TP53 transcriptional activation (Fig. 3C). Dependence of Tnv-6-induced cell death on TP53 was best demonstrated by rescue of cell viability without any change in SIRT1 expression levels if TP53 was knocked down before Tnv-6 treatment in wild-type TP53 TC252 cells (Fig. 3D). Cell death induction by Tnv-6 was dependent on SIRT1 but not on SIRT2, as SIRT2 knockdown failed to rescue TC252 cell death induced by drug treatment (Fig. 3E). Together, these results indicate that Ewing sarcoma cells are highly sensitive to Tnv-6 treatment and that the level of sensitivity depends on the presence or absence of intact TP53 and SIRT1.

The SIRT1/2 inhibitor Tnv-6 inhibits Ewing sarcoma growth and spread in a zebrafish xenotransplantation model

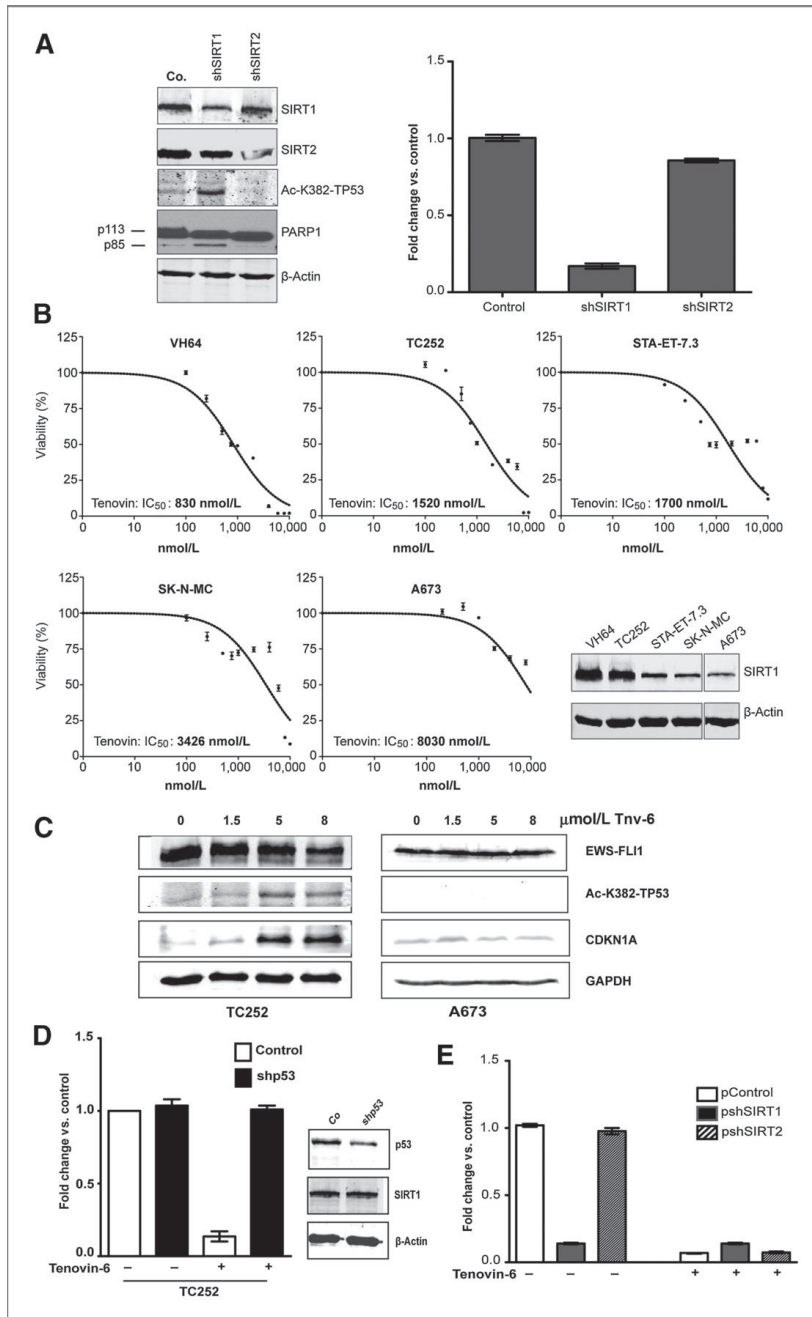
Because inhibition of SIRT1 was able to kill Ewing sarcoma cell lines, we tested Tnv-6 for tumor-inhibitory activity in an established xenotransplantation model in zebrafish embryos.³⁰ Two cell lines with high and low SIRT1 expression and distinct Tnv-6 *in vitro* sensitivity (Fig. 3B), the wild-type TP53 cell line TC252 and the TP53-mutant cell

line A673, were fluorescently labeled with mCherry and injected into the yolk sac of *fli1:EGFP* transgenic zebrafish embryos. Implanted embryos were either treated with solvent (DMSO) or 6 $\mu\text{mol/L}$ Tnv-6 for 4 days, and growth and spread of tumor cells through the embryo body were monitored by confocal microscopy (Fig. 4A). Figure 4B combines the results for all embryos injected in three independent replica experiments in a scatter plot that visualizes the distance and direction of migration for each object (cluster of tumor cells) for each embryo. As quantified in Fig. 4C, Tnv-6 not only significantly reduced tumor burden ($P < 0.0001$) but also significantly inhibited migration of TC252 cells ($P < 0.0001$) but not of A673 cells. These data show that pharmacologic inhibition of SIRT1 interferes with Ewing sarcoma growth and migration *in vivo*.

SIRT1 expression in Ewing sarcoma primary tumors and metastases

To validate SIRT1 expression in primary tumors, we screened 392 paraffin-embedded, formalin-fixed Ewing sarcoma samples on two series of TMAs (TMA1 and TMA2; Supplementary Fig. S4) for SIRT1 positivity by immunohistochemistry (IHC). Cases were scored semiquantitatively, and five groups were formed according to the percentage and intensity of mainly nuclear stained cells. Cases were scored as noninformative (necrosis, scant material, or artifact), negative (mild $< 5\%$), 1+ (mild staining in 5%–10% of cells), 2+ (moderate staining in 10%–50% of cells), or 3+ (strong staining in $>50\%$ of cells). Two hundred ninety-eight samples gave informative results, of which 272 samples and 26 samples were obtained from primary tumors and metastases, respectively. For 248 cases, information on disease extent was available (Supplementary Fig. S4). Figure 5A provides examples for the distinct staining patterns obtained. One hundred thirty-one (48%) primary tumors tested negative and 54 (20%) showed only mild staining, whereas 65 (24%) and 22 (8%) displayed moderate and strong nuclear SIRT1 staining, respectively (Fig. 5B). Focusing on primary tumors from patients with localized disease 109 (51%), 41 (19%), 53 (25%), and 11 (5%) showed no, mild, moderate, and strong staining. Corresponding numbers obtained for primary tumors from patients who presented with metastases at diagnosis were 12 (35%), 10 (29%), 5 (15%), and 7 (21%), suggesting a nonsignificant tendency toward higher positivity in patients with primary disseminated disease ($P = 0.550$). The site of metastasis was known for the informative primary tumors from patients with metastatic disease on TMA1 in 29 cases (Supplementary Table S2). Here, primary tumors associated with lung metastasis and primary tumors from patients with bone metastases tested positive in 50% and 40%, respectively.

Strikingly, this tendency turned into a significant difference ($P < 0.001$) when focusing on 26 informative metastasis-derived samples (Fig. 5B, last column). Here, two thirds of metastases showed SIRT1 expression in more than 10% of cells (8 moderately positive, 9 highly positive), whereas four samples tested negative and five metastases



showed SIRT1 positivity in less than 10% of cells (Fig. 5B).

To validate our finding of increased SIRT1 positivity in Ewing sarcoma metastases, we tested an independent series of 14 paired tissue samples for SIRT1 expression by IHC (Table 1, cases 1–14). Including 4 paired samples available from TMA1 and TMA2 (Table 1, cases 15–18), we found lung metastases to score positive in 88% and

Figure 3. Knockdown or pharmacologic inhibition of SIRT1 but not of SIRT2 kills Ewing sarcoma cells *in vitro*. A, silencing of SIRT1 but not of SIRT2 in TC252 cells induces TP53 acetylation and PARP1 cleavage (left) and reduces TC252 cell growth (right). The number of trypan blue-excluding cells was counted 4 days after transfection with the indicated constructs and is displayed relative to control scrambled shRNA transfection. Mean and SD for three experiments are shown. B, dose–response curves to Tnv-6 treatment and determination of IC₅₀ values for five Ewing sarcoma cell lines with distinct SIRT1 protein expression (inserted immunoblot) and TP53 gene status. VH64 and TC252 cells express wild-type TP53, STA-ET-7.3 expresses mutant, SK-N-MC truncated, and A673 no TP53 due to gene deletion (37). C, Tnv-6 induces acetylated TP53 and CDKN1A expression in TC252 cells but not in A673 cells. D, the growth-inhibitory effect of Tnv-6 depends on the presence of wild-type TP53. TC252 cells were transfected with control scrambled or TP53 shRNA and treated with 8 μmol/L Tnv-6 72 hours posttransfection. Trypan blue-excluding cells were counted after 72 hours of Tnv-6 treatment, and mean results and SDs from one representative of two experiments, each performed in triplicate, are shown relative to control treatment. TP53 modulation by shP53 and SIRT1 expression were monitored by immunoblot analysis. E, sensitivity of TC252 cells to Tnv-6 is independent of SIRT2. TC252 cells transfected with either control scrambled shRNA (pControl), or shRNA specific for SIRT1, or shRNA to SIRT2 were either treated with solvent (DMSO) or 8 μmol/L Tnv-6 for 72 hours 4 days posttransfection. Changes in cell numbers were determined relative to the number of cells before start of Tnv-6 treatment. Mean values ± SEM from three independent experiments performed in triplicates are shown relative to control transfections.

bone marrow metastases in 55% of cases similar to the frequency in the primary tumors of these metastatic patients (61%), a frequency twice as high as observed on the TMAs for the primary tumors of patients with localized disease. These results suggest that Ewing sarcoma metastases, specifically lung metastases are predominantly highly positive for SIRT1 by IHC, and that this positivity can frequently already be observed in the corresponding primary tumors at diagnosis.

Because this finding may imply a prognostic relevance of SIRT1 positivity, we independently tested a third previously published cohort of 43 patients with Ewing sarcoma with complete clinical follow-up for a median of 154 months for SIRT1 expression by IHC (TMA3; Supplementary Fig. S4; ref. 14). Six of 32 localized tumors (19%) and 6 of 11 tumors from patients with metastatic disease at diagnosis (55%) tested highly or moderately SIRT1 positive. Intriguingly, 5-year survival probability for the 12 SIRT1-positive patients was 25% as compared with 70% for the 31 SIRT1-negative patients (Supplementary Table

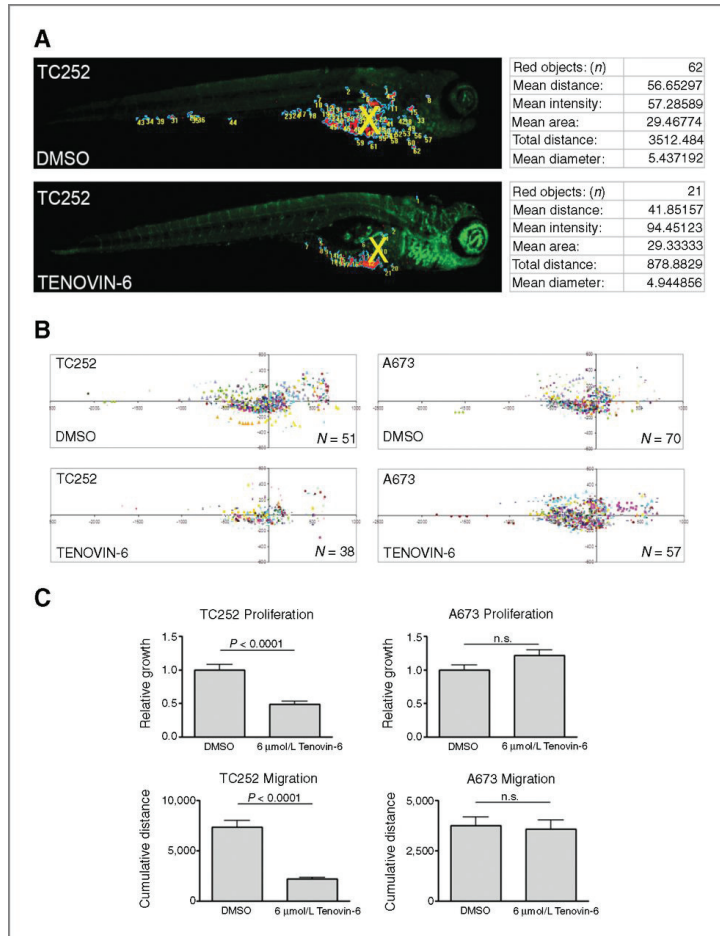


Figure 4. Effect of Tnv-6 treatment on Ewing sarcoma cells in zebrafish embryos. Five hundred cells of either wild-type *TP53*, high SIRT1 expressing TC252, or *TP53* mutant low SIRT1 A673 cell lines were implanted into the yolk sac of the indicated numbers of *TG(fli1:EGFP)* transgenic zebrafish embryos 2 days after fertilisation, and embryos were either control (DMSO) or Tnv-6 (6 μ mol/L) treated from day 1 to 4 after implantation. A, representative picture and quantitative analysis of TC252 implanted fish embryos. Algorithms use the green channel to find the outline of the *TG(fli1:EGFP)* embryo and estimate the site of implantation (X). Using the mCherry signal from ES cells, all tumor cell foci (objects) are outlined and numbered. To determine tumor burden per embryo, the number of objects was multiplied by the average size of objects. The distance of migration away from the site of implantation was determined per object and cumulative results for all embryos from three independent experiments are presented in scatter dot plots in B. Here, each color represents one embryo per group, each dot one cluster of tumor cells. Site of implantation: (x, y = 0, 0). C, cumulative results of tumor burden and migration of TC252 and A673 cells in embryos after three days of drug treatment, 4 days postinjection, normalized against DMSO. Shown are means \pm SEM of three

independent experiments with a total of 214 and 126 embryos for TC252 and A673, respectively. Statistical significance of results was analyzed by unpaired *t* test. n.s., no significant difference.

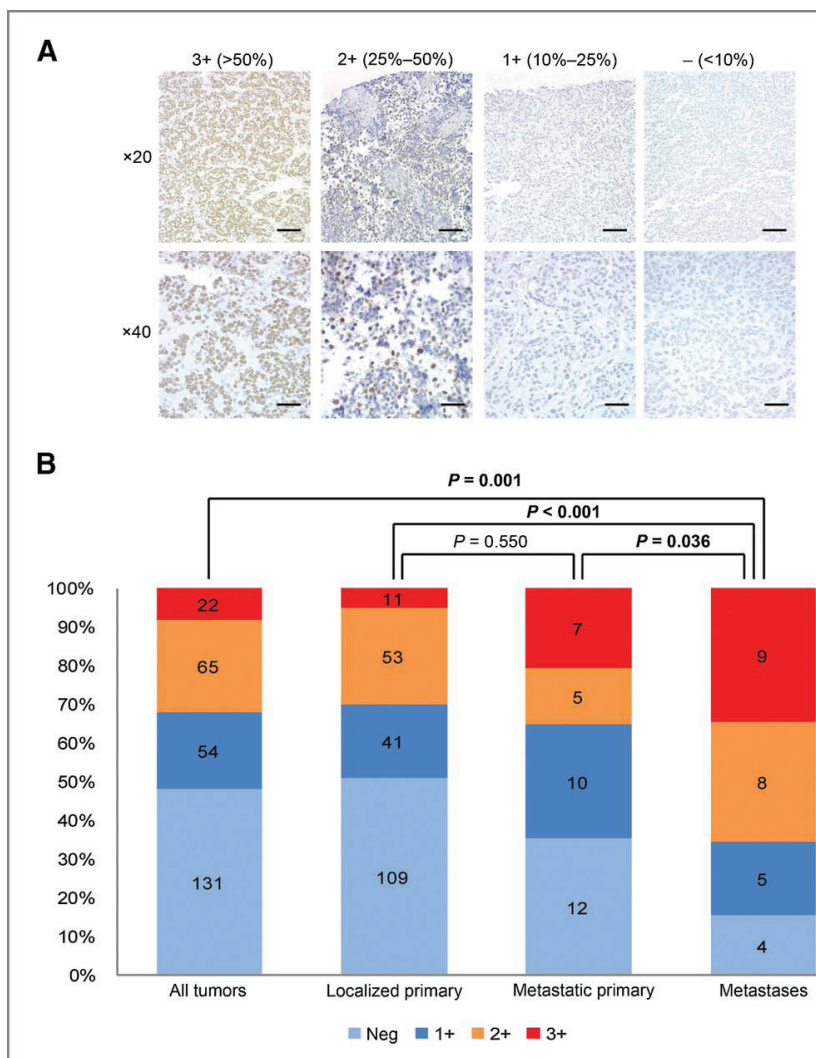


Figure 5. SIRT1 expression in primary human Ewing sarcoma samples by IHC. A, representative staining patterns for classification of SIRT1 positivity. Scale bars, top, 100 μ m; bottom, 50 μ m. B, combined results for the distribution of SIRT1 positivity levels among informative primary tumor samples and metastases from TMA1 and TMA2 (see Supplementary Fig. S2 for details). Numbers of tumors per SIRT1 positivity level are indicated in the bars. 3+ and 2+ staining patterns corresponding to >50% and >10% cells with nuclear SIRT1 staining are considered positive and indicated in red and yellow; 0 (no staining) and 1+ (<10% of SIRT1 staining cells) are considered as negative and are indicated in shades of blue. Statistical significance was assessed by 2×2 Fisher exact (2-tailed) test and is indicated for each comparison on top of the figure. See also Supplementary Table S2.

S3 and Supplementary Fig. S5). Although these results call for larger prospective studies to validate the potential prognostic importance of SIRT1 in Ewing sarcoma, our combined data strongly imply SIRT1 as a candidate therapeutic target in patients with Ewing sarcoma with metastatic disease.

Discussion

5

The NOTCH signaling pathway is well known for its complexity. Its role in cancer has been extensively studied in the context of oncogenic NOTCH mutations but little was known about its tumor-suppressive mechanisms. We here report on the mechanism by which HEY1 downstream of activated NOTCH induces TP53 and demonstrate that this mechanism is operative not only in Ewing sarcoma but also in other malignancies and tissues for which NOTCH activity has been linked to tumor suppression. We find that HEY1 consistently suppresses SIRT1 in Ewing sarcoma, B-ALL, and B-cell lymphoma cell lines and primary human keratinocytes, leading to TP53 acetylation, stabilization, and transcriptional activation. SIRT1 has previously been described to be involved in the epigenetic transcriptional repression of the HEY1 promoter. In the absence of NOTCH activation, SIRT1 forms a corepressor complex with LSD1, CoREST1, and CtBP1, leading to concerted repressive histone H4K16 deacetylation and H3K4 demethylation at the HEY1 promoter. Because we find SIRT1 (shown here) and also LSD1³¹ to be consistently expressed in Ewing sarcoma, and concomitantly HEY1 to be completely turned off⁵, this mechanism is likely operative in Ewing sarcoma. Upon activation and nuclear translocation of NICD and binding to the NOTCH regulated transcription factor CSL, this corepressor complex is replaced by mastermind-like (MAML) and co-activators, including the histone lysine acetyltransferase p300/CBP, leading to transcriptional activation.⁹ In addition, NICD stability has been reported to be prolonged by acetylation, which is modulated by SIRT1, with negative consequences on duration and amplitude of the NOTCH response.¹ Also, SIRT1 represses NOTCH1 transcription from a highly conserved region in the NOTCH1 promoter in endothelial cells.³² By demonstrating suppression of SIRT1 expression by HEY1, our results add an important negative feedback loop to NOTCH-driven gene regulation (Fig. 6).

It also adds a putative feedback mechanism of potential prognostic value to the regulation of TP53. Not only does SIRT1 modulate TP53 stability and activity but also TP53 has been demonstrated to suppress SIRT1 expression through transcriptional repression via binding to a TP53 response element in the SIRT1 promoter³³ and posttranscriptional regulation via TP53-activated microRNA hsa-mir-34a (Fig. 6; ref. 34). Interestingly, hsa-mir-34a and two other SIRT1 regulatory microRNAs, hsa-mir-132 and hsa-mir-93, were recently described components of a favorable prognostic signature in Ewing sarcoma.³⁵ Because we find SIRT1 positivity in Ewing sarcoma mainly associated with metastases,

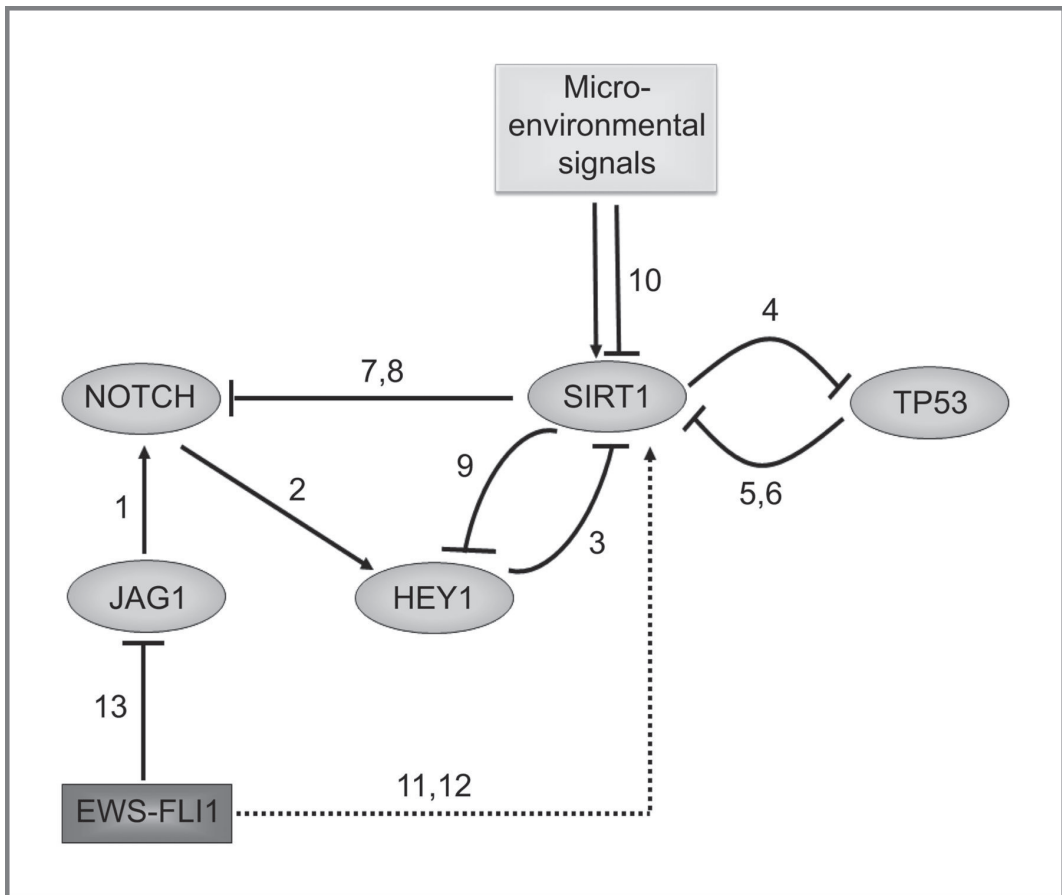
Table 1. SIRT1 staining results for paired primary tumor and metastasis-derived Ewing sarcoma samples.

Case	Origin ^a	Primary tumor	BM met	Lung met
1	FFPE	3+	3+	
2	FFPE	1+	1+	
3	FFPE	2+	2+	
4	FFPE	3+	3+	
5	FFPE	1+	3+	
6	FFPE	0	0	
7	FFPE	0	1+	
8	FFPE	0	1+	
9	FFPE	3+		3+
10	FFPE	3+		3+
11	FFPE	3+		3+
12	FFPE	3+		0
13	FFPE	3+		2+
14	FFPE	3+		3+
15	TMA1	1+		3+
16	TMA1	2+	2+	3+
17	TMA1	0	0	
18	TMA2	2+	3+	
% SIRT1 pos		61%	55%	88%

it is intriguing to speculate that the TP53/hsa-mir-34a/SIRT1 gene regulatory module plays a role in the suppression of metastases. In fact, our results in a zebrafish xenotransplantation model demonstrated that inhibition of SIRT1 prohibits Ewing sarcoma cell dissemination. Because the yolk sac, the site of tumor cell injection, is only poorly vascularized (as is visible from the absence of *fli:EGFP*-positive endothelial cells in Fig. 4), and tumor cells in control-treated animals migrated not only to the tail but also to the head region of the embryos, Tnv-6 likely inhibited active tumor cell migration, consistent with the documented role of SIRT1 in the regulation of cortactin.³⁶ This migration inhibitory effect could not be studied *in vitro* because of the strong cytotoxic effect of Tnv-6 and of SIRT1 knockdown observed in the Ewing sarcoma cell lines. Cell death induction upon perturbation of SIRT1 expression or activity was mainly due to activation of TP53 and could be rescued upon knockdown of TP53. In fact, sensitivity to pharmacologic SIRT1 inhibition was highest in wild-type *TP53* cell lines, which are representative of more than 90% of Ewing sarcoma.³⁷ However, also mutant TP53 cell lines proved sensitive to Tnv-6 treatment, albeit at much higher doses, which is likely due to the broad transcriptional and epigenetic roles of SIRT1 in genome-wide gene regulation as has previously been observed.²⁹ Although it cannot be excluded that part of the *in vitro* cytotoxic activity of Tnv-6 may be due to a non-SIRT1/non-TP53-related activity such as induction of autophagy as previously observed in CLL³⁸, it did not play a role in the zebrafish xenotransplantation model. Here, drug activity was dependent on high SIRT1 expression and the presence of wild-type TP53.

Our IHC study performed on a total of four independent ES cohorts reproducibly indicated increased SIRT1 expression in metastases, specifically in lung metastases. However, results for the frequency of SIRT1-positive staining in the primary tumors of patients presenting with metastases differed between the series. The UCL and the St. Jude cohorts implied high SIRT1 in metastatic patients, whereas in the Rizzoli and the Michigan cohorts, the frequency of SIRT1-positive primary tumors in localized and metastatic disease were comparable, still with a tendency toward higher numbers of positively staining tumor cells in metastatic cases. It is possible that tumor cell heterogeneity and focal SIRT1 expression might have led to an underestimation of SIRT1-positive cases in the primary tumors of metastatic patients on these TMAs. Also, we cannot exclude that decalcification of bone tumor specimens might have led to false negativity in some cases. Intriguingly, outcome results of the small retrospective St. Jude cohort suggested that not only metastatic patients but also patients with localized but SIRT1-positive tumors had an adverse prognosis. These results need to be confirmed on larger, prospectively collected sample series.

While there is already evidence that Sirtuin activators are clinically well tolerated, early clinical trials with SIRT1 inhibitors have only recently been initiated. Metastases are the main cause of treatment failure and death in cancer. Our findings of high SIRT1 positivity in metastases of



5

Figure 6. Model of the NOTCH/TP53 feedback regulatory loop and its regulation by EWS-FLI1 in Ewing sarcoma. 1, binding of the NOTCH ligand JAG1 to a NOTCH receptor results in 2 (proteolytic cleavage of NICD, which activates HEY1). 3, we show that HEY1 transcriptionally represses SIRT1. 4, SIRT1 suppresses TP53 activation by NAD⁺ dependent deacetylation. 5, TP53, when active, suppresses SIRT1 by direct binding to its promoter³³ and indirectly, by 6 (activating SIRT1 targeting microRNAs including miR-34a; ref. 40). 7, SIRT1 also modulates NOTCH activation by deacetylation of NICD¹ and by 8 (transcriptional regulation; ref. 32). 9, SIRT1 feeds back on its negative regulator HEY1 by epigenetically silencing its promoter.⁹ While NOTCH activation via HEY1 is able to suppress SIRT1, several additional mechanisms are known to activate or repress SIRT1, including transcriptional regulators HIF1 and 2 and HIC1^{39,41}, microRNAs⁴⁰, kinases⁴²⁻⁴⁷, and sumoylation⁴⁸ that integrate microenvironmental signals with SIRT1 expression/activity and may be responsible for the specific upregulation of SIRT1 observed in ES lung metastases in 10. 11, EWS-FLI1 directly binds to the SIRT1 promoter⁴⁹ and modulates SIRT1 regulatory microRNAs (no. 12; ref. 50), whereas 13 suppresses cell autonomous NOTCH activation by transcriptional repression of JAG1.

patients with Ewing sarcoma and sensitivity of SIRT1-positive tumor cell lines to SIRT1 inhibition in vitro and in vivo may therefore open an exciting new avenue to cancer treatment.

References

1. Guarani V, Deflorian G, Franco CA, Kruger M, Phng LK, Bentley K, et al. Acetylation-dependent regulation of endothelial Notch signalling by the SIRT1 deacetylase. *Nature* 2011;473:234–8.
2. Dotto GP. Notch tumor suppressor function. *Oncogene* 2008;27: 5115–23.
3. Ban J, Bennani-Baiti I, Kauer M, Schaefer KL, Poremba C, Jug G, et al. EWS-FLI1 suppresses NOTCH-activated p53 in Ewing's sarcoma. *Cancer Res* 2008;68:7100–9.
4. Kauer M, Ban J, Kofler R, Walker B, Davis S, Meltzer P, et al. A molecular function map of Ewing's sarcoma. *PLoS One* 2009;4:e5415.
5. Bennani-Baiti I, Aryee D, Ban J, Machado I, Kauer M, Muhlbacher K, et al. Notch signaling is off and is uncoupled from HES1 expression in Ewing's sarcoma. *J Pathol* 2011;225:353–63.
6. Gu W, Roeder RG. Activation of p53 sequence-specific DNA binding by acetylation of the p53 C-terminal domain. *Cell* 1997;90:595–606.
7. Luo J, Nikolaev AY, Imai S, Chen D, Su F, Shiloh A, et al. Negative control of p53 by Sir2alpha promotes cell survival under stress. *Cell* 2001;107:137–48.
8. Houtkooper RH, Pirinen E, Auwerx J. Sirtuins as regulators of metabolism and healthspan. *Nat Rev Mol Cell Biol* 2012;13:225–38.
9. Mulligan P, Yang F, Di Stefano L, Ji JY, Ouyang J, Nishikawa JL, et al. A SIRT1-LSD1 corepressor complex regulates Notch target gene expression and development. *Mol Cell* 2011;42:689–99.
10. Fang Y, Nicholl MB. Sirtuin 1 in malignant transformation: friend or foe? *Cancer Lett* 2011;306:10–4.
11. Vaziri H, Dessain SK, Ng Eaton E, Imai SI, Frye RA, Pandita TK, et al. hSIR2(SIRT1) functions as an NAD-dependent p53 deacetylase. *Cell* 2001;107:149–59.
12. Tang Y, Zhao W, Chen Y, Zhao Y, Gu W. Acetylation is indispensable for p53 activation. *Cell* 2008;133:612–26.
13. Machado I, Lopez Guerrero JA, Navarro S, Mayordomo E, Scotlandi K, Picci P, et al. Galectin-1 (GAL-1) expression is a useful tool to differentiate between small cell osteosarcoma and Ewing sarcoma. *Virchows Arch* 2013;462:665–71.

14. Lai R, Navid F, Rodriguez-Galindo C, Liu T, Fuller CE, Ganti R, et al. STAT3 is activated in a subset of the Ewing sarcoma family of tumours. *J Pathol* 2006;208:624–32.
15. Ghotra VP, He S, de Bont H, van der Ent W, Spaink HP, van de Water B, et al. Automated whole animal bio-imaging assay for human cancer dissemination. *PLoS One* 2012;7:e31281.
16. Brooks CL, Gu W. The impact of acetylation and deacetylation on the p53 pathway. *Protein Cell* 2011;2:456–62.
17. Kruse JP, Gu W. Modes of p53 regulation. *Cell* 2009;137:609–22.
18. Lim YP, Lim TT, Chan YL, Song AC, Yeo BH, Vojtesek B, et al. The p53 knowledgebase: an integrated information resource for p53 research. *Oncogene* 2007;26:1517–21.
19. Park JH, Smith RJ, Shieh SY, Roeder RG. The GAS41-PP2Cbeta complex dephosphorylates p53 at serine 366 and regulates its stability. *J Biol Chem* 2011;286:10911–7.
20. Lu Z, Wan G, Guo H, Zhang X, Lu X. Protein phosphatase 1 inhibits p53 signaling by dephosphorylating and stabilizing Mdmx. *Cell Signal* 2013;25:796–804.
21. Haneda M, Kojima E, Nishikimi A, Hasegawa T, Nakashima I, Isobe K. Protein phosphatase 1, but not protein phosphatase 2A, dephosphorylates DNA-damaging stress-induced phospho-serine 15 of p53. *FEBS Lett* 2004;567:171–4.
22. Mi J, Bolesta E, Brautigan DL, Lerner JM. PP2A regulates ionizing radiation-induced apoptosis through Ser46 phosphorylation of p53. *Mol Cancer Ther* 2009;8:135–40.
23. Li HH, Cai X, Shouse GP, Piluso LG, Liu X. A specific PP2A regulatory subunit, B56gamma, mediates DNA damage-induced dephosphorylation of p53 at Thr55. *EMBO J* 2007;26:402–11.
24. Dohoney KM, Guillerm C, Whiteford C, Elbi C, Lambert PF, Hager GL, et al. Phosphorylation of p53 at serine 37 is important for transcriptional activity and regulation in response to DNA damage. *Oncogene* 2004;23:49–57.
25. Serrano MA, Li Z, Dangeti M, Musich PR, Patrick S, Roginskaya M, et al. DNA-PK, ATM and ATR collaboratively regulate p53-RPA interaction to facilitate homologous recombination DNA repair. *Oncogene* 2013;32:2452–62.
26. Heisig J, Weber D, Englberger E, Winkler A, Kneitz S, Sung WK, et al. Target gene analysis by microarrays and chromatin immunoprecipitation identifies HEY proteins as highly redundant bHLH repressors. *PLoS Genet* 2012;8:e1002728.
27. Fischer A, Leimeister C, Winkler C, Schumacher N, Klamt B, Elmasri H, et al. Hey bHLH factors in cardiovascular development. *Cold Spring Harb Symp Quant Biol* 2002;67:63–70.

28. Consortium EP. A user's guide to the encyclopedia of DNA elements (ENCODE). *PLoS Biol* 2011;9:e1001046.
29. Lain S, Hollick JJ, Campbell J, Staples OD, Higgins M, Aoubala M, et al. Discovery, in vivo activity, and mechanism of action of a small-molecule p53 activator. *Cancer Cell* 2008;13:454–63.
30. van der Ent W, Jochemsen AG, Teunisse AF, Krens SG, Szuhai K, Spaink HP, et al. Ewing sarcoma inhibition by disruption of EWSR1- FLI1 transcriptional activity and reactivation of p53. *J Pathol* 2014;233:415–24.
31. Bennani-Baiti IM, Machado I, Llombart-Bosch A, Kovar H. Lysinespecific demethylase 1 (LSD1/KDM1A/AOF2/BHC110) is expressed and is an epigenetic drug target in chondrosarcoma, Ewing's sarcoma, osteosarcoma, and rhabdomyosarcoma. *Hum Pathol* 2012;43: 1300–7.
32. Xie M, Liu M, He CS. SIRT1 regulates endothelial Notch signaling in lung cancer. *PLoS One* 2012;7:e45331.
33. Nemoto S, Fergusson MM, Finkel T. Nutrient availability regulates SIRT1 through a forkhead-dependent pathway. *Science* 2004;306: 2105–8.
34. Yamakuchi M, Ferlito M, Lowenstein CJ. miR-34a repression of SIRT1 regulates apoptosis. *Proc Natl Acad Sci U S A* 2008;105:13421–6.
35. Nakatani F, Ferracin M, Manara MC, Ventura S, Del Monaco V, Ferrari S, et al. miR-34a predicts survival of Ewing's sarcoma patients and directly influences cell chemo-sensitivity and malignancy. *J Pathol* 2012;226:796–805.
36. Zhang Y, Zhang M, Dong H, Yong S, Li X, Olashaw N, et al. Deacetylation of cortactin by SIRT1 promotes cell migration. *Oncogene* 2009;28: 445–60.
37. Kovar H, Auinger A, Jug G, Aryee D, Zoubek A, Salzer Kuntschik M, et al. Narrow spectrum of infrequent p53 mutations and absence of MDM2 amplification in Ewing tumours. *Oncogene* 1993;8:2683–90.
38. MacCallum SF, Groves MJ, James J, Murray K, Appleyard V, Prescott AR, et al. Dysregulation of autophagy in chronic lymphocytic leukemia with the small-molecule Sirtuin inhibitor Tenovin-6. *Sci Rep* 2013; 3:1275.
39. Chen R, Dioum EM, Hogg RT, Gerard RD, Garcia JA. Hypoxia increases sirtuin 1 expression in a hypoxia-inducible factor-dependent manner. *J Biol Chem* 2011;286:13869–78.
40. Yamakuchi M. MicroRNA regulation of SIRT1. *Front Physiol* 2012;3:68.
41. Chen WY, Wang DH, Yen RC, Luo J, Gu W, Baylin SB. Tumor suppressor HIC1 directly regulates SIRT1 to modulate p53-dependent DNA-damage responses. *Cell* 2005;123:437–48.
42. Byles V, Chmielewski LK, Wang J, Zhu L, Forman LW, Faller DV, et al. Aberrant cytoplasm localization and protein stability of SIRT1 is regulated by PI3K/IGF-1R signaling in human cancer cells. *Int J Biol Sci* 2010;6:599–612.

43. Ford J, Ahmed S, Allison S, Jiang M, Milner J. JNK2-dependent regulation of SIRT1 protein stability. *Cell Cycle* 2008;7:3091–7.
44. Guo X, Williams JG, Schug TT, Li X. DYRK1A and DYRK3 promote cell survival through phosphorylation and activation of SIRT1. *J Biol Chem* 2010;285:13223–32.
45. Jang SY, Kim SY, Bae YS. p53 deacetylation by SIRT1 decreases during protein kinase CKII downregulation-mediated cellular senescence. *FEBS Lett* 2011;585:3360–6.
46. Lee CW, Wong LL, Tse EY, Liu HF, Leong VY, Lee JM, et al. AMPK promotes p53 acetylation via phosphorylation and inactivation of SIRT1 in liver cancer cells. *Cancer Res* 2012;72:4394–404.
47. Wen L, Chen Z, Zhang F, Cui X, Sun W, Geary GG, et al. Ca²⁺/calmodulin-dependent protein kinase kinase beta phosphorylation of Sirtuin 1 in endothelium is atheroprotective. *Proc Natl Acad Sci U S A* 2013;110:E2420–7.
48. Yang Y, Fu W, Chen J, Olashaw N, Zhang X, Nicosia SV, et al. SIRT1 sumoylation regulates its deacetylase activity and cellular response to genotoxic stress. *Nat Cell Biol* 2007;9:1253–62.
49. Bilke S, Schwentner R, Yang F, Kauer MO, Jug G, Walker RL, et al. Oncogenic ETS fusions deregulate E2F3 target genes in Ewing sarcoma and prostate cancer. *Genome Res* 2013;23:1797–809.
50. Ban J, Jug G, Mestdagh P, Schwentner R, Kauer M, Aryee DN, et al. Hsa-mir-145 is the top EWS-FLI1-repressed microRNA involved in a positive feedback loop in Ewing's sarcoma. *Oncogene* 2011;30: 2173–80.

Supplementary information

All supplementary data may be found at:
<http://cancerres.aacrjournals.org.gate2.inist.fr/content/74/22/6578/suppl/DC1>

Chapter 6

**Development of a high-throughput
zebrafish xenograft model for
Ewing sarcoma drug discovery**

Abstract

Ewing sarcoma tumours occurs predominantly in children and young adults. Circa one in four patients presents with metastatic disease at time of diagnosis. These patients have a poor outlook, and novel therapeutic agents are needed to provide a better projected survival. We propose automated robotic implantation of Ewing sarcoma cells into blastula-stage zebrafish embryos as a means to perform rapid screening of compound libraries.

In a previous study we have shown engraftment of Ewing sarcoma cells in 2-day-old zebrafish embryos provides a rapid method of screening drug-efficacy in a vertebrate *in vivo* setting. By immersing embryos in compounds with anti-cancer activity, reduction of proliferation and migration of Ewing sarcoma cells was observed *in vivo*.

To further expand upon this model and make it available for high-throughput screenings, we studied how manual and robotic engraftment of Ewing sarcoma cells in the yolk of blastula-stage zebrafish embryos compared to the previously described manual injections to the yolk of 2-day-old embryo. At blastula stage, the uniform shape of the embryos makes them more suited for large scale manipulation. Ewing sarcoma cells engrafted at blastula stage were able to proliferate, but migrated in relatively few cases. However, the readout of this model could be obtained more quickly than with the previous model, which is beneficial in large screening.

Automated robotic implantation was optimised, and using this method we have tested the effect of Vincristine, active (S)-YK-4-279 and inactive (R)-YK-4-279 compounds on the proliferation of Ewing sarcoma *in vivo* in three different cell lines. Response of the Ewing sarcoma cells *in vivo* was mostly comparable to *in vitro* results, though there were some discrepancies. These incongruities highlight the importance of testing drug efficacy in multiple cell lines in animal models. We conclude that promising initial findings warrants further expansion of this model to aid Ewing sarcoma research.

Introduction

Ewing sarcoma (EWS) is a bone- and soft tissue tumour affecting primarily children and young adults.^{1,2} Metastases at the time of diagnosis, indicative of a poor prognostic outlook, are found in approximately a quarter of all patients.² For these patients it is essential that newly developed compounds rapidly move from the lab bench to the clinic. In this study, we present a high-throughput zebrafish xenograft model for screening of anti-cancer compounds.

Employing zebrafish as a model for cancer development has become more prevalent over the recent years. Optical transparency

and external development of the embryos make them highly suitable for real-time *in vivo* visualization of processes involved in cancer and have led to transgenic³⁻⁵ and xenotransplantation models^{6,7} for various cancer types, amongst which EWS.⁸⁻¹⁰ Simultaneously, their low maintenance cost, high fecundity and ability to take up small molecule compounds from water, prompted their use in high-throughput chemical screens for a multitude of purposes, ranging from development¹¹ and teratogenicity¹² to inflammation¹³ and cancer.¹⁴ For melanoma, a presently on-going phase/II clinical trial of leflunomide combined with vemurafenib is the first to arise from one such zebrafish screens.^{15,16}

Anti-cancer compound screens in zebrafish are currently based on the analysis of deregulated processes by checking abnormal developmental phenotypes in embryos.^{17,18} Signalling pathways involved in oncogenesis are often also involved in embryonic development, so these screens can provide valuable insights into tumour progression.¹⁹ However, specific models are lacking for many cancer types, and well-defined xenotransplantation models are based on manual microinjection. Manual injection, while relatively fast, is a labour-intensive method for generating large numbers of implanted embryos for screening purposes. In 2006, Wang *et al.* first describes a fully automated robotic microinjection system for zebrafish embryos.²⁰ Designed to perform injections for genetic modulations (such as morpholino or mRNA injection), this system injects embryos within a few hours after proliferation, at a rate of 25 embryos per 2 minutes. In our group, a robotic injection system was developed which could perform such injections at a rate of 2000 embryos per hour.²¹ Moreover, this system could also be employed to inject other substances, for example *Mycobacterium marinum* bacteria for tuberculosis modelling. With this system for automated robotic implantation of cancer cells, sufficient amounts of embryos bearing human tumour cells may be obtained for extensive compound screening.²² In this study, we demonstrate the utility of this automated robotic implantation system for EWS research.

Previously, we have described a xenotransplantation model where we manually implant EWS cells in the yolk of 2-day-old zebrafish larvae.¹⁰ These cells induced angiogenesis in the larvae and could proliferate and migrate. Compounds known to be effective against EWS could severely impede these processes, showing the applicability of this model for testing anti-cancer properties of compounds. Here we have adapted this model to a high-throughput method, by engrafting EWS cells in an early embryonic blastula stage (between 2 and 4 hours post-fertilisation) by robotic implantation. We compared EWS cell behaviour after manual engraftment in the yolk of blastula stage embryos versus 2-day-old embryos. Subsequently, we optimised conditions to enable robotic injection of EWS cells, to generate large numbers of embryos bearing engraftments. Three cell lines were implanted and embryos were treated with different compounds to show the potential of this method for high-throughput screening.

Compounds chosen to validate the model were vincristine, and two enantiomers of YK-4-279. Vincristine is a classic chemotherapeutic agent employed in the treatment of Ewing sarcoma.²³ It is a member of the vinca alkaloid class of drugs, preventing microtubule formation by binding tubulin and blocking mitotic division.²⁴ The second compound used to inhibit EWS proliferation in this model was YK-4-279. YK-4-279 blocks the interaction between EWSR1-ETS, the oncogenic fusion protein characteristic for EWS, and RNA helicase.²⁵ This causes deregulation of transcription and has been shown to be effective in the inhibition of EWS growth in culture, mice and zebrafish.^{10,25} The YK-4-279 molecule bears a chiral centre, giving rise to two enantiomers, which Barber-Rotenberg *et al.* have separated with chiral HPLC.²⁶ They found that (S)-YK-4-279 is the functional enantiomer which blocks interaction between EWSR1-ETS and RNA helicase, whilst (R)-YK-4-279 cannot. In this study, we show that the robotic engraftment of EWS in blastula-stage embryos provides a rapid means of separating functional from non-functional compounds with regard to EWS inhibition. Both Vincristine and (S)-YK-4-279 were able to significantly reduce EWS proliferation in the zebrafish larvae, whilst (R)-YK-4-279 was not able to do so.

Materials and Methods

Cell culture

Ewing sarcoma cell lines (A673, EW7 and TC32) were cultured in IMDM (Life Technologies Europe, Bleiswijk, The Netherlands) supplemented with 10% fetal bovine serum (Life Technologies Europe) at 37°C and 5% CO₂. Stably fluorescent lines were produced by transduction with mCherry-expressing lentiviral vectors (kindly provided by Prof. Dr. R.C. Hoeben, LUMC).

Zebrafish maintenance

ABTL wildtype and *TG(fli1:EGFP)* zebrafish lines were handled compliant to local animal welfare regulations and maintained according to standard protocols (www.ZFIN.org). Fish were set up for mating in single-cross tanks with spacers, where one male and one female are placed on either side in the tank. Removing spacers at the same time ensured all eggs were fertilised at roughly the same time, an important requirement for automated injection.

Tumour cell implantation

Single-cell suspensions were diluted in 14% polyvinylpyrrolidone-40 (Sigma-Aldrich) at 2×10^8 cells/ml. For implantation, we used either 1.0mm OD x 0.78mm ID borosilicate needles (Harvard Apparatus, Holliston, MA) broken open manually around a 15 µm diameter, or custom-made needles with a 20 µm diameter opening (Qvotek, Mississauga, Canada). For robotic injection, zebrafish eggs up to 1K cell stage were placed on

a 1% agarose grid with a honeycomb pattern of 512 hemi-spherical wells, for optimal alignment. For manual injections, eggs were placed in a 1% agarose grid with 1mm wide grooves, in which eggs were placed side-by-side. Embryos of 2 dpf were placed on 1% agarose coated dishes, and water was removed to the point that the embryos were immobilized on the agarose surface. Per embryo, 4 nL of cell suspension was injected into the center of the yolk sac of embryos. After injection, embryos were rinsed and maintained with Instant Ocean egg water with 0,5 ppm methylene blue at 28°C. Two hours post-injection embryos were placed at 34°C, after removal of unfertilised and dead eggs.

In vivo toxicity test of chemical compounds and analysis

At 1 dpf, six embryos were placed per well of a 24-well plate, in a volume of 1mL Instant Ocean eggwater supplemented with chemical compounds or DMSO at a concentration equivalent to the highest concentration of chemicals compounds to be tested. Solutions were refreshed every other day for toxicity tests, or once at 4 dpf for treatment of injected cells, and surviving embryos were counted. At 5 dpf, embryos were fixed overnight (O/N) in ice-cold 4% paraformaldehyde (PFA) at 4°C. Embryos were imaged in glass-bottom 96-wells plates using a NIKON3 confocal microscope (4x lens). Image processing was performed with ImageJ 1.43 (National Institutes of Health, USA) and NIS-Elements Viewer (Nikon Instruments, Tokyo). ImagePro Analyzer 7.0 (Media Cybernetics, Rockville, MD) analysis was performed as described previously.²⁷

6

Proliferation assay in cell culture

For measurement of relative EWS cell survival of each treatment, 3000 cells/well in a volume of 100 µL were seeded in triplicate in full medium in a 96-wells microtiter plate. Next day, medium was replaced with medium containing indicated compound or vehicle concentrations. After indicated times, relative growth was measured using a WST-1-based colorimetric assay (Roche Diagnostics, Almere, The Netherlands), according to the manufacturer's instructions.

Immunohistochemistry and TUNEL staining

Whole-mount zebrafish immunohistochemistry was performed as described previously. The following antibodies were used: CD99-O13 (Covance, Rotterdam, The Netherlands), L-plastin (kindly provided by Dr. A. Huttenlocher), secondary anti-rabbit Alexa Fluor 488 (Life Technologies Europe), secondary anti-mouse Alexa Fluor 568 (Life Technologies Europe). TUNEL staining was performed using ApopTag Peroxidase in situ apoptosis detection kit (Merck-Millipore, Amsterdam, The Netherlands) and TSA-Plus Fluorescein system (Perkin-Elmer, Groningen, The Netherlands).

Statistical Analysis

A one-way ANOVA test with a Dunnet's post-test, or unpaired t-test was utilized to determine the *in vivo* drug treatment effects. All statistical tests were two-sided. Values were expressed as means with 95% confidence intervals. P-values less than 0.05 were considered statistically significant. Statistical analyses were performed using GraphPad Prism software V4 (GraphPad Software Inc, La Jolla, CA).

Results

Kinetics in EWS cell proliferation and migration differ between blastula and larval xenograft models

Zebrafish xenograft models for cancer are largely carried out in 2 days post-fertilisation (2 dpf) embryos by engrafting the cells in the yolk. Previously, we have described a 2 dpf zebrafish xenograft model for EWS, looking at proliferation and migration of EWS cells, as well as their interaction with the host. In order to adapt this xenograft model for high-throughput applications such as anti-cancer drug screenings, it is desirable that embryos engrafted with cancer cells are generated in an automated manner. Currently, automated injection systems for zebrafish are designed to inject embryos at early stages (up to 4 hours post-implantation (hpf)), as these are most easily handled and manipulated. In initial experiments, we sought to investigate how the blastula xenograft model compared to the 2 dpf xenograft model. TC32 EWS cells were manually implanted into the yolk of either 2 dpf (Figure 1A) or 2-4 hpf embryos (Figure 1B). From 4 days post-implantation (dpi), scoring was done of the percentage of embryos that showed 3 or more cells migrating out of the yolk area where cells were initially implanted. An example of migrating cells can be found in Figure 1C. Consistent with previous findings, in the 2 dpf xenograft model EWS cells migrated in subset of embryos from 4 dpi onwards, and migration increased during the course of the experiment (Figure 1D). In the blastula xenograft model, no migrating cells were found until 7 dpi, at which point few (1%) embryos showed migration. At 8 dpi, this percentage increased to 18% (Figure 1E).

Next, we looked at the kinetics of proliferation of EWS cells in the different xenograft models. As shown in Figure 1F and G, at 1 dpi initial tumour cell load per embryo (as determined by counting fluorescent pixels) differed between the two models. This difference is caused at the time of cell implantation: 2 dpf embryos are more robust, and up to 800 cells can be implanted into the yolk. Blastula stage embryos are more fragile, and implanting more than 250 cells per embryos will cause high lethality (data not shown). In kinetics, proliferation between the two models varied. The 2 dpf xenograft model showed an increase of tumour cell burden half-way through the course of the experiment at 3 dpi, which plateaued at 6 dpi. The blastula xenograft model showed an increase

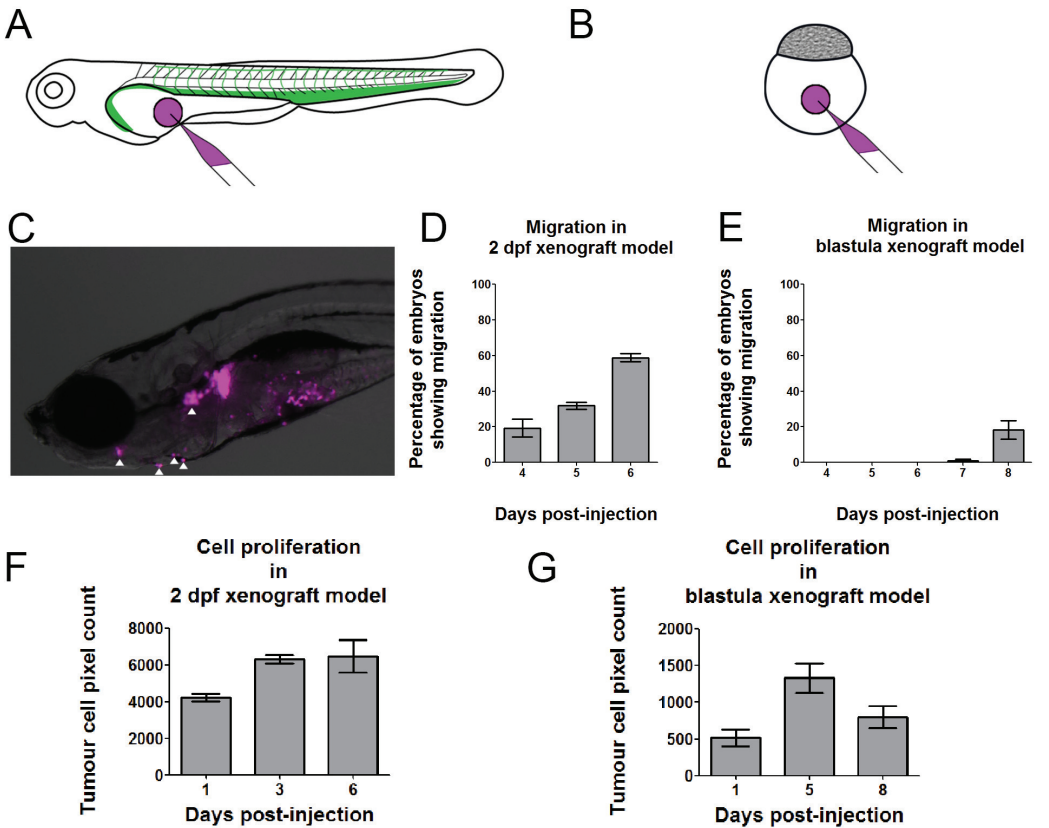


Figure 1. Comparison of 2 dpf and blastula zebrafish xenograft models. **A)** Schematic drawing of cell implantation in the 2 dpf xenograft model. The site of implantation in the yolk of a 2-day-old larva is indicated with a magenta circle. **B)** Schematic drawing of cell implantation in the blastula xenograft model. The site of implantation in the yolk of a 2- to 4-hour-old embryo is indicated with a magenta circle. **C)** Example of a 8 dpf zebrafish larva with migrating EWS cells (magenta; migrating cells indicated with arrowheads). **D)** Percentage of embryos with 3 or more cells migrating away from the site of implantation, from 4 dpi until 6 dpi in the 2 dpf xenograft model. **E)** Percentage of embryos with 3 or more cells migrating away from the site of implantation, from 4 dpi until 8 dpi in the blastula xenograft model. **F)** Tumour cell pixel count, indicative of proliferation, at 1, 3 and 6 dpi in the 2 dpf xenograft model. **G)** Tumour cell pixel count at 1, 5 and 8 dpi in the blastula xenograft model.

of burden half-way through the run of the experiment (5 dpi), and a subsequent reduction of tumour cell burden at the end of the experiment at 8 dpi.

Survival of blastula-stage engrafted EWS cells and interactions with the zebrafish host

In order to see if the cell burden reduction observed at 8 dpi in the blastula model was caused by increased cell death compared to the 2 dpf xenograft model, apoptotic cells were visualised using a whole-mount TUNEL staining (Figure 2A, B). The percentage of apoptotic cells present was tallied at 8 dpf, i.e. 6 dpi in the 2 dpf xenograft model, and 8 dpi in the blastula xenograft model. At this timepoint, both models had comparable percentages of apoptotic EWS cells (20% and 26%, respectively).

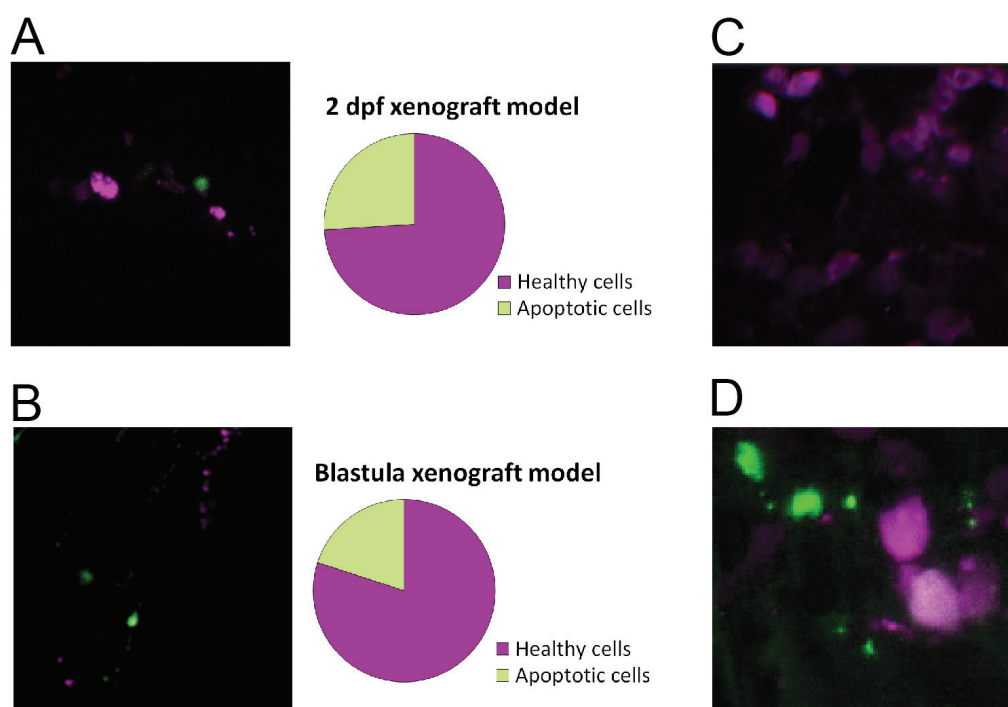


Figure 2. Behaviour of EWS cells in blastula xenograft model . A) Left panel: representative image of whole-mount TUNEL staining of EWS cells in the yolk of an 2 dpf-engrafted embryo, 6 dpi. Healthy cells are seen in magenta, TUNEL-stained apoptotic cells are green. Right panel: Proportion of healthy EWS cells vs apoptotic cells. ($N_{\text{embryos}}=15$). **B)** Left panel: representative image of whole-mount TUNEL staining of EWS cells in the yolk of an blastula stage-engrafted embryo, 8 dpi. Healthy cells are seen in magenta, TUNEL-stained apoptotic cells are green. Right panel: Proportion of healthy EWS cells vs apoptotic cells. ($N_{\text{embryos}}=15$). **C)** Whole-mount immunohistochemical staining of blastula stage-engrafted embryos with CD99, showing implanted EWS cells. **D)** Whole-mount immunohistochemical staining of blastula stage-engrafted embryos with L-Plastin, showing EWS cells (magenta) interacting with leukocytes (green).

In addition to observed cell burden reduction in the blastula, EWS cells also migrated less in this model. A possible explanation of the low amount of migration is reprogramming of EWS cells due to factors within the embryonic environment. Previous research states that loss of CD99 in EWS cell lines reduces their ability to migrate and form metastases.²⁸ We performed an immunohistochemical stain with the EWS marker CD99, which was still present on the cells (Figure 2C).

Cells engrafted in the blastula xenograft model may be taken up by leukocytes present in the host. An L-plastin immunohistochemical staining was performed on 8 dpi larvae, marking leukocytes (Figure 2D). Leukocytes were present near the engrafted EWS cells, and interacted with them. However, uptake was only observed in 2 out of 34 embryos within the experiment.

Optimisation of the blastula injection model for high-throughput robotic injection

While the blastula xenograft model did not result in many embryos with migrating cells in this time course, the data it gives on tumour-cell burden is valuable for investigation of anti-proliferative effects of compounds on EWS. For this, experiments could be run until 5 dpf, 3 days shorter than the previously described in 2 dpf xenotransplant model. For screening purposes, such a rapid initial readout is a benefit. Therefore, we continued investigations on how to automate blastula injections, which resulted in the following method.

Figure 3A shows a schematic representation of the robotic injector developed for the injection of *Mycobacterium marinum*.²¹ Embryos between 2 and 4 hpf are placed on a 1% agarose grid of 512 or 1024 hemispherical well roughly the size of a zebrafish egg, which allows for easy placement of the embryos at regular intervals using a small brush. A picture of an agarose grid with (injected) embryos can be seen in Figure 3B. The agarose grid with embryos is placed on a motorised stage which is computer-controlled. This computer similarly regulates injections parameters such as injection time, pressure, depth and speed. The motorised needle-holder grips glass capillary needles which are loaded with cell suspension, and inject the embryo by moving vertically. The motorised stage will position embryos underneath the needle. A camera underneath this set-up provides means to check of injections are performed correctly during the run.

Right after implantation, embryos with cells implanted in the yolk (Figure 3C) are placed at 28°C for an hour to recover from injection, before being placed at 34°C. The next day, embryos are checked under a fluorescent microscope: correctly implanted embryos (Figure 3D) are separated from non-implanted or incorrectly implanted embryos. Embryos are incorrectly implanted when cells are present in the body of the embryo (Figure 3E) or when cells are implanted in the yolk but simultaneously display a fluorescent glow throughout the yolk (Figure 3F).

The rate of successful implantation is highly dependent on the needle used for implantation. As the needle is mounted vertically in the needle holder, as opposed to the $\sim 45^\circ$ angle used with manual implantation, the cells will sink to the needle opening much faster. This is partially delayed by using high-viscosity 14% PVP to re-suspend cells, but needle-shape proved to be an important factor. Needles commonly used for manual implantation (Figure 3G, left needle) have long-drawn tips which can easily be broken open with tweezers to provide an opening with a small diameter which does minimal damage to the embryo. With

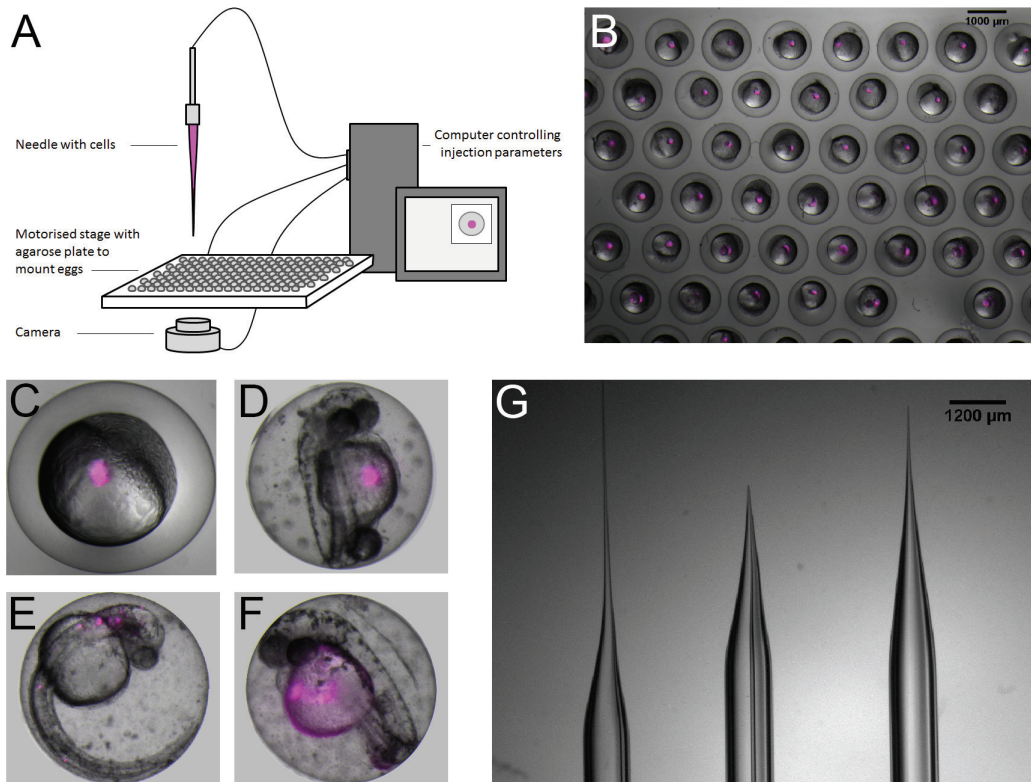


Figure 3. Automated robotic implantation of blastula zebrafish. **A)** Schematic drawing of the automated robotic set-up for cell implantation in the blastula xenograft model. **B)** Part of an agarose grid with zebrafish eggs implanted with EWS cells, immediately after implantation. **C)** Example image of a correctly implanted embryo, 30 minutes after implantation. **D)** Example image of a correctly implanted embryo, 24 hours after implantation, showing EWS cells in the yolk of the embryo. **E)** Example image of an incorrectly implanted embryo, 24 hours after implantation, showing EWS cells in the body of the embryo. **F)** Example image of an embryo, 24 hours after implantation, showing cells EWS cells in the yolk of the embryo, as well as a faint glow throughout the yolk. **G)** Different glass capillary needles used for implantation. Right and middle: closed needles pulled using different programmes of a Harvard Apparatus P-97 Micropipette Puller. Left: Commercially available needle with a 20 µm opening, custom made by Qvotek.

these needles clogging was a common problem, leading to interruptions to the experiment to reload a different needle, or low efficiency of injection. Using needles with a wider tip (Figure 3G, middle needle) reduced clogging, but there was more variation in upon breaking open the needle. Often, these needles had a large opening, which caused more damage to the embryos, and resulted in higher lethality. This could be reduced by opening the needles by grinding the tips down, rather than manually breaking open the needles with tweezers. Best results were achieved with custom-made Qvotek needles with a 20 μm opening (Figure 3G, right needle).

Finally, diligence in culturing conditions, confluence and cell suspension preparation were essential to ensure minimal clogging. After optimisation, a successful-injection percentage of 88% could be reached, with a capacity to inject 1024 embryos in a 30 minute run.

Effects of vincristine and two YK-4-279 enantiomers *in vitro*

To confirm the applicability of the automated robotic injection system for screening large compound libraries, we performed a test with three different compounds. Vincristine is a classic therapeutic agent used in the clinic to treat patients with EWS, often in combination with ifosfamide, doxorubicin and etoposide.^{23,29} YK-4-279 was shown previously to affect EWS growth *in vivo* in both mouse models and the 2 dpf zebrafish xenograft model.^{10,25} Separation of the racemic mixture into an active (S)- and an inactive (R)-enantiomer provides a positive and negative control for testing the model. Before moving to *in vivo* experiments, compounds were tested in culture.

Vincristine treatment of three EWS cells (A673, EW7 and TC32) caused a relative reduction of survival of 50% after 24 hours of treatment (Figure 4A). At this timepoint, with these concentrations, there was no dose-dependent response. TC32 cells were less sensitive to Vincristine treatment than A673 or EW7.

(S)-YK-4-279 reduced the survival of all three cell lines after 24 hours of treatment (Figure 4B). While a concentration of 3 μM (S)-YK-4-279 decreased EWS cell survival more than 1 μM , no difference was observed between concentrations of 3 μM or 30 μM at this timepoint. No effect on cell survival was observed after 24 hours of treatment with (R)-YK-4-279 (Figure 4C).

Cell culture experiments confirmed sensitivity of the three EWS cell lines to Vincristine and (S)-YK-4-279, whilst not being affected by (R)-YK-4-279.

Effects of Vincristine and two YK-4-279 enantiomers *in vivo*

Before applying compounds to the treatment of embryos engrafted with EWS cells, toxicity of these compounds to zebrafish embryo needed to be established. Treatment of embryos was started 1 dpf, when the embryo had undergone gastrulation, and segmentation. Results of these toxicity tests on non-injected wild-type embryos can be found in Figure

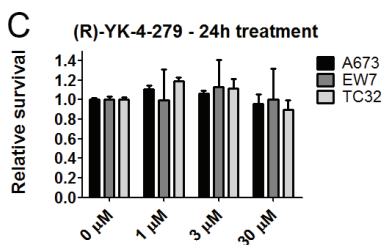
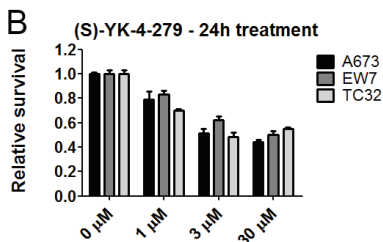
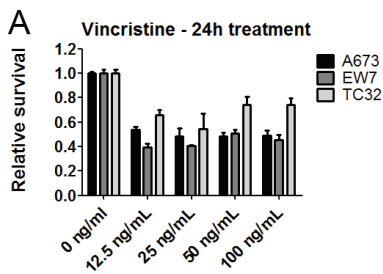


Figure 4. The effect of Vincristine and YK-4-279 enantiomers on EWS cells *in vitro*.

WST-1 colourimetric assay for measuring relative survival of A673, EW7 and TC32 cells treated for 24 hours with **(A)** Vincristine, **(B)** (S)-YK-4-279 or **(C)** (R)-YK-4-279. All measurements were performed in triplicates. Error bars represent SEM.

5. Both Vincristine and (S)-YK-4-279 caused lethality in over 80% of fish at the highest tested concentration (1 µg/mL and 5µM, respectively). Final concentrations to be used for treatment of the engrafted embryos were chosen to allow >80% survival of embryos in the case of Vincristine (i.e. 0.5 µg/mL) and (S)-YK-4-279 (i.e. 3 µM). The concentration of (R)-YK-4-279 was chosen to be equal to the (S)-YK-4-279 enantiomer. After implantation with A673, EW7 or TC32 cells in blastula-stage embryos, treatment with Vincristine or YK-4-279 enantiomers was started at 1 dpi. At 5 dpi, quantitative analysis as previously described²⁷ was performed on confocal images, providing information on the amount and size of tumour cell foci per embryo. Tumour burden (as obtained by the cumulative area of tumour foci) in treated groups was plotted relative to the DMSO control group in Figure 6.

Vincristine treatment of EWS cells in the xenograft transplantation model could significantly reduce tumour cell burden in embryo for all three EWS cell lines (Figure 6A-C). The mean reduction of tumour burden (MR) was highest in embryos engrafted with EW7 cells: 49%, with a 95% confidence interval (CI) of 30%-67% ($p < 0.001$). MR was the lowest in the A673-engrafted group (MR=28%, CI=6%-50%, $p < 0.01$).

However, while the MR was slightly lower in TC32-engrafted embryos, variance within this group was much higher (MR=30%, CI=0.1%-60%, $p < 0.05$).

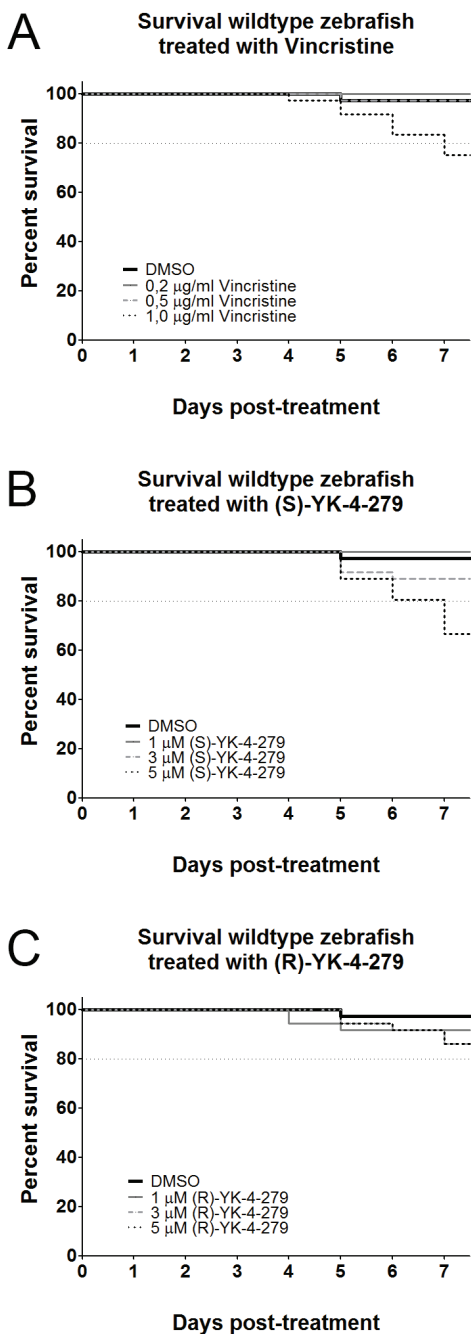


Figure 5. The effect of Vincristine and YK-4-279 enantiomers on zebrafish embryos. Toxicity test of (A) Vincristine, (B) (S)-YK-4-279 or (C) (R)-YK-4-279 on ABTL embryos treated from 1 dpf onwards. Embryos were checked twice daily, and deceased embryos were removed to avoid reduction of water quality. Compounds were refreshed every other day. $N \geq 36$ per condition.

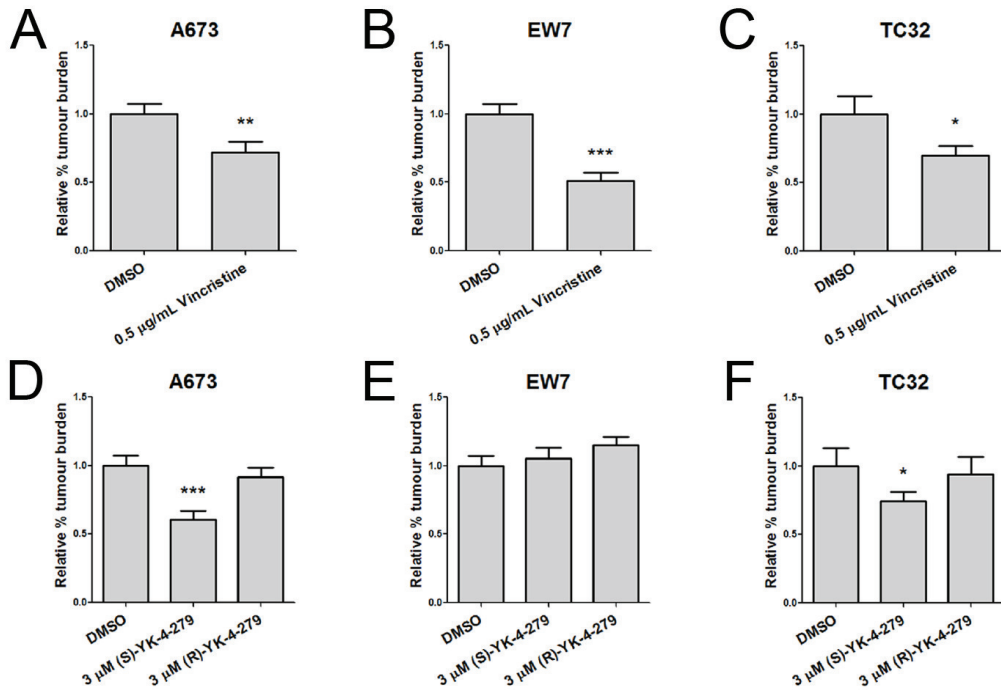


Figure 6. The effect of Vincristine and YK-4-279 enantiomers on EWS cells *in vivo*. **A-C)** Tumour burden of EWS cells in (robotic) blastula injected embryos at 5dpi, treated with 0.5 µg/mL Vincristine, 1-5 dpi, normalized against DMSO. **D-E)** Tumour burden of EWS cells in embryos, treated with 3 µM (S)-YK-4-279 or 3 µM (R)-YK-4-279, 5 dpi, normalized against DMSO. Differences between means were obtained by an unpaired t-test, or one-way analysis of variance (ANOVA) with a Tukey post-test. One star indicates a P-value < 0.05; two stars indicate a P-value < 0.01; three stars indicate a P-value < 0.001; no star indicates no significant difference with the DMSO control. Error bars represent standard error of the mean.

Treatment of engrafted embryos with the two enantiomers of YK-4-279 yielded a more varied response for the different EWS cell lines (Figure 6B). (R)-YK-4-279 did not induce a reduction of tumour burden in any of the groups, as expected based in previous research and *in vitro* tests. A673 engrafted embryos had the highest reduction of tumour cell burden (MR=39%, CI=21%-56%, $p < 0.001$). Reduction was less pronounced in the TC32 engrafted group (MR=25%, CI=3%-55%, $p < 0.05$). Treatment of EW7 with (S)-YK-4-279 did not elicit any response in terms of reduction of tumour cell burden in these experiments. It was previously shown that in the 2-day-old engraftment model a racemic mixture of YK-4-279 was able to inhibit proliferation of this cell line *in*

vivo. Difference may in part be explained by differences in treatment timespan.

These *in vivo* results largely recapitulated results previously found in culture, or what is known from literature and clinical data. We show that the model is suited to test the efficacy of multiple compounds on different EWS cells *in vivo* in a relatively short time.

Discussion

In this study, we investigated the possibility to develop an automated robotic injection system for engrafting Ewing sarcoma cells into blastula-stage zebrafish embryos. EWS is a malignant bone tumour affecting primarily children and young adults, a quarter of whom will have metastatic disease at the time of diagnosis. Prognostic outlook for these patients is poor, and novel therapeutic strategies are needed to improve event-free survival rate. We propose to employ the automated xenograft zebrafish model described here to facilitate high-throughput drug screenings.

As observed in our experiments with EW7 cells and (S)-YK-4-279, response of tumour cell *in vitro* to certain treatment regimens is not always recapitulated in an *in vivo* model. Responses are more complex as the microenvironment in which the tumour cells reside will also influence tumour cell survival and behaviour. Therefore it is essential to have thorough screening in *in vivo* settings before drugs are considered for clinical trials. The automated robotic implantation system we describe here can aid in speeding up such screenings. Compounds which are shown to be effective against EWS *in vitro* in initial screens can be selected further for their ability to reduce cancer cell malignancy *in vivo* in zebrafish. This way, compounds with the most potential can be further tested in murine models. Such models are costly and time consuming, and reducing the number of compounds with minimal influence *in vivo* will be helpful to get more effective compounds to clinical trials quicker.

While we focus on automated implantation here, more aspects can be considered to fully adapt this system for high-throughput drug screenings. When using large numbers of embryos, as is desirable for screening purposes, manual sorting of embryos correctly implanted embryos, transferring these to well plates and applying compounds can become a vast amount of work. To optimise the high-throughput pipeline, these tasks can be performed using a flow cytometer capable of analyzing, sorting and dispensing live multicellular organisms based on size, optical density and fluorescence intensity. Further optimisation in terms of image acquisition is also needed. Currently, confocal analysis is done in a semi-automated way, which is possible to do with large numbers of embryos, but labour-intensive. A VAST (Vertebrate Automated Screening Technology) BioImager platform developed by Union Biometrica is currently being tested to further automate imaging. This platform can take up embryos from a well plate, send them to a glass capillary mounted over a confocal microscope. By rotating the

capillary, embryos can be imaged in any orientation. This system, in addition to rapidly capturing images of the embryos, may also eject imaged embryos to different well plates, which provides the option to screen tumour cell response at multiple time points.

Screening at multiple time-points will provide more data on the kinetics of tumour cell expansion and migration with the embryonic host. This may be of interest not only for the blastula-stage xenograft model, but also the 2 dpf xenograft model. The latter model provides more information on the migration capabilities of the EWS cells, for which the blastula model is not well-suited. In the future, data on effective compounds discerned in initial large-scale screening in the blastula model can be augmented with data on effects on migration from the 2 dpf model. Furthermore, it should be noted that one drug on its own may not be sufficiently effective in curing EWS. As patients of this tumour are primarily children and young adults, it is imperative to have a complete curative effect as a goal, lest relapses occur later in life. Therefore, the effect of a combination of compounds with different targets is important to investigate, as well as their effects over a longer period of time.

In conclusion, here we describe the benefits of the blastula zebrafish xenograft model for the purpose of high-throughput anti-EWS drug screening applications. We show the applicability of this model for compound screening by applying Vincristine and two YK-4-279 enantiomers on 3 different EWS cell lines. Promising initial results certify further expansion of this model for the benefit of Ewing sarcoma research.

Acknowledgements

The authors would like to thank W. Veneman, A. Digenarro and A. Groenewoud for helpful discussions regarding the manuscript.

References

- 1 de Alava, E., Lessnick, S. L. & Sorensen, P. H. in WHO classification of tumours of soft tissue and bone (eds C.D.M Fletcher, J. A. Bridge, P.C.W. Hogendoorn, & F. Mertens) p. 305-309 (IARC Press, 2013)
- 2 Pizzo, P. A. & Poplack, D. G. *Principles and practice of pediatric oncology*. 6th edn, (Wolters Kluwer Health/Lippincott Williams & Wilkins, 2011).
- 3 Langenau, D. M. *et al.* Myc-induced T cell leukemia in transgenic zebrafish. *Science* **299**, 887-890, doi:10.1126/science.1080280 (2003).
- 4 Patton, E. E. *et al.* BRAF mutations are sufficient to promote nevi formation and cooperate with p53 in the genesis of melanoma. *Curr Biol* **15**, 249-254, doi:10.1016/j.cub.2005.01.031 (2005).

- 5 Santoriello, C. *et al.* Kita driven expression of oncogenic HRAS leads to early onset and highly penetrant melanoma in zebrafish. *PLoS One* **5**, e15170, doi:10.1371/journal.pone.0015170 (2010).
- 6 Lee, L. M., Seftor, E. A., Bonde, G., Cornell, R. A. & Hendrix, M. J. The fate of human malignant melanoma cells transplanted into zebrafish embryos: assessment of migration and cell division in the absence of tumor formation. *Developmental dynamics : an official publication of the American Association of Anatomists* **233**, 1560-1570, doi:10.1002/dvdy.20471 (2005).
- 7 Nicoli, S., Ribatti, D., Cotelli, F. & Presta, M. Mammalian tumor xenografts induce neovascularization in zebrafish embryos. *Cancer Res* **67**, 2927-2931, doi:10.1158/0008-5472.CAN-06-4268 (2007).
- 8 Embree, L. J., Azuma, M. & Hickstein, D. D. Ewing sarcoma fusion protein EWSR1/FLI1 interacts with EWSR1 leading to mitotic defects in zebrafish embryos and human cell lines. *Cancer Res* **69**, 4363-4371, doi:10.1158/0008-5472.CAN-08-3229 (2009).
- 9 Leacock, S. W. *et al.* A zebrafish transgenic model of Ewing's sarcoma reveals conserved mediators of EWS-FLI1 tumorigenesis. *Dis Model Mech* **5**, 95-106, doi:10.1242/dmm.007401 (2012).
- 10 van der Ent, W. *et al.* Ewing sarcoma inhibition by disruption of EWSR1-FLI1 transcriptional activity and reactivation of p53. *J Pathol* **233**, 415-424, doi:10.1002/path.4378 (2014).
- 11 Peterson, R. T., Link, B. A., Dowling, J. E. & Schreiber, S. L. Small molecule developmental screens reveal the logic and timing of vertebrate development. *Proc Natl Acad Sci U S A* **97**, 12965-12969, doi:10.1073/pnas.97.24.12965 (2000).
- 12 Van Leeuwen, C. J., Grootelaar, E. M. & Niebeek, G. Fish embryos as teratogenicity screens: a comparison of embryotoxicity between fish and birds. *Ecotoxicol Environ Saf* **20**, 42-52 (1990).
- 13 Wang, X. *et al.* Inhibitors of neutrophil recruitment identified using transgenic zebrafish to screen a natural product library. *Dis Model Mech* **7**, 163-169, doi:10.1242/dmm.012047 (2014).
- 14 Ridges, S. *et al.* Zebrafish screen identifies novel compound with selective toxicity against leukemia. *Blood* **119**, 5621-5631, doi:10.1182/blood-2011-12-398818 (2012).
- 15 White, R. M. *et al.* DHODH modulates transcriptional elongation in the neural crest and melanoma. *Nature* **471**, 518-522, doi:10.1038/nature09882 (2011).
- 16 White, R., Rose, K. & Zon, L. Zebrafish cancer: the state of the art and the path forward. *Nat Rev Cancer* **13**, 624-636, doi:10.1038/nrc3589 (2013).
- 17 Astin, J. W. *et al.* An in vivo anti-lymphatic screen in zebrafish identifies novel inhibitors of mammalian lymphangiogenesis and lymphatic-mediated metastasis. *Mol Cancer Ther*, doi:10.1158/1535-7163.MCT-14-0469-T (2014).
- 18 Terriente, J. & Pujades, C. Use of zebrafish embryos for small molecule screening related to cancer. *Dev Dyn* **242**, 97-107, doi:10.1002/dvdy.23912 (2013).

- 19 Ma, Y. *et al.* The relationship between early embryo development and tumourigenesis. *J Cell Mol Med* **14**, 2697-2701, doi:10.1111/j.1582-4934.2010.01191.x (2010).
- 20 Wang, W., Liu, X., Gelinas, D., Ciruna, B. & Sun, Y. A fully automated robotic system for microinjection of zebrafish embryos. *PLoS One* **2**, e862, doi:10.1371/journal.pone.0000862 (2007).
- 21 Carvalho, R. *et al.* A high-throughput screen for tuberculosis progression. *PLoS One* **6**, e16779, doi:10.1371/journal.pone.0016779 (2011).
- 22 Spaink, H. P. *et al.* Robotic injection of zebrafish embryos for high-throughput screening in disease models. *Methods* **62**, 246-254, doi:10.1016/j.ymeth.2013.06.002 (2013).
- 23 Juergens, C. *et al.* Safety assessment of intensive induction with vincristine, ifosfamide, doxorubicin, and etoposide (VIDE) in the treatment of Ewing tumors in the EURO-E.W.I.N.G. 99 clinical trial. *Pediatr Blood Cancer* **47**, 22-29, doi:10.1002/pbc.20820 (2006).
- 24 Himes, R. H., Kersey, R. N., Heller-Bettinger, I. & Samson, F. E. Action of the vinca alkaloids vincristine, vinblastine, and desacetyl vinblastine amide on microtubules in vitro. *Cancer Res* **36**, 3798-3802 (1976).
- 25 Erkizan, H. V. *et al.* A small molecule blocking oncogenic protein EWS-FLI1 interaction with RNA helicase A inhibits growth of Ewing's sarcoma. *Nat Med* **15**, 750-756, doi:10.1038/nm.1983 (2009).
- 26 Barber-Rotenberg, J. S. *et al.* Single enantiomer of YK-4-279 demonstrates specificity in targeting the oncogene EWS-FLI1. *Oncotarget* **3**, 172-182 (2012).
- 27 Ghotra, V. P. *et al.* Automated whole animal bio-imaging assay for human cancer dissemination. *PLoS One* **7**, e31281, doi:10.1371/journal.pone.0031281 (2012).
- 28 Rocchi, A. *et al.* CD99 inhibits neural differentiation of human Ewing sarcoma cells and thereby contributes to oncogenesis. *J Clin Invest* **120**, 668-680, doi:10.1172/JCI36667 (2010).
- 29 Ladenstein, R. *et al.* Primary disseminated multifocal Ewing sarcoma: results of the Euro-EWING 99 trial. *Journal of clinical oncology : official journal of the American Society of Clinical Oncology* **28**, 3284-3291, doi:10.1200/JCO.2009.22.9864 (2010).

Chapter 7

A versatile transgenic zebrafish model recapitulates genetic and histological features of Ewing sarcoma

Abstract

Ewing sarcoma, a highly malignant bone and soft-tissue tumour, is characterized by the presence of a translocation between *EWSR1* and a member of the ETS family of genes, most commonly *FLI1* or *ERG*. Despite knowledge of this key feature of Ewing sarcoma, so far no transgenic mouse models have been established that can accurately recapitulate this disease. The exact cell of origin for Ewing sarcoma is unknown, confounding which promoter is suitable to drive the expression of *EWSR1-ETS*. Thus far, attempts to make a murine model have led to embryonic death. Here, we have generated a zebrafish transgenic model for Ewing sarcoma, where expression of GFP-tagged *EWSR1-ERG* protein is driven by a Gal4-responsive UAS promoter. By crossing *TG(14xUAS:GFP-EWSR1-ERG)* fish with different transgenic driver lines expressing Gal4 by various tissue-specific promoters, we observed that neuronal cells are more permissive of *EWSR1-ERG* expression than cells in the notochord or muscles of the fish. Histology shows that these cells in the zebrafish larvae have round nuclei and scant cytoplasm, and bear a resemblance to cell features of human EWS tumour biopsies. Using next generation sequencing of embryos with neuronally expressed *EWSR1-ERG*, we validate how the zebrafish genes regulated in these embryos by the human oncogene compare to a previously described core *EWSR1-FLI1*-regulated gene set. The zebrafish *TG(14xUAS:GFP-EWSR1-ERG)* line provides a flexible method to investigate the effects of *EWSR1-ERG* expression in different background tissues and it is a promising tool to study processes involved in Ewing sarcoma development and testing potential treatments.

Keywords: Ewing sarcoma, transgenic animal model, zebrafish, gene expression profiling, oncogenic transformation

Introduction

Ewing sarcoma (EWS), the second most common bone sarcoma found primarily in children and young adults, is characterized by a reciprocal translocation between *EWSR1* and genes from the ETS family.¹ The resultant chimeric protein has strong transcriptional activity.² Additionally, it interacts with other transcription factors, causing further transcriptional deregulation.²⁻⁵ In 85% of all EWS cases, a t(11;22)(q24;q12) chromosomal location is found, which results in the oncogenic fusion gene *EWSR1-FLI1*.⁶ Another 10% of cases has an *EWSR1-ERG* fusion gene with t(21;22)(q22;q12) translocation.^{7,8} Gain of 1q, as well as alterations of *TP53* and *CDKN2A/CDKN2B* (p16), have been described to be correlated with an unfavourable prognosis.⁹⁻¹²

A quarter of EWS patients present with metastasis at the time of diagnosis¹³, and have a 2-year event-free survival of 20%.¹⁴ The 5-year event-free survival is 10% in case of recurrence.¹⁵ Finding more effective

treatments for these patients is needed, and in addition to established *in vitro* and xenotransplantation models, a transgenic animal model would be desirable for studying the mechanism of action of the chimeric protein *in vivo*, which potentially can lead to novel treatment regimes.

Despite knowing the genetic aberration responsible for driving oncogenesis of EWS, thus far no transgenic murine models have been established. A major issue hampering the development of a transgenic animal model for EWS is its elusive cell of origin, and toxicity of EWSR1-ETS to most normal cells. Stable expression of exogenous *EWSR1-FLI1* in cells *in vitro* has caused apoptosis or senescence in most normal cells, and many of such models depend on additional cellular modifications to tolerate expression of the chimeric protein.¹⁶⁻¹⁸ To date, only mesenchymal stem cells have been found to tolerate EWSR1-ETS expression and take on features of EWS.^{19,20} While this knowledge points to a mesenchymal origin of EWS, and can aid in finding suitable tissues to express the oncogene, all attempts at establishing transgenic mouse models have until now been unsuccessful. Similar to *in vitro* toxicity, expression of exogenous EWSR1-FLI1 in one murine model resulted in embryonic lethality.²¹ In another mouse model there was development of leukemia, but no formation of tumours resembling EWS.²²

In zebrafish, transient expression of human or zebrafish EWSR1-FLI1 led to mitotic defects in the developing embryo.²³ A stable transgenic zebrafish line with expression of EWSR1-FLI1 developed solid tumours with histologic features of small round blue cell tumours in a p53^{-/-} background.²⁴ This confirms that zebrafish provides a suitable background to research the role of EWSR1-FLI1 in tumour formation. However, this model simultaneously gives rise to malignant peripheral nerve sheet tumours, and tumours histologically similar to EWS are found in <10% of fish. Additionally, p53 mutations are found in only 10% of EWS patients²⁵, so further optimization is needed to mimic the situation in patients more closely.

To circumvent the problem of embryonic lethality upon expression of EWSR1-FLI1, we used the Gal4/UAS binary system to drive expression of the oncogene in zebrafish.²⁶ In this system, the gene of interest is placed under control of a UAS promoter, which becomes activated only in the presence of Gal4 element, expressed in transgenic lines under different promoters. Therefore, by placing *EWSR1-ETS* genes under control of the UAS promoter and introducing this construct into the germline, there will be no transcription of the gene until the transgenic fish is crossed with another fish line expressing Gal4. Simultaneously, the binary system provides a greater flexibility in expression than placing the gene of interest directly under a promoter. Crossing the UAS line with different Gal4 driver lines will allow expression at specific times and in specific tissues. This is an attractive feature for Ewing sarcoma research, considering the exact cell of origin for this cancer is, as of yet, unknown.

In this study, we show the transforming capabilities of human

EWSR1-FLI1 and EWSR1-ERG transiently expressed in zebrafish embryonic stages, and describe the establishment of *TG(UAS:GFP-EWSR1-ERG)*, a stable transgenic line to model EWS. Using different driver lines, we explore possible tissue tolerances to EWSR1-ERG expression. Expression in the notochord and muscle cells was mostly lost after 24 hours, but expression in the neurons of embryos was tolerated until at least 4 days post-fertilisation (dpf). Next generation sequencing and quantitative PCR showed that EWSR1-ERG regulated genes involved in cell structure, motility, proliferation and differentiation. Overlap between the zebrafish up- and down-regulated gene set and a core EWSR1-FLI1 regulated gene set was found. Furthermore, we explore possible routes of investigation for novel treatment regimes in zebrafish transgenic model

Materials and Methods

Zebrafish husbandry

Zebrafish lines were handled compliant to local animal welfare regulations and maintained according to standard protocols (www.ZFIN.org). During experiments, embryos were maintained in eggwater (60µg/ml Instant Ocean salts in demiwater) at 28.5°C and, when needed, anaesthetized with 0.001% tricaine (Sigma-Aldrich, St. Louis, MO). For wildtype fish, the standard laboratory strain AB/TL was used. The *Et(E1b:Gal4-VP16)s1101t, TG(UAS:Kaede)s1999t* line was generated in an enhancer trap screen described by Scott *et al.*²⁷ The *Et(kita:GalTA4,UAS:mCherry)hzm1* line was generated in an enhancer trap screen described by Distel *et al.*²⁸ The *TG(hsp70l:GAL4)1.5kca4* line was previously described by Scheer *et al.*²⁹ The *TG(14xUAS:GFP-EWSR1-ERG)* was newly generated in this study. Generation of novel transgenic zebrafish was approved by the animal care committee of the Leiden University Medical Center (UDEEC1135).

Generation of the *TG(UAS:GFP-EWSR1-ETS)* expression vectors

The coding sequence for GFP-EWSR1-FLI1 and GFP-EWSR1-ERG were amplified out of the pDEST225+GFP-EWSR1-FLI1 and pDEST225+GFP-EWSR1-ERG plasmids. The 5'-TCACAATTGGCAGAGCTGGTTTGTAGTGAACCG TC-'3 forward primer introduced an MfeI restriction site at the 5' end of the GFP-EWSR1-ETS ORF, whilst the 5'-TCAGCGGCCGCTCTAGATCCGGTGGATCA TCACCAC-3' reverse primer introduced a NotI at the 3' end. The resultant amplicon was cloned into the 14xUAS E1b Tol2 transposon-based vector (kindly provided by Prof. Dr. H. Baier, Max Planck Institute of Neurobiology, Martinsried, Germany).

Generation of *TG(UAS:GFP-EWS-ETS)* transgenic zebrafish lines

Tol2 transposase mRNA was generated by using a linearized pCS2FA-

transposase plasmid (kindly provided by Prof. Dr. K. Kawakami, National Institute of Genetics, Shizuoka, Japan)³⁰ as a template for mRNA synthesis with the mMESSAGING mMACHINE SP6 transcription kit (Life Technologies, Carlsbad, CA). mRNA was purified using the RNeasy MinElute Cleanup kit (Qiagen, Venlo, The Netherlands). The UAS:GFP-EWSR1-FLI1 or UAS:GFP-EWSR1-ERG construct (final concentration: 30ng/μl) was mixed with transposase mRNA (final concentration: 50ng/μl), phenol red (0.05%) and 1xDanieu's buffer (58mM NaCl, 0.7mM KCl, 0.4mM MgSO₄, 0.6mM Ca(NO₃)₂, 5mM Hepes, pH 7.6). Of this mixture, 1nl was injected into the cell of eggs at the 1-cell stage. Injected embryos were raised to adulthood, and F0 founders were identified by genotyping 24 hpf offspring via PCR. F1 fish and subsequent generations were genotyped by PCR on finclips. For genotyping, DNA was amplified using forward primer 5'-GTCTCAGCCTCACTTTGAGC-3' and reverse primer 5'-AGATGAACTTCAGGGTCAGC -3'.

Zebrafish embryonic heatshock

The transgenic *TG(hsp70l:GAL4)1.5kca4* and *TG(14xUAS:GFP-EWSR1-ERG)* lines were crossed, and their offspring were heatshocked at 6 hpf or 1 dpf for 2.5 hours by transferring them to eggwater prewarmed to 37°C, in a 37°C incubator. The next day, heatshocked embryos were checked for expression of GFP.

Histology

Embryos of *TG(14xUAS:GFP-EWSR1-ERG)* x *Et(E1b:Gal4-VP16)s1101t*, *TG(UAS:Kaede)s1999t* were fixed at 1 dpf with 4% paraformaldehyde (PFA) for 2 hours at room temperature. After 3 rinses with PBS-T (PBS containing 0.1% Tween-20), embryos were gradually dehydrated by sequential 30 min incubations in 70%, 80%, 90%, 98% and 100% MeOH. Embryos were then embedded in paraffin blocks and cut into 2μM sections. Sections were stained with H&E and analysed on histologic features of EWS.

RNA isolation

RNA isolation was performed by homogenizing 15 embryos per sample, using a Bullet Blender Homogenizer (Next Advance, Averill Park, NY), and subsequently extracting RNA using the RNeasy Micro Kit (Qiagen) according to the manufacturer's instructions.

RNAseq analysis

RNA samples of 3 dpf *TG(14xUAS:GFP-EWSR1-ERG)* x *Et(E1b:Gal4-VP16)s1101t*, *TG(UAS:Kaede) s1999t* and wildtype siblings were sequenced by ZF-Screens BV (Leiden, The Netherlands) on an Illumina HiSeq2500. Resulting FastQ files were uploaded on the GeneTiles website (www.genetiles.com). The GeneTiles software aligned reads to the ENSEMBL Zv9 zebrafish genome predicted cDNA sequences, and

uses DESeq to normalize the data and analyse differential expression between samples. The complete dataset has been deposited in NCBI's Gene Expression Omnibus and are accessible through GEO Series accession number GSE62273.

Information on enrichment was obtained by first converting zebrafish ENSEMBL gene IDs to human ENSEMBL gene IDs. These lists were uploaded on Database for Annotation, Visualization and Integrated Discovery (DAVID) v6.7.^{31,32}

cDNA synthesis and quantitative reverse transcriptase PCR (q-RT-PCR)

Complementary DNA synthesis from RNA samples of 3 dpf *TG(UAS:GFP-EWSR1-ERG)* x *TG(S1101T:Gal4;UAS:Kaede)* and wildtype siblings was achieved by combining 1 µg of RNA with 4 µL of 5x iScript reaction mix and 1 µL iScript reverse transcriptase (Bio-Rad Laboratories, Hercules, CA) in a total volume of 20 µL. These mixtures were incubated at 25°C for 5 min, 42°C for 30 min, and 85°C for 5 min, and diluted 1:25 in water. For each q-RT-PCR reaction, 5 µL of cDNA was mixed with 12.5 µL of 2x iQ SYBR Green Supermix (Bio-Rad Laboratories) and 10 pmol of each primer, in a total volume of 25 µL. In a iCycler Thermal Cycler (Bio-Rad Laboratories), samples underwent the following cycling parameters: 95°C for 3 min, followed by 40 cycles of denaturation at 95°C for 15 s and annealing/extension at 60°C for 45 s, followed by 1 min at 95°C and melting curve generation by 10 s at 55°C to 95°C, the temperature increasing with 0.5°C increments over 80 cycles. Fluorescence measurements were taken at the end of each cycle. Normalisation was done against the *β-actin* housekeeping gene, and results were analysed using the $\Delta\Delta C_t$ method.

Sequences for forward and reverse primers are given in Supplementary Table 1.

Statistical analysis

Statistical analysis was performed on q-RT-PCR data using a unpaired t-test. P values less than 0.05 were considered statistically significant, and are indicated with one star (*). P values less than 0.01 were indicated with two stars (**). Statistical analyses were performed using GraphPad Prism V4 (GraphPad, La Jolla, CA).

Results

Transient expression of human EWSR1-ETS in zebrafish embryos leads to oncogenic transformation

In order to establish a Ewing sarcoma (EWS) transgenic model, initial experiments sought to determine whether the introduction of the human translocation genes could result in oncogenic transformation in zebrafish

embryos. To test this, constructs bearing human *EWSR1-FLI1* or *EWSR1-ERG* with a GFP fluorescent tag, driven by a CMV ubiquitous promoter, were injected into 1- to 8-cell stage embryos (Figure 1A). At 6 hpf, GFP-positive cells could be found among the cell mass for both constructs (Figure 1B shows an *GFP-EWSR1-ERG* injected embryo). At 1dpf, similarly, mosaic expression of both constructs was observed, with transformed cells located in the head, trunk or tail (Figure 1C, 1D). At 3dpf, whilst some embryos had lost the fluorescent cells, others maintained expression in clusters of GFP positive cells (Figure 1E), perhaps owing to a more permissive cellular background. Higher magnification microscopy showed that some cells expressing *EWSR1-ERG* underwent division, whilst others showed membrane blebbing, indicating the onset of apoptosis (Figure 1F). Embryos were followed up to 5 dpf, at which point only few clusters of GFP positive cells remained.

Neuronal tissue is permissive for *EWSR1-ERG* expression

Using the Tol2 transposon principle (Figure 2) we generated a stable transgenic line, *TG(14xUAS:GFP-EWSR1-ERG)*; unfortunately our efforts to generate an *UAS:GFP-EWSR1-FLI1* were not successful. Further experiments were carried out with progeny of the *TG(14xUAS:GFP-EWSR1-ERG)* line, which will be referred to as UAS:EWS-ERG.

To determine which Gal4 driver line was suitable to investigate the zebrafish EWS model further, crosses with different Gal4 driver lines were performed. First was UAS:EWS-ERG was crossed with *TG(hsp70l:GAL4)1.5kca4*, a line in which Gal4 expression is driven by the heatshock protein 70 promoter (*hsp70*). *Hsp70* is normally expressed in the lens of developing embryos, but will be expressed throughout the embryo after heatshock at 37°C. Offspring from *TG(hsp70l:GAL4)1.5kca4* x UAS:EWS-ERG were given a heatshock at 6 hpf or 1 dpf. Heatshock at 6hpf resulted in expression of GFP- EWS-ERG in the yolk and part of the muscle cells of the embryos (Figure 3A, bottom left panel) at 24 hours post-heatshock (hph). In addition, muscles and notochord were poorly defined in these embryos compared to heatshocked control embryos (Figure 3A, upper middle panel). Fluorescence in these embryos was lost 48 hph, while abnormal muscle structure remained (Figure 3A, bottom middle panel).

Crossing UAS:EWS-ERG with *Et(kita:GalTA4,UAS:mCherry)hzm1* (hereafter referred to as *kita:Gal4*) produced offspring that expressed GFP-EWS-ERG primarily in cells along the notochord of the fish (Figure 3B, upper right and bottom left panel). In all embryos, expression of GFP present at 1 dpf was reduced at 3dpf (Figure 3B, bottom middle panel), and completely lost at 4 dpf (data not shown). As loss of fluorescence may be due to cell death, attempts to prevent this were made by injecting a morpholino against *TP53*. *TP53* knockdown can reduce cell death in zebrafish³³, but did not avert loss of fluorescent cells in these embryos (Figure 3B, bottom right panel).

Finally, UAS:EWS-ERG fish were crossed with *Et(E1b:Gal4-*

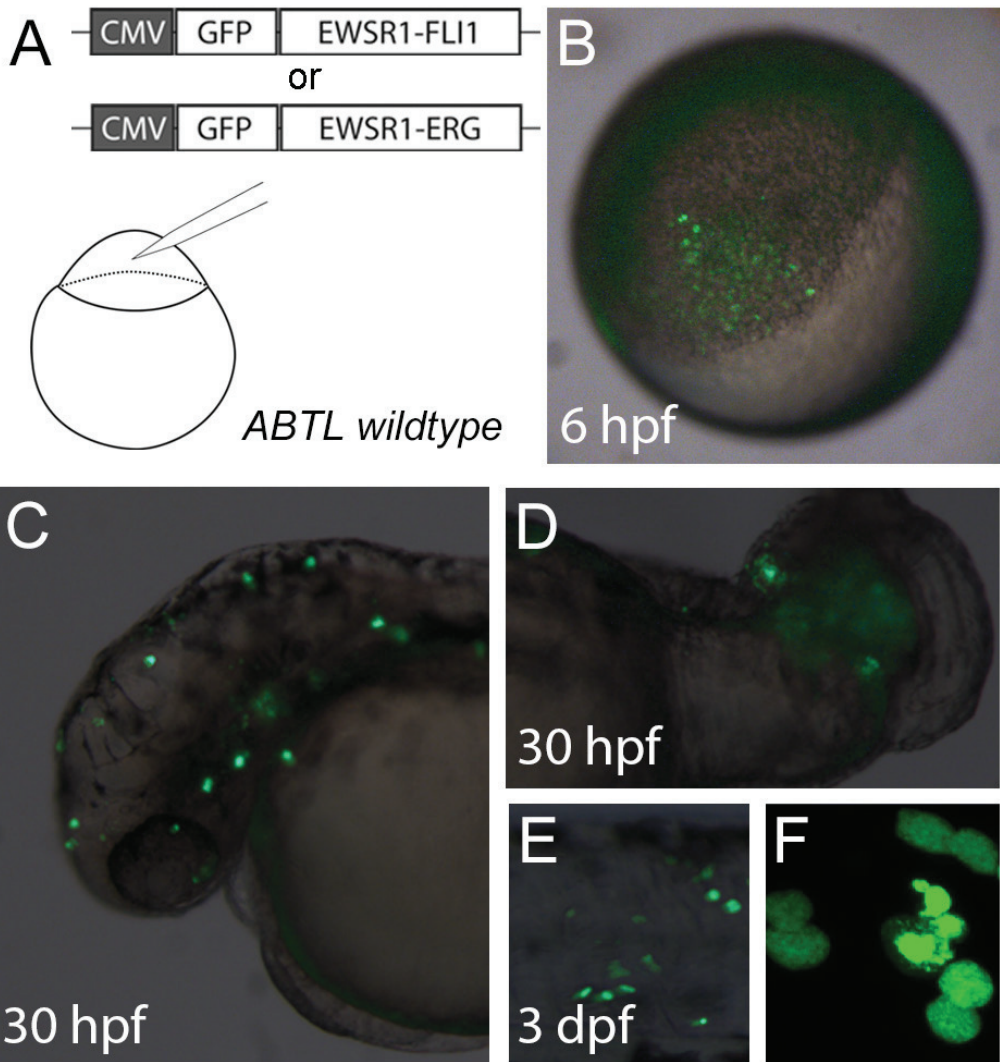


Figure 1. Transient expression of human EWSR1-ERG in zebrafish. **A)** Schematic of CMV:GFP-EWSR1-ETS constructs injected in to 1- to 8-cell stage wildtype embryos. **B)** Mosaic expression of GFP-EWSR1-ERG in a 6 hpf embryo. **C)** Mosaic expression of GFP-EWSR1-ERG in the head of a 30 hpf embryo. **D)** Mosaic expression of GFP-EWSR1-ERG in the tail of a 30 hpf embryo. **E)** Mosaic expression of GFP-EWSR1-ERG in the trunk of a 3 dpf embryo. Panels B-E are stereo microscopy images, original magnification: 20x **F)** Confocal image (original magnification: 60x) of dividing cells, and an apoptotic cell expressing GFP-EWSR1-ERG. Transient expression of EWSR1-FLI1 gave similar phenotypes (data not shown).

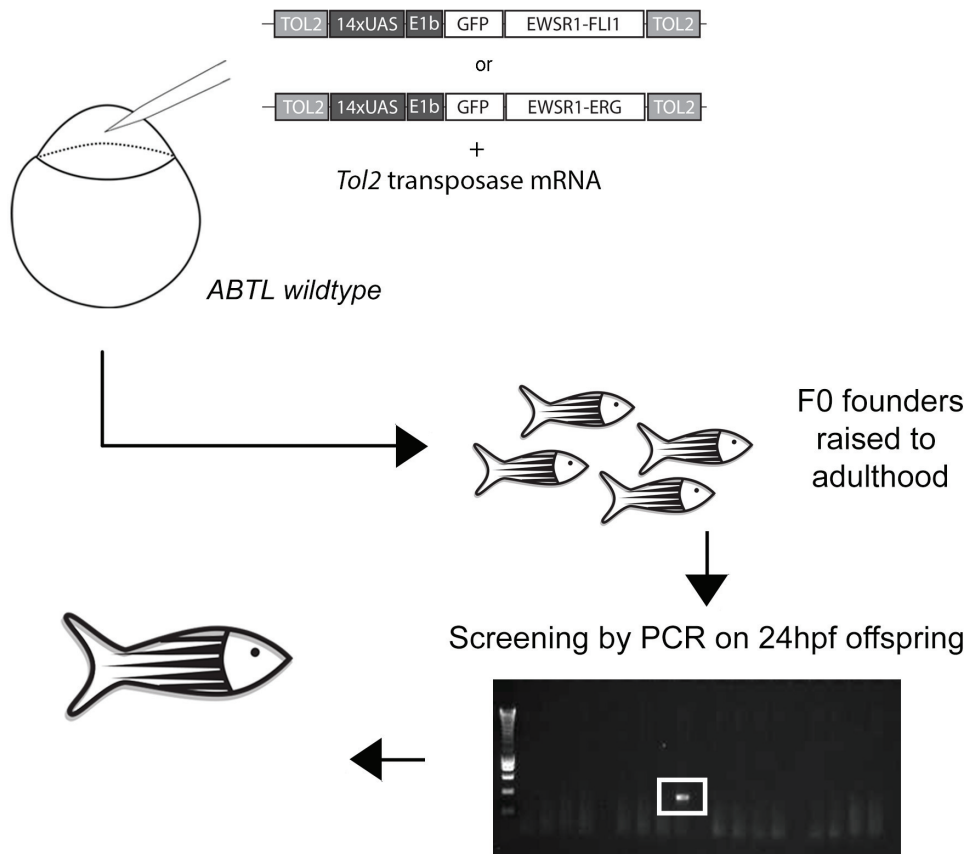


Figure 2. Generation of transgenic zebrafish Ewing sarcoma model. ABTL wildtype embryos were injected in the cell at 1-cell-stage with a mixture of a 14xUAS E1b Tol2-transposon-based DNA construct (containing either GFP-EWSR1-FLI1 or GFP-EWSR1-ERG) and Tol2 transposase mRNA. Injected embryos were raised to adulthood, and a PCR reaction on DNA isolated from their 24hpf was performed to confirm the insertion of the construct into the germline of F0 founder fish. This way, a F0 founder was found bearing the GFP-EWS-ERG construct, which we named *TG(UAS:GFP-EWSR1-ERG)*. An F0 founder bearing the GFP-EWS-FLI1 was not found.

VP16)*s1101t*, *TG(UAS:Kaede)s1999t* fish (hereafter referred to as S1101T:Gal4). In the offspring of this cross, expression of GFP-EWS-ERG and Kaede is localised to the neurons of the embryo, as early as 6 hpf (Figure 3C, bottom left panel). At 1 dpf, embryos expressing GFP-EWS-ERG were severely underdeveloped, with expression found throughout the body of the embryo (Figure 3C, middle panel). From the embryos showing this phenotype, embryos expressing the brighter, photo-convertible Kaede were removed, as not to complicate interpretation of the observed expression patterns. After dissociating these embryos, counting fluorescent versus non-fluorescent cells indicated that 40% of the cells were GFP-positive (95% confidence interval: 37%-43%). GFP-EWS-ERG expressing embryos maintained expression at least until 4 dpf. Development continued to the point where embryos showed rudimentary fins and a rhythmically contracting patch of cells at the site of the heart (Figure 3C, left panel, shows a representative embryo at 3dpf).

Transcriptome analysis of S1101T:Gal4/UAS:EWS-ERG transgenic zebrafish shows involvement of cancer-associated pathways

After observing the various phenotypes obtained by crossing UAS:EWS-ERG with a selection of Gal4 driver lines, further genetic profiling was performed. S1101T:Gal4 was chosen as a driver line, as these fish retained fluorescent cells for the longest period of time, and a large portion of cells in these fish were transformed.

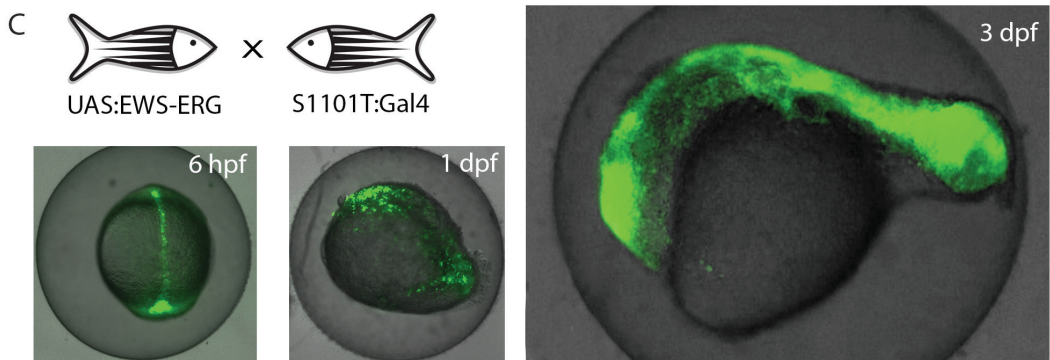
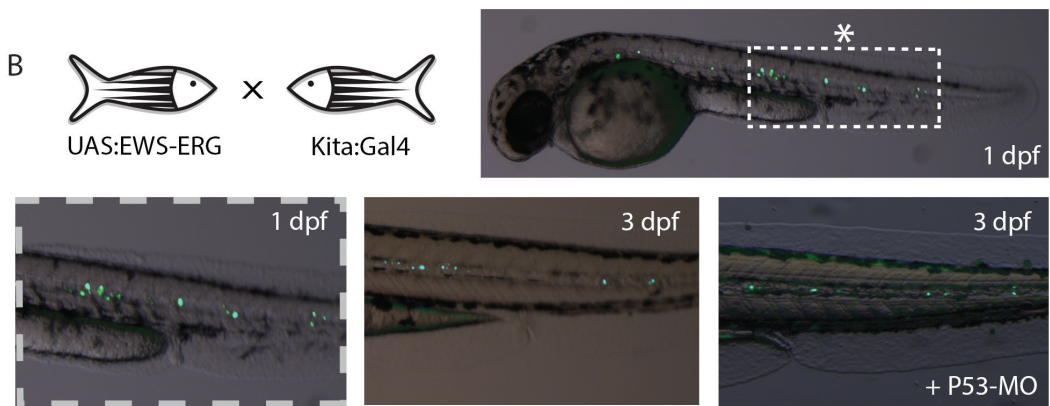
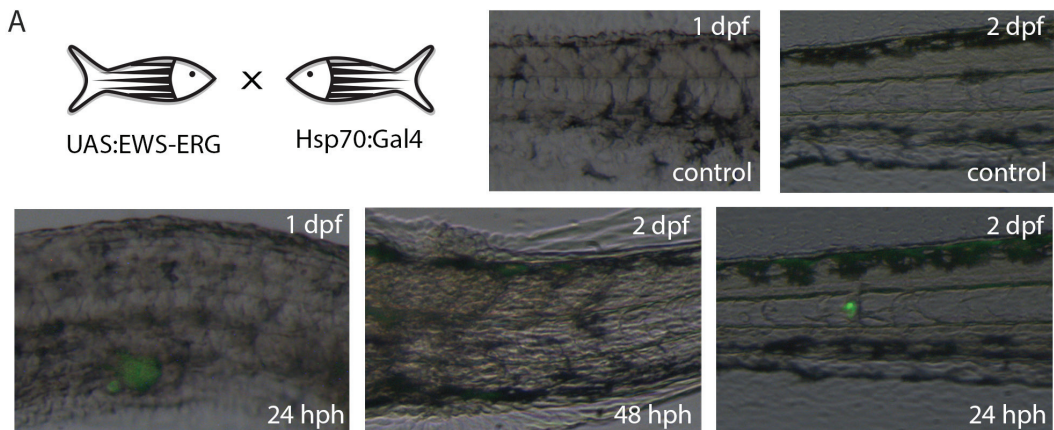
Deep sequencing of the transcriptome was performed on whole-embryo RNA samples from S1101T:Gal4/UAS:EWS-ERG and control siblings at 3dpf. The generated fastq files were analysed via GeneTiles, a bioinformatic software package developed within our research group to allow straightforward RNAseq analysis (www.genetiles.com).⁴⁴

To evaluate quality of the obtained expression data, variation between samples of the same group was calculated using Pearson product-moment correlation coefficient. There was little variation found between the samples, as seen by the mean R-values close to 1: mean $R_{\text{control}} = 0,9851$, mean $R_{\text{S1101T:EWS-ERG}} = 0,9656$.

Data was divided into two lists: genes at least 1.5-fold significantly

Figure 3. Expression of EWSR1-ERG in different Gal4 driver lines.

A) Offspring of UAS:EWS-ERG fish crossed with *Hsp70:Gal4* were given heatshock at 6 hpf and 1 dpf, and fluorescence was checked 24 hours post heatshock (hph) and 48 hph. Embryos heatshocked at 6 hpf showed few fluorescent cells and undefined notochord and muscle structure 24 hph (bottom left panel) compared to heatshocked controls at the same timepoint (upper middle panel). These embryos lost fluorescent signal 48 hph, while muscle structure remained abnormal (bottom middle panel), compared to 2 dpf controls (upper right panel). Embryos given heatshock at 1 dpf showed single



cells with GFP expression 24hph. **B)** UAS:EWS-ERG crossed with Kita:Gal4 resulted in expression in cells along the notochord. Images taken of the same embryo at 1 dpf and 3 dpf (upper right, bottom left and bottom middle panel) show that cells expressing GFP-EWSR1-ERG disappear over time. This loss of GFP+ cells could not be rescued by P53 morpholino injection (bottom left panel). **C)** UAS:EWS-ERG crossed with S1101T:Gal4 resulted in expression in the neurons from 6 hpf onwards (left panel), and causes malformation of the developing embryo at 1 dpf (middle panel). Expression of GFP-EWSR1-ERG remained stable at 3 dpf (right panel).

($p \leq 0,05$) upregulated, and genes at least 1.5-fold significantly downregulated. This way, 574 up- and 948 downregulated genes were found. When compared to the gene expression pattern of the EWS adult transgenic zebrafish model described by Leacock *et al.*²⁴, there was overlap of six genes (upregulated: *cathepsin L. 1*; downregulated: *annexin A5a*, *defensin beta-like 1*, *3-hydroxy-3-methylglutaryl-CoA synthase 1*, *transferrin-a*, *zgc:195245*). This low number of commonly regulated genes could be due to comparing an embryonic whole-body expression profile to an adult tumour-only expression-profile. When we compared our model to the embryonic transgenic model described in the same paper, we similarly observed impaired development. With enrichment analysis, we aimed to look further into this and other biological processes on a genetic level.

For enrichment analysis, the zebrafish ENSEMBL gene IDs were first converted to human ENSEMBL gene IDs, and analysed using the Database for Annotation, Visualization and Integrated Discovery (DAVID) v6.7.^{31,32} Table 1 shows enrichment in gene ontology (GO) terms and KEGG Pathways for the upregulated and downregulated gene set. The abnormal development of these embryos is reflected in the enrichment of terms such as 'Developmental process', 'P53 signalling pathway' and 'Apoptosis'. The expression of EWS-ERG specifically in the neurons of the embryos can explain the extremely low p-value for enrichment of 'Neurological systems process'. Introduction of the oncogene caused a significant downregulation of genes involved in neuron differentiation. In addition to these expected enrichments, introduction of EWS-ERG also affects biologic processes and pathways linked to cancer, such as the MAPK signalling pathway that plays an important role in orchestrating cell survival and division. Genes involved in cell adhesion and motility are both altered, as well as cytoskeleton organization.

Gene expression profile of S1101T:Gal4/UAS:EWS-ERG transgenic zebrafish overlaps with core EWSR1-FLI1 regulated gene set

Next, we investigated how the gene expression profile found in these transgenic S1101T:Gal4/UAS:EWS-ERG embryos compared to other transcriptome sequencing studies performed in human and murine *in vitro* models. A core gene set regulated by EWSR1-FLI1 was described by Hancock and Lessnick, by comparing 13 such studies.³⁴ From the 574 genes upregulated in embryonic the transgenic zebrafish model, 20 human orthologues were also identified within the core EWSR1-FLI1 upregulated gene set. For the downregulated gene set, 22 out of 948 zebrafish genes showed overlap with the gene set described by Hancock and Lessnick. These genes were involved in various processes such as metabolism, signalling and transcriptional and translational activity (Figure 4A). The change in expression of these genes was validated by quantitative q-RT-PCR (Figure 4B). One of the upregulated genes is *gstm*, encoding a glutathione-S-transferase enzyme which is involved in detoxification of xenobiotics.³⁵ Inhibition of these enzymes

Table 1. Enrichment analysis of S1101T:Gal4/UAS:EWS-ERG transgenic zebrafish.

Upregulated genes

<u>GO Term</u>	<u>Number of genes</u>	<u>P-value</u>
Regulation of cell proliferation	74	2.4E-7
Apoptosis	50	5.8E-4
Developmental process	195	7.1E-4
Cytoskeleton organization	35	7.5E-3
Cell surface receptor linked signal transduction	110	4.4E-2

<u>KEGG Pathway</u>	<u>Number of genes</u>	<u>P-value</u>
Regulation of actin cytoskeleton	31	1.1E-5
MAPK signaling pathway	28	5.4E-3
P53 signaling pathway	11	7.2E-3
Cell adhesion molecules (CAMs)	16	1.3E-3

Downregulated genes

<u>GO Term</u>	<u>Number of genes</u>	<u>P-value</u>
Neurological system process	175	1.1E-20
Neuron differentiation	63	1.3E-7
Response to drug	33	6.0E-5
Developmental process	275	7.1E-5
Cell adhesion	75	3.5E-4
Vesicle-mediated transport	56	1.5E-2

<u>KEGG Pathway</u>	<u>Number of genes</u>	<u>P-value</u>
Glycolysis / Gluconeogenesis	18	6.4E-7
PPAR signaling pathway	18	5.3E-6
Drug metabolism	13	3.5E-5

7

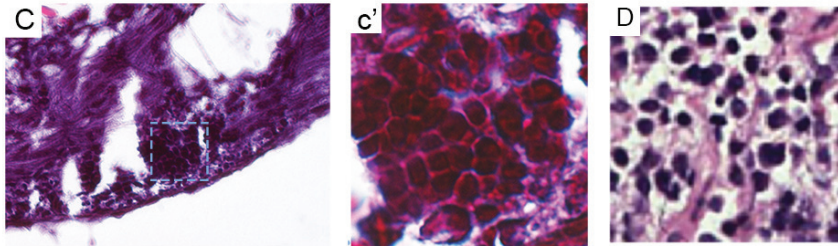
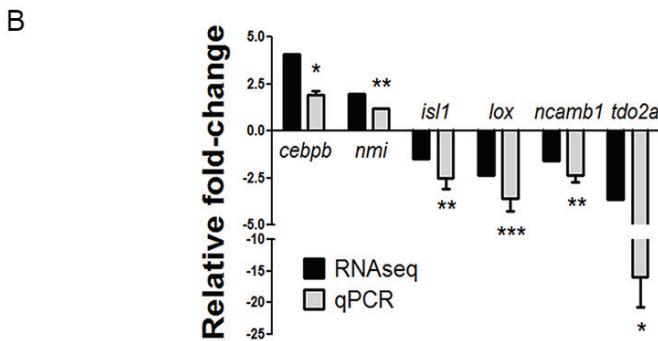
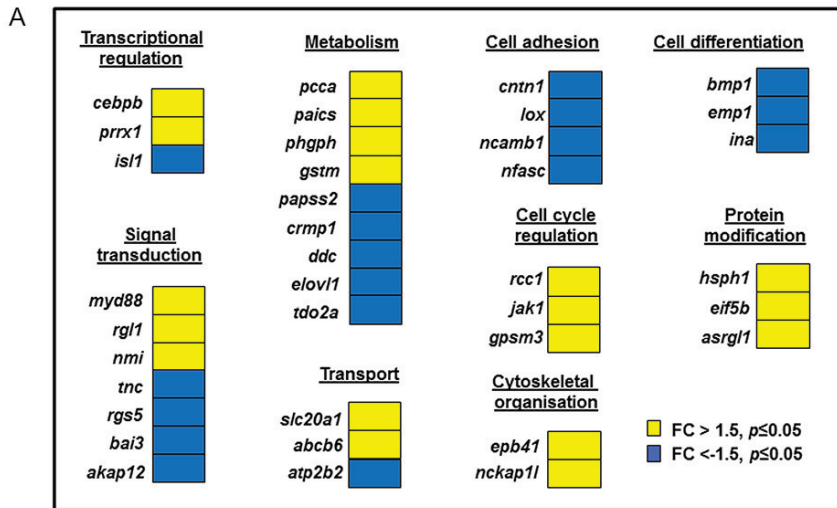


Figure 4. Comparison of transgenic zebrafish Ewing sarcoma model to human Ewing sarcoma and murine models. A) Transcriptional profile of genes differentially expressed in S1101T:Gal4xUAS:EWS-ERG at 3 dpf, as determined by deep-sequencing, which additionally show overlap with a core regulated gene-set as determined by comparison of human and murine microarray experiments. **B)** Relative fold change of genes as determined by RNAseq or quantitative RT-PCR. For q-RT-PCR, p-values were calculated by unpaired t-test, and significance indicated as follows: *p ≤ 0,05; **p ≤ 0,01; ***p ≤ 0,001. **C)** H&E staining of sections from S1101T:Gal4xUAS:EWS-ERG at 1dpf (magnification: 40x), showing muscle tissue in the trunk of the embryo, interspersed with clusters of cells with scant cytoplasm (**c'**: 60x magnification of boxed region). **D)** H&E staining of sections from human EWS tumour.

has been shown to increase sensitivity of EWS cell lines to conventional chemotherapeutics.³⁶ Also upregulated were Janus Kinase 1 (*jak1*) and N-Myc and STAT interactor (*nmi*). JAK inhibition was shown to decrease EWS cell growth *in vitro* via deactivation of STAT3.³⁷ Among the downregulated genes, lysyl oxidase (*lox*) was found. This gene acts as a tumour suppressor when ectopically re-expressed in EWS cell lines, preventing cell proliferation.³⁸

Cells expressing human EWS-ERG in zebrafish share histologic features with EWS biopsies

S1101T:Gal4/UAS:EWS-ERG embryos were fixed at 1 dpf, and embedded in paraffin for sectioning and H&E staining, to compare morphology of transformed cells to those found in EWS tumour biopsies. In Figure 4C and 4c', within regular muscle tissue, clusters of cells were observed with round nuclei and little cytoplasm, bearing a resemblance to cell features of H&E stained sections of EWS tumour biopsies.

Discussion

In this study, we have aimed to generate a transgenic zebrafish model for Ewing sarcoma (EWS) to facilitate *in vivo* research on these tumours, for future usage of this model for preclinical screens in searching for a new drug treatments. Thus far, the generation of a transgenic murine model has been unsuccessful, due to the toxicity of EWSR1-FLI1, the oncogenic fusion protein characteristic for EWS. Similar difficulties were found with the only other stable transgenic model, a zebrafish which can produce small blue round cell tumours expressing EWSR1-FLI1 within one year.²⁴ These fish required a p53-mutated background, found in <10% of actual EWS patients, for these tumours to arise in addition to malignant peripheral nerve sheet tumours. A previous transient embryonic zebrafish model, where mRNA for human EWSR1/FLI1 or zebrafish *ewsr1a/fli1a* was injected, resulted in mitotic defects and neurologic, trunk and tail malformation.²³

We circumvented problems of embryonic lethality by placing the expression of the *EWSR1-ERG* and *EWSR1-FLI1* oncogene under a UAS promoter, which is silent in the absence of Gal4, allowing transgenic fish to reach adult stages. Even though integration of *EWSR1-FLI1* was not successful, we were able to generate for the first time a transgenic fish expressing human *EWSR1-ERG* oncogene. By the crossing these fish with a variety of driver-lines of fish expressing Gal4 under different promoters, we could study the effect of GFP-tagged EWSR1-ERG expression in various tissues in zebrafish larval stages. We observed the toxic effects of EWSR1-ERG expression as most embryos lost expression of the GFP-tagged oncogene. This could be due to apoptosis of the cells. With the heatshock-inducible Gal4 driver line, it is possible

to induce local heatshocks with a focused laser. Performing these in different locations at different stages of development may improve survival of cells expressing the oncogene. Another possible cause of losing oncogene expression, is silencing of the gene. The 14xUAS promoter is prone to methylation, which can cause transcriptional silencing.³⁹ Using a promoter with fewer UAS copies may diminish this event.

Embryos resulting of a cross between the *TG(UAS:GFP-EWSR1-ERG)* and a fish expressing Gal4 in its neurons so far has proved the most tolerant of EWSR1-ERG expression. This observation was interesting considering various lines of evidence point to neural crest as the currently unknown tissue of origin for EWS⁴⁰⁻⁴³, a tissue which also gives rise to neurons. However, characterization of EWSR1-ERG expression in other tissues at other time points is a good possibility for further investigation. More detailed characterization of the embryos neuronally expressing EWSR1-ERG revealed an overlap of genes regulated in the embryonic zebrafish transgenic model, and a core set identified by comparison of various other transcriptional studies investigating the role of EWSR1-FLI1 in EWS.³⁴ Several of the genes found this way have been shown to be involved in different processes of EWS tumourigenesis and survival. It would be interesting to see how the phenotype of the transgenic embryos is affected by targeting pathways linked to these genes. This can be done with chemical inhibitors added to the water of the embryos, or by genetic modulation with morpholino injection. For example, knock down of *gstm*, encoding glutathione-S-transferase, should increase sensitivity of EWS transformed cell to conventional chemotherapeutics. Also, inhibition of Janus Kinase 1 (*jak1*) or re-expression of lysyl oxidase (*lox*) should decrease EWS cell growth in the zebrafish model.

It should be noted that the core gene set identified by Hancock and Lessnick is based on datasets investigating gene expression profiles as regulated by EWSR1-FLI1, and RNAseq in this study was performed on offspring of *TG(UAS: GFP-EWSR1-ERG)* fish. This could be one explanation as to why there was a relatively low overlap between the two data sets. However, genes which did show overlap may belong to a set of genes regulated by both EWSR1-FLI1 and EWSR1-ERG, and possibly other EWSR1-ETS fusion products. Such similarities despite different translocation types could point to key genes essential for EWS malignancy, filtering out those specific for one particular translocation. Furthermore, sequencing was performed on whole-embryo RNA isolates, where part of the cells do not express EWSR1-ERG. This causes an underestimation of regulated genes within the samples.

In conclusion, we have generated a transgenic zebrafish model to aid in the research of Ewing sarcoma. The flexibility of expression of EWSR1-ERG provided by the use of the Gal4/UAS binary system allows for adaptation of the model as knowledge about the tissue of origin of Ewing sarcoma grows. Furthermore, the current neuronal-expression model shows overlap with other studies previously done, validating its use for

further investigation of these genetic pathways in the progression of this disease.

Acknowledgments

The authors are grateful to Wouter Veneman, Shuxin Yang and Rubén Marín-Juez for assistance with transcriptome analysis, Gerda Lamers for assistance with histology, and Tim Salbert and Raygene Martier for assistance with experimental procedures. This study was supported by Stichting Kinderen Kankervrij (Grant No. 30677).

References

1. Fletcher CDM, World Health Organization., International Agency for Research on Cancer. 2013. WHO classification of tumours of soft tissue and bone. 4th ed. Lyon: IARC Press. 468 p. p.
2. Erkizan HV, Uversky VN, Toretsky JA. 2010. Oncogenic partnerships: EWS-FLI1 protein interactions initiate key pathways of Ewing's sarcoma. *Clin Cancer Res* 16(16):4077-4083.
3. Nishimori H, Sasaki Y, Yoshida K, Irifune H, Zembutsu H, Tanaka T, Aoyama T, Hosaka T, Kawaguchi S, Wada T, Hata J, Toguchida J, Nakamura Y, Tokino T. 2002. The Id2 gene is a novel target of transcriptional activation by EWS-ETS fusion proteins in Ewing family tumors. *Oncogene* 21(54):8302-8309.
4. Watson DK, Robinson L, Hodge DR, Kola I, Papas TS, Seth A. 1997. FLI1 and EWS-FLI1 function as ternary complex factors and ELK1 and SAP1a function as ternary and quaternary complex factors on the Egr1 promoter serum response elements. *Oncogene* 14(2):213-221.
5. Zwerner JP, Joo J, Warner KL, Christensen L, Hu-Lieskovan S, Triche TJ, May WA. 2008. The EWS/FLI1 oncogenic transcription factor deregulates GLI1. *Oncogene* 27(23):3282-3291.
6. Turc-Carel C, Aurias A, Mugneret F, Lizard S, Sidaner I, Volk C, Thiery JP, Olschwang S, Philip I, Berger MP, et al. 1988. Chromosomes in Ewing's sarcoma. I. An evaluation of 85 cases of remarkable consistency of t(11;22)(q24;q12). *Cancer Genet Cytogenet* 32(2):229-238.
7. Sorensen PH, Lessnick SL, Lopez-Terrada D, Liu XF, Triche TJ, Denny CT. 1994. A second Ewing's sarcoma translocation, t(21;22), fuses the EWS gene to another ETS-family transcription factor, ERG. *Nat Genet* 6(2):146-151.
8. Zucman J, Melot T, Desmaze C, Ghysdael J, Plougastel B, Peter M, Zucker JM, Triche TJ, Sheer D, Turc-Carel C, et al. 1993. Combinatorial generation of variable fusion proteins in the Ewing family of tumours. *EMBO J* 12(12):4481-4487.
9. Huang HY, Illei PB, Zhao Z, Mazumdar M, Huvos AG, Healey JH, Wexler LH,

- Gorlick R, Meyers P, Ladanyi M. 2005. Ewing sarcomas with p53 mutation or p16/p14ARF homozygous deletion: a highly lethal subset associated with poor chemoresponse. *J Clin Oncol* 23(3):548-558.
10. Lopez-Guerrero JA, Pellin A, Noguera R, Carda C, Llombart-Bosch A. 2001. Molecular analysis of the 9p21 locus and p53 genes in Ewing family tumors. *Lab Invest* 81(6):803-814.
 11. Mackintosh C, Ordonez JL, Garcia-Dominguez DJ, Sevillano V, Llombart-Bosch A, Szuhai K, Scotlandi K, Alberghini M, Sciot R, Sinnaeve F, Hogendoorn PC, Picci P, Knuutila S, Dirksen U, Debiec-Rychter M, Schaefer KL, de Alava E. 2012. 1q gain and CDT2 overexpression underlie an aggressive and highly proliferative form of Ewing sarcoma. *Oncogene* 31(10):1287-1298.
 12. Wei G, Antonescu CR, de Alava E, Leung D, Huvos AG, Meyers PA, Healey JH, Ladanyi M. 2000. Prognostic impact of INK4A deletion in Ewing sarcoma. *Cancer* 89(4):793-799.
 13. Pizzo PA, Poplack DG. 2011. Principles and practice of pediatric oncology. 6th ed. Philadelphia: Wolters Kluwer Health/Lippincott Williams & Wilkins., 1531 p. p.
 14. Meyers PA, Krailo MD, Ladanyi M, Chan KW, Sailer SL, Dickman PS, Baker DL, Davis JH, Gerbing RB, Grovas A, Herzog CE, Lindsley KL, Liu-Mares W, Nachman JB, Sieger L, Wadman J, Gorlick RG. 2001. High-dose melphalan, etoposide, total-body irradiation, and autologous stem-cell reconstitution as consolidation therapy for high-risk Ewing's sarcoma does not improve prognosis. *J Clin Oncol* 19(11):2812-2820.
 15. Bacci G, Ferrari S, Longhi A, Donati D, De Paolis M, Forni C, Versari M, Setola E, Briccoli A, Barbieri E. 2003. Therapy and survival after recurrence of Ewing's tumors: the Rizzoli experience in 195 patients treated with adjuvant and neoadjuvant chemotherapy from 1979 to 1997. *Ann Oncol* 14(11):1654-1659.
 16. Arvand A, Bastians H, Welford SM, Thompson AD, Ruderman JV, Denny CT. 1998. EWS/FLI1 up regulates mE2-C, a cyclin-selective ubiquitin conjugating enzyme involved in cyclin B destruction. *Oncogene* 17(16):2039-2045.
 17. Deneen B, Denny CT. 2001. Loss of p16 pathways stabilizes EWS/FLI1 expression and complements EWS/FLI1 mediated transformation. *Oncogene* 20(46):6731-6741.
 18. Lessnick SL, Dacwag CS, Golub TR. 2002. The Ewing's sarcoma oncoprotein EWS/FLI1 induces a p53-dependent growth arrest in primary human fibroblasts. *Cancer cell* 1(4):393-401.
 19. Miyagawa Y, Okita H, Nakajima H, Horiuchi Y, Sato B, Taguchi T, Toyoda M, Katagiri YU, Fujimoto J, Hata J, Umezawa A, Kiyokawa N. 2008. Inducible expression of chimeric EWS/ETS proteins confers Ewing's family tumor-like phenotypes to human mesenchymal progenitor cells. *Mol Cell Biol* 28(7):2125-2137.
 20. Riggi N, Suva ML, Suva D, Cironi L, Provero P, Tercier S, Joseph JM, Stehle

- JC, Baumer K, Kindler V, Stamenkovic I. 2008. EWS-FLI-1 expression triggers a Ewing's sarcoma initiation program in primary human mesenchymal stem cells. *Cancer Res* 68(7):2176-2185.
21. Lin PP, Pandey MK, Jin F, Xiong S, Deavers M, Parant JM, Lozano G. 2008. EWS-FLI1 induces developmental abnormalities and accelerates sarcoma formation in a transgenic mouse model. *Cancer Res* 68(21):8968-8975.
 22. Torchia EC, Boyd K, Rehg JE, Qu C, Baker SJ. 2007. EWS/FLI-1 induces rapid onset of myeloid/erythroid leukemia in mice. *Mol Cell Biol* 27(22):7918-34.
 23. Embree LJ, Azuma M, Hickstein DD. 2009. Ewing sarcoma fusion protein EWSR1/FLI1 interacts with EWSR1 leading to mitotic defects in zebrafish embryos and human cell lines. *Cancer Res* 69(10):4363-4371.
 24. Leacock SW, Basse AN, Chandler GL, Kirk AM, Rakheja D, Amatruda JF. 2012. A zebrafish transgenic model of Ewing's sarcoma reveals conserved mediators of EWS-FLI1 tumorigenesis. *Dis Model Mech* 5(1):95-106.
 25. Neilsen PM, Pishas KI, Callen DF, Thomas DM. 2011. Targeting the p53 Pathway in Ewing Sarcoma. *Sarcoma* 2011: 746939.
 26. Brand AH, Perrimon N. 1993. Targeted gene expression as a means of altering cell fates and generating dominant phenotypes. *Development*. 118(2):401-15
 27. Scott EK, Mason L, Arrenberg AB, Ziv L, Gosse NJ, Xiao T, Chi NC, Asakawa K, Kawakami K, Baier H. 2007. Targeting neural circuitry in zebrafish using GAL4 enhancer trapping. *Nat Methods* 4(4):323-326.
 28. Distel M, Wullimann MF, Koster RW. 2009. Optimized Gal4 genetics for permanent gene expression mapping in zebrafish. *Proc Natl Acad Sci U S A* 106(32):13365-13370.
 29. Scheer N, Riedl I, Warren JT, Kuwada JY, Campos-Ortega JA. 2002. A quantitative analysis of the kinetics of Gal4 activator and effector gene expression in the zebrafish. *Mech Dev* 112(1-2):9-14.
 30. Kawakami K, Takeda H, Kawakami N, Kobayashi M, Matsuda N, Mishina M. 2004. A transposon-mediated gene trap approach identifies developmentally regulated genes in zebrafish. *Dev Cell* 7(1):133-144.
 31. Huang da W, Sherman BT, Lempicki RA. 2009a. Bioinformatics enrichment tools: paths toward the comprehensive functional analysis of large gene lists. *Nucleic Acids Res* 37(1):1-13.
 32. Huang da W, Sherman BT, Lempicki RA. 2009b. Systematic and integrative analysis of large gene lists using DAVID bioinformatics resources. *Nat Protoc* 4(1):44-57.
 33. Robu ME, Larson JD, Nasevicius A, Beiraghi S, Brenner C, Farber SA, Ekker SC. 2007. p53 activation by knockdown technologies. *PLoS Genet* 3(5):e78.
 34. Hancock JD, Lessnick SL. 2008. A transcriptional profiling meta-analysis

reveals a core EWS-FLI gene expression signature. *Cell Cycle* 7(2):250-256.

35. Luo W, Gangwal K, Sankar S, Boucher KM, Thomas D, Lessnick SL. 2009. GSTM4 is a microsatellite-containing EWS/FLI target involved in Ewing's sarcoma oncogenesis and therapeutic resistance. *Oncogene* 28(46):4126-4132.
36. Pasello M, Manara MC, Michelacci F, Fanelli M, Hattinger CM, Nicoletti G, Landuzzi L, Lollini PL, Caccuri A, Picci P, Scotlandi K, Serra M. 2011. Targeting glutathione-S transferase enzymes in musculoskeletal sarcomas: a promising therapeutic strategy. *Anal Cell Pathol* 34(3):131-145.
37. Yan S, Li Z, Thiele CJ. 2013. Inhibition of STAT3 with orally active JAK inhibitor, AZD1480, decreases tumor growth in Neuroblastoma and Pediatric Sarcomas In vitro and In vivo. *Oncotarget* 4(3):433-445.
38. Agra N, Cidre F, Garcia-Garcia L, de la Parra J, Alonso J. 2013. Lysyl oxidase is downregulated by the EWS/FLI1 oncoprotein and its propeptide domain displays tumor suppressor activities in ewing sarcoma cells. *PLoS One* 8(6):e66281.
39. Goll MG, Anderson R, Stainier DY, Spradling AC, Halpern ME. 2009. Transcriptional silencing and reactivation in transgenic zebrafish. *Genetics* 182(3):747-755.
40. Cavazzana AO, Miser JS, Jefferson J, Triche TJ. 1987. Experimental evidence for a neural origin of Ewing's sarcoma of bone. *Am J Pathol* 127(3):507-518.
41. Khan J, Wei JS, Ringner M, Saal LH, Ladanyi M, Westermann F, Berthold F, Schwab M, Antonescu CR, Peterson C, Meltzer PS. 2001. Classification and diagnostic prediction of cancers using gene expression profiling and artificial neural networks. *Nature Med* 7(6):673-679.
42. Staeger MS, Hutter C, Neumann I, Foja S, Hattenhorst UE, Hansen G, Afar D, Burdach SE. 2004. DNA microarrays reveal relationship of Ewing family tumors to both endothelial and fetal neural crest-derived cells and define novel targets. *Cancer Res* 64(22):8213-8221.
43. Suh CH, Ordonez NG, Hicks J, Mackay B. 2002. Ultrastructure of the Ewing's sarcoma family of tumors. *Ultrastruct Pathol* 26(2):67-76.
44. Veneman WJ, de Sonnevile J, van der Kolk KJ, Ordas A, Al-Ars Z, Meijer AH, Spaink HP. 2015. Analysis of RNAseq datasets from a comparative infectious disease zebrafish model using GeneTiles bioinformatics. *Immunogenet.* 67(3):135-47

Supplementary Table 1. Primer sequences

cebpb FW	GCAGGCAACCTATCACCTACATAC	q-RT-PCR
cebpb REV	CGCAAGTTTCACCGACTACAAGT	q-RT-PCR
nmi FW	CCTGCTCGCTAATATCGGCT	q-RT-PCR
nmi REV	GTGCTCTCGTCCTGAAACTGA	q-RT-PCR
isl1 FW	TAGTCGGCAGCTCATCCCA	q-RT-PCR
isl1 REV	GGGCTCTGCTGCCATTTGTAAAG	q-RT-PCR
lox FW	GAGGTTTCCACAGCGAGTCA	q-RT-PCR
lox REV	CTGTGGTAGTGCTGATGGCA	q-RT-PCR
ncamb1 FW	TCTGCTATCAACGGCAAGGG	q-RT-PCR
ncamb1 REV	GAGGACTGGGCTCTCCTTGA	q-RT-PCR
tdo2a FW	AGGTCAGAGGAGGCTGTCTT	q-RT-PCR
tdo2a REV	TCTAGGCTCCTCCCTGTAGA	q-RT-PCR
β -actin FW	GGCACCCAGCACAATGAAGAT	q-RT-PCR
β -actin REV	AAGTCATAGTCCGCCTAGAAGCAT	q-RT-PCR
eb1 FW	GTCTCAGCCTCACTTTGAGC	genotyping
gfp REV	AGATGAACTTCAGGGTCAGC	genotyping
mfel-EWS FW	TCACAATTGGCAGAGCTGGTTTAGTGAACCGTC	cloning
EWS-NotI REV	TCAGCGGCCGCTCTAGATCCGGTGGATCATCA CCAC	cloning

Chapter 8

**Quantitative analysis of protein
expression in zebrafish embryos
neuronally expressing human
EWSR1-ERG oncogene**

Abstract

Ewing sarcoma, a pediatric sarcoma affecting bone and soft tissue, is characterized by a translocation event which merges between EWSR1 and a member of the ETS family of genes. In 85% of the patients an EWSR1-FLI1 fusion gene is present, another 10% of patients harbor an EWSR1-ERG fusion gene. While much is known about the effects that these EWSR1-ETS fusions can have on a transcriptomic level, much less studies have been dedicated to investigate the proteome after introduction or knockdown of EWSR1-ETS. Previously, a zebrafish binary transgenic model for Ewing sarcoma was described where expression of human *EWSR1-ERG* is driven by the conditional UAS promotor. This promotor is silent and requires Gal4 element for its activation. Crossing UAS-GFP-EWS-ERG fish with fish expressing Gal4 under neuronal promotor generates offspring with EWSR1-ERG expression localized to the neurons as monitored by GFP expression. Massive expression of EWSR1-ERG transformed cells leads to developmental malformations notable from 1 day post-fertilisation (dpf) onwards. At this stage, the majority of embryos with neuronal EWSR1-ERG expression have no discernable tissues or organs, and show a mix of GFP-expressing and non-expressing cells in no obvious organized pattern. This phenotype is maintained until at least 4 dpf. A number of embryos form rudimentary structures like eyes, fins or contracting patches of cells, but do not resemble normally developing siblings. In this study, we have performed comparative LC-MS/MS on the wild type embryos and embryos expressing a driver of Ewing sarcoma at 3 dpf, to investigate the effect of the human EWSR1-ERG oncogene on the zebrafish proteome. We show the up- and downregulation of proteins in various pathways which are transcriptionally regulated in EWS. For example, we found that Notch proteins levels were lower in transgenic embryos in comparison to wild type embryos. The downregulation of the Notch protein was confirmed *in vivo* in zebrafish embryos expressing Notch reporter and is in line with previously described transcriptional downregulation of Notch pathway in EWS by the EWSR1-FLI1 oncogene.

Introduction

EWSR1-FLI1 and EWSR1-ERG are the two most commonly occurring translocations in Ewing sarcoma (EWS), in respectively 85% and 10% of all cases.¹⁻⁴ The cell or tissue of origin of these tumours is not yet known; the two main candidates are currently mesenchymal stem cells, or the neural crest. In previous work, we have shown how the exogenous expression of human EWSR1-ERG in zebrafish embryos can give rise to clusters of cells expressing the gene that are undergoing proliferation and apoptosis (chapter 7 of this thesis). Additionally, when using a GAL4/UAS expression system, we observed variances in permissiveness of

expression of this gene in different tissues and at different time points. The transcriptomic profile of embryos expressing EWSR1-ERG in the neurons, as determined by RNAseq at 3 days post-fertilisation (dpf), showed that various cancer-associated pathways were affected in these embryos. Simultaneously, a number of genes identified in a core set of EWSR1-FLI1 regulated genes (based on microarray expression profiling of various EWS models⁵), were also found to be significantly up- or down-regulated in our model.

While there have been numerous studies published on the effect of EWSR1-FLI1 knockdown or ectopic expression in cell lines on an RNA level, much less is known on a protein level. The direct involvement of EWSR1-FLI1 on a protein level has been investigated by looking at the interactome⁶, or by knockdown of EWSR1-FLI1 and investigating changes in the phosphorylation profile in A673 cells.⁷ Other studies described changes in protein expression after interference with genes of interest in EWS.^{8,9} Here, we have applied LC-MS/MS to quantify changes in protein expression in 3 dpf zebrafish embryos neuronally expressing EWSR1-ERG.

LS-MS/MS with spectral counting is a label-free method to quantify the most abundant proteins present in a sample. Label-free quantification is a relatively rapid method of protein quantification. It offers a cheaper alternative to stable-isotope labeling, which is important in large-scale experiments. Furthermore, although stable-isotope labeling approaches have been used in zebrafish to study tissue regeneration and organ protein expression profiling, it is challenging to find appropriate isotopically enriched feed for both larvae and adults.¹⁰ Label-free quantification provides a method to measure the relative amount of abundantly expressed proteins in two or more samples.

This study shows the effects of expression of human EWSR1-ERG in the neurons of 3-day-old zebrafish embryos on the proteome, using LC-MS/MS. Analysis of the protein quantification reveals that embryos expressing EWSR1-ERG have altered protein expression enriched in various pathways which are relevant for EWS progression. Many proteins were enriched in the gene ontology term 'oncogenesis', and proteins of the Wnt and Notch pathway were also found to be altered. Downregulation of Notch was confirmed *in vivo*, using Notch signaling reporter fish.

Materials and Methods

Zebrafish husbandry

Zebrafish lines were handled compliant to local animal welfare regulations and maintained according to standard protocols (www.ZFIN.org). During experiments, embryos were maintained in eggwater (60µg/ml Instant Ocean salts in demiwater) at 28.5°C and, when needed,

anaesthetized with 0.001% tricaine (Sigma-Aldrich, St. Louis, MO). The *TG(14xUAS:GFP-EWSR1-ERG)* was newly generated in the Leiden University laboratory. Generation of novel transgenic zebrafish was approved by the animal care committee of the Leiden University Medical Center (UDEEC1135). The *Et(E1b:Gal4-VP16)s1101t, TG(UAS:Kaede)s1999t* line was generated in an enhancer trap screen described by Scott *et al.*¹¹ The *TG(EPV.Tp1-Mmu.Hbb:nlsMCherry)^{ia7}* notch reporter line was generated by Schiavone *et al.*¹², and was used to create the *Et(E1b:Gal4-VP16)s1101t, TG(EPV.Tp1-Mmu.Hbb:nlsMCherry)^{ia7}* line.

Proteomics sample preparation

For proteomics, 20 zebrafish embryos anesthetized using 0.001% tricaine (Sigma-Aldrich, St. Louis, MO) were placed in an Eppendorf tube, and deyolked using deyolking buffer (116 mM NaCl, 2.9 mM KCl, 5.0 mM HEPES, 0.3 mM PMSF, 1 mM EDTA, pH 7.2) and trituration with a 200 μ L pipette tip. Deyolked embryos were rinsed several times in calcium-free Ringer's solution (116 mM NaCl, 2.9 mM KCl, 5.0 mM HEPES, pH 7.2) and snap-frozen in liquid nitrogen until further use.

10 μ L of urea buffer containing 8 M urea, 75 mM NaCl, 50 mM Tris-HCL pH 8.2, 50 U/mL benzonase (E1014-5KU, Sigma-Aldrich), 2 mM MgCl₂, and protease inhibitors (cOmplete ULTRA tablets, mini, EDTA-free, Roche, Basel, Switzerland) was added to the samples. For homogenization 0.5 mm zirconium oxide beads were added and the samples were homogenized in the Bullet Blender (Next Advance, Averill Park, NY) at speed setting "8" for 3 min. Subsequently placed at 4 °C for 30 minutes, centrifuged at 16,000g at 4 °C for 15 min and the supernatant was taken. A second protein extraction was performed using 10 μ L SDS buffer containing 1% SDS, 50 U/mL benzonase, and 2 mM MgCl₂, followed again by homogenization and centrifugation. Protein concentration of both extractions were measured by a bicinchoninic acid (BCA) protein assay kit (Thermo Fischer Scientific, Waltham, MA)

Circa 40 μ g of protein was loaded on a 1 mm 10-well 4-12% NuPAGE® Bis-Tris gel (Invitrogen, Carlsbad, CA). Proteins were separated in the gel for 90 min at 180 V. The gel was stained in NuPAGE® Colloidal Blue (Invitrogen) overnight at room temperature and de-stained with milli-Q water until the background was transparent. The gel lanes were cut into 48 identical slices fractions using a custom-made OneTouch Mount and Lane Picker (The Gel Company, San Francisco, CA). Each slice was placed into one well in a 96-well polypropylene PCR plate (Greiner Bio-One, Frickenhausen, Germany). Using 50 and 250 μ L Rainin 8-channel multi-pipettors, each gel slice was washed twice for 30 minutes at room temperature with 30% acetonitrile in 25 mM ABC. Cystines were reduced by addition of 75 μ L 10 mM DTT in 25 mM ABC and the plate incubated at 56°C for 20 minutes. After discarding the DTT solution, cysteines were alkylated by addition of 75 μ L 55 mM iodoacetamide in 25 mM ABC with incubation at room temperature in darkness for 20 minutes. The gel pieces were washed again as above

and the supernatant discarded. The proteins were digested in-gel by addition of 15 μL of 5 ng/ μL porcine trypsin (Promega, Madison, WI) and incubation for ~ 12 hours at 37°C , after which the digestion was quenched with the addition of 1 μL 5% trifluoroacetic acid (TFA). The solution was removed, followed by a second extraction with 20 μL 0.1% TFA for 1 h and the solution pooled with the first extraction. The plate was stored at -80°C until analysis by LC-MS/MS.

Liquid Chromatography – Tandem Mass Spectrometry

For each analysis, 10 μL of sample was loaded and desalted on a C18 PepMap 300 μm , 5 mm-i.d., 300 \AA precolumn (Thermo Scientific) and separated by reversed-phase liquid chromatography using two identical 150 mm 0.3 mm-i.d. ChromXP C18CL, 120 \AA columns (Eksigent, Dublin, CA) coupled parallel and connected to a split less NanoLC-Ultra 2D plus system (Eksigent) with a linear 45-minute gradient increasing from 4 to 35% acetonitrile in 0.05% formic acid and with a constant flow rate of 4 $\mu\text{L}/\text{minute}$. The LC system was coupled to an amaZon speed ETD ion trap (Bruker Daltonics, Billerica, MA) configured with an Apollo II ESI source. After each MS scan, up to 10 abundant multiply charged species in the mass range of 300-1300 m/z were selected for tandem mass spectrometry and actively excluded for one minute after having been selected twice. The LC system was controlled by HyStar 3.2 and the ion trap by trapControl 7.1.

The raw LC-MS/MS data was first converted to mzXML¹³ using compassXport version 3.0.4. These mzXML files contain all MS/MS data from each acquired spectrum, and in trans proteomic pipeline they were searched with X!Tandem¹⁴ using the k-score against a *Danio rerio* sequence database (UniProtKB, 20120403, 39559 proteins). A theoretical probability was assigned using Peptide Prophet. Afterwards the raw LC-MS/MS data were searched against a zebrafish Spectral library using SpectraST.¹⁵ The data of both searches were combined using IProphet.¹⁶

Gene ontology/pathway analysis

Enrichment analysis was performed using DAVID (Database for Annotation, Visualization and Integrated Discover, v6.7, Frederick, MD)^{17,18} or GATHER.¹⁹ For the DAVID analysis, the identifiers of all significantly regulated proteins were first converted to the ENSEMBL gene IDs of their closest human orthologue. Lists of these ENSEMBL gene IDs were uploaded to DAVID, and GO term enrichment was checked, as well as involvement of specific pathways (using the Panther, KEGG and Reactome databases). For analysis in GATHER, lists of regulated protein names could be uploaded directly for analysis. GATHER returns GO term enrichment values, as well as performing KEGG pathway analysis.

In vivo imaging

Expression of Notch was analysed in embryos anesthetized with 0.001% Tricaine at 2 dpf after embedding in 1% low melting point agarose (Sigma Aldrich). Confocal images were made on a Zeiss LSM5 Exciter / AxioObserver with a 10x objective, or on a Leica MZ16FA stereo fluorescent microscope with a DFC420C digital colour camera.

Results

Quantitative analysis of protein expression

In order to assess changes on a protein level in embryos expressing human EWSR1-ERG, crosses were made between the *TG(14xUAS:GFP-EWSR1-ERG)* and *Et(E1b:Gal4-VP16)s1101t, TG(UAS:Kaede)s1999t* lines. Offspring of these fish that receive both a copy of the UAS-driven GFP-EWSR1-ERG gene and the Gal4 gene have EWSR1-ERG expression localized to the neurons. As the EWSR1-ERG protein is tagged with a fluorescent reporter, expression of the protein can be confirmed using a stereo microscope. An example of such an embryo at 3 dpf (from now on referred to as EWS-ERG), and a wild-type sibling (referred to as WTcontrol), can be found in Figure 1A and B.

Deyolking and protein isolation was performed on 20 embryos of 3dpf. A simplified schematic in Figure 1C shows how these samples were prepared for LC-MS/MS, which is also described in higher detail in the material and methods. Briefly, deyolked embryos were taken up in NuPAGE® LDS Sample Buffer and separated on gel. For each sample, two lanes were used, which were subsequently cut into 2x 48 pieces, which were then placed in a 96 well plate. Reduction of disulphide bonds with DTT and digestion of the protein with trypsin took place in the pieces of gel in the plate. Subsequently, the 96 samples were measured by LC-MS/MS using a 45 minute gradient. For each group, WTcontrol and EWS-ERG, two replicates were made and measured.

Using LC-MS/MS, 1849 proteins were identified to be present in at least one of the samples. To evaluate the quality of the obtained protein expression data, variation between replicates from the same group was calculated. Correlation was high, as seen by the coefficients of determination: $R_{WTcontrol}^2 = 0.9942$ and $R_{EWS-ERG}^2 = 0.9624$ (seen also in Figure 2A and B, respectively). Subsequently, the fold changes between the WTcontrol and EWS-ERG were calculated for both sets of samples, and 1245 consistently upregulated and 369 consistently downregulated proteins were identified in the EWS-ERG groups, compared to the WTcontrol groups.

Calculating P-values to determine if the observed fold changes were significant would not be proper, as there were only two replicates for each group. Therefore, inspiration was drawn from a common analysis method used for SILAC experiments. Analysis of these experiments can be problematic when isotope incorporation is not efficient, as in

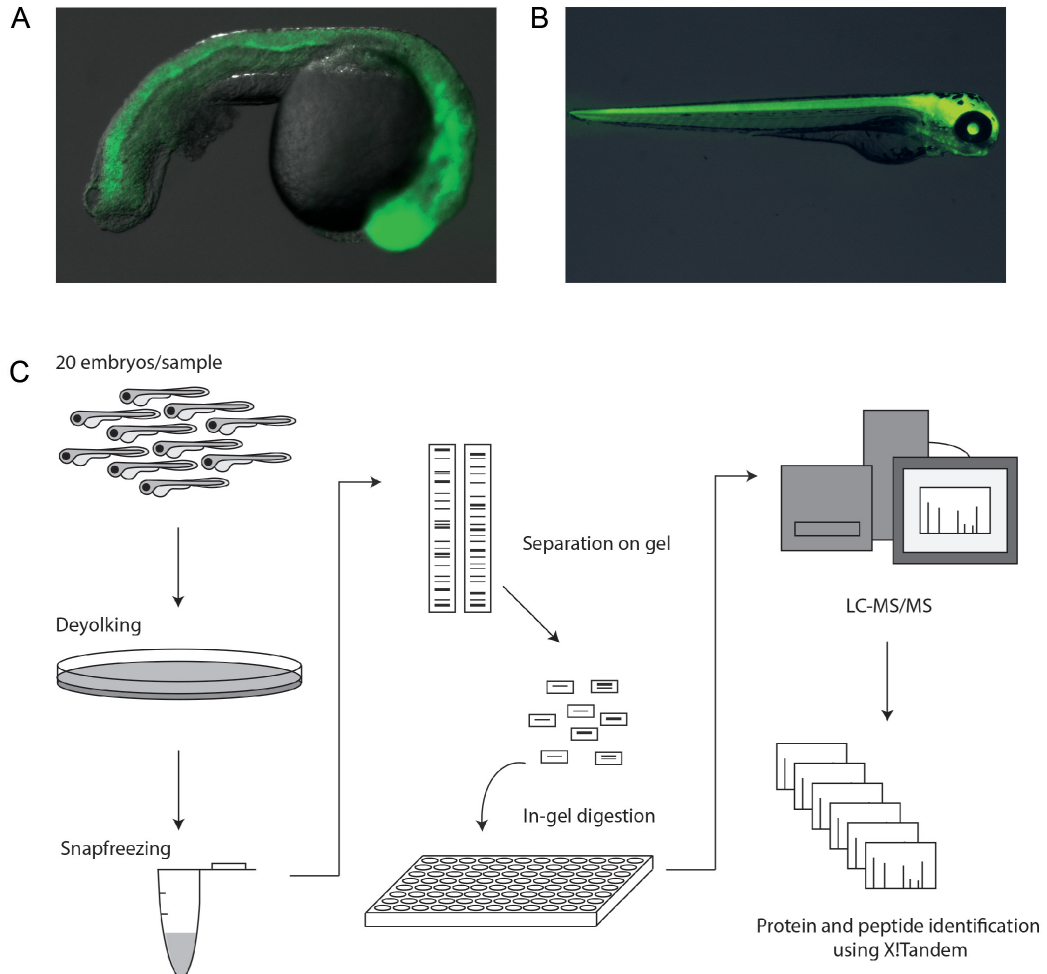


Figure 1. Sample preparation for LC-MS/MS analysis. A) 3dpf embryos resultant from a cross between the *TG(14xUAS:GFP-EWSR1-ERG)* and *Et(E1b:Gal4-VP16)s1101t, TG(UAS:Kaede)s1999t* zebrafish line, neuronally expressing human EWSR1-ERG tagged with GFP (green). **B)** A wildtype sibling resultant from the same cross as in (A), with expression of Kaede (green) in the neurons. **C)** Schematic overview of sample preparation for LC-MS/MS. For each sample, 20 3dpf embryos were de-yolked in using de-yolking buffer, before being snap-frozen until further use. Proteins were taken up in sample buffer and loaded onto gel for separation. Each gel lane was cut into 48 pieces, which were placed in a 96 well plate, after which proteins were digested in-gel using porcine trypsin. Each fraction of proteins was then analysed using liquid chromatography – tandem mass spectrometry (LC-MS/MS). Using X!Tandem and PeptideProphet, peptides and proteins were identified from the tandem mass spectra.

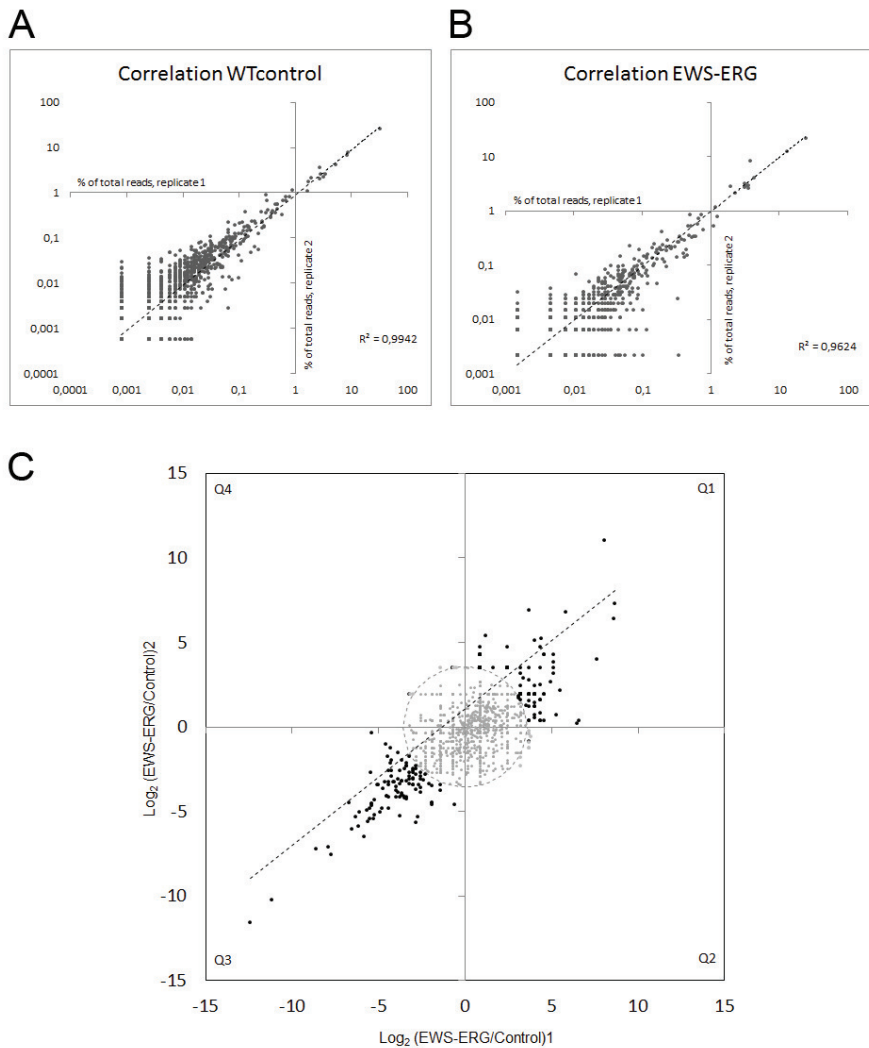


Figure 2. Quantitative analysis of protein expression. Plots showing the correlation of read-percentages for replicates of the **A**) wildtype control group ($R^2=0.9942$), and **B**) EWS-ERG expressing group ($R^2=0.9624$). **C**) Scatterplot illustrating the correlation of the fold changes between biological replicates. The excess of protein fold changes in quadrants 1 and 3 are due to agreement and reproducibility between biological replicates. Since there are also a number of proteins with small fold changes in Q2 and Q4, where the direction of the change was not reproducible, we removed (grey circle) proteins with similar small fold changes also from Q1 and Q3. The remaining proteins (black) represent up- (Q1) and down- (Q3) regulated proteins in the EWS-ERG samples of both replicates compared to the control group with an approximate FDR of 0.05.

primary cell lines with low longevity and replication time. Therefore, it is suggested by Park *et al.* to perform a label swap for such experiments, where the stable isotope is first incorporated in one, and then the other experimental condition.²⁰ Protein fold changes can then be plotted against each other for the label-swapped biological replicates. Such a graph was generated based on fold changes between EWS-ERG and WTcontrol for the two replicates, with a FDR of 0.05, shown in Figure 2C. In this graph, the significantly regulated proteins (FDR = 0.05) were indicated with black dots, whereas the remaining proteins are indicated in grey. After this cut-off, 294 and 100 proteins were found to be up- and downregulated, respectively.

Analysis of deregulated proteins

Further investigation into the up- and down regulated proteins was done by analyzing their enrichment in various pathways and biological processes using the Database for Annotation, Visualization and Integrated Discovery (DAVID) v6.7.^{17,18} For this purpose, the obtained protein names were first converted to the ENSEMBL gene ID of their human homologs, as DAVID is most suited for this type of input. Additionally, protein names were also run through GATHER (Gene Annotation Tool to Help Explain Relationships)¹⁹, for further annotation. Table 1 shows a selection of gene ontology terms (GO terms), biological processes, and pathways for both the up- and downregulated genes, as were found to be enriched using DAVID and GATHER.

In the upregulated gene set, various processes and pathways were found to be enriched. Amongst these, 'apoptosis' and 'cell cycle checkpoints' are reflecting the abnormal development of these embryos. The highest number of genes could be grouped under the GO term 'oncogenesis'. One of the proteins categorized in this group is Necdin-like 2. Necdin is a member of the melanoma antigen (MAGE) family of proteins, and promotes the differentiation and survival of neurons. Necdin has been shown in mice to increase the binding between Sirt1 and p53.²¹ Sirt1 in turn suppresses p53-mediated apoptosis by regulating the p53 acetylation. Interestingly, SIRT1 has previously been linked to EWS, via NOTCH and HEY1.²² NOTCH is downregulated by EWSR1-FLI1; when NOTCH expression is restored in EWS cells, the HEY1 effector suppresses SIRT1 expression and activates TP53. In the LC-MS/MS data, protein levels of Notch2 were also found to be downregulated in the embryos with EWSR1-ERG expression.

Another enriched pathway was 'signalling by wnt'. Two upregulated proteins were Wnt5a, and Frizzled homolog 8b (Fzd8b). Analysis of several EWS cell lines revealed expression of various WNTs and FZDs on RNA level.²³ In another study, WNT5a was shown to promote cellular migration in Ewing sarcoma, via regulation of CXCR4 expression levels.²⁴

With a FDR of 0.05, 100 proteins were found to be downregulated. However, 24 of these proteins could not be characterized. A further

number of identified proteins could not be converted to a human homologue, which is needed for analysis with DAVID. With this relatively low number of proteins, enrichment analysis yielded only few significantly regulated processes of pathways, shown in Table 1. Most genes were found in the broad GO term 'cellular process'. For other significantly enriched terms and pathways only one or two genes relevant to the downregulated dataset were involved.

***In vivo* analysis of Notch signaling**

For *in vivo* analysis of Notch activity, the *TG(EPV.Tp1-Mmu.Hbb:nlsmCherry)^{ia7}* was used. In this line, the expression of mCherry is driven by a Notch-responsive box containing 12 copies of the Epstein Barr Virus terminal protein 1 (TP1) promoter with 12 Rbp-Jk binding sites. This line was crossed with the *Et(E1b:Gal4-VP16)s1101t, TG(UAS:Kaede)s1999t* line. Fish without UAS:Kaede were selected, as the Kaede signal may interfere with interpretation of the mCherry Notch activity reporter. The *Et(E1b:Gal4-VP16)s1101t, TG(EPV.Tp1-Mmu.Hbb:nlsmCherry)^{ia7}* fish were crossed with the *TG(14xUAS:GFP-EWSR1-ERG)* line, to generate embryos expressing human GFP-tagged EWSR1-ERG in the neurons, in which Notch activity could also be monitored. Due to heterozygosity of the parents for 14xUAS:GFP-EWSR1-ERG, not all embryos expressed EWSR1-ERG. These siblings were used as the wildtype control.

In the regular development of zebrafish embryos, mRNA of Notch homologs of maternal origin can be found in the 2-cell stage, and maintains present in all cells until gastrulation. During gastrulation and stages thereafter, Notch expression remains present in different patterns throughout the development of the embryo.²⁵ When introducing neuronally targeted EWSR1-ERG, no Notch activity could be observed in embryos at 1, 2 and 3 dpf. In the wildtype siblings without EWSR1-ERG expression, regular expression patterns of Notch activity could be observed (Figure 3).

Discussion

EWSR1-ERG is the second most commonly occurring translocation in EWS patients, and is found in 10% of EWS cases. The most common translocation occurs between EWSR1 and FLI1, and there have been many investigations in the effect of knockdown or exogenous expression of EWSR1-FLI1 on a transcriptomic level. On a protein level, much less is known about the effects of either EWSR1-FLI1 or EWSR1-ERG. Here, for the first time, the effect of exogenous expression of EWSR1-ERG *in vivo* is shown. For this purpose, we have employed LC-MS/MS on 3 dpf zebrafish embryos expressing human EWSR1-ERG in the neurons. Numerous proteins were identified this way, the majority

Table 1. Enrichment analysis of up- and downregulated proteins.

Upregulated proteins

<u>GO Terms</u>	<u>Number of proteins</u>	<u>P-value</u>
Oncogenesis	33	8.2E-19
Cellular catabolic process	19	5.9E-3
Cellular respiration	6	2.0E-3
Cell organization and biogenesis	11	1.0E-2
Translation	9	1.2E-2
Cell surface receptor linked signal transduction	2	2.0E-2
Transcription activator activity	9	3.5E-2

<u>Pathways (KEGG, Panther, Reactome)</u>	<u>Number of proteins</u>	<u>P-value</u>
Oxidative phosphorylation	5	1.0E-3
Proteasome	5	2.0E-3
Apoptosis	7	3.5E-3
Signalling by Wnt	5	5.3E-3
Gene expression	11	5.9E-3
Cell cycle checkpoints	6	9.3E-3
Lysosome	5	4.6E-2

Downregulated proteins

<u>GO Terms</u>	<u>Number of proteins</u>	<u>P-value</u>
Nucleoside, nucleotide and nucleic acid metabolism	14	1.3E-2
Cellular process	28	3.4E-2
Positive regulation of small GTPase mediated signal transduction	2	3.6E-2
Cell differentiation	8	5.0E-2

<u>Pathways (KEGG, Panther, Reactome)</u>	<u>Number of proteins</u>	<u>P-value</u>
Notch signalling pathway	1	9.0E-3
Starch and sucrose metabolism	1	1.0E-2
Angiogenesis	3	3.2E-2

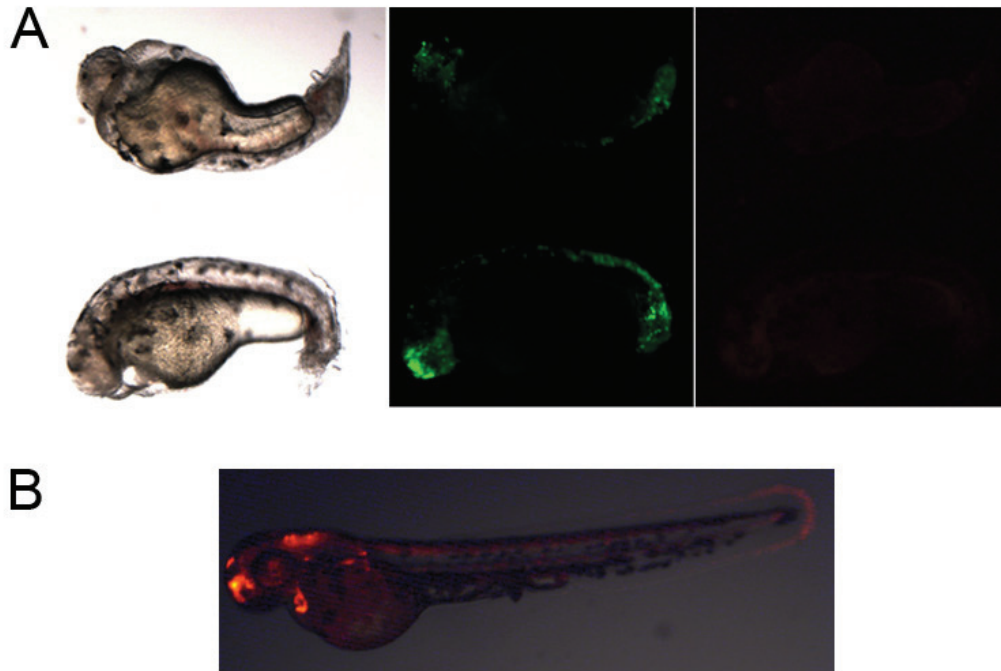


Figure 3. *In vivo* expression of Notch. A) Two representative 2 dpf embryos resultant from a cross between the *TG(14xUAS:GFP-EWSR1-ERG)* and *Et(E1b:Gal4-VP16)s1101t,TG(EPV.Tp1-Mmu.Hbb:nlsMCherry)^{ia7}* line. These embryos express GFP human EWSR1-ERG in the neurons (middle panel), while there is an absence of Notch reporter activity in these embryos, as seen by the lack of fluorescent signal in the right panel. **B)** A wild-type sibling without expression of EWSR1-ERG, showing Notch reporter activity in various tissues.

8

of which upregulated (294, versus 100 downregulated proteins). The significantly regulated proteins were involved in a variety of pathways and processes, such as oncogenesis, transcription and translation, and cellular respiration. Some of the proteins deregulated by EWSR1-ERG in this model are known to be involved in EWS, from previous studies.

Several WNT proteins and Frizzled proteins have been shown to be expressed in EWS cell lines; this includes WNT5a and FZD8, of which homologs were found expressed in this model.²³ The Wnt/Frizzled pathway active in EWS cells is suggested to be regulated (in part) by the Wnt inhibitor Dickkopf1 (DKK-1), which is repressed by EWSR1-FLI1.²⁶ Furthermore, WNT5a specifically has been shown to mediate EWS migration via CXCR4 expression.²⁴ Although CXCR4 was not found regulated in these samples (possibly due to protein levels below the detection threshold), previously performed RNA-seq analysis did show regulation of *cxcr4* and its ligand *cxcl12*. The CXCR4-CXCL12 axis has

been shown to play a role in EWS tumour growth.²⁷

Another protein identified was Necdin-like 2. Its murine homolog Necdin has been shown to be involved in the neuronal development, by regulating post-mitotic neuronal apoptosis.²¹ It suppresses apoptosis by increasing the interaction between Sirt1 and p53. This increased binding causes an increase in deacetylation of p53 by Sirt1, which leads to its deactivation. Not only Necdin, but also NOTCH has previously been shown to be linked to regulation of TP53 via SIRT1 activity.²² In EWS cell lines, NOTCH induced the reactivation of TP53 via HEY1 activation, which is a direct suppressor of SIRT1. Upon chemical treatment with a SIRT1/2 inhibitor, EWS cells engrafted in zebrafish showed reduced capacity of proliferation and migration. In this study, Notch2 was shown to be downregulated, and notch signalling overall was lost in these embryos, as observed via the Notch activity reporter fish *in vivo*. These results strengthen the case for investigating reactivation of the notch pathway as a therapeutic strategy.

In conclusion, this is the first proteomic analysis of an *in vivo* EWS model system. Using LC-MS/MS with spectral counting, we could quantify the changes in protein abundance as an effect of EWSR1-ERG expression in zebrafish in a time- and cost-effective manner. Various proteins, processes and pathways identified in this model, such as the downregulation of notch signalling, were comparable to other EWS models. Therefore, we believe that this model provides relevant insights into the effect of EWSR1-ERG *in vivo* and can be of great benefit in the search of a targeted therapy against EWS.

References

1. Turc-Carel C, Aurias A, Mugneret F, *et al*. Chromosomes in Ewing's sarcoma. I. An evaluation of 85 cases of remarkable consistency of t(11;22)(q24;q12). *Cancer Genet Cytogenet* 1988; **32**: 229-238.
2. Delattre O, Zucman J, Plougastel B, *et al*. Gene fusion with an ETS DNA-binding domain caused by chromosome translocation in human tumours. *Nature* 1992; **359**: 162-165.
3. Zucman J, Melot T, Desmaze C, *et al*. Combinatorial generation of variable fusion proteins in the Ewing family of tumours. *EMBO J* 1993; **12**: 4481-4487.
4. Sorensen PH, Lessnick SL, Lopez-Terrada D, *et al*. A second Ewing's sarcoma translocation, t(21;22), fuses the EWS gene to another ETS-family transcription factor, ERG. *Nat Genet* 1994; **6**: 146-151.
5. Hancock JD, Lessnick SL. A transcriptional profiling meta-analysis reveals a core EWS-FLI gene expression signature. *Cell Cycle* 2008; **7**: 250-256.
6. Elzi DJ, Song M, Hakala K, *et al*. Proteomic Analysis of the EWS-Fli-1 Interactome Reveals the Role of the Lysosome in EWS-Fli-1 Turnover. *J Proteome Res* 2014.
7. Anderson JL, Titz B, Akiyama R, *et al*. Phosphoproteomic profiling reveals IL6-mediated paracrine signaling within the Ewing sarcoma family of tumors. *Mol Cancer Res* 2014; **12**: 1740-1754.
8. Grunewald TG, Diebold I, Esposito I, *et al*. STEAP1 is associated with the invasive and oxidative stress phenotype of Ewing tumors. *Mol Cancer Res*

- 2012; **10**: 52-65.
9. Somasekharan SP, Stoynov N, Rotblat B, *et al.* Identification and quantification of newly synthesized proteins translationally regulated by YB-1 using a novel Click-SILAC approach. *J Proteomics* 2012; **77**: e1-10.
 10. Westman-Brinkmalm A, Abramsson A, Pannee J, *et al.* SILAC zebrafish for quantitative analysis of protein turnover and tissue regeneration. *J Proteomics* 2011; **75**: 425-434.
 11. Scott EK, Mason L, Arrenberg AB, *et al.* Targeting neural circuitry in zebrafish using GAL4 enhancer trapping. *Nat Methods* 2007; **4**: 323-326.
 12. Schiavone M, Rampazzo E, Casari A, *et al.* Zebrafish reporter lines reveal in vivo signaling pathway activities involved in pancreatic cancer. *Dis Model Mech* 2014; **7**: 883-894.
 13. Pedrioli PG, Eng JK, Hubley R, *et al.* A common open representation of mass spectrometry data and its application to proteomics research. *Nat Biotechnol* 2004; **22**: 1459-1466.
 14. Craig R, Beavis RC. TANDEM: matching proteins with tandem mass spectra. *Bioinformatics* 2004; **20**: 1466-1467.
 15. Lam H, Deutsch EW, Eddes JS, *et al.* Development and validation of a spectral library searching method for peptide identification from MS/MS. *Proteomics* 2007; **7**: 655-667.
 16. Shteynberg D, Deutsch EW, Lam H, *et al.* iProphet: multi-level integrative analysis of shotgun proteomic data improves peptide and protein identification rates and error estimates. *Mol Cell Proteomics* 2011; **10**: M111 007690.
 17. Huang da W, Sherman BT, Lempicki RA. Systematic and integrative analysis of large gene lists using DAVID bioinformatics resources. *Nat Protoc* 2009; **4**: 44-57.
 18. Huang da W, Sherman BT, Lempicki RA. Bioinformatics enrichment tools: paths toward the comprehensive functional analysis of large gene lists. *Nucleic Acids Res* 2009; **37**: 1-13.
 19. Chang JT, Nevins JR. GATHER: a systems approach to interpreting genomic signatures. *Bioinformatics* 2006; **22**: 2926-2933.
 20. Park SS, Wu WW, Zhou Y, *et al.* Effective correction of experimental errors in quantitative proteomics using stable isotope labeling by amino acids in cell culture (SILAC). *J Proteomics* 2012; **75**: 3720-3732.
 21. Hasegawa K, Yoshikawa K. Necdin regulates p53 acetylation via Sirtuin1 to modulate DNA damage response in cortical neurons. *J Neurosci* 2008; **28**: 8772-8784.
 22. Ban J, Aryee DN, Fourtouna A, *et al.* Suppression of deacetylase SIRT1 mediates tumor-suppressive NOTCH response and offers a novel treatment option in metastatic Ewing sarcoma. *Cancer Res* 2014; **74**: 6578-6588.
 23. Uren A, Wolf V, Sun YF, *et al.* Wnt/Frizzled signaling in Ewing sarcoma. *Pediatr Blood Cancer* 2004; **43**: 243-249.
 24. Jin Z, Zhao C, Han X, *et al.* Wnt5a promotes ewing sarcoma cell migration through upregulating CXCR4 expression. *BMC Cancer* 2012; **12**: 480.
 25. Bierkamp C, Campos-Ortega JA. A zebrafish homologue of the Drosophila neurogenic gene Notch and its pattern of transcription during early embryogenesis. *Mech Dev* 1993; **43**: 87-100.
 26. Navarro D, Agra N, Pestana A, *et al.* The EWS/FLI1 oncogenic protein inhibits expression of the Wnt inhibitor DICKKOPF-1 gene and antagonizes beta-catenin/TCF-mediated transcription. *Carcinogenesis* 2010; **31**: 394-401.
 27. Berghuis D, Schilham MW, Santos SJ, *et al.* The CXCR4-CXCL12 axis in Ewing sarcoma: promotion of tumor growth rather than metastatic disease. *Clin Sarcoma Res* 2012; **2**: 24.

Chapter 9

Summary and concluding remarks

Summary and concluding remarks

Ewing sarcoma (EWS) is a disease with a high need for novel therapeutic strategies. It is the second most common bone- and soft-tissue sarcoma affecting children and young adults, and a quarter of patients present with metastases at the time of diagnosis. When metastases are present, the outlook of patients diminishes greatly: from an event-free survival rate of 60-70% in the case of localised disease, to only 20-30% when metastases are present. In this thesis, zebrafish is brought forth as an innovative model organism for EWS research. The zebrafish has been increasingly used in cancer research over the years. Between human and zebrafish, there is a high conservation of tumour suppressor genes and oncogenes, which supports the translational value of transgenic zebrafish cancer models. With regard to xenograft models, an attractive feature of the zebrafish is the segregation in time of innate and adaptive immune system development. Before 4 weeks post-fertilisation, there is no mature adaptive immune system, permitting the engraftment of human cancer cells without additional immunosuppression until this time point.

The zebrafish engraftment model (employed in **Chapter 4 and Chapter 5**), where EWS cells are implanted to the yolk of 2-day-old zebrafish, is a useful new tool in the field of EWS research. It provides a rapid method of looking at the proliferation and migration properties of cancer cells *in vivo*, and the changes of these behaviours upon compound treatment or gene interference. An attractive feature of this model is its supreme aptness for doing non-invasive live *in vivo* imaging. While only used sparingly in this thesis, zebrafish embryos can be used for time-lapse microscopy by embedding them in low melt-point agarose; with a correct setup, this can even be done over a period of multiple days. A whole array of transgenic and mutant zebrafish lines is available, aiding in the investigation of interactions of tumour cells with the vasculature, the immune system, and other components of the microenvironment in the host. Fluorescent reporter lines for specific signalling pathways (such as the *TG(EPV.Tp1-Mmu.Hbb:nIsmCherry)^{ia7}* fish for the Notch pathway, used in **Chapter 8**) allow monitoring of pathway activity in live embryos in real-time. With the development of the CRISPR/Cas9 system, producing mutant zebrafish lines has become a relatively quick and easy feat. This is in addition to the long-standing morpholino technology, which can produce transient gene knockdown by injection of oligonucleotides. All these available technologies make it a very flexible model to study the process of EWS progression. However, no technique is without its limitations: this model is designed primarily for early stages of tumour development. Starting with circa 800 cells in the yolk, migration away from the site of injection can be observed, and also the proliferation of these cells. Due to the timeframe of the experiment, we have not followed the development of cells that have settled at these distant locations. These micro-metastases were occasionally observed

at 4 dpi, though usually at 6 dpi, which coincides with the final day of most zebrafish experiments due to local animal experimentation regulations. Although regulatory permission to investigate tumour formation in the xenograft model beyond this timepoint must be requested, other factors then will come into play, such as the need for immunosuppression once the immune system develops further. Considering the tumour burden is relatively high for the embryos, especially at the site of injection, lethality may be significantly increased in these embryos when they are maintained for a longer time frame. As such, the major appeal of the presented 2-day-old engraftment model will be for rapid investigation of early processes of EWS tumour development.

As is demonstrated in **Chapter 3**, many efforts are ongoing to utilize the full potential of the zebrafish embryonic model organism for high-throughput screenings for drug discovery. We present the work we have done with this goal in mind in **Chapter 6**, and show the dynamics of EWS cell behaviour after robotic implantation into blastula-staged embryos. Implantation into blastula-staged embryos differed in some aspects from engraftment into two-day-old embryos. Firstly, the embryos at this stage of development are more fragile, and cannot withstand a high number of cells, as lethality will become a problem. Secondly, EWS cells engrafted in these embryos do not show much migration. This may be due to reprogramming of the EWS cells under influence of the embryonic environment. While these cells were still positive for the expression of EWS marker CD99, further characterization of these cells would be interesting to see how they are affected by the embryonic microenvironment. Another possible explanation of the lack of migration would be that there are simply too little amount of cells to achieve migration. Only a subset of EWS cells are migratory, as is also seen in the manual xenograft model in 2-day-old embryos. In the same line of thought, perhaps this subset of cells is stimulated by other cells in the microenvironment to achieve migratory properties. Considering that the blastula model has three to four times less cells implanted than in the manual model, it could be that no cells are triggered to move from their current microenvironment. Despite this lack of migration, however, this model is useful in screens to look at drug-treatment response. We showed in Chapter 6 that the effect of drugs *in vitro* does not always comply with the same conditions *in vivo*. While most EWS cell line/drug treatment combinations concurred between the two experiments, EW7 failed to respond to treatment with (S)-YK-4-279 in this model. Interestingly, in the 2-day-old engraftment model a racemic mixture of YK-4-279 was able to inhibit proliferation of this cell line *in vivo*. A large amount of developed drugs do not make it from the bench to the clinic, partially due to inadequate effects *in vivo*. It is important to remove these compounds from the testing pipeline as early as possible, to avoid investing time and costs into their development. The proposed model allows for testing of compounds in an *in vivo* setting, while at the same time, being a rapid screening method with relatively low costs. Additionally, both the

engraftment models presented in Chapter 2 and Chapter 3 may be further developed to use for patient-derived xenografts (PDX). These experiments would be quick and use relatively low amounts of cells, which is advantageous when little tumour material is available.

In addition to the xenograft model, this thesis also describes a novel transgenic zebrafish model for EWS in **Chapter 7**. As the cell of origin for EWS is unknown, making transgenic animal models for this disease has proven to be a difficult task. The defining molecular aberration in EWS, an *EWSR1-ETS* translocation gene, is highly toxic when introduced in cells, and caused embryonic lethality when expressed in mice. A previous attempt to introduce the *EWSR1-FLI1* gene in zebrafish with mutated p53 did lead to tumour formation in a subset of fish reaching adulthood. However, the majority of these were malignant peripheral nerve sheath tumours arisen from the p53-mutated background. About 5% of the fish presented with solid small round blue cell tumours (SRBCTs). Another 3% of fish in the same group developed more diffuse, leukaemia-like SRBCTs. Possibly the low amount of fish presenting with SRBCTs is due to the cellular context in which *EWSR1-FLI1* was expressed. Therefore, in our design of a transgenic zebrafish model, we anticipated the need of flexibility of expression by using a binary expression system. By placing *EWSR1-FLI1* and *EWSR1-ERG* under control of a UAS promotor, expression only takes place when there is also GAL4 present to activate the UAS promotor. Using different GAL4 driver lines, *EWSR1-ETS* expression can be targeted to various tissues at different times. One setback in these experiments was that we were not able to generate the *EWSR1-FLI1* transgenic line, to represent the most common translocation in EWS. Possibly, this may be due to leakiness of the promoter: if there is inadvertent expression of *EWSR1-ETS* in early development, the fish may die in embryonic stages. In the case of the *EWSR1-ERG* transgenic line, out of circa 150 injected embryos raised to adulthood, only one founder fish was identified. The expected percentage of founders when using the Tol2 transposase system is around 10%, so this is quite low and may be explained by similar leakiness of the promoter. Nonetheless, with the progeny of the *EWSR1-ERG* founder we did identify, we could investigate which GAL4 lines were suitable to drive expression. Neuronal expression of *EWSR1-ERG* was shown to have pronounced effects on embryonic development. The expression of *EWSR1-ERG* was maintained in these embryos, whereas it was lost in embryos where expression was targeted to different tissues. Further investigation into the transcriptome showed that there was an overlap of genes expressed in these embryos and a core set of genes identified to be regulated by *EWSR1-FLI1* in other models, suggesting that the expression of the human driver of EWS resulted in partial transformation of zebrafish embryonic cells, and has a translational value. These findings are a promising start, and further investigation with this model by combination with other GAL4 driver lines should yield interesting insights into the mechanisms of the *EWSR1-*

ERG oncogene.

Additional characterization of the transgenic model was done by a proteomic analysis of embryos neuronally expressing EWSR1-ERG at 3dpf (**Chapter 8**). Using LC-MS/MS with spectral counting, we could identify significantly regulated proteins, several of which are known to be involved in EWS pathogenesis. One upregulated protein identified in the proteomics study of **Chapter 8** was *necdin*. This protein was interesting because upregulation of *Necdin* in a murine model was shown to increase the binding between Sirt1 and p53, as a mechanism to regulate post-mitotic neuronal apoptosis. In **Chapter 5**, SIRT1 was also implicated in EWS malignancy. It was shown that restoration of Notch signalling in human cells caused SIRT1 suppression via HEY1, which in turn caused reactivation of p53 signalling. In the proteomics study of Chapter 8, one of the downregulated proteins was *notch2*. By using signalling reporter lines, the downregulation of Notch signalling in these embryos was confirmed *in vivo*.

In conclusion, in this thesis three novel *in vivo* models for EWS research are presented. The manual xenograft model into two-day-old embryos and the high-throughput xenograft model into blastula-staged embryos provide two rapid methods of testing the efficacy of chemical or genetic inhibition on EWS malignancy. The transgenic model can provide a more fundamental understanding of the effects of exogenous expression of EWSR1-ERG in a variety of cellular contexts. Given the relative ease with which the zebrafish genome can be manipulated, the models can be adapted as further insights in EWS development are obtained, and so provide a lasting, valuable contribution to the field of EWS research and the search for novel patient treatment regimens.

Chapter 10

Nederlandse samenvatting

Samenvatting en afsluitende commentaren

Ewing sarcoom (EWS) is een ziekte waarvoor er grote behoefte is aan nieuwe therapeutische strategieën. Het is het tweede meest voorkomende bot- en weke delen sarcoom wat kinderen en jongvolwassenen aangrijpt, en een kwart van patiënten presenteert met metastasen op het moment van diagnose. Wanneer metastasen aanwezig zijn, is het vooruitzicht van de patiënt slecht: waar er met lokale ziekte een 60-70% kans van overleven zonder terugval is, neemt dit af naar slechts 20-30% in het geval van aanwezige metastasen. In dit proefschrift wordt de zebravis naar voren gebracht als een innovatief model organisme voor EWS onderzoek. De zebravis is gedurende de laatste decennia meer en meer gebruikt in het veld van kankeronderzoek. Er is een hoge mate van conservatie van tumor suppressie genen en oncogenen tussen mens en zebravis, wat de translationele waarde van transgene zebravis kankermodellen ondersteunt. Met betrekking tot xenograft modellen, is de scheiding in tijd tussen ontwikkeling van het aangeboren en adaptief immuunsysteem een aantrekkelijk kenmerk van de zebravis. Tot 4 weken na fertilisatie is er geen volledig ontwikkeld adaptief immuunsysteem, wat toelaat humane kanker cellen te implanteren zonder additionele immunosuppressiva tot dit tijdstip.

Het zebravis implantatie model (toegepast in **Hoofdstuk 4 en Hoofdstuk 5**), waarbij EWS cellen worden geïmplaneerd in de dooier van 2 dagen oude zebravis embryo's, is een nuttige nieuwe techniek in het veld van EWS onderzoek. Het biedt een snelle methode om te kijken naar deling en migratie van kanker cellen *in vivo*, en de veranderingen van deze eigenschappen wanneer behandeling met chemische stoffen of genetische ingrepen worden toegepast. Een waardevol kenmerk van dit model is diens buitengewone bekwaamheid voor het uitvoeren van niet-invasieve, live microscopie *in vivo*. Hoewel slechts incidenteel toegepast in dit proefschrift, kunnen zebravis embryo's gebruikt worden voor het maken van timelapse-videos door ze in te bedden in agarose met een laag smeltpunt; met de juiste opstelling, kunnen deze zelfs over een periode van meerdere dagen worden uitgevoerd. Er is een batterij aan transgene en mutante zebravis lijnen beschikbaar, wat uitkomst biedt bij het onderzoek naar interactie tussen tumor cellen en het bloedvatenstelsel, het immuunsysteem, en andere componenten van de tumor micro-omgeving in de gastheer. Fluorescente reporter lijnen voor specifieke signalleringsroutes (zoals de *TG(EPV.Tp1-Mmu.Hbb:nlsMCherry)*^{ia7} vis voor de Notch signalleringsroute, gebruikt in **Hoofdstuk 8**) maken het mogelijk de activiteit van signaaltransductie in levende embryo's te volgen. Met de ontwikkeling van het CRISPR/Cas9 systeem is het produceren van mutante zebravislijnen en relatief snel en makkelijk proces geworden. Hiernaast is tevens de veelgebruikte morpholino technologie beschikbaar, waarmee transiënte verlaging van genexpressie wordt bewerkstelligd door injectie van oligonucleotiden. Al deze beschikbare technologieën samen maken de zebravis een zeer

flexibel model om het proces van EWS voortgang in te bestuderen. Echter, geen enkele techniek is zonder haar beperkingen: dit model is ontworpen met vooral de eerste stadia van tumor progressie in gedachte. Beginnend met circa 800 cellen in de dooier, kan migratie weg van de plek van implantatie waargenomen worden, evenals proliferatie van deze cellen. Door het tijdsbestek van deze experimenten, hebben we de verdere ontwikkeling van cellen gevestigd op secundaire locaties niet gevolgd. Deze micrometastasen werden soms waargenomen op 4 dagen post-injectie (dpi), maar meestal op 6 dpi, wat samenvalt met de laatste dag van het merendeel van zebavis experimenten als gevolg van geldende proefdier regelgeving. Hoewel het mogelijk is toestemming aan te vragen om de tumor ontwikkeling na dit tijds punt in het implantatie model, zullen andere factoren in zulke experimenten een rol spelen. Bijvoorbeeld de noodzaak van immunosuppressiva, naarmate het immuun systeem zich verder ontwikkelt. Gezien de tumor massa relatief groot is voor de embryo's, vooral op de plek van implantatie, is het goed mogelijk dat sterfte significant toeneemt in de embryo's wanneer zij voor een langere tijd aangehouden worden. Als zodanig zal de grote aantrekkingskracht van het gepresenteerde implantatie model zijn voor snel onderzoek naar vroege processen in de ontwikkeling van EWS tumoren.

Zoals is aangetoond in **Hoofdstuk 3**, zijn er veel ontwikkelingen gaande om het volledige potentieel van het embryonale zebavis model organisme te benutten voor hoge-doorvoer screenings met als doel het ontdekken van nieuwe medicijnen. Wij presenteren het werk gedaan met dit doel in ogen in **Hoofdstuk 6**, en laten de dynamiek van EWS cel gedrag zien na geautomatiseerde implantatie in embryo's op blastula stadium. Implantatie in blastula-stadium embryo's verschilde in enkele aspecten van implantatie in 2 dagen oude embryo's. Allereerst zijn de embryo's op blastula stadium kwetsbaarder, en tolereren geen groot aantal cellen, gezien dit een hogere mate van letaliteit als gevolg heeft. Daarnaast vertonen EWS cellen geïmplanteerd op dit stadium niet veel migratie. Dit is mogelijk een gevolg van herprogrammering van de cellen door de embryonale omgeving. Hoewel deze cellen nog altijd positief waren voor de EWS marker CD99, zou verdere karakterisering van deze cellen interessant zijn, om te zien hoe zij beïnvloed worden door de embryonale micro-omgeving. Een andere mogelijke verklaring voor het gebrek aan migratie kan zijn dat er simpelweg te weinig cellen aanwezig zijn voor het plaatsvinden van migratie. Slechts een deel van de cellen kunnen migreren, wat ook geobserveerd werd in het handmatige implantatie model in 2 dagen oude embryo's. Ook wordt deze deelverzameling van cellen mogelijk tot migratie gestimuleerd door andere cellen in de micro-omgeving. Gezien het blastula model 3 tot 4 keer minder cellen geïmplanteerd in de dooier heeft dan het handmatige injectiemodel, kan het zijn dat de cellen niet gestimuleerd worden om uit hun huidige micro-omgeving te migreren. Ondanks het gebrek aan migratie, is dit model echter nog altijd nuttig voor het screenen van

respons op behandeling met potentiële geneesmiddelen. In Hoofdstuk 6 laten we zien dat het effect van medicijnen *in vitro* niet altijd overeenkomt met dezelfde condities *in vivo*. Hoewel de meeste EWS cellijn/geneesmiddel behandeling combinaties dezelfde resultaten gaven tussen de verschillende experimenten, vertoonde EW7 geen respons na behandeling met (S)-YK-4-279 in dit model. Opmerkelijk genoeg was een racemische mix van YK-4-279 in het handmatige implantatie model in 2 dagen oude vissen wel in staat tot het verminderen van deling van deze cellijn *in vivo*. Een groot deel van ontwikkelde geneesmiddelen halen het niet van werkbank naar de kliniek, deels door ontoereikende effecten *in vivo*. Het is belangrijk deze medicatie zo snel mogelijk uit de pijn te verwijderen, zodat er zo min mogelijk tijd en geld in hun ontwikkeling wordt gestoken. Het in dit hoofdstuk voorgestelde model staat toe geneesmiddelen *in vivo* te testen, terwijl het tegelijk een snelle screening methode is met relatief lage kosten. Daarnaast kunnen zowel de implantatie modellen gepresenteerd in Hoofdstuk 2 als Hoofdstuk 3 verder ontwikkeld worden voor implantatie van patiënt-afgeleide xenografts (PDX). Deze experimenten zouden snel zijn, en relatief weinig cellen gebruiken, wat voordelig is wanneer er weinig tumor materiaal beschikbaar is.

Naast het implantatie model, beschrijft dit proefschrift een nieuw transgeen zebrafish model voor EWS in **Hoofdstuk 7**. Daar de cel van oorsprong onbekend is voor EWS, is het maken van een transgeen diermodel moeilijk gebleken voor deze ziekte. De definiërende moleculaire afwijking, een *EWSR1-ETS* translocatie gen, is zeer toxisch wanneer geïntroduceerd in cellen, en veroorzaakt embryonale letaliteit wanneer tot expressie gebracht in muizen. Een voorgaande poging om het *EWSR1-FLI1* gen in zebrafish met p53 mutaties te introduceren, leidde tot tumor ontwikkeling in een deel van de vissen die het volwassen stadium bereikten. Echter, het merendeel waren maligne perifere zenuwschedetumoren, die ontstonden als gevolg van de p53-gemuteerde achtergrond. Ongeveer 5% van de vissen presenteerden met solide tumoren bestaande uit kleine ronde cellen (Engels: small round blue cell tumours, afgekort als SRBCTs). Verder ontwikkelde 3% van de vissen uit dezelfde groep meer diffuse, leukemie-achtige SRBCTs. Mogelijk is het lage aantal vissen met SRBCTs te verklaren door de cellulaire context waarin *EWSR1-FLI1* tot expressie werd gebracht. Hierom hebben wij in ons transgene zebrafish model geanticipeerd op een behoefte aan flexibiliteit van expressie, en gebruik gemaakt van een binair expressie systeem. Door *EWSR1-FLI1* en *EWSR1-ERG* onder controle van een UAS promotor te plaatsen, vindt expressie alleen plaats wanneer er ook GAL4 aanwezig is om de UAS promotor te activeren. Gebruik makend van verschillende GAL4 lijnen kan *EWSR1-ETS* expressie in verscheidenen weefsels en op specifieke tijden tot expressie gebracht worden. Een tegenslag in deze experimenten was dat wij niet in staat waren de *EWSR1-FLI1* transgene lijn te genereren, die de meest voorkomende translocatie representeert. Mogelijk komt dit

door het “lekken” van de promotor: wanneer er ondanks afwezigheid van GAL4 toch expressie is van EWSR1-ETS in vroege stadia van ontwikkeling, kunnen de vissen sterven in het embryonale stadium. In the geval van de *EWSR1-ERG* transgene lijn is er, uit circa de 150 geïnjecteerde embryo's die volgroeid zijn tot volwassen, slechts één 'founder' vis gevonden (een vis met het beoogde transgen geïntegreerd in de kiemlijn). Het verwachte percentage founders, wanneer gebruik wordt gemaakt van het Tol2 transposase systeem, ligt rond de 10%. Het gevonden percentage is dus relatief laag, en zou eveneens door het lekken van de promotor verklaard kunnen worden. Desalniettemin, met het nageslacht van de gevonden *EWSR1-ERG* founder konden we onderzoeken welke GAL4 lijnen geschikt waren om op expressie van het gen aan te drijven. Neuronale expressie van EWSR1-ERG toonde aanzienlijke effecten op de embryonale ontwikkeling. De expressie van EWSR1-ERG werd door deze embryo's in stand gehouden, waar het verloren ging in embryo's die het gen in andere weefsels tot expressie brachten. Verdieping in het transcriptoom liet zien dat er een overlap was tussen de genen tot expressie gebracht in de embryo's met neuronale EWSR1-ERG, en een set aan genen gedefinieerd als de kern-set van gereguleerde genen in EWS aan de hand van andere modellen voor de ziekte. Dit suggereert dat de expressie van het humane gen dat EWS aanstuurt, in zebrafish embryonale cellen een gedeeltelijke transformatie bewerkstelligd, en van translationele waarde is. Deze bevindingen zijn een veelbelovend uitgangspunt, en verder onderzoek met dit model in combinatie met andere GAL4 lijnen zou interessante inzichten in de mechanismes van werking van het EWSR1-ERG oncogen op kunnen leveren.

Verdere karakterisatie van het transgene model is gedaan door een analyse op eiwit niveau (proteomics) van drie-dagen-oude embryo's die EWSR1-ERG neuronaal tot expressie brachten (**Hoofdstuk 8**). Gebruik makend van LC-MS/MS met spectral counting, konden wij significant gereguleerde eiwitten identificeren, waarvan van meerdere reeds bekend was dat zij betrokken zijn bij EWS pathogenese. Een van de omhoog gereguleerde eiwitten geïdentificeerd door proteomics in **Hoofdstuk 8** was *Necdin*. Dit eiwit is interessant omdat in voorgaande studies in een muismodel de inductie van *Necdin* binding tussen Sirt1 en p53 stimuleerde, als mechanisme op post-mitotische neuronale apoptose te reguleren. In **Hoofdstuk 5** is SIRT1 ook betrokken bij EWS maligniteit. Het is aangetoond dat herstel van Notch signallerings in humane cellen SIRT1 onderdrukt via HEY1, wat op zijn beurt reactivatie van p53 signallerings als gevolg heeft. In de proteomics studie van Hoofdstuk 8, is notch2 een van de gereduceerde eiwitten. Door gebruik te maken van vislijnen die signallerings activiteit aan kunnen tonen middels aanwezigheid of afwezigheid van fluorescente signalen, kon deze vermindering van Notch signallerings activiteit in de embryo's bevestigd worden *in vivo*.

Ter conclusie; er zijn in dit proefschrift drie nieuwe *in vivo* modellen voor EWS onderzoek gepresenteerd. Het handmatige xenograft

model in twee-dagen-oude embryo's en het geautomatiseerde model in blastula-stadium embryo's voor hoge-doorvoer doeleinden bieden twee snelle methoden om de efficiëntie van genetische of chemische inhibitie op EWS voortgang vast te stellen. Het transgene model kan een meer fundamenteel inzicht bieden in het effect van exogene EWSR1-ERG expressie in verschillende weefsels of celtypen. Gezien het gemak waarmee het zebravisgenoom gemanipuleerd kan worden, kunnen de modellen aangepast worden naarmate verdere inzichten in EWS ontwikkeling verkregen worden. Hiermee bieden zij een blijvende, waardevolle contributie aan het veld van EWS onderzoek en de zoektocht naar nieuwe patient behandel methodes.

Chapter 11

Curriculum Vitae

Curriculum vitae

Wietske van der Ent was born on the 19th of May, 1986 in Albrandswaard, The Netherlands. She attended secondary school at CSG Maarten Luther in Rotterdam and obtained her atheneum diploma in 2004. From 2004 to 2007 she studied Biology at Leiden University in order to obtain her BSc degree. During this period, she performed an internship entitled “*Optimalisation of heterologous protein production in Aspergillus niger and Aspergillus awamori*” under the supervision of Dr. Arthur F.J. Ram and Dr. Sandra de Weert at the department of Molecular Microbiology at the Leiden University. In 2007 she continued her MSc research at the same university, choosing to pursue the track of Molecular and Cellular Biosciences, which she successfully completed in 2009 (cum laude). Results obtained in her MSc internship under the supervision of Dr. B. Ewa Snaar-Jagalska and Dr. S.F. Gabby Krens led to a grant application at Foundation KiKa by Dr. Snaar-Jagalska and Prof. Dr. Pancras C.W. Hogendoorn, which was awarded. This grant, entitled “*Zebrafish: a new engraft model to study Ewing’s sarcoma progression*” funded her PhD research at the Molecular Cell Biology department of Leiden University (headed by Prof. Dr. Herman P. Spaink) and the department of Pathology at the Leiden University Medical Centre (headed by Prof. Dr. Hogendoorn). In March 2015, she started her postdoctoral research in laboratory of Prof. Dr. Olivier Delattre, MD at Institut Curie in Paris, France.

Chapter 12

List of publications

Publication List

Jager MJ, Cao J, Yang H, Carita G, Kalirai H, **van der Ent W**, de Waard N, Cassoux N, Aronow ME, Coupland SE. *Animal models in ocular oncology*. Accepted in Experimental Animal Models of Ophthalmic Diseases

van der Ent W, Burrello C, van der Velden PA, Jochemsen AG, Jager MJ, Snaar-Jagalska BE. *Embryonic zebrafish, different phenotypes after injection of human uveal melanoma*. Accepted in Ophthalmic Research - special issue Animal Models in Ocular Oncology

van der Ent W, Veneman WJ, Groenewoud A, Chen L, Tulotta C, Hogendoorn PCW, Spaik HP, Snaar-Jagalska BE. *Automation and manipulations for cancer discovery*. Accepted in Springer publication 'Cancer and Zebrafish: Mechanisms, Techniques, and Models'

Ban J, Aryee DN, Fourtouna A, **van der Ent W**, Kauer M, Niedan S, Machado I, Rodriguez-Galindo C, Tirado OM, Schwentner R, Picci P, Flanagan AM, Berg V, Strauss SJ, Scotlandi K, Lawlor ER, Snaar-Jagalska E, Lombart-Bosch A, Kovar H. *Suppression of deacetylase SIRT1 mediates tumor suppressive NOTCH response and offers a novel treatment option in metastatic Ewing sarcoma*. Cancer Res. 2014 Oct 3. pii: canres.1736.2014

van der Ent W, Burrello C, Teunisse AF, Ksander BR, van der Velden PA, Jager MJ, Jochemsen AG, Snaar-Jagalska BE. *Modelling of human uveal melanoma in Zebrafish xenograft embryos*. Invest Ophthalmol Vis Sci. 2014 Sep 23. pii: IOVS-14-15202

van der Ent W, Jochemsen AG, Teunisse AF, Krens SF, Szuhai K, Spaik HP, Hogendoorn PC, Snaar-Jagalska BE. *Ewing sarcoma inhibition by disruption of EWSR1-FLI1 transcriptional activity and reactivation of p53*. J Pathol. 2014 Aug;233(4):415-24

Spaik HP, Cui C, Wiweger MI, Jansen HJ, Veneman WJ, Marin-Juez R, de Sonnevile J, Ordas A, Torraca V, **van der Ent W**, Leenders WP, Meijer AH, Snaar-Jagalska BE, Dirks RP. *Robotic injection of zebrafish embryos for high-throughput screening in disease models*. Methods. 2013 Aug 15;62(3):246-54

Ghotra VP, He S, de Bont H, **van der Ent W**, Spaik HP, van de Water B, Snaar-Jagalska BE, Danen EH. *Automated whole animal bio-imaging assay for human cancer dissemination*. PLoS One. 2012;7(2):e31281

Chapter 13

List of abbreviations

ANOVA	One-way analysis of variance
CI	Confidence interval
DMSO	Dimethyl sulfoxide
dpf	Days post-fertilisation
dpi	Days post-implantation/injection
ES	Ewing sarcoma (only Chapter 5)
EWS	Ewing sarcoma
hpf	Hours post-fertilisation
hph	Hours post-heatshock
hpi	Hours post-implantation/injection
IHC	Immunohistochemistry
LOC	Lab-on-chip
MCD	Cumulative migration distance
MPC	Mesenchymal progenitor cell
MR	Mean reduction
MSC	Mesenchymal stem cell
O/N	Overnight
PAS	Periodic acid-Schiff
PBS	Phosphate buffered saline
PDX	Patient-derived xenografts
PFA	Paraformaldehyde
PTM	posttranslational modifications
PVP	Polyvinylpyrrolidone
PVS	Perivitelline space
SIV	Subintestinal <i>vein</i>
SOI	Site of implantation/injection
SRBCT	Small round blue cell tumours
TFA	Trifluoroacetic acid
TMA	Tissue microarray
VAST	Vertebrate Automated Screening Technology Chemotherapeutic protocol using vincristine, ifosfamide, doxorubicine and etoposide
VIDE	